THE EFFECT OF BIOFILM COLONIZATION ON THE STABILITY OF NON-COHESIVE SEDIMENTS

By

ELISA VIGNAGA

MSc, BEng

Submitted in fulfilment of the requirements for the Degree of Doctor of Philosophy

SCHOOL OF ENGINEERING

UNIVERSITY OF GLASGOW

Abstract

In the past decades, engineers have started to realize the importance of the interaction between vegetation, biota and water flow, in riverine and marine environments; a discipline that has been named "Eco-Hydraulics". Scientists have valued this coupled phenomenon for much longer than their engineering colleagues. As early as 1970, marine researchers presented the evidence that colonies of micro-organisms might alter the stability of fine cohesive sediments (Neuman *et al.*, 1970). However traditional models of sediments transport (e.g. Shields, 1936) have been derived using abiotic sediments and did not consider that most wet surfaces would soon be colonized by micro-organisms and their extracellular polymeric substances (EPS), a combination called "biofilm" (Lock, 1993). Scientists during the 1990s, after observing this phenomenon in the field, coined the term "biostabilization". During this period they showed that colonies of cyanobacteria and diatoms coating fine sand or cohesive sediments can increase their stability by up to 960% compared to abiotic sediments (Grant and Gust, 1987; Dade *et al*, 1990; Paterson 1997). Only recently have engineers started to take into consideration the effect of such increased cohesion and adhesion due to biogenic forces within the sediment transport model (Righetti and Lucarelli, 2007); yet all of those studies have low applicability because they are linked to specific environmental conditions. Moreover no data are available on the effect of biofilm on larger sediments (e.g. coarse sand and gravel).

The present thesis provides experimental data carried out in a flume laboratory pertaining to biostabilization of non-cohesive coarse sand and gravels at a scale representation of a real river system (from 0.2m to 1m). Four sediment substratum (glass spheres of D_{50} = 1.09mm and 2.00mm; sand of D_{50} = 1.20mm and gravel of D_{50} = 2.20mm) were colonized under unidirectional flow by a cyanobacterium (*Phormidium* sp.) for between 1 and 10 weeks. The increase in erosion threshold for biotic sediment is then investigated using a series of different methods ranging from traditional sediment transport techniques (e.g. Yalin, 1972), to image thresholding and particle image velocimetry (PIV) assessments of flow modification due to biofilm presence. Moreover, tensile strength analysis of ex-situ biofilm/substratum specimens will be presented to understand better the mechanical property of this composite material.

Data indicates that: i) biostabilization of sediments in the range of coarse sand and gravel occurs (9%-150% more shear stress required to induce entrainment compared to abiotic sediments) but to a lower extent compared to critical entrainment thresholds for fine sand and cohesive sediments (Paterson, 1997); ii) flume experimentation can be employed to control specific variables affecting biostabilization and could help to unfold the complicated interactions between environmental variables, and the affect of flow on the growth and strength of biofilm colonization over sediments; iii) strong biofilm growth generated a more uniform velocity field, with reduction in shear stress (up to 82% compared with abiotic sediments) and decreases in roughness length of the bed (up to 94% compared to abiotic sediments); iv) Composite biofilm/substratum specimens presented a clear elastic behaviour when tensile tested; v) Conventional models of sediment transport (e.g. Wiberg and Smith, 1987) do not consider the presence of biofilm and will not work in the case of bio-mats smoothing the surface of the bed; hence the need for new models which include the biofilm elasticity and the bio-mat smoothing process. This thesis suggests two theoretical examples where the biofilm action is considered at a grain to grain and bio-mat scale.

Keywords: Biostabilization, sediment transport, non-cohesive sediments, flume, erosion, Eco-Hydraulics, PIV, tensile testing.

TABLE OF CONTENT

List of Tables

List of figures

Acknowledgment

My first big thank you goes to my two supervisors, **Heather and Bill**: you have been models to follow throughout the course of this journey; you really have passed on to me your enthusiasm about research and the desire to achieve the best science. It is only thanks to you that I have made it so far.

Stuart: without your fundamental help I would have not been able to finish this thesis. Thank you for always being there.

Thank you to the two external examiners, Prof David Paterson and Prof Trevor Hoey, for the precious help in improving the quality of my thesis.

Amanda, Barbara, Eileen, Alan, Bobby, Ian, Robert, Tim, Kami: you have been fundamental for me! Always there to help and with a bright smile in any occasion.

Dr V.R. Phoenix, Dr T. Beattie, Dr A. Fernandes, Dr M. Jarvis, Dr G Collins, Sarah Haigh, Dr J. Cooper: thanks for the technical input that all of you have given me at different points during my PhD. It really meant a lot for this project.

Department of Civil Engineering, University of Glasgow (and in particular the former Heads of the Department Alan, Simon and Chris): thanks you very much for the support that you have given me during the past 4 years.

GU68: A special thank you to you for having believed in me and for the award I received: with the help you given me, my data (especially in chapter 5) have improved in quality substantially. Without you the science I have produced would not have been at the right standard.

Alan Ervine: a big thank you to Alan, for having believed in me as a researcher. You will always be a model for all of us.

For the old PhD folks Annie, Doug, Miguel, Iain, Jen: I am glad we met and if it wasn't for this academic journey I would have never got to know you guys! You have been all special for me and made the journey go smoother and faster. Thanks for being there all the time. I won't forget it.

For all the great friends I have met on the way thanks to this PhD: Marnie and Jay, Melanie and Jake, Sarah and Martin, Ross and Jay, Graeme and Kirsten, James, Doug and Hayley, Siding. You guys have been a huge help and a lot of fun. I am lucky that we all met! Thanks for all the things we have done together and for always being there.

Friends in UK: Silvia, Simona, Alessandro e le bambine, Filippo, Lotta, Giancarlo, Alessia, Jesus, Moha, Marie, Megan, Daniele, you are my family here. Thanks for being there always.

Italian friends: Sonia, Daniele, Marina, Paolo, Karen, Ilaria, Laura, Erica, Andrea, Giacomo, Massimiliano, Luca, Monica, Giuseppe, Batta, Giada, Raffaele, Stefano, Silvia, Manuel, Marzio, Mauro, Sara Busatto, Moreno, Laura, Valentina,

Irene, Alessandra thanks for making me feel your support, even from Italy! Even if we are distant, every time we see each other, is like no time has passed and you are always with me!

Manolo, Silvia, Estelle: you guys, even if we do not see each other very often, I have always known you are there for me and this meant a lot! I will come and visit you once I am done!

Finally, Seb: thank you for having been such a good support for me. For everything I had to complain about, you have been there. I would never have made it without you in my life and without your precious suggestions and advice. Grazie amore mio.

Vale: my best friend, I don't think I would have made it so far without you. You have always been there in all the decisions: from leaving Italy to starting a PhD. You have been indispensable for me: I have to really thank you for never leave me alone.

My family: Mamma, Papa', Antonio thanks just for being there in good and bad moments and always believe in my crazy ideas. You have given me all I could possibly want. Without your support and understanding I would have never gone anywhere. Grazie davvero.

Author's declaration

I declare that no portion of the work in this thesis has been submitted in support of any application for any other degree or qualification of this or any other university or institute of learning. I also declare that the work presented in this thesis is entirely my own contribution unless otherwise stated.

Elisa Vignaga

Definitions

a: small grain diameter;
A: the area;
A_w: the wet area;
b: intermediate grain diameter: this is the one measured with a sieve;
B: the width of the channel;
c: longest grain diameter;
C_D: drag coefficient;
cm: centimetres;
cm/s: centimetres per second, a measure of velocity;
d: displacement height in the "law of the wall", where the velocity profiles goes to zero;
D: grain diameter;
D_{50}: sediment grain diameter for which 50% of the material is lower;
E: Young's modulus of elasticity;
E_r: the erosion rate;
F_A: adhesive force;
F_D: drag force;
F_D: drag force;
F_L: lifting force;
F_R: resistance force;
Fr: the Froude number:
f_s: the sand fraction;
g: the gravity acceleration (9.81m/s^2);
H: flow depth;
k: Von Karman constant (0.4);
k_s: sediment roughness parameter;
L: length;
m: metre;
m/s: metre per seconds, a measure of velocity;
M: mass;
mm: millimetres;
M_o: overturning moment due to F_D or F_L;
M_r: resisting moment depending on W_S and F_R;
n: the critical number of grain moving according to the Yalin criterion;
Pa: Pascal, equal to kgm/s^2 and used to measure shear stress intensity;
Q: the flow;
R_e: Reynolds number;
R_{ep}: particle Reynolds number;
R_h: the hydraulic radius, defined as wet area (A_w) over wet perimeter (P);
s: seconds;
S: is the slope of the bed;
S_b: the slope of the bed:
S_e: the slope of the energy;
S_p: the shape factor;
S_w: the slope of the water level;
t: the time of application of the Yalin criterion;
T: time;
u^*: shear velocity;
u: instantaneous velocity in the downstream direction;

U: the mean cross sectional velocity;
u': deviation from the mean velocity U;
u_c^*: the critical friction velocity;
U_C: average critical velocity at incipient motion;
v: instantaneous velocity in the vertical direction (normal to the boundary);
v': vertical velocity fluctuation;
w: instantaneous velocity in the lateral direction;
W: weight of a particle;
w': lateral flow fluctuation;
W_s: submerged weight;
x: longitudinal coordinate;
y: vertical coordinate;
z_0: hydraulic roughness;
γ_s: the specific weight of a grain;
δ: boundary layer length;
ε: eddie viscosity/Yalin criterion (1972), equal to $1*10^{-6}$;
ε_f: the empirical floc erosion rate;
μ: the molecular (or dynamic) viscosity;
μm: micrometers;
ν: the kinematic viscosity;
ρ_s: the density of the material;
ρ_w: the water density;
τ: shearing force or shear rate, defined as the force applied on the area F/A;
τ_b: the bed shear stress;
τ_C: the critical bed shear stress for initiation of sediment motion;
Φ: Logarithmic scale for grain scale;
ω: terminal fall velocity.

Abbreviations

BGB: biofilm grown over beads (SGS);
BGS: biofilm grown over sand;
BO: biofilm only specimens;
Box_1: boxes used in the preliminary experiment with length scale equal to 1m;
$Box_{0.2}$: boxes used in the preliminary experiment with length scale equal to 0.2m;
CSM: cohesive strength meter;
dH_2O: distilled water;
DOM: dissolved organic matter;
EPS: extracellular polymeric substances;
LGS: large glass sphere (D_{50}=2.00mm);
LS: large scale of observation for the image thresholding (0.2m by 0.2m in chapter 4 and 0.5m by 0.3m in chapter 5);
PAR: photosynthetically active radiation;
PIV: particle image velocimetry;
SGS: small glass sphere (D_{50}=1.09mm);
SS: small scale of observation for the video recordings (50mm by 30mm in chapter 4 and in chapter 5).

CHAPTER 1

Introduction

"One can learn much from a river.

From the river I have learned too: everything comes back"

H. Hesse, *Siddharta*

1.1 Sediment transport and biological interaction: from an ancient past to present

The success and development of civilization has always been based on river systems, with a tendency of both maximizing the benefits and limiting the damages caused by rivers (Yang, 2003). The nature of lotic systems (streams and rivers) is complex and dynamic: natural streams constantly reshape their course through cycles of transport, scour and deposition of sediments. This combination of processes goes under the name of "sediment transport". In order to tackle the complexity by which physical forces induce sediment motion, engineers have for many years resolved to analyze simplified versions of the natural problem, by implementing laboratory experiments in channels, known as flumes (the manipulative experiment, Rice *et al.*, 2010a). DuBuat carried out the first ever recorded experiment as early as 1871 on the resistance of soil (from clay to "the size of an egg") under fluid velocities. Early experimental studies on sediment incipient motion by Gilbert (1914), Kramer (1932), Casey (1935) were used by Shields (1936) to draw the still most commonly used curve for predicting sediment transport. Yet, in the past century many engineers and geomorphologists (e.g. Mantz, 1977; Miller *et al.*, 1977; Yalin and Karahan, 1979; Buffington, 1999; Garcia, 2000) have attempted to improve the applicability of Shields work, which fails in a number of cases. The lack of a complete understanding of sediment transport is the reason why even in present times

engineering structures are badly affected by erosion, to the point of becoming ineffective (e.g. silting up of dams, bridge pier scour, and river banks erosion).

It is not only engineers who are facing issues related to sediment transport; in recent times environmental scientists have found themselves having to deal more and more with problems of habitat preservation, enhancement and the fate of pollutants and of pathogens (e.g. *E. coli*, Droppo *et al.*, 2009) in river systems. It is widely recognized that fine eroded sediments represent the best carrier for pollutants together with the "sticky exopolysaccharide matrix" (Salant, 2011), produced by micro-organisms naturally present in river systems. Those micro-organisms, ranging from viruses to algae, live in colonies bound together by extracellular polymers substances (EPS) and are known as "biofilms" (Neu, 1994). Biofilms have been extensively studied by biologists and ecologists in the past century, partly because they are part of the food web and biogeochemical cycles and partly because they influence fluxes of nutrients, energy and matter (Battin and Sengschmitt, 1999; Battin *et al.*, 2003a). A well known fact is that biofilm growth benefits from constant flow, hence micro-organisms preferentially colonize submerged substrata such as sediments and rocks, which provide an ideal location for anchoring and maximizing their exposure to nutrients (Anderson-Glenna *et al.*, 2008). The direct link among flow and biofilm growth is the reason why micro colonies are present in both marine and riverine environments. Despite the very many studies published on the effect that flow have on the development of biofilms (a search in the database *Web of Knowledge* for biofilm structure/flow provides 590 papers on the subject on the 31/03/12), it is only recently that publications have started to show that biofilms can also have an effect on flow and hydraulic variables. Some examples are: (i) increase the frictional resistance of ships such that 18% more power is required to match the speed of a non-biofouled ship (Schultz and Swain, 1999); (ii) reduce the power output of Hydroelectric Power Stations by as much as 17% and affect water distribution utilities (Andrewartha *et al.*, 2010); (iii) change the hydraulic roughness of rocks: Nikora *et al. (*1997, 1998) draw the conclusions that biofilms increase bed roughness whereas Biggs and Hickey (1994) and Graba *et al.* (2010) found that biofilms (micro colonies attached to rocks and bed material) induce a decrease in hydraulic roughness of the sediment substratum.

The evidence that epilithic biofilms (biofilms growing on the surface of rocks) affect flow and turbulence suggests that those might also produce physical modification on the erosion processes of small size sediments. Examination of the early seventies literature indicates that field samples, in the sizes of fine sand sediments and smaller, colonized by mats of filamentous green algae (cyanobacteria) were five time more resistant to erosion than bare zones of sediment (Scoffin, 1970; Neumann *et al.*, 1970). Since then, evidence that the phenomenon is widespread has grown (Grant and Gust, 1987; Black *et al.*, 2002; Lelieveld *et al.*, 2003). In particular in marine environments it appears that sediment samples that comprise mineral grains and a microbial biofilm often require shear stresses several orders of magnitude higher than those suggested by the models (e.g. Shields, 1936) to be entrained (Paterson, 1997; Black *et al.*, 2002; Righetti and Lucarelli, 2007). As scientists have delved deeper into the processes by which biofilms bind sediments, they have begun to recognize the complexity of the biological – physical interactions, which has been named "biostabilization" and defined as "a decrease in sediment erodibility caused directly or indirectly by biological action" (Parerson and Daborn, 1991) or "the process whereby microbial growth and production of extracellular polymeric substances (EPS) in conjunction with sediment colonization by other organisms such as fungi and algae result in the increased stabilization of bed sediment due to the sticking together of individual particles and floc" (Droppo *et al.*, 2001). The definitions presented above revealed an unexplored process of sediment erosion happening when the substratum is "carpeted" by bio-mats: those biotic grains behave differently from single particles but more like a fabric; hence it is not surprising that models of sediment transport based on equilibrium of forces acting on single grains (White, 1940) fail when biofilms prevail.

The general trend emerging from the studies presented above is that understanding and modelling sediment erosion can only be progressed once biological and chemical interactions are taken into account (Rice *et al.*, 2010a). However, our knowledge of sediment transport has relied for many years on models derived from experimentation on clean sediments. The need for gaining a better knowledge of the subject has led researchers, mainly from geosciences and engineering, to create networks unified by the name "Eco-hydraulics" (Rice *et al.*, 2010b), intended to embrace ecology and biology into hydraulics for a

better understanding of the science behind erosion. However, the scale at which eco-hydraulics has been confidently applied is generally much larger than the micro-organism level. The majority of experimental studies in eco-hydraulics are focussed upon the effect that grasses, bushes and trees have on flow (a search in the database *Web of Knowledge* for flow/vegetation/flume provides 224 papers on the subject on the 31/03/12); very few quantitative data from flumes are presented on the mutual effect of biofilms, flow and sediment stability (a search for flow/biofilm/flume presents 23 available publications and flow/biofilm/sediments/flume shows only 15 papers on the 31/03/12). Furthermore amongst this literature there is very little written on the behaviour of fine non-cohesive sediment when coated by biofilms, allowing them to behave as cohesive sediments. I believe this is one of the most challenging and less investigated areas of research at present, with the result that the only theoretical physical models for non-cohesive sediments coated by biofilm is presented for the first time in this thesis. Borsje *et al*. (2008) were first to introduce the modification of commercially available software, such Delft3D, accounting for the biological component in the erosion of cohesive sediments. However, Borsje *et al*. (2008) inclusion of biological factor in a model remains an empirical site specific study with very restricted applicability. Hence there is the need for a mechanical model that could be universally applied. In order to achieve this point there is still a long way to go since many are the discrepancy among different methodologies to investigate sediment transport (benthic flumes, CSM, visual techniques).The experimental project presented here embarks upon answering some of the unresolved questions presented above. In particular, it investigates the effect of biofilm colonization in time on the entrainment of small non-cohesive sediments (gravels and sands). This has been carried out by implementing a complete flume based approach, which spans from growth to testing of the colonized samples. The intention was to create as little as possible disruption in the samples we produced. However, as stated by Rice *et al*. (2010a), the simplification of flume studies can be at the cost of realism. In particular, flume studies tend to prioritize the requirement of matching Froude scales between the model and prototype, paying less attention to the modifications of the fluid characteristics (e.g. water temperature is often controlled to minimize viscous effects and achieve sensible turbulent condition). When ecology is included into flume studies, the environmental conditions could

affect greatly the growth of any organisms; however it is easier to control single variables and their effect on the organism under experiemtnal conditions, which is impossible to obtain in the field. Biofilms are, for the most part, very fragile and, although field samples have been used (Grant and Gust, 1987; Lelieveld *et al.*, 2003; Righetti and Lucarelli, 2007) in flume tests, it has been argued that this technique might cause irremediable physically and biologically disruption and consolidation of the samples (Tolhurst *et al.*, 2000; Maa *et al.*, 2007), leading to overestimation of the erosion strength. To obviate this problem *in-situ* instruments such as benthic flumes (Aberle *et al.*, 2003; Aberle *et al.*, 2004) have been exploited. Their limitation is on the maximum sediment size detectable; large aggregates and bedload cannot be measured by the turbidity sensors used in this flume's set-up, and the narrow nature of these flumes would induce erosion unrepresentative of the real condition once larger sediments are present. Furthermore, instruments such as the cohesive strength meter (CSM; Paterson, 1989), an erosion device based on the effect of a water jet impacting the sediment surface and recording a change in transmission, have limitations in the dimension of the area analyzed (28mm in diameter) and of the maximum sediment size that can be investigated (designed for mixed cohesive sediments smaller than 1.5mm). Moreover, the CSM fires a vertical jet of water onto the biotic sediments, which might induce earlier failure of the bed compared to the typical horizontal shear in unidirectional flows. Similarly, when alternative experiments have been conducted in the laboratory, they have often been undertaken at small scales where the hydraulics are unrepresentative of real river systems (Tolhurst *et al.*, 2008). Therefore, in order for "biostabilization" to be less of a qualitative and situation-bound effect, it is necessary to carry out experimental investigations at a scale comparable to the one of real river systems.

1.2 Research aims

This experimentally based project intends to measure specific variables pertaining to biostabilization and non cohesive sediments (e.g. flow, time and nutrients supply during biofilm growth period, sediments shape and size,

horizontal shear stress increase and bio-mats failure) and move towards a generic mathematical description of the process of biotic erosion. We will present and compare the results of flume experiments for which a single species cyanobacterium (*Phormidium sp*.) was cultured in boxes of different sizes over four different non-cohesive substratum (artificial and natural sediments, ranging from coarse sand to fine gravels according to the Wentworth scale (1922)).

The specific aims of this project are to: (i) induce a single species biofilm, common to marine and riverine environments, to colonize non-cohesive sediments in a laboratory environment at different scales, comparable to river ones; (ii) introduce a standardized criterion of motion for biotic sediment by applying sediment transport methods and evaluate their applicability (e.g. Yalin criterion ε (1972)); (iii) investigate the mechanical properties of the material biofilm only and the composite material biofilm/substratum, in order to account for the force inducing failure on the bio-mat; (iv) assess the modifications generated by different times of biofilm growth on the flow profile by using a non invasive particle image velocimetry (PIV) technique; and, (v) define a mathematical model which predicts biotic incipient motion by accounting for the elastic properties of the biofilm and the modifications on the hydraulic variables previously measured (e.g. hydraulic roughness and velocity field).

In detail:

- Chapter 2 will present: (i) a brief overview of the concept of sediment transport and the new issues that need to be addressed related to the increased stability of cohesive sediment due to biotic colonization (section 2.1); (ii) the available literature and most up-to-date engineering research in sediment transport, for cohesive and non-cohesive sediment (section 2.2); (iii) the introduction to emerging cross-disciplinary called “Eco-Hydraulics” and “Eco-Geomorphology”, which accounts for mutual effects among flow and biota (section 2.3); (iv) the findings of environmental scientists and biologists on the increased field stability of sediment (biostabilization) due to the presence of micro-organisms such as micro-algae, fungi, bacteria (section 2.4); (v) the evidence of research gaps in sediment transport when colonies of micro-organisms are present (section 2.5). As a conclusion (section 2.6), the evidence presented in this

chapter will form a solid argument for conducing laboratory experimentation on the stability of non-cohesive sediments coated by filamentous bacteria at larger length scales comparable to hydraulic structures and sediment patches found in real river systems (i.e. cm to m scale).

- Chapter 3 comprises the methodology chosen for the experimental studies and will show: (i) the rationale for choosing the sediment sizes used in this thesis (section 3.3); (ii) the set-up chosen for the flume used as incubation chamber (Yalin flume) plus the explanation on the bacterium selection (section 3.4) ; (iii) the set-up and instrumentation details of the flume used to test the Preliminary Experiments at the cm scale (Shields flume, section 3.5); (iv) the set-up and instrumentation of the fume used to test Series 1 experiments at the m scale (Ervine flume, section 3.6).

- Chapter 4 will present the first set of the flume experimental results: Preliminary Experiments (length scale 0.2m). Here 4 different non-cohesive sediments (glass spheres of D_{50} = 1.09mm and 2.00mm; sand of D_{50} = 1.20mm and gravel of D_{50} = 2.20mm) have been colonized up to 10 weeks in boxes 0.2m long by 0.2m wide by 20mm high and eroded under quasi-uniform flow steps. This chapter presents the experimental procedure followed (entrainment technique and image analysis, section 4.3) and erosion results (section 4.4). Incipient motion threshold for abiotic sediments will be used as a benchmark, focusing on the effect of sediments shape and size. For biotic sediments, results will articulate upon variables such as: (i) time length of biofilm colonization under unidirectional flow; (ii) sediment shape and size and their correlation to bio-mats strength; (iii) biological analysis in terms of biomass; (iv) scale of observation (small scale (SS, which is a 4% of the box area) versus large scale (LS, which is the whole box area).

- Chapter 5 includes the second set of flume experimental results: series 1 experiments (length scale 1m). Here the same 4 non-cohesive sediments as used in chapter 4 have been colonized up to 4 weeks in boxes 1m long by 0.3m wide by 20mm high and eroded under steady and uniform flow steps. Selected experimental procedures are in line with chapter 4, with

section 5.3 outlining additional methodologies introduced compared to chapter 4 (particle image velocimetry (PIV) set up, to obtain non-invasive measurements of the hydraulic flow field, and EPS analysis). The incipient motion threshold for clean and biotic sediments will be investigated again in terms of sediment shape, size and biomass with the addition of average flow characteristics (flow field, shear velocity and hydraulic roughness, sections 5.4).

- Chapter 6 investigates experimentally the mechanical properties using a *Tinius Olsen H1KS* tensile test machine of biofilm only or biofilm grown under constant unidirectional flow over sandy substratum. First, an overview on the elastic properties of biofilms at different scales will be offered in section 6.2. Section 6.3 will present the details of the instrumentation used, followed by the hypothesis (section 6.4) made on the basis of the previous flume testing. Results (section 6.5) will be shown for biofilm only samples and composite specimen biofilm/substratum, together with Young's modulus of elasticity (E). In the case of gravel size sediments (section 6.6), tensile tests have not been possible to conduct because bio-mats did not generate over those sizes. However an adhesive experiment with physical proofs will be shown as a proof of concept, showing biofilm "stickiness" also in gravel size sediments.

- Chapter 7 will discuss the results in relation to the initial aims and objectives presented herein; in particular attention will be given to the variable selected such as: (i) flow at growth; (ii) size and shape of the sediments; (iii) time of growth and biomass generated; (iv) change in roughness assessed through the hydraulic investigation (PIV) and (v) mechanical properties of the biofilm.

- Chapter 8 will report the conclusions (section 8.1) and the future refinements of the project presented (section 8.2). Evidence will be given of the effect that biofilm colonized from real river water can have on the stability of artificial non cohesive sediment (D_{50} = 0.85mm). This was a concluding, very simple experiment, carried out to show that laboratory conditions are representative of a real phenomenon, which needs much more investigation due to the many variables involved into the growth of

biofilm (e.g. seasonality, nutrients, flow, and species). Among the future recommendation we will present a theoretical mathematical model for biotic incipient motion, based on a modification of the Wiberg and Smith (1987) work and a new conceptual model based on the interaction of the biological membrane with sediment and flow. Finally a brief discussion on an ideal and hypothetical facility combining tensile testing in a flume will be given in section 8.3.

CHAPTER 2

Literature review

"We cannot command nature except by obeying her"

Sir Francis Bacon

2.1 Background

Sediment transport is a central issue for the disciplines of engineering, geoscience, chemistry and ecology. In engineering, it influences infrastructure stability and operational efficiency in a plethora of ways; scour and erosion undermines bridges, piers, embankments with implications for transportation, shoreline dynamics and navigation safety, whilst siltation reduces reservoir capacity, precludes hydroelectric operation, increases flood risk (see figure 2.1a, b, c). Similarly, in environmental science it controls the benthic community composition (Hall, 1994), dispersal of pollutants and dredge soil, harbour and beach maintenance, geochemical fluxes and animal-sediment relations (McCave, 1976). Thus, man has held awareness of the physical implications of this phenomenon and sought to cope with their impact for many centuries (e.g. irrigation channel in China, waterways in Mesopotamia and domestic water supply in the Roman Empire). Yet, Graf's (1984) review of the history of sediment transport clearly defines man's approach towards the discipline as an "art" until 200 years ago, when sediment transport became a branch of fluid mechanics and was more robustly underpinned by mathematical explanations and measurements.

Figure 2. 1. Sediment transport effects: a) Infrastructure damage; b) Bank erosion and c) Dam silting up (after Haynes, 2011).

A plethora of studies over the last Century have focussed on the fundamental physical mechanics of sediment entrainment, transport and deposition (e.g. Gilbert, 1914; Shields, 1936; Hjulström, 1935) to considerably improve sediment transport model predictions. Whilst researcher knowledge and capabilities in particle dynamics has become ever more advanced, in the last century engineers have focussed their attention on the problems of applied mechanics, without fully considering the associated environmental implications (chemistry, biology, geomorphology). This trend has changed in the past decade, with engineers investigating the interactions of flow and large vegetation in river channels (e.g. Finnigan, 2000; Wilson *et al.*, 2003; Nikora *et al.*, 2008).

Only recently have more studies have been presented by engineers on the processes that occur at the micro scale (e.g. nutrient exchange into the sediment surface and increased sediment stability in natural sediments; Li *et al.*, 2012; Righett and Lucarelli, 2010). More research at this scale has been carried out in the past decades by geoscientists and ecologists who have been motivated by understanding the environmental pollutants fate (Macklin *et al.*, 1997; Owen, 2007; Luoma and Rainbow, 2008; Gerbersdorf *et al.*, 2011). On entering a river system, contaminants are gradually adsorbed or bound onto sediments that are either suspended in the water column or on the bed (Droppo *et al.*, 2009); whilst these may be slowly assimilated by local biology, the pollutant-bound sediment is transported through the aquatic environment by cyclical erosion-deposition. The residence time and chemical nature of this pollutant within the system can cause a severe impact on water quality and habitat (Haag and Westrich, 2002). With the advent of nano-toxicology, sediment-related pollutant transport remains as topical an issue today as it has been over the last few decades of research into mine-waste, wastewater, and

agricultural pollutant transport. Implicit within this issue is that fine and/or cohesive sediments are generally the preferential carrier for pollutants (Owens, 2007); yet, the behaviour of cohesive sediments is still puzzling researchers as Lick *et al.* (2004) state that "very little is known".

The nature of cohesive sediments, with their large surface area to weight relationship, surface charge and/or organic content (Parker, 1997) is ideal for trapping pollutants. These characteristics in themselves change the entrainment and transport mechanics of sediment particles; rather than discrete particle entrainment they flocculate to stabilise as larger aggregates. Similarly, micro-organisms colonize any wetted surface (Lock, 1993), inducing an additional degree of cohesive strength. Yet, this modification of the sediment substratum by microbes appears to be the least well researched of all environmental-sediment interactions. In fact, Grabowski *et al.* (2011) suggests that at the moment researchers are unable to define or quantify the "propensity to erosion" of cohesive sediments due to the lack of appropriate instrumentation to investigate this property. What can be measured is the rate of erosion or mass eroded (E_r) using benthic flumes for example (Tolhurst *et al.*, 2000; Aberle *et al.*, 2003).

Moreover no mathematical modelling of this effect for non-cohesive sediments (more common in river systems) exists and a reason for this is that the data available are scarce, because expensive to collect (Borsje *et al.*, 2008) and often biased by the collection method (Tolhurst *et al.*, 2000). Yet the possibility that biology might affect the arrangement of sediment systems and mediate the response of the bed to physical forcing has recently started to be taken into account by scientists engaged in field work (Dade *et al.*, 1990; Madsen *et al.*, 1993; Yallop *et al.*, 1994). In particular, attention has focused on bacteria and their binding effect in intertidal and marine environments, characterized by fine cohesive sediments. Organisms inhabiting sediments may have three different influences on sediment erodibility (Paterson, 1997): neutral (no effect), negative (decreasing stability called bioturbation, expressed by reworking or packing of the sediment by organisms) or positive (increasing stability). The positive effect on sediment, due to the presence of micro-organisms, is known as *biogenic stabilization or biostabilization* and it has been defined by Paterson and Daborn (1991, pg. 111-119) as "a decrease in sediment erodibility caused directly or

indirectly by biological action" (see section 2.4 for in detail information). A large *in situ* dataset for the stability of cohesive sediments coated by micro-organisms has been collected over the years and correction for biological variables such as water content, chlorophyll *a* and bulk or dry density have been also introduce into erosion equations for this cohesive size fraction (Amos *et al.*, 1998; Tolhurst *et al.*, 1999). Even though it is well known by researchers that biofilms can colonize rock surfaces and modify the flow around the substratum (Nikora *et al.*, 1998; Graba *et al.*, 2010), practically no information are given on the erosion properties of non-cohesive sediments in the size of sand and fine gravel when coated by biofilm. Yet these sediment sizes are very common in river systems and their transport is important for river management and restoration.

This thesis will focus on trying to unfold, experimentally, the complex relationship between biofilms, sediments and biostabilization. Before embarking on this an in depth review of the processes inducing sediment transport and the core physics behind it is presented in section 2.2. Section 2.3 introduces the modern concept of eco-hydraulic and eco or bio-geomorphology. Section 2.4 presents evidence of the effect that the biota can have on sediment stability and the need of a unified field of research that involves different disciplines to generate the "best science" (Gerbersdorf *et al.*, 2011). Finally, the limitations in current knowledge that motivated this project are presented in section 2.5.

2.2 Physical modelling of sediment entrainment

In order to understand the relevance of biostabilization to sediment transport, it is first necessary to explain the fundamental physics. *Entrainment* represents the process by which a particle resting on a river bed is forced to move by the flowing fluid. This occurs when the forces induced on the sediment by the fluid overcome the frictional forces or the immersed weight of the grains; the threshold shear stress for initial motion τ_c (Buffington and Montgomery, 1997) is normally used as an index to the onset of entrainment. This might seem a very simple concept but in reality the initiation of motion is driven by a series of inter

correlated factors which are difficult to separate including *inter alia*: i) *sediment size*, which is usually classified using the Wentworth scale (1922) and uses sieve-based fractionation of a sediment sample; ii) *shape*, influencing the structure and the arrangement of river beds, the surface area exposed to the flow and the rollability (Powers, 1953) of a particle; iii) the *flow characteristic* (laminar vs. turbulent), bearing in mind that turbulent flow is more common within natural river flows, due to the relatively low fluid viscosity and high inertia; laminar flow is broken down by fluctuations in the water column. This is via flow structures of highly irregular shapes with a wide range of sizes, termed *eddies* (Middleton and Southard, 1984). Even though many physical studies have been carried out in order to determine the threshold of erosion (see for a review Buffington & Montgomery, 1997) of sediment from cohesive to non cohesive, uncertainties can still be found and these gets complicated even further once the system considered is a natural one and hence includes more inter –related variables.

Crucially to the present study is the distinction between **cohesive and non-cohesive abiotic sediment**, which according to the Wentworth scale (1922) lies at the silt-clay (0.062mm) transition. Particles smaller than this have cohesive properties (i.e. surface charge) and therefore flocculate to form larger particles of greater size and submerged weight (Parker, 1997); these characteristics serve to stabilise the floc. Conversely, particles larger than this do not exhibit cohesive effects and behave discretely. However, when micro-organisms coat sediments, they induce cohesion due to the adhesive properties of the biofilm. Hence, if fine non-cohesive particles are coated by biofilm, they might present a certain degree of cohesiveness that has never been accounted before in models of incipient motion based on the balance of force action on sediments (e.g. Wiberg and Smith, 1987).

Hence in the following section of this thesis an overview of the forces responsible for incipient motion of abiotic sediment will be presented (section 2.2.1) together with the most common and used techniques for the individuation of the entrainment threshold (section 2.2.2) and in section 2.2.3 the methodology used for defining cohesive sediments entrainment will be illustrated.

2.2.1 Forces involved in the incipient motion

Halow (1973) stated that the entrainment of sediment particles can occur in four different ways: i) rolling, ii) sliding, iii) lifting and iv) bouncing. The most important types of entrainment are generally considered rolling and lifting. Following Yang's (2003) theory, the external forces acting on a grain can be seen in figure 2.2. The forces are: i) F_D, drag force; ii) F_L, lifting force; iii) F_R, resistance force; iv) W_s submerged weight.

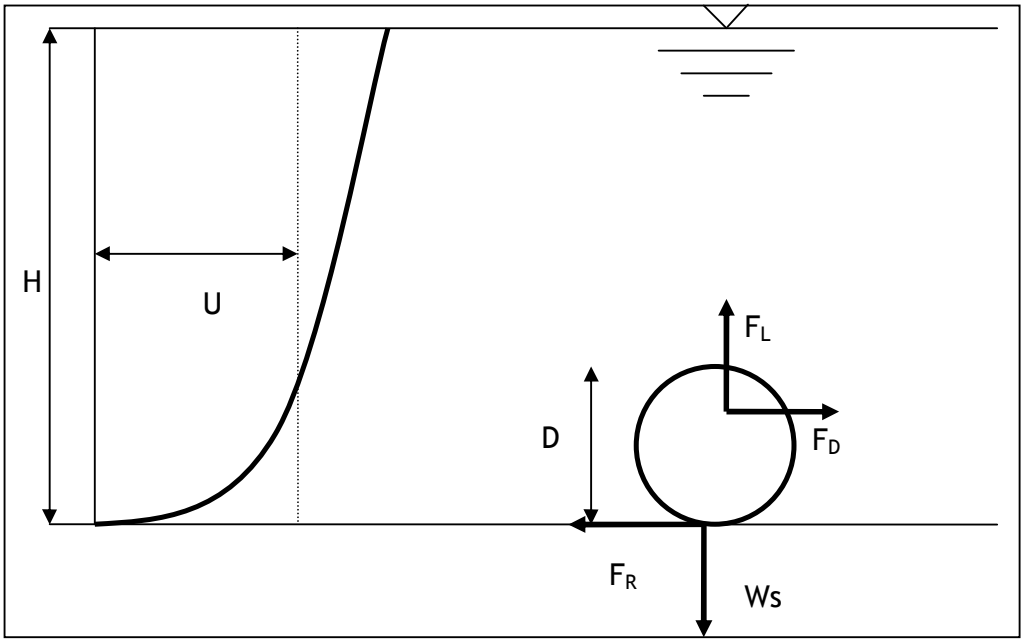

Figure 2. 2. Forces acting on a grain: F_D, drag force; F_L, lifting force; F_R, resistance force; W_s submerged weight. H is the flow depth and U is the average velocity (Modified after Yang, 2003).

For incipient motion, which is the state immediately prior to the onset of motion, one of the following statements is satisfied:

$$\begin{aligned} F_L &= W_s \\ F_D &= F_R \\ M_o &= M_R \end{aligned} \quad , \qquad \textbf{Equation 2. 1}$$

where, M_o is the overturning moment due to F_D or F_L and M_R is the resisting moment depending on W_S and F_R. Wu and Chou (2003) observed that the threshold of entrainment occurs when the stability of a particle is disturbed, due to the imbalance of the forces or force moments exerted on the particle in the flow (Ling, 1995).

Whilst the physics of this is correct, complexities arise. For example: firstly, it is difficult to simultaneously measure all these variables at a given instant due to the complexity of 3D turbulence; in fact, as suggested by Reynolds (1895), turbulence can be considered as random fluctuations around a time-average velocity value. Hence descriptors based on more general characteristics of flow velocity, grain properties and fluid properties would be preferable; secondly, the instant at which the forces balance cannot be directly observed, as no actual motion has taken place. Thus, researchers have developed a number of methodologies and models for defining and determining incipient motion. Use of one method over another remains controversial and up to the individual researcher to defend, therefore section 2.2.2 gives an in depth analysis of sediment entrainment approaches.

2.2.2 Sediment entrainment theory

In section 2.2.2.1 the four most common methodologies generally used to define the threshold condition for sediments will be illustrated. Section 2.2.2.2 will instead present the evidence that turbulent related structure can as well be responsible for particles initiation of motion. Finally, section 2.2.2.3 will illustrate the most common expressions used up to date to identify the entrainment processes of cohesive sediments, differentiating among biotic and abiotic.

2.2.2.1 Traditional methods for investigating incipient motion of sediment (from cohesive to non-cohesive)

Four of the most common methods used by sediment researchers for defining incipient motion and can be summarized as:

1. **the visual observation** (Gilbert, 1914; Kramer, 1935; Shields, 1936; Yalin and Karahan, 1979), page 17;

2. **the reference transport method,** which is based on the extrapolation of bedload transport rates to either a zero or a low reference value (Day, 1980; Parker and Klingeman, 1982), page 18;

3. **the largest grain method,** which depends on competence functions (Andrews, 1983; Komar, 1987), page 19;

4. **the probabilistic method** (Grass, 1970; Komar, 1996), page 19.

The first three methods fall into the class of deterministic approaches, whereas the last one is classified as stochastic. Each method will be presented in detail below.

Visual Observation: Kramer in 1935, by observing experimentally the motion of sediment, defined the threshold of motion as when:

> "several of the smallest particles are in motion, in isolated spots and in countable numbers"

Until the intensity of erosion reached a maximum and was classified by Kramer as:

> "grains up to and including the largest are in motion and movement is occurring in all parts of the bed at all times. It is sufficiently vigorous to change the bed configuration".

Shields (1936), in order to derive the famous curve relating shear stress and grains characteristics, adopted a similar method, defining the flow at threshold

to be when “small number of detachments” were experienced. However, both of those methods are largely subjective and cannot be widely applied. It is only in 1972 that Yalin standardized the way of visually assessing sediment transport by introducing an empirical relationship for the number of sediment grains that need to move from a specific observed area in a selected amount of time for sediment transport to be deemed to have occurred:

$$\varepsilon = \frac{n}{At}\left(\frac{\rho D^5}{(\rho_s - \rho)g}\right)^{\frac{1}{2}} \quad \textbf{Equation 2. 2}$$

where a lower limit of ε was defined as 1.0 x 10^{-6}, based on the number of mobile grains (n) observed over a given area (A) over a specified time (t). The recommendation in using this formula derives from the fact that in order to resolve the entrainment threshold, considered as a spatially and temporally random process due to turbulent fluctuations, it is required that the area of observation, *A*, should be ‘large’ in comparison to the grain area and the time, *t*, of the observation should be ‘large in comparison to the average time period of turbulent fluctuations’ (Yalin, 1972). This method has been successfully employed by many researchers (Paphitis and Collins, 2005; Haynes and Pender, 2007).

Before presenting the reminder of the methods, it is necessary to introduce the concept of absolute and relative sediment size. Considering that gravel and sand are both present in natural rivers, another way of looking at the bulk sediment characteristics is to consider the relative grain size distribution, defined as D/D_{50}. Sediment transport is directly dependent on sediment sizes and it is induced as a result of competition among absolute and relative grain size effects (Wilcock and Kenworthy, 2002). The absolute size effect generates a decrease in transport as the sediment size increases and finer sediments will be transported much more easily than coarse one. When different grain sizes are present, interaction between grains (for example in determining grain protrusion or hiding, or in the development of a coarse surface layer) leads to relative size effects tending to increase the transport rate of larger grains and to decrease that of smaller grains; this phenomenon depends on the composition of the

mixture, which can change during transport in response to variation in flow and sediment supply (Wilcock and Kenworthy, 2002). More details on the transport processes of sediment mixtures can be found below.

The reference transport method. This method is based on bedload, which is classified as the transport of sediments that takes place as rolling, sliding and sometimes jumping of sediments (Yang, 2003). Specifically, the reference transport method allows one to obtain values of dimensional shear stress based on a critical shear stress associated with either a zero or low reference bedload transport rate. This rate is extrapolated from paired shear stress and bed load transport measurements. Parker *et al*. (1982) used a reference transport criterion to provide a deterministic description of the first sediment motion, which is now widely used in most investigations of this type in both field and laboratory studies (Wilcock, 1993; Wilcock *et al.,* 1996; Shvidchenko *et al*., 2001; Ockelford and Haynes, 2011). One of the limitations of using this technique is that in condition of size selective entrainment a single reference based transport rate cannot be found, as presented by Komar (1987). Thus, it is clear that such an approach remains sensitive to the extrapolation technique used (Paintal, 1971; Wilcock, 1988).

Largest Grain Method: The third deterministic method is not very commonly used in present times. This method is based on the establishment of competence based functions that relate shear stress to the largest mobile grain size, from which the critical shear stress for a given size of interest can be determined (Andrews, 1983). Predicting incipient motion in this way assumes that the largest mobile grain size collected in a bed load trap is indicative of the initial motion conditions. Competence functions are sensitive to the size and efficiency of sediment trap, sample size, sampling strategy, and availability of coarse grain sizes (Wathen *et al*., 1995). It is also inappropriate for sediment that exhibits equal mobility, as the competence approach relies on selective transport (Wilcock, 1988). Hence this method was not suitable to test uniform size material as used in this thesis.

Probabilistic Method: The final method presented is the stochastic one: it is classified as such because it examines the role of turbulence on the threshold of initial motion. The approach is based on the concept that the bed shear stress

(τ_b) is an average estimation in time and it varies as a function of the turbulence intensity. Moreover the motion of a particle on a gravel bed depends on a series of factors: i) the location of a grain with respect to the particles of different sizes or bedforms; ii) the instantaneous turbulence acting on the particle; iii) the orientation of the grain. All of these conditions make the incipient motion process probabilistic (Yang, 2003). A possible way to account for the instantaneous nature of the shear stresses due to turbulent motion is using a probabilistic approach (Grass, 1970; Paintal, 1971), for which the shear stress can be defined as a random variable, characterized by a probability distribution; another random variable can be the susceptibility of grains to movement, due to size, protrusion, exposure, friction angle variability, imbrication (Komar, 1996; see figure 2.3).

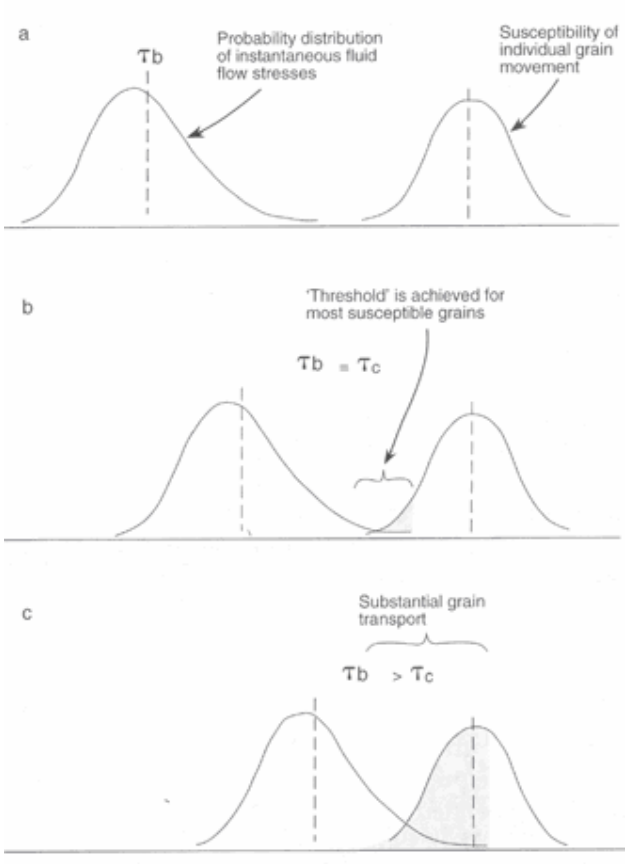

Figure 2. 3. Illustration of a probability distribution of instantaneous bed shear stresses (τb) and a probability distribution of the susceptibility of individual grains to movement dependent on the critical bed shear stress (τc). The threshold of initial motion is achieved when the two probability distributions overlap; the degree of overlap represents the amount of sediment movement. Modified after Komar (1996).

When the flow velocity increases, the probability distribution of instantaneous bed shear stress τ_b may overlap the susceptibility to grain motion τ_c (Grass, 1970; Komar, 1996). The threshold of motion for sediment particles is found when a significant overlap between the distributions takes place; the larger the overlap the more the quantity of sediment movement. No motion is observed where the curves do not overlap. This method uses a force balance in order to predict initial motion thresholds and is particularly sensitive to parameters such as protrusion, packing, and friction angle, which are hard to collect in the case of colonized sediments, where the thickness of the biofilm under water is not easily identifiable. Hence it was not chosen in this thesis.

As stated by Buffington and Montgomery (1997), none of these four methods is better than the other but some methods may be more appropriate for particular applications (Carson and Griffiths, 1987). For example bed load transport investigation is better assessed using the reference transport method because this method accounts only for the bedload component when defined.

Crucial to this thesis is the fact that visually based methods are more appropriate for conditions in which the spatial heterogeneity of the bed is relevant. They record the local incipient motion and are best applied to characterise the mobility of spatially distinct patches. Patchy biofilms often occur as a result of heterogeneous environmental conditions and thus the visual method proposed by Yalin (1972) was chosen as the preferred tool in this thesis.

In section 2.2.2.2 a brief overview of the effect that hydraulic roughness and turbulent structures can have on the incipient motion of sediment will be presented. This is a very recent field of study and it has seen its improvements since the late 90s due to the implementation of novel flow visualization techniques, such as particle image velocimentry (see chapter 3), which non invasively have allowed researchers to obtain large scale temporal flow information.

2.2.2.2 Incipient motion and turbulence: coherent structures

As seen from section 2.2.2.1, the turbulence affects the entrainment of sediment (see probability method above). Advances in laboratory techniques (e.g. flow visualization and particle image velocimetry - PIV (see chapter 3)), have allowed a greater understanding of turbulent flow and it has became evident that turbulence in boundary shear flows (so common for rivers) is not as random as it was once thought (Hardy *et al.*, 2009). Instead, quasi-random complex flow structure can now be decomposed into elementary organized structures with spatial and temporal coherence (Adrian, 2007).

Gravel beds usually experience shallow flow conditions, with the ratio between mean water depth and roughness height, called the relative roughness height, during floods in the region of 10-20. These flow conditions have been shown to influence significantly the generation, development and dissipation of *coherent flow structures* (Hardy *et al.*, 2009). Flow structures are considered by some researchers to be directly related to sediment transport (Shvidchenko and Pender, 2001; Hardy *et al.*, 2009). Best (1993) indicated that sediment transport happens in the turbulent boundary layer, and in particular is connected to the structures, instantaneous Reynolds stresses and lift forces F_L exerted in this zone.

Grass (1970) observed that entrainment is associated to peak Reynolds stresses, generated by a particular type of structure termed ***sweep*.** This can be defined as an inrush of higher than average downstream velocity fluid. Many researchers (e.g. Grass, 1971; Best 1992) have suggested that sweeps may contribute to a large portion of the Reynolds stress and they are also associated with the initiation of sediment motion. Conversely ***burst*s** are considered to be the breakdown of near bed flow during violent events; as such *bursting* is though to be one of the principal events associated to sediment transport (figure 2.4). In later models (e.g. Lu and Smith, 1991) bursting is associated with lifting and stretching of vortex loops form the surface, which are considered to be the fundamental structures in well-bounded shear flows.

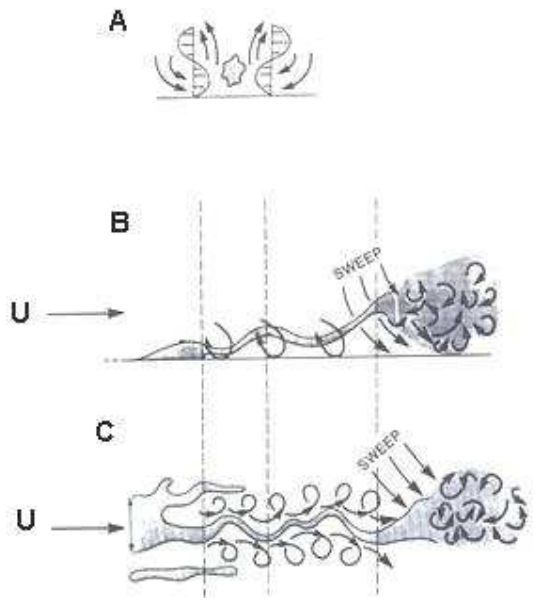

Figure 2. 4. Fluid bursting in wall-bounded shear flow. a) Downstream elevation; b) side elevation and c) plan view (modified after Williams, 1996).

However, even if the mechanics of those coherent structures is becoming better understood, the effect that smoothing of a gravel bed (usually induced by an increased amount of fine infiltration clogging the river bed pores) has on the turbulent structure generation is still poorly understood. The smoothing of the surface of the bed will: i) decrease the local grain friction; ii) reduce the loss of fluid momentum from the wake of the particle; iii) reduce the bed permeability. Furthermore, if a large grain is entrained in a smoothed bed then, it will move faster, following a process called "gravel overpassing" (Carling, 1990).

Hardy *et al*. (2009) found that the effective roughness is fundamental for coherent structures to generate. Their research showed that, if effective roughness increases, then the coherent structures become more visible through the water depth and tend to have an angle with the bed increasing from 45° to 60°. The direction given by this angle is considered to be the one in which sediment transport occurs. Moreover if the effective roughness increases, a reduction in stream wise flow velocity and turbulence, occurring in the upstream side of the coherent structure, becomes more evident.

The study presented in the next chapters considers the smoothing of non cohesive beds induced by the presence of biofilm. Even if turbulent studies have

been conducted on the modification of the flow characteristics induced by biofilm coating large rocks and some researcher found the smoothing to occur due to biogenic colonization (Graba *et al.*, 2010; see section 2.3.2), no study related the entrainment properties of colonized non-cohesive sediments to the hydraulic conditions (change in hydraulic roughness z_0). To obviate this limitation, in chapter 5 we will introduce a detailed investigation on the modified sediment surface roughness due to the growth of biofilms in time using PIV and the relative transport obtained.

The next section will present the famous curves used by engineers to estimate the entrainment threshold based on two different approaches: 1) the bed shear stress τ_b (Shields, 1936); 2) average flow velocity *U* (Hjulström, 1935).

2.2.2.3 The engineering curves

A body of water flowing over a surface will exert a force on that surface. In turbulent rivers this is called the **bed shear stress (τ_b),** which is dependent on the velocity gradient and on flow structures of highly irregular shapes termed *eddies* (Middleton and Southard, 1984). A very common way of defining the bed shear stress in uniform flow (UF) conditions is using the so called "depth-slope equation" (Yang 1973, equation 2.3), which is based on the geometry of the channel:

$$\tau_b = \rho_w g R_h S \quad \textbf{Equation 2. 3}$$

Where *S* is the bed slope and R_h is the hydraulic radius, ρ_w the water density and *g* is the gravity acceleration. Bed shear stress τ_b is often converted to the shear velocity (u^*), given by:

$$u^* = \sqrt{\frac{\tau_b}{\rho_w}} \quad \textbf{Equation 2. 4}$$

u^* can be derived using the "law of the wall" (Prandtl, 1925; von Karman, 1930; Wilcock, 1996) from the vertical time-average velocity profile, as follows:

$$\frac{U}{u^*} = \frac{1}{\kappa}\ln\left(\frac{z-d}{z_0}\right) \qquad \textbf{Equation 2. 5}$$

Where κ is the Von Karman constant (κ=0.4), z is the position in the water column; z_0 is the roughness length and d is the displacement height, which is where the velocity profile apparently goes to zero. Typically the velocity profile close to the bed is highly variable (Wilcock *et al.*, 1996). Hence spatially averaged velocity profiles (Smith and McLean, 1977) are often preferred because they give a more representative and accurate estimation of the average local bed shear stress and roughness length. The accuracy of the calculation of shear velocity u^* increases with the possibility of obtaining numerous velocity measurements in the near bed region (e.g. the bottom 20%). However Lawless and Robert (2001) stated that at greater distances above the bed surface velocity profiles and corresponding velocity gradients still reflect the roughness exerted by the bed, making a distance of 40% from the bed acceptable, as it has been done in this thesis.

However, in real river system the measurement of the near bed velocities is not always possible (Yang, 2003). Hence many researchers have found simpler to relate the averaged velocity in the dominant direction of flow, (U) to the entrainment of sediments.

The incipient motion is typically termed the "critical" or "threshold" of entrainment, defined mathematically by the sub-script "c" i.e. u^*_c or τ_c and this underpins incipient motion descriptions and comparisons. Whilst Buffington and Montgomery (1997) provide a detailed review of entrainment studies, salient and updated details of sediment entrainment theory are briefly considered in the following sections, to further elucidate upon both velocity U and shear stress τ_b approaches as relevant to the present thesis. Below the difference of the approaches using the averaged velocity U (Hjulström, 1935; Yang 2003) and the shear stress τ_b (Shields, 1936) to define the commonly used curve for incipient motion in engineering will be presented.

- **The velocity approach: the Hjulström curve and Yang's approach**

The easiest approach to determining when a particle will be entrained would be a simple relationship between grain size and the mean velocity of the overlying flow. An early study by Hjulström (1935), therefore, collected a detailed dataset of the movement of uniform material related to the average cross section velocity *U* in deep channels (>1m). His results are intuitive, with figure 2.5 indicating that for grain sizes greater than 0.1mm a positive linear relationship occurs with increased size (i.e. submerged weight) and applied velocity (i.e. shear force). For particles smaller than 0.1mm, as the particle size decreases, the velocity required to entrain the particle increases. The dashed line in figure 2.5 presents the values for the settling velocity that is directly proportional to the diameter of the sediments.

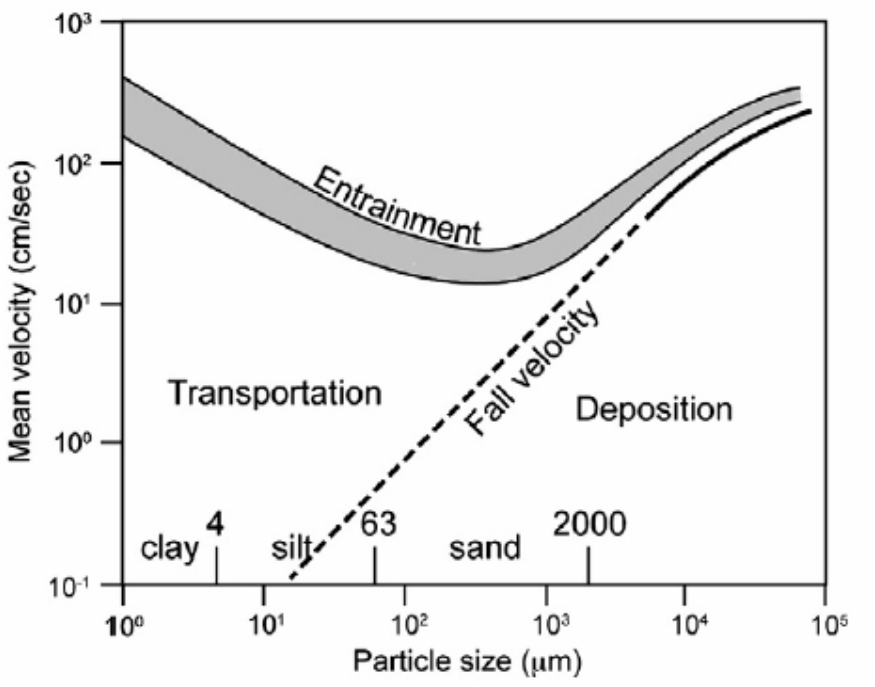

Figure 2. 5. Hjulström curve for erosion and deposition (1935). (After Graboski *et al*., 2011).

The importance of this curve is that it produces an initial and intuitive model to follow for the entrainment threshold of sediments only by using a depth average velocity *U*, which is more easily obtained than a near bed value. However this

curve was generated using flow depth of 1m. In laboratory conditions this equation is rarely used due to the low flow depth used. Moreover the curve was specific to a dataset in which fixed sediment density and water temperature were used, making it less applicable to the wider engineering issues. Also, as stated by Grabowski *et al*. (2011), data for sediment with diameter lower than 0.1mm could not be collected in the field but instead from flume experiments.

To overcome the shortcomings of Hjulström's research, a number of revisions were made. Of these, possibly the most notable was that of Yang (1973), who introduced a novel approach for the incipient motion of a spherical particle based on a dimensionless critical velocity (U_c/ω). Here, U_c is the critical average flow velocity and ω is the terminal fall velocity for a certain grain size (D), which is reached by a spherical particle when balance between drag force and submerged weight of the particle is reached. Thus, if the fall velocity of the particle in question is known, then Hjulström's issues of fluid and sediment density would be somewhat overcome. However, the whole theory is based on the fact that the fall velocity ω is known and reproducible for a specific sediment; in case of discrete particles this may be the case (hence equivalent methodology has been readily applied in entrain studies such as Wallbridge *et al.*, 1999), yet is less viable in situations where flocs develop of varying size and shape. This deficiency appears critical therefore when sediment-biofilm flocs vary considerably in dimension and weight due to interdependent variables such as time, nutrient, flow at growth. Hence more investigations are needed on how biofilms affect the settling velocity if equations such as Yang (1973) are to be applied. Also the hydraulic flow structure at the interface among bed and biofilm have indicated to be extremely important (Nikora *et al.*, 2002; Graba *et al.*, 2010) in unfolding the turbulence structure generating due to biofilm colonization; in section 2.2.2.2 it has been shown that this can be extremely relevant for the entrainment of sediments.

Thus, for biotic systems it appears that velocity approaches based on average-depth velocity or settling velocity are inappropriate and alternative approaches should be considered. Below the shear stress τ_b approach will be presented.

- **The shear stress approach and Shields curve**

Shields (1936) believed that it is impossible to analytically define the entrainment threshold of sediment particles; hence applying a non-dimensional analysis to his laboratory experiments using abiotic sediments, he was able to generate the well known diagram for incipient motion (see figure 2.6), which is still readily employed by researchers and practicing engineers today.

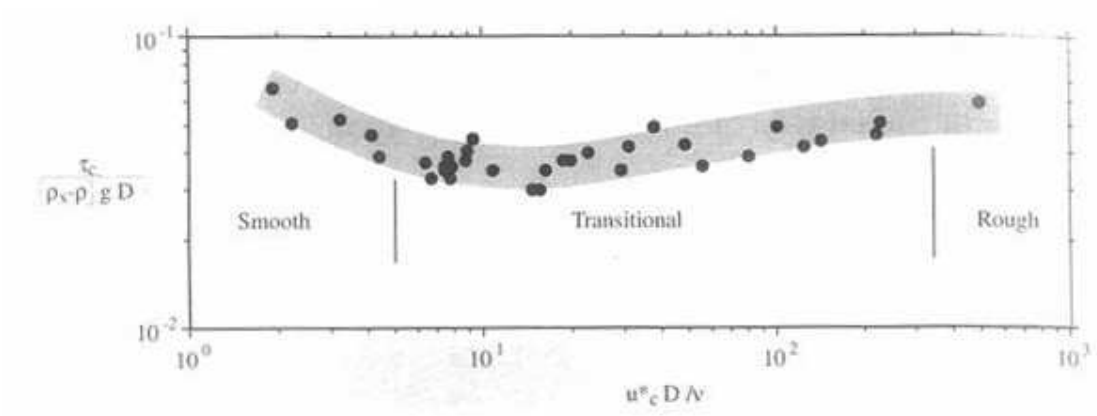

Figure 2. 6. Shield's diagram for incipient motion redrafted from Rouse (1939). Data laying below the curve are stable and not subjected to entrainment; data on the curve are at threshold and data above the curve are in full transport. Note that higher shear stress is needed for fine cohesive sediment (left of the curve) to be entrained.

The experiments carried out by Shields consisted in the identification of particles initial motion through visual observation of flume bed surface, following the 'weak-movement' criteria proposed by Kramer (1935). Specifically entrainment threshold was qualitative in that the definition applied was "...several of the smallest particles are in motion, in isolated spots, and in countable numbers"; yet quantitative in that a deterministic threshold was produced by Shields based upon five measurable variables i.e. the critical shear stress τ_c, the particle diameter D, the kinematic viscosity ν, the gravitation acceleration g and the difference in density between sediment and fluid (ρ_s- ρ_w). He defined the incipient grain motion using the dimensionless ratios:

$$D\frac{(\tau_c/\rho_w)^{1/2}}{\upsilon} = \frac{Du_c*}{\upsilon}$$

$$\theta = \frac{\tau_c}{D(\rho_s - \rho_w)g} = \frac{\tau_c}{D\gamma[(\rho_s/\rho_w)-1]}$$

Equation 2. 6

Where θ is the Shields' parameter, τ_c is the critical bed shear stress for initiation of sediment motion and u_c* the relative shear velocity, g is the acceleration due to gravity, D sediment grain size, corresponding to the median grain size of his hydraulically unworked sediment mixture ($D = D_{50}$). After obtaining equilibrium conditions, which Shields does not specify, he measured flow depth, water surface slope, bedload transport rate and bedform morphology (Buffington, 1999). He then used the depth-slope equation (section 2.2.2.3, equation 2.3) to obtain the bed shear stress; the critical shear velocity was then calculated keeping in mind the relationship for which:

$$\tau_c = \rho_w u_c^{*2}. \quad \textbf{Equation 2. 7}$$

Shields demonstrated that the dimensionless critical shear stress of the median size of unworked laboratory mixtures varies as a function of the critical particle Reynolds number $R_{ep,}$ defined as $u*_cD/\upsilon$. The particle Reynolds number expresses the nature of the flow around rough elements, classifying the flow as hydraulically rough or smooth. Hence this parameter expresses the inter-relationships between hydraulics, boundary roughness and sediment size with regard to particle entrainment. To summarise Fig. 2.6, if conditions lie above the curve then the sediments are mobile, whilst conditions lying below the curve would be stable, without sediment entrainment or transport. Whilst Shields himself employed non-cohesive grain sizes ranging from 0.36mm to 3.44mm (Shields, 1936) to indicate a positive relationship between particle size and the shear stress required to entrain it, his data set was extended to finer grains using supplementary data of Gilbert (1914), Kramer (1932), Casey (1935) and the U.S. Waterways Experiment Station (1935). This agreed with Hjulström's (1935) findings that very fine material required higher shear stresses to entrain due to cohesion and flocculation.

Whilst many limitations of the Shields curve have been discussed in well-cited reviews (see Buffington and Mongomery, 1999; Yang, 2003), possibly the most

relevant omissions pertinent to the present thesis include: drag force dominance; definition of entrainment threshold; and, abiotic sediments. Firstly, the lifting force F_L was completely neglected (Yang, 2003), such that Shields' assumption of only the drag force being responsible for erosion is quite limiting in case of coarse sand and gravel sediments that experience large flow through the bed. Secondly, Kramer's definition of entrainment threshold is qualitative and irreproducible. This has largely been overcome in more recent research by using quantitative approaches such as particle visual counts over defined area-time combinations (Yalin, 1972) or back-calculation from transported load data (e.g. reference transport approach of Parker, 1982); Buffington and Montgomery (1997) well illustrate the ongoing debate regarding quantitative descriptors and chapter 3 considers this in more detail regarding justification of the methodological approach taken in the present thesis. Thirdly, in the context of the present thesis, the restriction of data to abiotic sediments appears to be a deficiency of the "Shields diagram", with recent studies indicating its limited prediction precision when applied to field samples where biotic sediment is present (Black *et al.*, 2002; Lelieveld *et al.*, 2003; Righetti and Lucarelli, 2007). This therefore raises the question as to whether the Shields curve or indeed any abiotic-derived entrainment threshold models can be "corrected" for use in biotic situations affected by cohesion, adhesion and biological binding. The first step in ascertaining this is to review alternative descriptors specific to the effects of cohesion in abiotic sediments, i.e. clays.

As can be seen in figure 2.7, engineering curves have been also used by marine scientists: for example Manzenrieder (1983) showed that almost all the biotic fine sands colonized in the field and tested were entrained at values of the critical Shield's parameter θ much higher than for abiotic sediments.

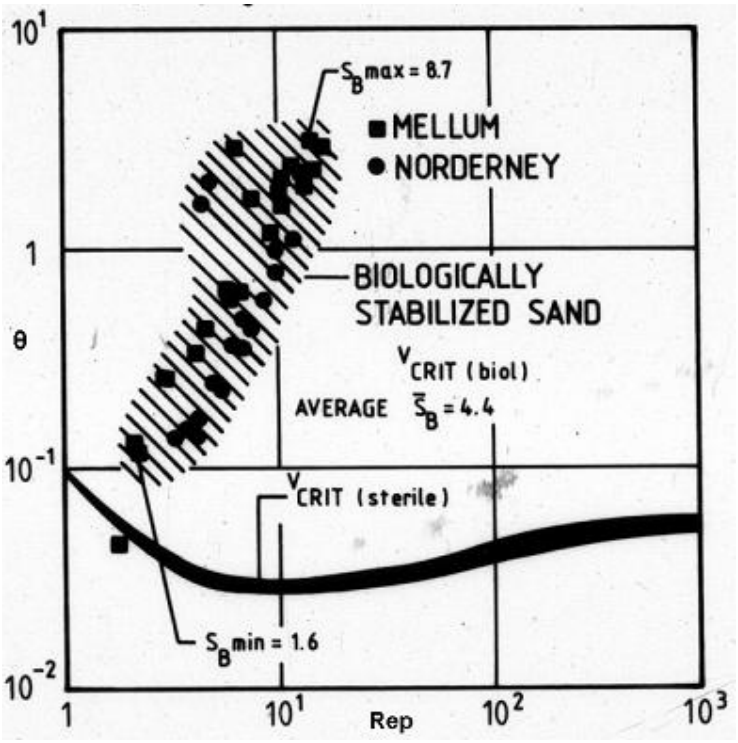

Figure 2. 7 Manzenrieder (1983) presented evidence that biotic sands (a part from an outlier in the bottom left corner) present higher stability than abiotic sediments of the same size measured by Shields (1936).

However more common in marine studies is classifying sediment erosion using a "reference transport approach": this approach is preferred because of the limitations in defining clear floc dimensions and density during tests and in natural conditions. In the next section a brief overview will be presented of the equations used to assess the entrainment of cohesive sediments in marine environments for abiotic and biotic sediments.

2.2.2.4 Erosion formula for fine sediments

Even though this thesis does not purport to investigate the erosion of cohesive sediments, colonized non-cohesive sediments could demonstrate some adhesive or cohesive properties due to the biogenic component and thus there are commonalities. The erodibility of cohesive sediments has been presented in the literature as related to a threshold for erosion or as an erosion rate (Sanford, 2008); herein I will refer in particular to the latest, which is the mass of

sediment eroded per unit time, occurring once the threshold is exceeded. For a detailed review on the behaviour of cohesive sediments see Yallop *et al*. (1994), Black *et al*. (2002), Tolhurst *et al*. (2009) and Grabowski *et al*. (2011).

Much of the biogeochemical cycling in rivers occurs in cohesive sediments (Grabowski *et al*., 2011), which also harbour and transport pollutants (Droppo *et al*., 2009). Hence it is important to be able to predict the transport of cohesive sediments. Cohesive sediments are generally transported in suspension (rather than the bedload mode of coarser sands and gravels of earlier section 2.2.2.1).

Field and laboratory investigations of cohesive beds have remained focused on the bottom shear stress τ_b as it is responsible for the initiation of motion. Pathaniades (1962) in a laboratory study using a straight recirculating channel, found that flow bottom shear stress τ_b was related to the erosion rate (E_r, in $kgm^{-2}s^{-1}$). From there E_r has been defined as constant in time or decreasing in time according to the structure of the bed (Black *et al*., 2002). Moreover, researchers indicate a degree of preference towards an erosion rate (E_r) defined as a function of scour depth (y); this yields a power law relationship between E_r and shear stress (Lick, 1982; Maa *et al*., 1998), such as:

$$Er = m[\tau_b - \tau_c(y)]^n \quad \textbf{Equation 2. 8}$$

Where m and n are empirical constants; τ_b the bed shear stress, τ_c is the critical bed shear stress for initiation of sediment motion and y the depth of erosion. Other researchers preferred an exponential form (Amos *et al*., 1992), expressed as:

$$Er = \varepsilon_f \exp(\alpha[\tau_b - \tau_c(y)]^\beta) \quad \textbf{Equation 2. 9}$$

Where ε_f is the empirical floc erosion rate and α and β are empirical constants. Equation 2.9 is used for defining Type I erosion, which is when τ_c increases with depth into the bed and limits the extent of the erosion. Whereas equation 2.8 is used to define the Type II erosion, in which erosion takes place with a single and constant value of τ_c that does not change with the depth into the sediments.

Sandford and Maa (2001) specify that the definition of τ_c used in the past published works to compute equations 2.8-2.9 is not so obvious: many researchers used the initiation of motion value (Young and Southard, 1978), whereas others employed a value for which "significant" erosion occurred (e.g. Maa *et al.,* 1998). Moreover very many different techniques have been involved to obtain datasets which makes it difficult to draw comparisons (Sandford and Maa, 2001). This shows how complicated the field of cohesive sediment transport is and how hard it is to define the "propensity to erosion" of the bed (Grabowski *et al*., 2011).

Even more complicated is the case in which sediments become coated by biofilms (Paterson, 1997; Black *et al*., 2002). Bacteria adhesion is related to the secretion of EPS (Allison, 2003), which sticks to grains changing their density and clogging their pores. Dade *et al*. (1996) suggested that 60% more shear stress was required to entrain microbially bound marine clays. Black *et al*. (2002) was the first of many researchers (Lelaiveld *et al*., 2003; Righetti and Lucarelli, 2007; Righetti and Lucarelli, 2008) to state the limitations of the Shields' curve when applied to sediments from the field with sizes larger than 0.020mm. However to date, even though a considerable number of studies have been carried out on the increased stability due to microbial adhesion (see for more details section 2.4), comparisons between the experimental results are often very difficult to draw due to the difference in instrumentation used from the field to the laboratory (Paterson, 1997; Tolhurst *et al*., 2000). The lack of a unified assessment technique comes also from the poor understanding of the variables influencing the transport of non-cohesive colonized sediments. Until the mechanical properties governing biofilm adhesion and cohesion are better understood, no modifications of existing mathematical models can be undertaken to account also for the biology. In this thesis I will attempt to improve this understanding: hence an in depth review of the mechanical characteristics of biofilm strength is given in chapter 6, together with a new approach to quantify for the increase adhesion that coated grains experience.

As seen above, engineers cannot separate their study from the presence of biota. Section 2.3.1 will introduce the concept of "eco-hydraulics", which has seen many engineers to be involved in research pertaining large scale vegetation and flow interaction. Section 2.3.2 will present the evidence that also smaller

scale organisms have in the past interested engineering research: in particular biofouling will be briefly presented. Finally, with the concept of eco or bio-geomorphology it will become clear that processes taking place in sediments and river cannot be separated from the biological life that herein takes place.

2.3 The emergence of eco-hydraulics and eco-geomorphology

Environmental engineers dealing with river management have found that a well designed project, based only on sediment transport equations, is no longer sufficient; sustainability of the natural system has become an integral part of good design. Thus many commentaries and review articles in journals interested in sedimentology and lotic systems (streams and rivers) published in the past decade have called for improved interdisciplinarity between fields such as hydraulics, geomorphology, ecology, and biology (e.g. Le Hir *et al.*, 2007; Rice *et al.*, 2010a; Rice *et al.*, 2010b; Nikora, 2010; Gerbersdorf *et al.*, 2011) to facilitate significant gains in our understanding of environmental systems. Thus, there is an emerging trend for traditional disciplines to add the prefix "eco-" to their denomination (e.g. eco-hydraulics, eco-geomorphology). A brief description of the two disciplines will be presented below: eco-hydraulics in section 2.3.1, which relates more to the interaction of flow and macro-scale vegetation, and eco-geomorphology in section 2.3.3. As part of eco-hydraulics I will introduce the effect of micro-organisms on surface/flow interaction, a concept known by engineers as biofouling (section 2.3.2). This will lead into the verification that micro-organisms can modify the hydraulic roughness of sediments and hence the flow characteristics and turbulence, affecting then the entrainment properties.

2.3.1 Eco-hydraulics

Eco-hydraulics is a branch of hydraulics which has seen its birth in 1996 through an IAHR forum, described as a "nascent field created by necessity" (Black *et al.*, 2002). The concept of Eco-hydraulics was born with the idea of generating a subject that would take into consideration the flow and macro-scale vegetation interaction (e.g. macrophytes and flow/sediment interaction in Kouwen and Unny, 1973). It has then developed more into the analysis of large-scale effects due to vegetation in the flow.

However, as will be crucially presented in this thesis, the concept of biostabilization (see section 2.4.4) and the mutual effect among micro-organisms and flow has a great importance for water related disciplines. For example, Battin *et al.* (2003) studied for many years the effects of river flow on the growth and establishment of microbial organisms such as bacteria, algae and fungi, which represent the first colonizers of river systems and are fundamental part of the nutrient web of those eco-systems. Many environmental scientists have gone further and looked at the interactions among those micro-organisms and fine sediments (Paterson, 1997; Droppo *et al.*, 2001; Gerbersdorf *et al.*, 2011), basing their studies on evidence that they have gained from the field. Yet, due to the journals targeted and nuance in language, none of those studies appear in geoscientist or hydraulics led review articles such Rice *et al* (2010a,b); this both underlines the separation among researchers in different disciplines and demonstrates the resulting incomplete knowledge of even the finest researchers working in complementary research (possibly with duplication of effort).

Only a few engineers have related the core of hydraulics to the study of sediment transport when other than physical forces are involved (e.g. Righetti and Lucarelli, 2007). The split between the subjects is unfortunate when the sharing of knowledge and expertise would be to mutual benefit of all. The problem is partly related to scientific language barriers. However, Nikora (2010) suggests that a common interest in the nomenclature does not solve the problems of finding unified goals, methods and terminology among different disciplines. A general agreement upon moving towards more synergistic research

activities at the life-science, morphology and hydraulics interface in river systems is being sought by geographers and engineers (e.g. Rice *et al.,* 2010a), but even to date, only 18 published papers citing eco-hydraulics have been published by *engineering* departments (Rice *et al.*, 2010b). It is significant that in 2002 Black *et al*. stated that very few engineering books included reference to biologic processes in sediment transport; yet 10 years later we are still facing the same issue.

An area of eco-hydraulics that engineers have started to investigate more and more in the past decade is related to the concept of biofouling of surfaces. Since this subject will be crucial in this thesis, the next section will present some of the results presented by researchers investigating the effect of micro-organisms on flow after colonization of either smooth surfaces or artificial rocks.

2.3.2 Micro-organisms and flow interaction

Engineers have in the past century spent time assessing the effect of biofiouling onto man made structures. For example colonies of micro-organisms are known to increase the frictional resistance of ships such that 18% more power is required to match the speed of a non-biofouled ship (Schultz and Swain, 1999). Hence a lot of research for more than 50 years has been concentrated on developing modern and efficient antifouling paints, in order to limit the economical loss (e.g. *Marine fouling and its prevention,* 1952). In particular it was found that a 68% increase in skin friction was generated with a slime biofilm growing on ship's hull, whereas 190% more skin friction was obtained in correspondence to filamentous green algae. Moreover fresh water diatoms have been considered as responsible for reducing the power output of hydroelectric power stations by as much as 17%, with a direct impact on water distribution utilities (Andrewartha *et al.*, 2010). In particular this study presented a gelatinous diatom generating a 50% increase in skin fiction and filamentous algae inducing an increase of 310% of the same parameter. Hence these studies present the evidence that biofilm growing on impermeable surface can cause a severe modification of the hydraulic roughness and hence of the flow induced around them.

However, biofilms colonize any surface and hence will be seen also in rocks and sediments in river systems. Not surprisingly engineers have identified this issue and have often used the easiest laboratory approach to try to control some of the variable affecting the biofilm growth, with the intent to study the relationships among flow structure and turbulence due to the presence of micro-organisms (Nikora *et al.*, 2002; Labiod *et al.*, 2007; Graba *et al.*, 2010). Salant (2011) presents a comprehensive review of the "handful of studies" carried out on the hydraulic modifications induced by biofilm colonizing sediments. Nikora *et al.* (2002), Labiod *et al.* (2007) and Salant (2011) found a general increase in turbulence intensity and shear velocity and Dodds and Biggs (2002) experienced, in general, velocity attenuations; these are all effects due to an increase in hydraulic roughness (similar to the finding for filamentous biofilm of Schultz and Swain (1999) and Andrewartha *et al.* (2010)), possibly due to the filamentous nature of the biofilm affecting the flow structure.

However in case of bio-mats, then the roughness decreases together with the turbulent flow shear (Godillot *et al.*, 2001) and dampening of the turbulence (Black *et al.*, 2002) was experienced. Moreover other researchers found that biofilm growth can decrease the roughness of the substratum (Biggs and Hickey, 1994) or even in case of filamentous streamers extending into the flow can smooth the gravel bed and induce acceleration of the average flow, especially at the interface with the biofilm (Graba *et al.*, 2010). Crucially it is evident that the subject is complicated and, as presented by Moulin *et al.* (2008), the relative hydraulic roughness is related to the growth characteristics of the biofilm (smooth mat or filamentous), which is proportional to the flow structure. Hence there are many variables coming into play and more studies are needed in order to integrate the few investigations published with variables related to the growth characteristics of the biofilm, which affect the resulting flow structure, as stated by Moulin *et al.* (2008).

From this section one concept comes across very clearly: this is that biofilm has the ability to alter the roughness of any surface it colonizes, whether permeable or impermeable, and hence to modify its structure and in case of sediments its geomorphology. Salant (2011) published in a geomorphological journal the evidence of the effect that micro-organisms can have on flow/bed interaction: in particular it has been highlighted that biofilm can modify infiltration and

deposition of sediment, by clogging pores and this can modify the entrainment properties of sediments. This is a process that fall into the events investigated by another new subject of study, called “eco or bio-geomorphology”, which will be briefly presented below.

2.3.3 Eco or bio-geomorphology

Ecology and geomorphology interactions in research date back to the 1800s (Wheaton *et al.*, 2011). However the terms eco or bio-geomorphology (which according to Hupp *et al.* (1995) are synonyms) were coined in the 1990s; they differed because bio-geomorphology has paid more attention on to how chemical and physical weathering are amplified and modulated with biological feedbacks; eco-geomorphology is more related to the study of erosion and deposition processes (Wheaton *et al.*, 2011). The concept is based on the mutual interaction of landscape and biota, which can be trees, animals or microbes.

Recently the study of the interaction between sediment and micro-organisms has been classified as part of Bio-Geomorphology (Borsje *et al.*, 2008). For biota it is intended both micro and macro organisms (e.g. benthic organisms, modifying the hydraulic and geomorphological characteristics of sediment beds; Borsje *et al.*, 2008). Research done by Noffke *et al.* (2001) presents the large effect that micro-organisms colonization can have in the development of strong sedimentary structures. Hence the research field is vibrant and has acquired much more interest by researchers in earth science, whereas engineers seems to have only grasped the tip of the iceberg so far (Righetti and Lucarelli, 2007; Moulin *et al.*, 2008).

Whilst the present thesis stems from an engineering focus, the research seeks specifically to better integrate the ecological, geoscience and hydraulic engineering knowledge. Thus, a detailed review of existing literature at this interface is provided in the next few sections, which focussed on the small body of evidence available specific to how biology affects both sediment and flow dynamics pertaining to the sediment entrainment process. The following sections provide an introduction to microbial ecology relevant to freshwater

substratum (section 2.4.1); a definition of the concept of "biofilm" will be given in section 2.4.2. Then reviews of the impact of EPS on and on the role in increased adhesion will be presented in section 2.4.3 and finally the available information on the biostabilization potential and its evidence will be given in section 2.4.4.

2.4 Biostabilization of sediments

Before presenting the concept of biostabilization (section 2.4.4) it is important to introduce what are the components that comprise a biofilm. Micro-organisms characteristics will be firstly introduced, followed by a brief chronological review of the concept of biofilms and its connection to the presence of EPS. This will lead to the introduction of the core of this thesis, which is the increased stability that sediments can show when coated by micro-organisms.

2.4.1 Micro-organisms and their characteristics

The word micro-organism is used to describe an organism not normally seen without the use of a microscope (Nicklin *et al.,* 1999). **Viruses, bacteria, fungi, protozoa and some algae** belong to this category, ranging in dimension from 0.01μm to several metres (table 2.1).

Micro-organisms	Approximate range of sizes
Viruses	0.01-0.25 μm
Bacteria	0.1-10 μm
Fungi	2 μm->1m
Protozoa	2-1000 μm
Algae	1 μm –several meters

Table 2. 1. Types of micro-organisms and their sizes (modified after Nicklin *et al.,* 1999).

Freshwater environments include all these micro-organisms; the different communities that develop in different environments depend, in a large part, on the physical and chemical variations taking place. Thus, an array of appropriate

terminology is employed by ecologists to describe the environment, organism and community. It is evident that diatoms and cyanobacteria, which are common in all aquatic systems (Callow, 1993), are the organisms that induced the most biostabilization (Paterson, 1997; Neuman, 1970; Grant and Gust 1986, 1987). Hence, the focus of the thesis will be on these organisms (chapter 3) and the following apply:

Lotic: flowing freshwater environments such as rivers and canals (Sigee, 2005).

Prokaryotes: organisms that do not have a distinct nuclear membrane, organelles associated with energy generation (e.g. mitochondria and chloroplasts) or complex internal membranes. All bacteria and archaea are prokaryotes, whilst all other microbial cells are eukaryotes (Nicklin *et al.,* 1999).

Phototrophs: Microbes which derive their energy from sunlight are called *phototrophs*. Alternative classifications include: *chemotrophs* (gain energy from chemical reactions), *autotrophs* (synthesise their organic compounds) or *heterotrophs* (depend on preformed organic compounds) (Ananthanarayan and Jayaram Paniker, 1996).

Aerobic: Aerobic bacteria require oxygen for growing. Alternatives include *microaerophilic* bacteria that grow better in the presence of a low oxygen tension and *anaerobic* bacteria which grow in absence of oxygen

Bacterial growth may depend also on the temperature and the temperature at which growth occurs best is known as “optimum temperature”. Bacteria which grow best at temperature of 25-43 °C are called *mesophilic* (e.g. *Pseudomonas aeruginosa*); *Thermophiles* are those bacteria that grow best at high temperature of 55-80 °C (Ananthanarayan and Jayaram Paniker, 1996).

Bacteria tend to group into colonies, which are called “biofilm”; a brief definition of the term is presented below in section 2.4.2.

2.4.2 Biofilm

The first use of the term "biofilm" was found in proceedings of the Dhalem Conference on microbial adhesion and aggregation in 1984 (Neu, 1994): "A biofilm is a collection of micro-organisms and their extracellular products bound to a solid (living or inanimate) surface (termed as substratum)" (Marshall, 1984).

The term biofilm was later extended and linked with the concept of adhesion, directly related to the presence of extracellular polymeric substances (EPS) (section 2.4.3): "A biofilm is a surface accumulation of micro-organisms, frequently characterized by large amounts of organic polymers of microbial origin that bind cells and other organic and inorganic materials together and to the substratum" (Characklis and Wilderer, 1989).

Many researchers have found that the EPS are effectively what induces the adhesion of biofilm.

2.4.3 EPS and adhesive properties

EPS is an abbreviation for extracellular polymeric substances. It is comprised mainly by polysaccharides (95%) with the remaining balance made by lipo (protein), which can vary depending on the type of EPS (Stal, 2003). EPS is a flexible, viscoelastic material (when hydrated) and comprised by organic aggregates. Looking to the individual cell, EPS can occur in two different forms: *capsular*, in which the EPS are strictly associated to the single cell surface and under a more loosely attached form. Biopolymers have been largely mentioned in literature for being involved in grain to grain adhesion induced by microbial exudates or mucus produced by macrofauna and meiofauna (Costerton *et al.*, 1978, 1987; Amos and Droppo, 1996). EPS also facilitates the spatial arrangement of any consequent attachment of a different species within a biofilm. Thus, essentially EPS can be considered to provide the 'skeleton' into which bacteria and their products are inserted (Allison *et al.*, 2003).

Paracelsus (1493-1541) was the first who discovered and identified EPS as connected to the stabilization of sediments. One of the most representative descriptions of the activity of the EPS was given by Characklis and Wilderer (1989) who stated that: "EPS – Organic polymers of microbial origin which in biofilm systems are frequently responsible for binding cells and other particulate materials (e.g. sand, pebble) together (cohesion) and to the substratum (adhesion)".

Numerous studies have shown the importance of EPS in modifying sediment hydraulic properties; this is intuitive, as any visco-elastic membrane will adsorb turbulent energy far more effectively than an inflexible surface such as sediment substratum (Jenkinson *et al.*, 1991). Dade *et al*. (1990) using a mix of experimental and in situ analysis of different sediment plugs (40mm in diameter and comprised of: a control sand; sand with added polymer from a bacteria and sand with a bacteria grown *in-situ*) found that the stability potential of fine quartz sand (ranging from 0.125 to 0.177mm) was increased due to the added exopolymer alone or EPS generated during in situ growth of the bacterium *Alteromonas atlantica*. In particular the latter allowed the highest stability which required double the critical shear velocity u_c^* to entrain the sediments. Tolhurst *et al*. (2001) obtained similar results employing isolated bacterial polymer (xanthan gum) on sand and mud.

From what presented above it is not surprising that biostabilization, a concept that was first introduced by Paterson and Daborn in 1991, is so strictly related to the presence of EPS (Gerbersdorf *et al*., 2008, 2009). In detail definition of this process will be given below.

2.4.4 Biofilm and biostabilization

Any wetted surface submerged in a river will be coated by micro-organisms over relatively short timescales (Lock, 1993). As early as 1868, the development of microbial coating of substratum was described in scientific papers by Huxley (1868) as "all-pervasive slime or mucilage" observed on the ocean bed. Yet, it took more than 100 years before terminology evolved specific to the content and

nature of this "slime", leading ultimately to use of two terms: "biofilm" (see section 2.4.2) and "bio-mat". With regard to the complementary term **"bio-mat"** its origin appears slightly earlier, from a benchmark study by Scoffin (1970) and Neumann *et al*. (1970) in the Bimini Lagoon, Bahamas. The term was used for colonies of organisms that can physically smooth and embed sediments in a "carpet" like form. They presented results for which subtidal environments showed laterally extensive coatings of filamentous green algae overlaying sediments; their similarity to green carpets or mats gave way to the "bio-mat" terminology still used today. Interestingly some researchers believe that if the biofilm is present as a complete sheet, it represents a protective barrier against erosion due to its isolation of the sediment from the flow (Droppo *et al*., 2001). However, after development of techniques such as laser scanning confocal microscopy (CLSM; Lawrence *et al.,* 1991), it was more evident that biofilms are a complex structure, comprised by channels, which extended to the surface. This further complicates the hydraulic pattern that could take place around those assemblages.

Crucially, these early studies of bio-mats showed they were five times more resistant to erosion than bare zones of sediment in the same sub-tidal environment. In light of these preliminary observations, Paterson (1994) for the first time defined the concept of "**biostabilization"** as the process for which sediments increase their stability due to the fixation by micro-organisms such as diatoms, cyanobacteria, fungi and others. Droppo *et al*. (2001) redefined this only slightly as "*the process whereby microbial growth and production of EPS, in conjunction with sediment colonization by other organisms such as fungi and algae, result in the increased stabilization of bed sediment due to the sticking together of individual particles and floc*". This was augmented in terms of the specific biotic influences on natural cohesive sediment being clarified and explained further by Black *et al*. (2002), in that: (i) *EPS secretion* by bacteria and microphytobenthos enhances cohesion, promotes flocculation and deposition; (ii) *network effects by* filamentous biota (e.g. cyanobacteria) ramify through the sediment matrix binding sediment particles together; (iii) *sediment armouring* by the organism coating over the sediment surface protects it from erosion; (iv) *boundary layer effects* smooth the sediment surface to reduces interface stress by decreasing bed roughness and near bed turbulence of the

fluid flow. This list of interactions clearly shows the need for well integrated sediment-flow-ecology data if biostabilization effects in different environments are to be quantified, contrasted and modelled; this therefore underpins the present thesis (chapters 3-8).

As early as 1997, Paterson presented a review of existing results found by different researchers on biostabilization of both cohesive and fine non-cohesive sediments; this was fundamental to the research discipline, as it concluded that there was a common trend of increased stability when biotic sediments are compared to control samples and, armed with this knowledge, there appeared grounds for working towards biotic corrections of traditional sediment models that had existed for nearly a century. However a comparison of the results is very difficult due to the difference in experimental and field methodology. Hence his summary table refers to a % increase not referred to a hydraulic vale (such as u^*_c or τ_c) because all of these results are somehow site dependant but instead to the increase over the control sediments. His summary table is reproduced in table 2.2 and additional data have been inserted with the most novel research in biostabilization.

Substratum	Date	Biota	Relative stabilization % increase over control
NON-CHESIVE			
Neumann et al.	1970	Algae/cyanobacteria	500
Manzenrieder	1983	Bacteria/Algae	300-700
Grant and Gust	1987	Purple sulphur bacteria Cyanobacteria	390 350
Dade at al.	1990	Bacteria	200
Madsen et al.	1993	Diatoms/bacteria	300
Yallop et al.	1994	Diatoms/cyanobacteria	>960
Vos et al.	1988	Microbial mat	100% (compared u^*_c)
Lelieveld et al. **CHOESIVE**	2003	Bivalves	10-46% (compared u^*_c)
Rhoads et al.	1978	Unidentified microbes	300
Parchure	1984	Unidentified microbes	200
Black	1992	Diatoms/bacteria	500
Yallop et al.	1994	Diatoms/bacteria	300
Lelieveld et al.	2003	Bivalves	133-210% (compared u^*_c)
Righetti and Lucarelli	2007	Benthic sediments and diatoms	52% (compared τ_c)

Table 2. 2. Selected measurements of the biogenic stabilization from literature (modified after Paterson, 1997). According to the table the highest stability for non-cohesive sediment is reached using a mix of diatoms and cyanobacteria.

From the analysis of the table above some clear points can be highlighted. First of all none of the studies to my knowledge seem to consider coarse sand or fine gravel in the investigation of the biostabilization effect on sediments. Those sizes are typical of river systems and hence subjected to micro-organisms colonization and completely ignored by researcher. However, as it has been seen in section 2.3.2 the effect that biofilm has onto sediments can modify the hydraulic roughness and hence the propensity towards entrainment. Secondly many researchers listed in table 2.2 used visual techniques to assess the threshold of incipient motion in an objective manner; Grant and Gust (1987) embraced the concept of "weak movement" (Kramer, 1935), whereas Lelieveld *et al*. (2003) considered two stages of initial motion (Mantz, 1977), for which the first u^*_c was defined as the initiation of grain rolling for stopping at a short distance and the second u^*_c was recorded when at least 20 grains were moving simultaneously. Both the methods led to differences in defining a commonly accepted threshold of motion. The necessity to unify the methods of entrainment identification in order to be able to objectively compare results for biotic sediments is then evident. Thirdly it seems that many scientists preferred the usage of the critical shear velocity as a comparisons for incipient motion (Grant and Gust, 1987; Dade *et al.*, 1990; Lelieveld *et al.*, 2003), whereas engineering studies such as Black *et al*. (2002) and Righetti and Lucarelli (2007) seem to prefer the critical shear stress, due to the direct application to the curves such as the Shields one. Again this evidence that there is still a different approach being used among different research field: this might be the reason why common research has not spread among the different disciplines (Black *et al.*, 2002).

In light of all of what presented above, section 2.5 presents some of the clear research gaps that this thesis wants to partially fill.

2.5 Discussion: the research gap for biotic sediment transport

The complexity of biostabilization has led researchers to collect results from the field, obtaining comparative indication of the biostabilizing effect but offering very little hydraulic insight. Some of examples of this process are: i) *in-situ* core collection and flume testing (Grant and Gust, 1987; Rigehtti and Lucarelli, 2008), with the complication of too many variables to control; ii) benthic flumes (Black and Paterson, 1997; Tolhurst *et al.*, 2000; Aberle *et al.*, 2003), which work well for fine sands and smaller fractions but cannot estimate the effect on non-cohesive sediments); iii) The Cohesive Strength Meter (CSM) (Paterson, 1989).

Benthic flumes have been employed for testing real natural and complex samples (e.g. Black and Paterson, 1997, Tolhurst *et al*. 2000, Aberle *et al.*, 2003). Those flumes are suitable to test cohesive sediments and very fine sand, which by being transported in suspension can be detected by turbidity probes. More issues arise when non cohesive sediments that get transported as bedload are present. Another complication is that benthic flumes are usually very narrow and this could influence the erosion process by inducing fast flows over the samples, especially if the sediment size is larger than fine sand. Hence these instruments would not be effective for testing biostabilization in riverine environments.

An alternative was proposes by researchers such as Righetti and Lucarelli (2007), who tested cores of cohesive sediments extracted from a lake in a flume. A similar approach was taken by Grant and Gust (1987) and by Lelieveld *et al* (2003). However, it cannot be forgotten that testing cores extracted from the field add a series of variable due to the complexity of the sample that cannot be controlled. Moreover many researchers have shown that sampling and laboratory testing of cohesive sediments can lead to overestimations of their erosion strength due to physically and biologically disruption and consolidation (Tolhurst *et al.*, 2000; Maa *et al.*, 2007).

Hence the Cohesive Strength Meter (CSM, Paterson, 1989; Tolhurst *et al.*, 1999; Vardy *et al.*, 2007) has been extensively used in the past decade in order to obviate to the problems presented above. This is a portable instrument which blasts a jet of water vertically into sediments and measures the ensuing turbidity. However the instrument starts to be limited as soon as the dimension of the sediments increases and could induce an erosion pattern not comparable to the one due to shear friction induced by unidirectional flow. As seen in section 2.2.2.2, coherent structure happen at 45° to 60° degrees to the bed; (Hardy *et al.*, 2009); incipient motion is believed to be related to these structures, which are longitudinal. The usage in the field of the CSM, which generates vertical ejections, might induce unrealistic erosion patterns because not directed as these turbulent structures. The results is that, even if the instrument is extremely important as a comparative tool for testing bed strength, it does not offer real hydraulic estimates of the shear stress at entrainment. A major improvement in assessing biostabilization strength would be to develop methodologies to test strength in the direction of predominant shear; thus, for a river bio-mat this would mean applying shear in the downstream direction over the surface of the mat and evaluate the strength of the biofilm in this direction. To overcome this problem I have introduced the usage of tensile testing (chapter 6) as the most appropriate method to investigate the strength and failure mechanisms of bio-mats under shear flow. My aim is to couple this finding with a calibration of the erosion threshold from flume studies, in order to obtain a clear model of erosion based not only on single particle pivoting, but also on the idea that particles can be fully coated and carpeted by biofilms.

Another approach to improve the quality of the data acquired was introduced by Dade *et al*. (1990) and Tolhurst (2008), who obviated the complexity of the in situ testing and coring extraction by culturing their sample in the laboratories, controlling the relevant environmental factors in order to avoid the transportation issue. The limitation of their studies lies in the sample scale and on the constrains generated by the edges of the containers (Petri dishes have been used). Therefore, if flow was applied to the bed, the shear stress could only be related to the surface of the sample, because no flow through the sample could be achieved. I believe that their approach of culturing and

controlling environmental conditions is the easiest to implement and the one that would generate the largest number of answers to the many questions available in the literature. This is why this thesis will focus on culturing biofilm over sizes of sediments that have been neglected in the literature so far (large non-cohesive sediments), controlling the environmental conditions during biofilm growth. The objective is to define a unified threshold of motion criterion based on visual assessment of the patchy nature of the substratum coated by biofilm. This will be done in chapter 4 and chapter 5 using the Yalin criterion (1972) in a subscale of the sample coupled with image analysis at the full scale of the experiment. Moreover using the law of the wall and PIV analysis, I will be able to increment the knowledge on the effect that biofilm has on the hydraulic roughness z_o at different flow conditions. This is the first attempt in literature to achieve such a comprehensive dataset.

Finally biostabilization relationship with biological variables is fairly well researched by scientists. Some of the most investigated variables are chlorophyll *a*, EPS and biomass. Positive correlations have been demonstrated for biomass and stability of very fine particles (Yallop *et al.*, 2000; Righetti and Lucarelli, 2010). It is also evident that the adhesive properties of EPS in biofilms and their environmental conditions during growth are particularly relevant to the final biostabilization potential (De Brouwer *et al.*, 2000; De Deckere *et al.*, 2001). Ideally researchers auspicated that biological factors such as biomass or EPS could be used as proxy values to correct entrainment threshold models for biotic interaction (Black *et al.*, 2002); however more and more evidence have been given that biomass development is affected by flow characteristics and will mutually alter the flow structure of the overlying fluid in a two-way interaction (Moulin *et al*, 2008). This clearly shows how complicated it is to generate a model that accounts for all the variables that might influence the biofilm growth. An attempt will be presented in chapter 8, where in the future refinement of this project I included a modification of a traditional model of sediment transport by adding in the equilibrium balance the force relative to the biofilm presence.

2.6 Chapter summary

In light of what presented above, the core theory of sediment transport (Shields, 1936; Hjulström, 1935), even if still widely used, presents large limitations in particular when related to cohesive sediments. A challenge is to obtain valid models predicting the entrainment of cohesive sediments (Grabowsky *et al.*, 2011) and almost no space in literature is given to the behaviour of non-cohesive sediments that become cohesive due to the coating of micro-organisms. However this chapter has presented the evidence that biofilm can modify sediment behaviour by different means. Biostabilization acts:

i) embedding fine sediment (small sand and finer) into bio-mats (up to the meter length), which has been seen to be eroded into a carpet like fashion (Grant *et al.,* 1986; Grant and Gust, 1987; Walker and Grant, 2009);

ii) increasing the mechanical strength of sediments due to the natural elasticity of the EPS and bio-mats, with the result that mechanical properties related to the elasticity of the material are needed in order to model effectively this phenomenon (see chapter 6 for a review);

iii) changing the hydraulic flow field over the sediments and creating a difference in the turbulence processes taking place, hence on the erosion processes (Nikora *et al.,* 2002; Graba *et al.*, 2010).

Various quantitative results and field experiments are available on the first point for cohesive and fine non-cohesive sediments, even though there isn't a common approach used widely in the research community to investigate biotic sediment entrainment. However no research up to date has been found on the investigation of the relevance of biostabilization for larger sediment sizes (coarse sand and fine gravels), which are most common in river systems.

Also very little in literature is available on the second two points presented. The available data are usually difficult to interpret, because they are dependent on too many different variables or situation bound.

Finally only a hand full of models are available (Rigetti and Lucarelli, 2007; Borsje *et al.*, 2008) that account for the biotic component in sediment transport; however these are difficult to apply widely to other environmental conditions because site specific. Also, in case of bio-mats carpeting the bed, it seems clear that traditional models of sediment transport (e.g. Wiberg and Smith, 1987, based on single particle pivoting on each other) are redundant and a new approach is largely needed, which account for the cohesion and adhesion introduced by the biofilm.

All of the limitations presented above were the starting point of this project which, by culturing in a laboratory biofilm at a scale comparable to that of real river systems, wants to investigate the effect that biostabilization can have on non-cohesive sediments. The methodology used for this thesis will be presented in chapter 3. Chapter 4 and chapter 5 will illustrate the results of the entrainment investigation at different scales (0.2m and 1m; chapter 4 and chapter 5 respectively). Chapter 6 will deal with the mechanical properties of biofilms and their elasticity by using tensile testing to obtain Young's moduli of elasticity (*E*) for different bio-mats. Finally chapter 7 and chapter 8 will present the discussion and the conclusions and future recommendations.

CHAPTER 3

Experimental instrumentation and set-up

"When you try to explain the behaviour of water, remember to demonstrate the experiment first and the case next"

The great experimentalist, Leonardo Da Vinci (1452-1519)

3.1 Introduction

In this chapter the experimental program used for culturing and testing the effect of micro-organisms colonization on non cohesive sediments will be presented. To my knowledge the experiments carried out in the flumes of the Civil Engineering Department of the University of Glasgow are novel, in that they specifically investigate the effect of biostabilization on non-cohesive sediments and have characteristic length scales representative to real river systems.

The experimental techniques herein underpin the quantitative results of biostabilization presented later in chapter 4 and chapter 5. Implicit to this are decisions regarding entrainment threshold definition, measurement accuracy and the environmental conditions under which the biofilm were colonized (i.e. **sediment size, scale, flow at growth, nutrient supply**). Section 3.2 will present a brief overview of the experimental studies with relative numbers of experiments carried out. Section 3.3 will introduce the choice of the material used for the experiments followed by the growth set up adopted in the "Yalin" flume (section 3.4): here a detailed rational for the selection of the bacterium and the environmental conditions during growth will be given. Section 3.5 will present the set up of the "Shields" flume, in which the preliminary experiment testing the colonizing length scale of 0.20m took place. In section 3.6 the set up for the core of the experimental study of this thesis can be found, carried out in the "Ervine" flume testing the colonizing length scale of 1m. Here the usage of

PIV will be introduced with a brief overview of the theory, data collection, processing and specific set up for this study.

3.2 Overview of experimental studies

The experimental laboratory programme was conducted using flumes in the School of Engineering, University of Glasgow, United Kingdom. Here a suite of standard Armfield flume facilities were available for hydraulic research, including the "Yalin" flume (0.6m wide x 5m long) and "Shields" flume (0.3m wide x 15m long) Two sets of experiments were run between August 2008 and March 2011; 5 months of this period (spring 2010) was spent constructing a purposely built environmental flume christened the "Ervine" flume (see section 3.6). Moreover, a dedicated 4 month period was required (summer 2010) to calibrate a bespoke PIV system (section 3.6.3.2).

The **first set of experiments** was designed to improve our limited understanding of the biostabilization potential on non-cohesive sediments: here four different non-cohesive sediments were cultured in boxes 0.20m by 0.20m by 20mm (which from now on will be termed box0.2) for up to 5 weeks and tested every week for erosion by applying steps of quasi-uniform flow. This colonization stage took place in the "Yalin" flume (see section 3.4). Subsequently, testing took place in the "Shields" flume (section 3.5), where a combination of visual assessment at two different scales (Small scale (SS) ~50mm by ~30mm and Large Scale (LS) 0.20m by 0.20m) allowed a comprehensive analysis of the erosion process in time. For the data yielded, the biofilm erosion results indicated sensitivity to flow fluctuations implicit to the flow control system of a traditional "Shields" flume set-up for low flows; thus leading to the bespoke construction of a new flume for the subsequent data set. This **second set of experiments** was performed in the new environmental flume, called the "Ervine" flume (section 3.6) and consisted of the main part of the project; this is because it was conducted at a scale directly comparable to the one of a real river system (1m, in box1). Moreover the growing and testing conditions were largely improved in this set of experiments (see light supply in section 3.4.4.3; flume pump and

control in section 3.6.2 and PIV for flow measurement in section 3.6.3.2). A detailed breakdown of all experiments undertaken is given in Appendix 3.A.

A total of 49 experiments were carried out; 29 preliminary experiments (section 3.5 and chapter 4) and 20 further runs undertaken in the second experimental programme (section 3.6 and chapter 5). A total time of growth of 140 weeks was undertaken (equivalent to 2 years and 7 months, considering a year comprised of 52.18 weeks and 4.3? weeks in a months), which for the majority of the experiments took place simultaneously (the incubation flume could host 4 box1 and 6 box0.2 at the time); this ensured that the effective growth, facility/instrumentation development and comprehensive data analysis could fit into the 3.5 year timeframe of this PhD project. Following the prescribed growth time, sample biostability was tested by incrementally increasing the flow in a series of quasi-uniform steps of 5 to 10 minutes duration. The analysis of the erosion and of biostabilization was carried out using **still images at the large scale (LS).** Here a colour-based thresholding process (*ImageJ,* Abramoff *et al.*, 2004) was employed for ~700 images. In addition, **video** recordings were used **for the small scale (SS)** to verify the effectiveness of the Yalin criterion (1972). For every flow step 2 minutes (usually the 1^{st} and the 5^{th} of every recording) were analyzed and the number of grains moving was counted (flocs were visually deconstructed to provide a discrete particle equivalent count as required by the criterion). In total, 880 minutes (~15 hours) of recorded data was analysed.

Whilst the present chapter discusses the general instrumentation required for each experiment, more detailed methodology is provided specific to the analysis undertaken in chapters 4 and chapter 5.

3.3 Sediment details

Four different uniform substrata were tested: (i) small glass spheres, SGS, with D_{50}=1.09mm; (ii) natural sand with D_{50}=1.20mm; (iii) large glass spheres, LGS, with D_{50}=2.00mm; and, (iv) natural gravel with D_{50}=2.20mm (see figure 3.1)

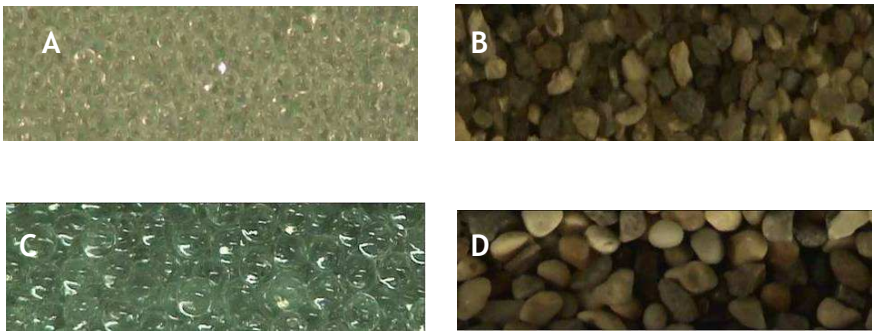

Figure 3. 1. Sediments used in the experiments. A) SGS with D_{50}=1.09mm; B) natural sand with D_{50}=1.20mm; C) LGS with D_{50}=2.00mm and D) natural gravel with D_{50}=2.20mm.

The characteristics of the sediments can be found in table 3.1. According to the Wentworth classification (1922), SGS and sand can be classified as "very coarse sand", whereas LGS and gravel fall in the classification of "very fine pebbles". Important to note is that every material chosen was classified as non-cohesive: this is the focal point of the project presented in this thesis. In fact to my knowledge this work is the first in the literature to present experimental results on the biostability of sediments in the range of such coarse particles.

	D_{50} (mm)	Density (kg/m^3)	Shape	Sphericity (Supplier)	Material	Supplier
SGS	1.09	2500	Spherical	92%	SiO_2	Potters Europe
LGS	2.00	2500	Spherical	87%	SiO_2	Jablonex
Sand	1.20	2650	Sub-angular/ Angular	****	****	Murchie sand (glacial deposit, Isle of Arran). Obtained from uniform material in size 1.00-1.41mm
Gravel	2.20	2650	Sub-rounded/ Rounded	****	****	Murchie gravel (glacial deposit, Isle of Arran). Obtained from uniform material in the range of 2.00-2.38mm.

Table 3. 1 Characteristics of the four sediments employed in the experiments: size (D_{50}, mm); density (kg/m^3); shape (Powers, 1953); Sphericity for beads, information given by the supplier; Material composition and Supplier.

The substrata were deliberately selected to enable comparison of the effect of both sand and gravel grain sizes on biostabilization potential. However, whilst these natural material is representative of field sediments, it is commonplace in hydraulic flume studies to undertake simplified experiments on spherical particles (SGS and LGS) at the outset of a new disciplines of entrainment-based research (e.g. Chepil, 1959; Cheng and Chiew, 1998; Wu and Chou, 2003). This is

considered beneficial as it removes “shape” effects, thus providing to easily calculate surface area and volume as appropriate for mathematical modelling purposes. Also, by using glass spheres the material chemistry is unreactive and uncontaminated, further simplifying complexities in the sediment environment. Thus, both natural grains and glass spheres are compared and contrasted throughout this thesis; results in chapter 4 defend the underpinning motivations described here.

Looking at figure 3.1 it is evident that the natural sand employed in the experiments could be classified as tending to sub-angular, whereas the natural gravel tended to sub-rounded following the Powers (1953) shape classification (figure 3.2). These shapes are common in river systems in the UK and, whilst the distinction is reflective of the different quarried sources of the materials, the shape classifications similar to each other (i.e. neighbours on Powers’ classification). The initial decision towards more angular sand was specific to evaluating differences in growth compared to the spheres. As equally angular gravel was difficult to source, the closest (i.e. sub-rounded) shape was elected; when using natural materials this is a reasonable approach and wild deviation of results would not be anticipated due to such small distinction in the shape classifications of the sand and gravel. Yet, review after the first set of experiments does indicate a possible shape effect on biostabilization (in that glass spheres may biostabilize most; chapters 4 - 6); however this effect cannot be specifically separated from material type (glass v. sediment). This is elaborated upon in later discussion of the data.

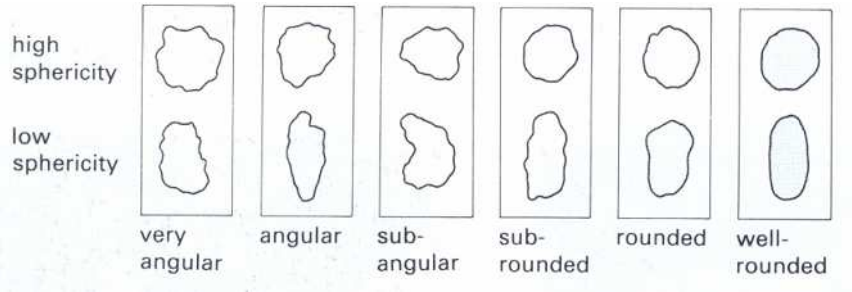

Figure 3. 2. Grain shape classification (after Powers, 1953).

The sediments were then placed into Perspex boxes, such that they could be transferred without disturbance between the colonisation Yalin flume to the

testing flumes of Shields or Ervine. Each box comprised perforated walls (0.8mm mesh size) to permit subsurface flow and nutrient exchange, as would naturally occur in the field; this was considered essential as subsurface forces acting on a surface-based biofilm may impact its growth and structure. Two different sets of boxes were fabricated: the *first* set used in the preliminary experiment were boxes with length scale equal to 0.2m (box0.2) in the x and y directions (i.e. downstream and cross-stream); the depth of the box (z) was equal to 20mm so 10-20 layers of sediment comprised the bed; this latter scaling is considered important in establishing realistic subsurface flow paths and permitting biofilm penetration during growth. The *second* set of experiment upscaled the test samples to approach length scales more comparable to those in a real river. Boxes were extended to 1m long (box1) and 300mm wide. To reduce flexion during box extraction from the flume, the box bases were strengthened and 2 bolts were screwed into the base of the box to allow temporary handles to be connected (see section 3.4).

3.4 Introduction to growth set up

The following section highlights the stages that were undertaken to select and culture the single specie bacterium as used to generate biostabilization of the non cohesive sediments. Detail description of the rationale for the selection of the bacterium, a description of the flume set-up for culturing the biofilms and the development the growth set up for the different scales tested will be given herein.

3.4.1 Bacterium details

A phototrophic cyanobacterium *Phormidium* sp (strain PP03) from the culture collection of V. R. Phoenix (Phoenix and Holmes, 2008) was chosen as the single species to colonize over the various substratums. Justification for using this species of bacteria is that it is common to freshwater biofilm (Callow, 1993) and cyanobacteria are known to stabilize sediments (in the range of cohesive and

fine non cohesive sediments) up to values of 960%, when compared to abiotic ones (Grant and Gust, 1987; Paterson, 1997; Yallop *et al.*, 1994).

An initial investigation of the bacterium growth structure was carried out using an Environmental Scanning Electron Microscope (ESEM, School of Geographical and Earth Sciences, University of Glasgow). Figure 3.3 shows the *Phormidium* biofilm grown over silica sand (D_{50}=0.3-0.5mm) for 5 weeks under agitated flow conditions (i.e. a bidirectional flow created via a rocking machine); a continuous light intensity generating a PAR (Photosintetic Active Radiation) values of 25 μmol m^{-2} s^{-1} as generated by LED strip lights placed in the incubation chamber; this was in agreement with the range of irradiance between 10-100 μmol m^{-2} s^{-1} found by Gerbersdorf *et al.* (2009) to allow diatom communities to grow and develop in a natural riverine environment. It needs to be noted that the 24 hours cycle was not ideal as it was not representative of natural conditions; this cycle was selected to generate a fast biofilm growth so that tests could be carried out in the ESEM. A more realistic approach is presented in Chapters 4 and 5, where a cycle of 12:12 light darkness was employed. It is evident from the image that the biofilm is filamentous, and its fabric like structure at maturity encompasses sediment particles of the substratum; these characteristics are considered to contribute to the mechanical strength of the biofilm as relevant to a study of biostabilization. Additionally, *Phormidium* is well-known to produce large amounts of Extracellular Polymeric Substances (EPS; Ramanan *et al.*, 2010) associated with enhanced biostabilization potential (De Brouwer *et al.*, 2000; De Deckere *et al.*, 2001; Gerbersdorf *et al.*, 2005; Gerbersdorf *et al.*, 2008). Whilst the ESEM images do not illustrate the EPS specifically, it would be logical to assume that the filaments are embedded within an EPS matrix, providing adhesion properties at the sediment surface. With both adhesive and mechanical properties evident, this bacterium was appropriate to culture the sediments.

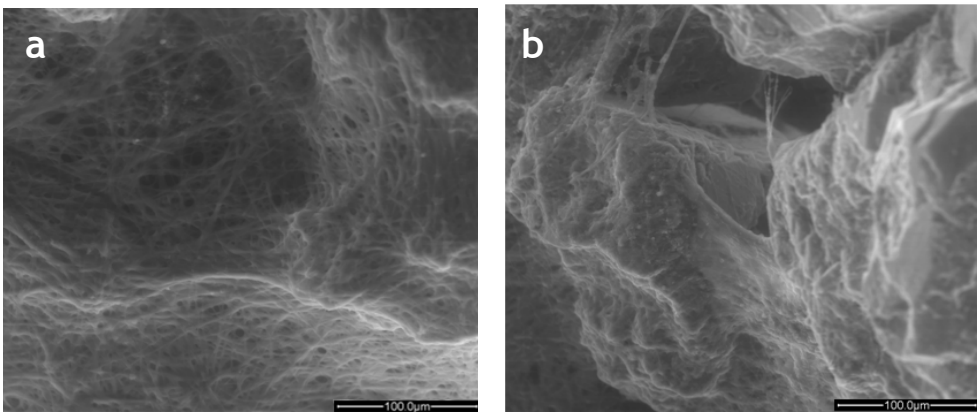

Figure 3. 3. ESEM images (scale 100µm) of *Phormidium sp* biofilm grown over a sand bed (D_{50} = 0.3-0.5mm) for 5 weeks under flowing water conditions. The filamentous, fabric-like structure (a) entwines particles from the bed surface into the bio-mat (b) during growth.

3.4.2 Yalin flume description and operation

The inoculation and growth was conducted in the "Yalin" flume, a fibreglass recirculating flume (5m long by 0.6m wide and 0.40m deep). Whilst this style of Armfield flume is developed for sediment scour observations (and hence includes a deep step in the bed), it was reconfigured to a planar bed and manually tilted to a physical slope of ~1/200. The flume used a *Calpeda*® pump, which generated flows up to 15l/s and controlled by a bespoke power inverter. This recirculated flow from the outlet tank (capacity 400l) back to the upstream header tank; it should be noted that sediment was not recirculated. The header tank was filled with marbles (D_{50}=16mm) resting onto a perforating plate; this combination would allow smoothing the turbulence generated by the pump and improves conditions of uniform flow over the test section. Flow depth and water slope within the channel was controlled via the tail gate (windlass control), used to regulate the quasi uniform flow conditions.

Importantly, flow was measured using an acoustic portable instrument, temporarily installed onto the recirculating pipe (*Portaflow SE)*. The instrument is comprised by two sensors directly in contact to the outside of the return pipe: a transmitter sends an acoustic pulse through the pipe and this is transported through the water and recorded by a receiver. The time between the emission and receiving phase allows measuring the speed of the flow. The flow information is obtained after setting parameters relative to the specific set up (such as the pipe material, thickness and lining). The velocity resolution

obtained is in the region of ± 0.1m/sec. Good signal strength and quality (i.e. R^2>75%) was obtained in all runs; this compared well to manufacturer recommended minimum values of 40%. In order to achieve this accuracy, some reconfiguration of the flume was required, in that the instrument placement needed an offset distance 10 pipe diameters away from the pump with location not on the suction side: this removed problems of air entrainment/bubbles on sensor accuracy. Detailed information on flow values can be found in section 3.4.4.1.

3.4.3 Instrumentation on the Yalin flume

3.4.3.1 Pointer gauge

A *Mitutoyo SD Series 572* pointer gauge measured the vertical distance of water surface and bed surface, as taken relative to an arbitrary datum. Used to establish water slope, bed slope and therefore uniform flow conditions, the instrument records to an accuracy of ± 0.01mm and measurements were taken at 0.3m intervals along the length of the flume. The uniform flow information was collected prior to start the inoculation and assumed to remain approximately valid during growth; this assumption is justifiable given that no sediment was transported during the colonisation period, thus any changes are reflective of biofilm development, which was designed to be the experimental variable.

3.4.3.2 Light set up

The flume was equipped with a light system to allow the phototrophic bacterium to grow. For the preliminary experiment the light set up was initially done with two rows of three 12V hot wire spot lights, which would provide an average light intensity or PAR (Photosintetically Active Radiation) of ~120 µmol m^{-2} s^{-1} over an area of 400cm^2, measured with a *Q203 Quantum Radiometer (Macam)*. A range of irradiance between 10-100 µmol m^{-2} s^{-1} has been shown to allow diatom

communities to grow and develop in natural riverine environment (Gerbersdorf *et al.*, 2009), hence choosing a value at the upper end of this spectrum was considered appropriate to encourage growth in laboratory conditions. The light system was organized so that the spot lights would be centered on the boxes and constant illumination (24/7) was provided.

Yet, issues regarding constant illumination, unequal areal diffusion of light and generated heat led to regions of "extreme-growth" (see figure 3.4), which generated biofilm trapped bubbles of oxygen. Those represented a clear weakness in the biofilm and could induce erosion of the biofilm because exposed to the flow, decreasing the biostabilization potential. The disadvantage of this particular set up was the large heat generated under the bulb, which resulted in an uneven growth (high PAR values in the centre of the sample170-230 µmol m^{-2} s^{-1} and low PAR at the extremities 16-45 µmol m^{-2} s^{-1}).

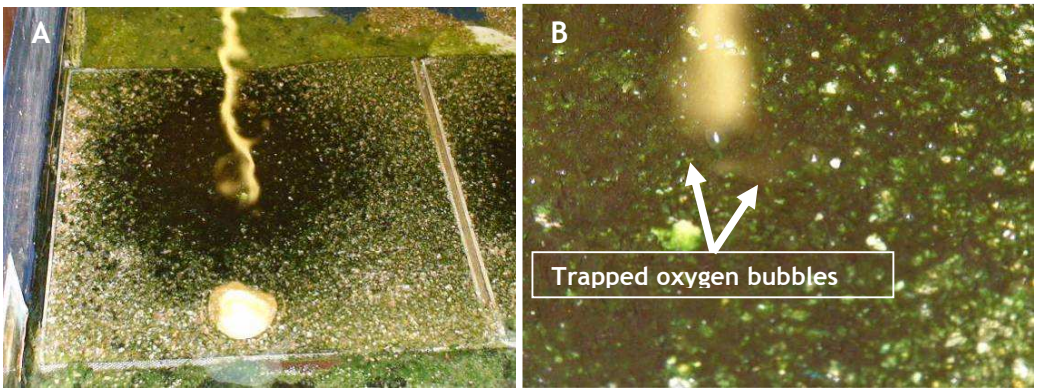

Figure 3. 4. A) Circular biofilm growth directly underneath the spot light after a week of growth; B) Oxygen bubble trapped by the biofilm. These bubbles are exposed to the flow and represent a weakness of the biofilm, which could be easily eroded.

Thus, throughout the course of the thesis the lighting was incrementally refined and improved towards:

- a light: dark cycle of 12:12 hours (this is used in all experiments except for SGS box0.2, chapter 4);
- reduced PAR to 26 µmol m^{-2} s^{-1} by use of LED (used in chapter 5);
- more evenly diffused lighting via LED strip systems (used in chapter 5).

Each of these improvements led to more uniform growth across the sample area and characteristics closer to those observed in the field as compared to Noffke *et al*. (2001).

3.4.4 Inoculation

The aim of this project was to investigate in the available time the effects that bacteria inoculation at the two different scales (0.2m and 1m) had on the stability of the 4 different materials (SGS, sand, LGS and gravel). Therefore no repetitions were carried out in this thesis due to time restrictions, prioritizing instead the analysis of biostabilization on a variety of not previously tested sediment substrata. Hence the analysis of the results in chapter 4 and chapter 5 needs to be interpreted in light of this experimental limitation.

3.4.4.1 Flow

In all experiments the flow at growth was kept constant and at sub-threshold conditions (i.e. no motion of sediments). In the first set of experiments (chapter 4) flow in the Yalin flume was 0.88l/s (i.e. shear velocity u^*=2.06cm/s, τ_b=0.42Pa). Measurements indicated that this was 35-50% that of the abiotic shear stress threshold for sand size sediment and 25-30% that of the abiotic entrainment threshold for gravel sediments. Given that the flows are sub-threshold, this slight difference in relative shear between materials would not be expected to significantly alter either the bed or biofilm growth; this assumption is further discussed in chapter 4. Thus, keeping the flow constant over all sediments permitted simultaneous colonization of multiple boxes and development of a much-needed comprehensive data set within the PhD timeframe.

Considering the second set of experiments (box1, chapter 5), it was understood from the growth characteristics of box0.2 that gravel sediment experienced an excessive biofilm growth under the spot lights. This would induce the biofilm to grow in a “spongy” manner, opposite to the bio-mat stage that has been shown to be extremely important for sediment stability (Grant and Gust, 1987; Walker

and Grant, 2009). Hence in chapter 5, in order to achieve the highest biostabilization potential, the two variables that could affect the growth (light (see section 3.4.3.2) and flow) were modified to improve the strength of the biofilm culture generated. Because of this, for box1 higher flow at growth was implemented for gravel size sediments (LGS and gravel), so that the shear stress τ_b during growth would match that of sand size sediments (35-50% of the critical (τ_c)). This was achieved using a flow equal to 2.22l/s which generated a shear velocity u^*=2.53cm/s and τ_b=0.64Pa.

3.4.4.2 Temperature

In order to culture bacteria into the flume, the header tank was equipped with a 3KW Resistance (controlled by a thermostat with a solid state relay for safety reasons on the header tank), which provided a water temperature of 28 ± 0.5 ºC throughout the experiments. This temperature was chosen to maximise biofilm growth rate (after personal communication with Dr Phoenix, who collected and cultured the bacterium and found this condition to be the one generating the fastest biofilm growth). Using this temperature reduces the realism of the project since natural rivers in Scotland experience an average temperature of about ~10ºC over the calendar year (Natural Heritage Trends of Scotland, 2006); however this choice was made so that more tests could be analyzed on samples presenting similar growth structure to that of biofilm in the field. Important to note is that water temperature used to test the entrainment conditions was of about 22.5 ºC and a discussion on temperature variations and its effect on transport can be found in section 3.5.To compensate for the evaporation taking place, a ball cock valve was installed into the header tank and set at the working water level of the flume during growth. Once this level decreased, the valve would allow flow from the main water supply to refill the tank via a trickle of water. This gentle intake of water allowed stability of the water temperature which varied of no more than +/-1 ºC during the course of any experiment.

3.4.4.3 Nutrients

Full strength BG11 (with $NaNO_3$) nutrient (Ripkka *et al.*, 1979; See Appendix 3.B for details) was added to the outer tank, where they were dissolved and circulated through the system overnight. 200ml of this bacteria and nutrient solution (absorbance of 0.375 at a wave length of 720µm) was then added into the flume end tank and left to recirculate again overnight. The boxes were then inserted and the experiment commenced. The pH and the dissolved oxygen (DO) were measured 10 days after inoculation; values obtained were pH=8.07 and the DO=8.06 and are comparable to river systems (South Yakima Conservation District, 2008). The inoculation was carried out only once at the start of the experiment, and no subsequent top-up of nutrients or bacteria was employed.

3.4.4.4 Development of the growth set up

For the preliminary experiments a grid of box0.2 were arranged into 2 rows of 3 boxes (See figure 3.5). Upstream and downstream of the boxes the bed was "fixed" by gluing a layer of SGS onto marine plywood; this was essential for two reasons: (i) to permit unhindered and equivalent turbulent structures along the length of the flume by way of "uniform" hydraulic roughness along the length of the test bed; (ii) ensuring that boxes could be extracted easily from the flume.

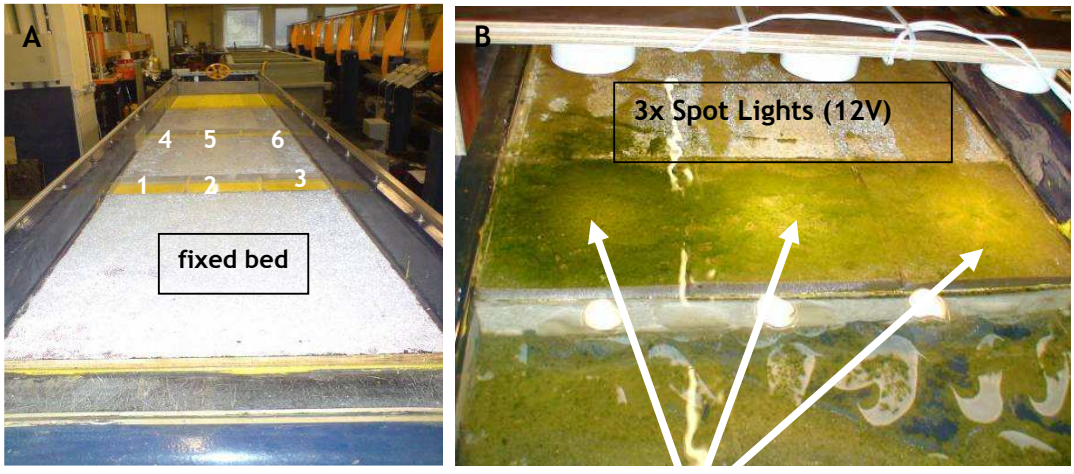

Figure 3. 5. A) Yalin flume set up with the 2 rows of 3 box0.2 (see numbers for location of the box) and plywood coated with glued SGS; B) particular of one of the row with the spot lights on top during growth.

After carefully investigating the growth pattern for SGS, it was noted that the centre box had growth stages different from the boxes attached to the walls (see figure 3.6). Specifically, the centre box was subjected to higher flow velocities (and therefore shear) as no wall-induced resistance had to be overcome in this locality; this meant that growth was far faster and subject to greater shear and failure during colonization. Hence for the remainder of the experiments (i.e. with the exception of SGS, chapter 4), only the boxes exhibit similar growth patterns near the walls were tested for entrainment threshold. The central boxes were used instead to collect samples for biomass analysis and tensile testing (See chapter 4, chapter 5 and chapter 6). Whilst this set-up was employed for box0.2 runs (chapter 4), it was refined in the second set of experiments (chapter 5) using box1; here only two rows of boxes (both subject to equivalent wall-effects) were used in the Yalin flume (figure 3.7). This was considered appropriate to best practice within the time constraints of the study.

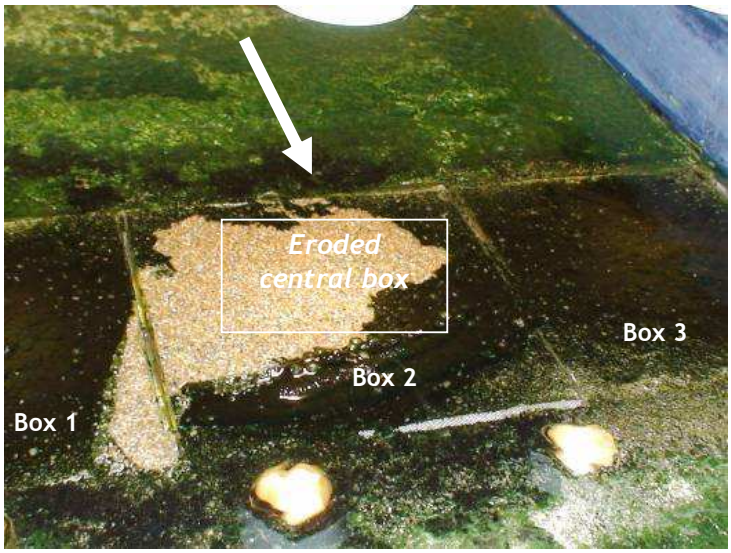

Figure 3. 6. Growth characteristics of the central box of the rows. As it is visible from the image, due to the different flow patterns in the centre of the box (see arrow) not subjected to wall effects, the growth was different from the other boxes. Hence the decision of testing only the boxes directly in contact with the walls (e.g. box 1 and box 3).

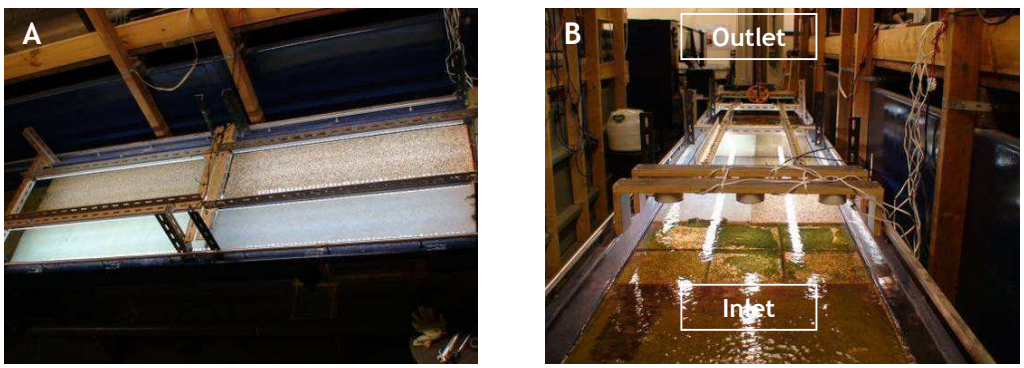

Figure 3. 7. A) Growth set up in the Yalin flume for the last set of experiments. LED strip lights were placed directly above the centre of the 1m long boxes; B) Final Yalin arrangement for growth of the 1m long boxes; the spot lights were used to grow sample to be tensile tested.

3.4.4.5 Extraction of the boxes and cores for biological analysis

Once the selected growth stage was reached, boxes were carefully extracted from the Yalin flume and moved across to either the "Shields" flume (see section 3.5) or to the "Ervine" flume (see section 3.6) for individual testing of entrainment threshold using tightly-controlled hydraulic conditions. The extraction was not very trivial in case of box0.2. The flume was stopped for a short amount of time so that the extraction could take place with still water; the tailgate was then lowered down to allow some of the overhead to be displaced into the outlet tank. At this point the box could carefully be extracted from the flume by holding the outer edges comprised by the 0.8mm mesh. After, the box was promptly placed into the Shields flume, where a gap in the bed material was created before starting the experiment.

In case of the box1 the extraction was more complex. The boxes were made of a very stiff material which would ensure that the bottom of the box would not bend under the weight of the wet sediments. In order to extract a box from the Yalin flume, a set of removable handles (metal plates) could be hooked to the extreme ends of each box, where 2 screws were inserted in each side during the design. Lifting the box was performed by two people, after the flume was stopped and drained as described for box0.2. Once the extraction was achieved the box was placed towards the end of the Ervine flume, 1.5m from the outlet. Here, after the box was carefully inserted, the remainder of the bed was inserted around the box. In all the cases no evident movement of the sediments/biofilm composite could be seen.

Biomass quantification using the loss on ignition technique (HIMOM, 2005) was carried out for both box0.2 and box1 experiments. In chapter 5 EPS assessment was also performed (for details of the technique, see section 5.3.5). Both samples for biomass and EPS analysis were collected before the beginning of every experiment by extracting at the end of each week of growth two sediment

cores of the entire depth of the bed (diameter 26mm) for every material. Only two cores per sample were collected, in order to limit the disruption to the remaining substrata. The whole process from the extraction to the starting of the erosion test did not take longer than 30 minutes. The location of the cores was firstly chosen as the downstream end of both box0.2 and box1, replacing the missing material with coarse gravel (D=4-6mm). In case of box1 the samples were taken from a region outside the testing area and hence this process did not affect the final result; however, after coring the downstream end of box0.2 for SGS, a disruption (~10%) of the testing sample was evident, affecting the quality of the results. Hence, since as seen in section3.4.4.4 the central box0.2 in the Yalin flume were not used, samples were collected from a region of these central boxes that had a visually similar coverage compared to the test boxes. This process is not ideal and in future experiments more cores should be collected from the tested sample, in order also to investigate the patchiness of the biofilm growth.

In the next two sections more in depth description of the flume used for testing the boxes will be given. In particular section 3.5 will illustrate the characteristics of the "Shields" flume used for the length scale of 0.20m whereas section 3.6 would present the "Ervine" flume used for testing the 1m long boxes.

3.5 Introduction to flume preliminary experiments (0.2m scale)

3.5.1 Shields flume description and operation

The preliminary set of experiments was conducted in the "Shields" flume, an *Armfield* recirculating and tilting channel (15m long by 0.3m wide by 0.45m deep). The flume was equipped with glass side-walls, a smooth steel floor and had a rectangular cross section. The slope was adjusted using a flying wheel at the upstream end, which by pivoting on a point in the centre of the channel length, allowed to obtain slopes ranging from 0.005 to 0.035.

The flume allowed recirculation via a *Calpeda* pump, which permitted flows up to 30l/s to be obtained from reservoirs tanks containing ~2000 litres of water at an average temperature of 22.5ºC. This temperature is induced by the overheating of the pump and it is much higher than the average in natural river systems (see Section 3.4.4.2); the consequence is that for small values of R_{ep} (R_{ep}<5) an increase in temperature corresponds to an increase in sediment transport, whereas for intermediate values of R_{ep} (5< R_{ep} < 50) an increase in temperature decreases the transport (Taylor and Vanoni, 1971). The effect of temperature is not surprising since the kiematic viscosity ν varies from $1.52*10^{-6}$ m^2/s at 5°C to $0.95*10^{-6}$ m^2/s at 22.5°C, which is ~40% difference when compared to natural conditions. Recirculation, flow control and measurement, header tank configuration and tail gate operation was identical to that already outlined in section 3.4 for the Yalin flume. The specific set up of the sediment arrangement is presented in figure 3.8. The pre-colonized testing box (box0.2) was placed 3.5m downstream the inlet; with a turbulent boundary layer inducement length of 2.13m (Monin and Yaglom, 1971) this set up is justifiable. Upstream of this location was a 1m fixed bed of plywood board with SGS glued on it (see Sec. 3.4.4.4 for full justification); as this fixed bed section ensured that no "foreign" sediment entered the test section, other reaches of the flume comprised coarse immobile sediment (D=13-18mm) to maintain roughness and turbulence structure (this was both, simpler to execute than a stable bed over the full flume length and, better accommodated slight dimensional differences in the tested boxes). Both the fixed and coarser surrounding gravels (immobile) were set with their surfaces parallel to the bed slope and 40mm above the flume bed.

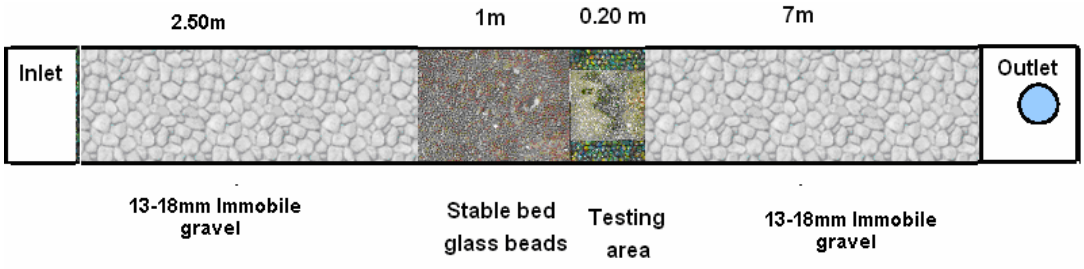

Figure 3. 8. Shields flume set up. The testing area is located 3.5m downstream the inlet. An immobile gravel bed (D=13-18mm) was placed after the inlet up to the stable bed for 2.5m. After that a 1m stable bed obtained with a plywood board where a single layer of glass beads (D_{50}=1.09mm) were glued on top. The test section was 0.2m in length and it was followed by immobile gravels up to the outlet.

3.5.2 Instrumentation on the Shields flume

Whilst information regarding the pointer gauge can be found in 3.4.3.1, the Shields flume was also equipped with visualization (imaging) capabilities. A *Sony HDR-SR5E* 4 Mega pixel camera was used to investigate the erosion rate during the experimental testing with all images taken in planform (i.e. a bird's eye view of the bed surface). Two different scales were analyzed: large scale (LS; 0.20mx 0.20m) and a small scale (SS; ~ 50 x 30mm). The former was dedicated to taking still images at the beginning and at the end of every flow step (a part from SGS in chapter 4, where images were taken only at the end of every flow step) specific to assessing changes in the areal coverage of biofilm (green pixel thresholding (see chapter 4 for more details). The latter employed a macro function to zoom sufficiently close to the bed such as to resolve and easily identify individual grains; this was essential to count the number of grains moving as required by the Yalin criterion (1972) definition of entrainment.

With reference to Yalin, his definition notes that the area analyzed should be "large" in comparison with the grain diameter and that the length of the time of observation should be 'large' in comparisons with the average period of turbulent fluctuations (Yalin, 1972). Taking each of Yalin's requirements in turn: *Firstly,* with regard to area (A), the main criteria for camera set-up was dictated by the need to resolve the full-box field-of-view and limitations on macro capabilities from this prescribed elevation. In spite of this the area observed in the macro setting is compliant with Yalin's criterion in that 300-1200 particles are present in all images (intuitively more 1mm beads than 2mm gravels particles comprise an equivalent area). In each of these images of the LS, the resolution that was achieved with the camera was of ~6pixels/mm: this allowed comfortably resolving the smallest particles (SGS) and the coverage that would interest them (this is significantly better than standard accepted photogrammetry (see Butler *et al.,* 1998) where resolution is rarely better than 1mm). *Secondly,* with regard to time (*t*), video recordings for the entire duration of the flow step were applied (10 minutes for the preliminary SGS experiment and 5 minutes for every other experiment) after for every flow step the flow had

stabilized (3 minutes from the increase in flow through the power inverter). Of this, 2 minutes of footage (the 1st and the 5th minute) were used to calculate the number of grains that moved from the small area. These times were selected because: i) in the 1st minute was likely that the most movement would occur as a consequence of the application of the new shear stress, hence the largest tendency to movement was expected; ii) the 5th minute was used because, if after the longest water-working period still the critical number of sediment were entrained, then a flow could be comfortably defined at threshold. In order to improve image quality, a glass plate was lowered onto the water surface so as to remove the distortion due to the ripples present on the water surface (this is a well-used method in flume based research and the small adjustments to the water surface are not thought to propagate to the bed in a manner influential on entrainment threshold data (Haynes and Pender, 2007; Cooper and Tait, 2008)).

3.6 Introduction to flume series 1 experiments (1m scale)

3.6.1 Ervine flume description and operation

The erosion tests for box1, representing the main experimental program, were conducted in the "Ervine" flume. This was a purposely built flume, specific to testing biostabilization with increased hydraulic precision at this scale. The basic configuration was an *Armfield* recirculating and tilting channel (5m long by 0.3m wide by 0.45m deep), equipped with glass side-wall rectangular cross section with an average water temperature of 22.5 ºC. The slope was adjusted using a fly- wheel at the downstream end, which was set to the same 1/200 slope as the colonisation (Yalin) flume. Specific upgrades on this facility included: (i) a smaller *Calpeda* ® pump of 15l/s as required to improve control at the low flows specific to biofilm testing i.e. to remove undesirable flow pulsations; (ii) fitting a more advanced power inverter of *Jaguar VXR, 1.5kW*to provide finer control (+/-1% accuracy) of the pump at low flows, by way of a closed loop function, as described below.

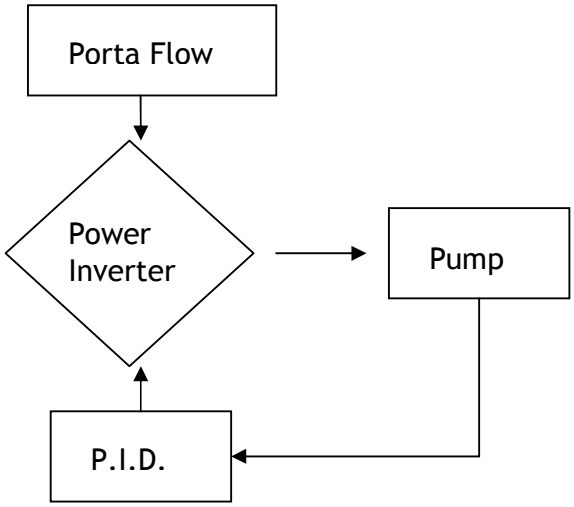

Figure 3. 9. Schematic diagram of flow control devices of the Ervine flume.

A Proportional integrative derivative (P.I.D) function, inbuilt in the *Jaguar VXR* was used to increase the accuracy of the flow by calculating the 'error' in the system recorded as the difference between a measured process variable (*U*) and a desired set point, the programmed flow velocity. The power of the P.I.D function stands on the possibility of generating a closed loop feedback (See figure 3.9). The loop works as follow: the speed from the pump and the flow velocity is recorded by the *Portaflow*; this recorded flow velocity is then fed into the P.I.D. function until the desired and achieved flow velocities are the same. The desired flow can be achieved to a 1% accuracy of that required.

The set up for the sediment arrangement is presented in figure 3.10 with the testing box1 placed 2m downstream the inlet and a section of 4-6mm gravels; with a turbulent boundary layer inducement length of 1.84m (Monin and Yaglom, 1971) this set up is justifiable. Justification for this set-up is as previously highlighted in section 3.5.1 and section 3.5.2.

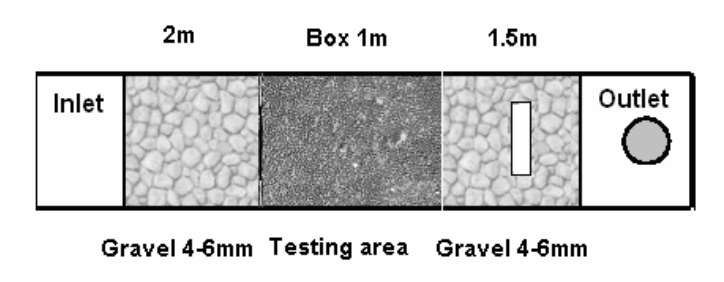

Figure 3. 10. Ervine Flume set up. The testing area is located 2m downstream the inlet. Gravel (*D*=20mm) were used in the first 0.3m to induce a turbulent boundary layer; 1.7m of gravel (*D*=4-6mm) followed this section. The 1m testing area was located immediately after that. Following the testing area there was a section filled with sediments 4-6mm up to the outlet.

3.6.2 Instrumentation on the Ervine flume

Whilst pointer gauge and visualization techniques are identical to those described in section 3.5, hydraulic data was additionally collected in the Ervine flume by means of a PIV system. As this considerably benefits entrainment threshold determination and shear stress evaluation at threshold, in depth description of PIV set-up, data acquisition and analysis is presented below.

3.6.2.1 Particle image velocimetry: theory, data collection and processing.

Particle image velocimetry (PIV) was installed to the Ervine flume in the summer 2010. From June to September 2010, the set up and calibration of the instrument was performed. Below the **theory of the technique, the data collection and processing will be presented**. The last section will illustrate the specific set up carried out in the Ervine flume.

Theory. Particle image velocimetry (PIV) is a velocity measuring technique that measures the motion of regions of a fluid by observing the locations of markers in images at two or more consequent times (Adrian, 1991). PIV is part of the optical methods family, which are extremely used in fluid dynamics because they do not necessitate of a submerged probe and hence generate less disturbance of the flow. Moreover optical methods have the advantage of: i)

collecting larger data sets because usually focused into larger portion of the flow and ii) offering more accurate data reading than a submerged probe.

The strength of the PIV technique depends on the fact that it is “indirect”; it measures the velocity of seeding particles added to the flow and neutrally buoyant, which follow the flow because their gravity and inertia are minimized. PIV is based on the fundamental definition of velocity:

$$U(x,t) = \frac{\Delta x(x,t)}{\Delta t} \qquad \textbf{Equation 3. 1}$$

Where Δx is the displacement of the tracer particle, located at x in time t after an interval of Δt between two different images. PIV relies on the illumination of the seeding particles by an external source (a laser), which allows them to shine and reflect clearly the light. In this way a camera focussed on the plane of the laser can record, even at very short Δt, the displacement of the seeding particles.

The PIV system is comprised by what can be seen in figure 3.11: a high speed camera; a synchronizer; a laser; a computer and analyzing software. The camera needs to be good enough to resolve very small Δt; some of the most up to date types of camera are high speed, which means that they can work up to 1000Hz. Lasers have been usually designed to be pulsed and can vary in power: the higher the power of the laser, the smaller the seeding particle can be with less effect on the flow and better buoyancy. However in recent years continuous laser have been employed together with high speed cameras, offering a safer system that can resolve very small time distances among video frames (time resolved PIV); this particular set up was preferred for this thesis due to: 1) its safer nature due to the lower power compared to any of the double frame systems; 2) its ability to resolve turbulence at a very high hertz rate (up to 1000), hence capturing very fine turbulent development. The synchronizer has the fundamental role to tune the laser pulses to the camera recording: without a synchronizer the time of image sequence collection would not match, inducing errors in the translation to flow velocity. Finally the software allows storing the sets of images recorded by the camera and performing visual enhancement and cross correlations sequences, in order to generate velocity from particle

displacements. Of great importance is the memory stored on the computer: the data collection of PIV systems is memory intense (e.g. the raw data in chapter 5 on a specific week of growth would occupy about 24Gb of space, without any processing done).

The principle of PIV can be subdivided into three different phases: 1) Data collection; 2) Data processing; 3) Data Analysis.

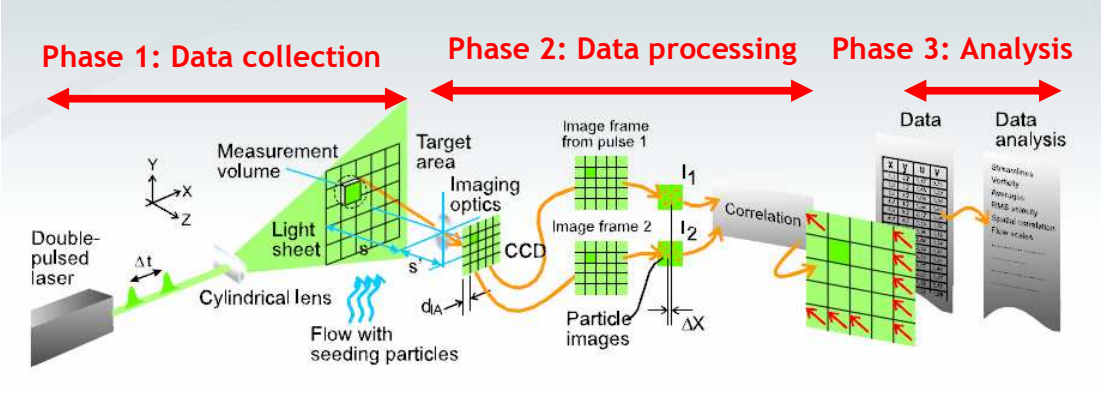

Figure 3. 11. Principle of PIV and different phases: 1) Data collection; 2) Data processing; 3) Data analysis. (Modified after Niels Anker Andersen, Dantec Dynamics, May 2007).

Data collection. A laser source is fired into the flow and seeding particles are added to the water. The laser is the most important light source in a PIV system and can be of two different types: pulsed or continuous. Usually pulsed laser are very powerful and use Q-switching to provide short and bright light; these lasers are easy to synchronize because they do not require a shutter for the camera. The final wavelength is in the green spectrum (532nm). Due to their high power, the pulsed lasers are extensively used in air. The continuous laser have lower power than the pulsed one and are very important in time resolved PIV, where a high speed camera can record very fast time sequences (up to 1000Hz), so that detailed turbulent measurements can be achieved. Moreover, as said before, these lasers provide a safer version than the pulsed laser system for any operator.

The seeding particles are another fundamental part of the system. The light scattered by the particles depends on: (i) ratio of the refractive index of the particles to that of the surrounding medium; (ii) particle size; (iii) particle shape; (iv) particle orientation (Raffel *et al.*, 2007). Size, material and

concentration of the seeing particles are important variables that can affect the final result of the PIV. The size usually depends on the power of the laser: the more powerful the laser the lesser the size of the particle needed (that can go from 1 up to 200μm). The material usually depends on the type of flow analyzed (e.g. air or water): for air flow it is common to use oil atomized (smoke, 1-2μm), whereas in water is much easier to find neutrally buoyant material (e.g. polychristalline material, 30μm). Another important variable related to the seeding particles is their optical properties. By definition in PIV, the seeding particle has to produce light scattering that will be collected and acquired by a camera, set perpendicular to the laser sheet as shown in Phase 1 of figure 3.11. To maximize the light scattering in water, silver coated particle are used; this needs to be carefully considered because their weight is larger than any other particle, resulting in unwanted errors due to the sinking of the particles.

Data processing. The displacement in PIV is obtained by superimposing couples of consecutive frames of an image sequences collected by the camera. The idea is to shift frames with respect to one another, until the best fit is reached: the displacement of the images represent the average particle displacement. In more detail, the field of view (FoV) is subdivided in smaller areas (called Interrogation area, IA), which can vary in size (e.g. 16 by 16 pixels; 32 by 32 pixels; 64 by 64 pixels), and the analysis is done for the movement of minimum of 6 particles per IA (Dantec, 2001). The displacement of this group of particle is evaluated by the PIV software (*Dynamic Studio*), which uses a process called cross-correlation. This is the application of the Fast Fourier Transformation (FFT) to obtain a correlation function and individuate a peak of correlation for the best matching of the displacement (Raffel *et al.*, 2007). After a calibration process has been performed, which takes into account the dimension of the FoV and the time displacement Δt, then the image displacement is converted into velocity (see figure 3.12).

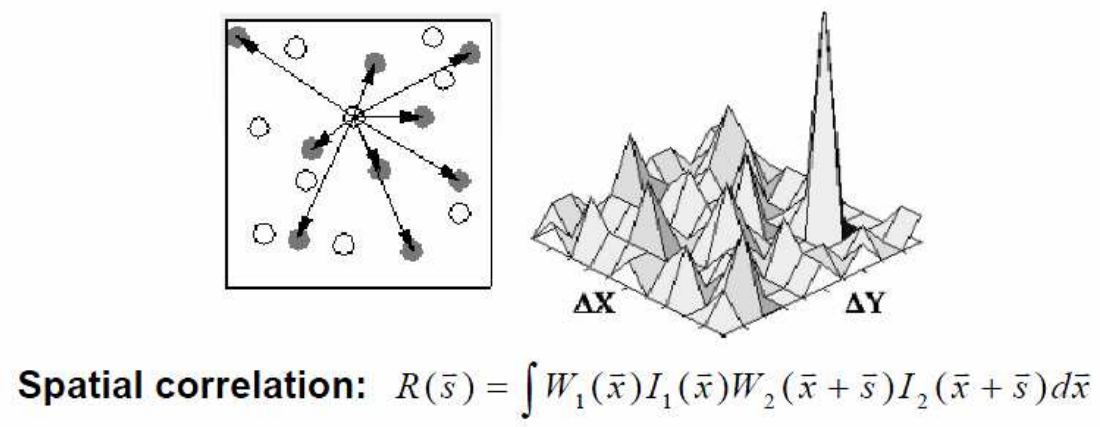

Figure 3. 12. Illustration of the process leading to the superimposition of consecutive images to find the displacement for every single Interrogation Area (IA). This is done by applying a mathematical spatial correlation. Once the displacement is known, then a velocity can be put in the place of the IA. (Modified after Niels Anker Andersen, Dantec Dynamics, May 2007).

Data analysis. This involves the verification that the cross correlation process generated the correct flow pattern. It is done by individuating the "wild" vectors, which are these that do not follow the neighboring vectors trend. In order to correct for these vectors (which might be generated by a non homogeneous seeding concentration in a certain IA or by a dark region near the bed), validation methods such as the moving average validation or the adaptive correlation (Dantec, 2010) are adopted. For this thesis, the first method was preferred because it works better in situations with less particle density and allows increasing the signal to noise ratio, which generates a clearer peak for the cross correlation. Moreover processes such as the masking of the bed could be implemented to get rid of unwanted regions of the bed.

In the following section, specific information will be given of the PIV system used in the experiments, followed by a detailed clarification of the set up on the Ervine flume.

3.6.2.2 PIV system and operation

The system acquired by the University of Glasgow was a 2D Time Resolved PIV (*Dantec*). Set-up details are presented in table 3.2:

Component	Name/Constructor	Specifications
Laser	*Raypower 2000*	Continuous green laser; wavelength 532nm; 2W power
Camera	*iNanoSense 3E*	High speed camera; 60mm lenses; FoV 1280x1024; 1000Hz, 4Gb ram which could store up to 3300 images; CMOS instead of CCD allows higher frame rate and lower laser power
Software	*Dynamic studio 3.14*	Used in Single Frame Mode, IA=64x64pixels, Calibration FoV=77.6mm*62.1mm (scale factor: 5.051); Overlap 50%, Displacement (y) 6 pixels
Seeding particle	*Talisman 30*	~100-150μm polyolefin powder

Table 3. 2. 2D Time Resolved Specifications. In particular details are given for the Laser, Camera, Software and Seeding particles.

A continuous laser *Raypower 2000* was mounted on to a carriage and connected to a boroscope via a set of mirrors. Placed perpendicular to the bed, the submerged head of the borescope (~20mm in height and ~10mm in thickness) fired a vertical laser sheet along the length of the flume. The head was placed 1m downstream the area of interest, termed the "interrogation area", in order to minimize its effect on local fluid turbulence structure (see figure 3.13a). Whilst a submerged continuous laser has lower power than alternative pulsed versions, this set-up is not constrained by pulse frequency limitations (usually ~50Hz); thus, the high speed camera employed in the present study was able to capture time sequences (up to 1000Hz), appropriate to more detailed turbulent measurements. Moreover, continuous lasers provide a safer version than the pulsed laser system for any operator; thus, the flume did not need to be "enclosed" and all processes pertaining to biofilm failure at entrainment threshold could be visualized simultaneously using a range of measurement techniques such as videography etc. (sec. 3.5.1-3.5.2) – this was essential to this thesis.

The alignment is a fundamental phase of the setting up of a PIV system: if the particles are not in the plane of the laser sheet, many wild vectors will be generated and hence the displacement of a set of particles would become almost impossible to asses. To do this, a purposely built instrument called the alignment device (see figure 3.13b) was designed and used in the Ervine flume. The alignment device consists of a crossed shape metallic frame, with two long arms placed right in the centre of the flume in the longitudinal direction. The device could be adjusted to the exact slope of the flume, thanks to four screws

and a slot to sit a digital inclinometer. At the edge of the long arms there were 2 metal bars perpendicular to the bed. The one closer to the laser was characterized by a 1mm slot (roughly the thickness of the laser) (see figure 3.13c): this would allow the laser to shine through and reflect on the back metal strip. In this way the direction of the laser sheet and its perpendicularity to the bed could be verified accurately.

Once the perpendicularity was verified, a metal plate with a ruler bolted into it was placed in the centre line of the flume, in such a way to be exactly into the laser sheet (see figure 3.13d, c). Tape colored with pink highlighter was placed on the plate: once illuminated by the green laser this color fluoresces and allows double-checking the position of the calibration ruler, even wearing the safety goggles, compulsory when the laser is switched on.

The camera was then focussed on the calibration plate under flowing water conditions: this ensured a correct calibration for the experiments, which were conducted under flowing water. The position of the camera was chosen so that the highest of the flow depth could be imaged (see figure 3.13e). It was levelled using the bubbles and fine adjustment controls on the tripod (*Manfrotto;* see figure 3.13f). The camera was tilted slightly so that it would be parallel to the slope of the flume (1/200). This was done by aligning FoV to the box wall. The camera position and it perpendicularity to the laser bin was crucial for the PIV technique to be successful. The FoV of the camera was kept at is maximum (minus the circularity of the intensifier) which was of 1000pixels, corresponding to about 70mm in the long direction and the depth was adjusted according to the flow height.

Moreover this system allowed avoiding the usage of a plate to still the surface of the water, which would have affected the flow conditions, especially for low flow conditions. Instead, the boroscope was positioned in the centre of the flume and aligned carefully to generate a laser sheet (1-2mm in thickness), perfectly perpendicular to the bed.

Seeding particles (see table 3.2 for characteristics) were fed into the system by a water tank, suspended 1m upstream the area of interest, recorded by the speed camera. The particles were mixed with water and stirred before adding to

the flow. The feed was delivered via a trickle of water right in the centre of the flume, where the laser was placed. This ensured in the large part of the experiments a good density of seeding material and a good quality of the analysis.

A total of 240 image sequences (2000 images) were collected for the whole set of experiments conduced in the Ervine flume. Those were subdivided into: 4 materials x 5growth times (from 0 to 4 weeks) x 6 flow steps x 2 sets of 2000 images per flow step. The analysis was conducted only on the first recorded set at every flow step (for a total of 120 image sequence), after verifying that the time analyzed was sufficient to resolve single turbulent structures and due to the long time processing that required almost 3h for every image sequence (e.g. 45 full days of processing) of constant presence at the computer. The software in fact requires the operator to input geometries for the masking process and to manually perform specific operations; only a minor averaging part can be automated. As will be seen in chapter 5, of the 120 image sequences, only 70 offered results with the desired resolution: in all cases, at higer flow rate the seeding concentration resulted to high, so that the particles reflection become less efficient, reducing the ability of the software to individuate the right displacement.

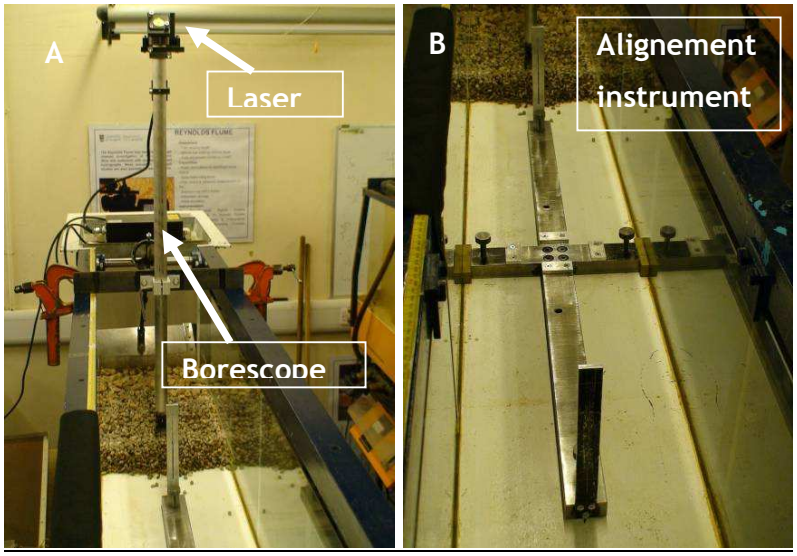

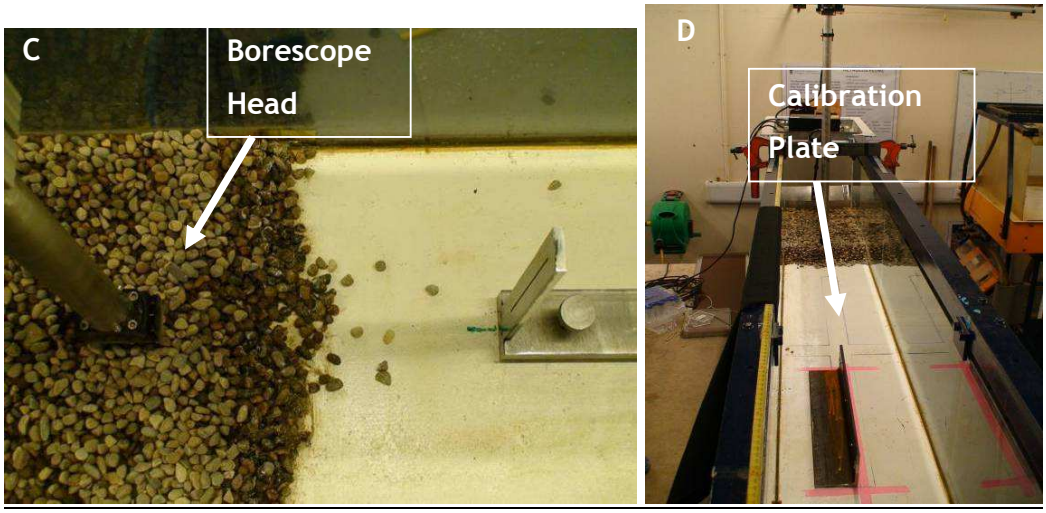

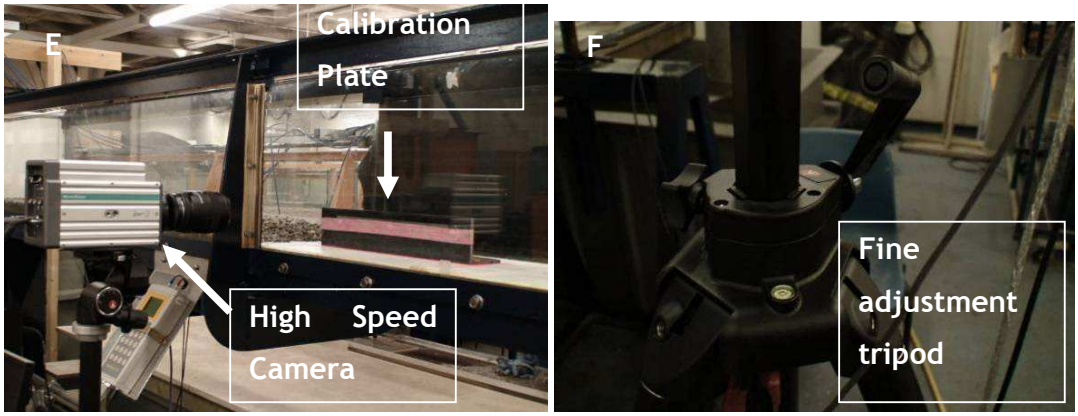

Figure 3. 13. Alignment device: A) particular of the alignment instrument; B) Laser, Boroscope and alignment instrument set up; C) Boroscope and laser adjustment to shine in the slot 1mm; D) Calibration plate placed in the centre of the flume and perpendicular to the high speed camera; E) high speed camera focussed don the calibration plate and tilted with the same slope of the flume (1/200); F) Manfrotto tripod, where the camera was rested: the figures shows the fine adjustment on the tripod which allowed refining 3 degrees of movement of the camera.

Concerning the data collection, as seen before in figure 3.13 the laser was mounted on a carriage running on the Ervine's flume rails and parallel to the flume bed. The laser was fired via a submerged boroscope (*Olympus*; See next section). The borescope was placed 1m downstream the tested area, in order to generate as low as possible disturbance on the flow (see figure 3.13). The resulting seeding of the flow for IA equal to 64x64pixels and after masking of the bed can be seen in figure 3.14a. Moreover an example of the cross correlation results (with very low concentration of wild vectors, always lower than 5%, as suggested by Dantec) can be seen in figure 3.14b.

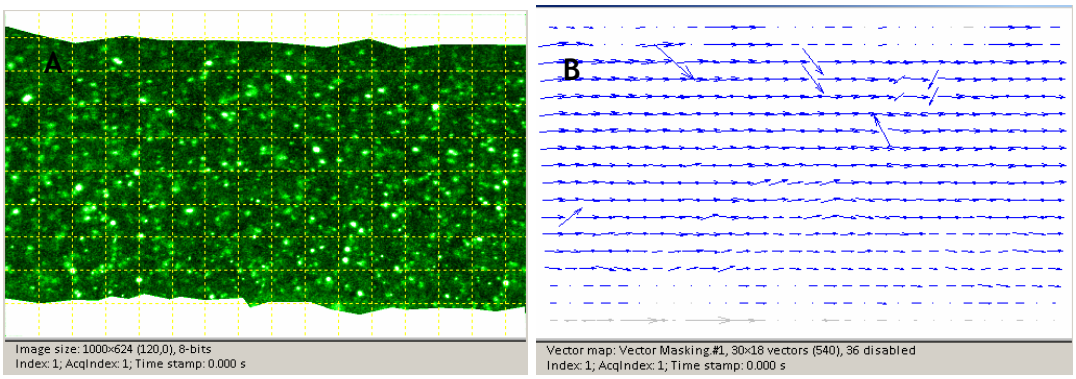

Figure 3. 14. A) Seeding concentration and in yellow the IA (64x64pixels). The white areas on top and bottom are the result of the masking of the bed and of the free surface without water. B) Result of the cross correlation process on the image sequence presented in A. As it can be seen, the number of wild vectors is well below the 5% advised by Dantec.

Once a seeing concentration as the one seen in figure 3.14 was achieved, reliable data could be collected. More information on the resulting settings applied during the experiments in the Ervine flume will be given in chapter 5.

3.7 Summary of Experimental Studies

This chapter has presented the overview of the experimental set up used to test the biofilm effect on the stability of non-cohesive sediments (see chapter 4 and chapter 5). Three different flumes have been employed for this purpose:

The Yalin flume (section 3.4): this was the incubation flume, in witch box0.2 and box1 have been cultured for up to 10 weeks. Light, flow, nutrients and temperature of the water have been controlled to obtain the best and strongest biofilm colonization.

The Shields flume (section 3.5): this is the flume where box0.2 and the preliminary set of experiment have been conducted. Visual analysis at two different scales (SS and LS) offered a first comprehensive data set of the effect of biofilm on sediment typical in river system. The results for this set of experiments will be provided in chapter4.

The Ervine flume (section 3.6): here the last and main experimental program has been carried out using box1. The usage of PIV will allow obtaining not only the trend of erosion at SS and LS but also to infer the modification of the longitudinal velocity trend and the hydraulic roughness (z_0) induced by the biofilm colonizing the sediments.

Hence, in the next two chapters a sediment transport method (the Yalin criterion, 1972), commonly used in engineering, will be evaluated in terms of its applicability to biotic sediment. Secondly the usage of different visual techniques, which have the advantage of being non invasive, will be assessed in their effectiveness; thirdly a series of improved methodologies to measure hydraulic variables will be undertaken in chapter 5. Here, instead of using the depth- slope equation (see chapter 2, section 2.2.4.3), based on flow and geometry of the channel cross sections for the bed shear stress τ_b calculation, I implemented the Particle Image Velocimetry (PIV) coupled with the Law of the Wall equations (see chapter 2, section 2.2.2.3): this allowed obtaining parameterizations of the bed roughness length z_0 in case of biotic sediments, as largely advocated by Black *et al*. (2002), and defining the variations of the longitudinal velocity over a colonized bed.

CHAPTER 4

Preliminary experiments: length scale 0.2m

"A theory is something nobody believes, except the person who made it. An experiment is something everybody believes, except the person who made it."

Albert Einstein

4.1 Introduction

Chapter 2 has provided clear evidence that biofilms can bind sediments by a complex biological – physical interaction (Paterson, 1997; Droppo *et al.*, 2001), i.e. "biostabilization". The strongest biostabilization potential appears to be associated with cyanobacteria and diatoms, linked to secretion of the EPS, fundamental for the adhesion of bacteria to surfaces. With increases in entrainment threshold up to 960% higher than those found in equivalent sediment (Yallop *et al.*, 1994), there is emerging consensus that these microbial interactions may (partly) account for well-known uncertainty in traditional sediment transport models when applied in the field.

Given the complexity of inter-related environmental variables (e.g. flow, light and temperature) in natural aquatic systems, this thesis was borne out of the need to isolate and analyse independent variables via the exact experimental flume systems, which originally bore the abiotic empirical entrainment equations (in agreement with Rice *et al.*, 2010a). However, chapter 2 has determined biostabilization knowledge gaps for a number of variables; (i) grain size – specific to coarse, non-cohesive sediments; (ii) time of growth; (ii) biomass; (iv) EPS; (v) spatial scale of analysis; (vi) direct measure of mechanical/adhesive strength in the direction of applied fluid shear. Whilst all these will be considered in detail in the following chapters, chapter 4 specifically relates traditional quantitative visual sediment entrainment

thresholds (i.e. Yalin criterion, 1972) to the time of growth of a cyanobacterial biofilm.

Following this approach, this chapter will illustrate the results of preliminary flume experiments conducted in the Shields flume over 0.2m boxes; details of substratum, species and environmental set-up can be found in chapter 3, sections 3.3, 3.5. Results of the present chapter are sub-dived into two parts: section 4.3 focuses on the methodology used for the entrainment threshold analysis at the small scale (Yalin) and at the LS (image segmentation). Section 4.4 will present the results starting from the assessment of the growth characteristics compared to the field one, presented by Noffke *et al*. (2001) characterisation; moreover the rational for the maximum length of colonization used will be introduced together with the biomass analysis for every experiment. Finally the result of the entrainment threshold identification will be given for SS and LS. The conclusions in section 4.5 will discuss the key finding of this chapter and the limitations that will be resolved in chapter 5.

4.2 Hypothesis

From chapter 2 the hypotheses anticipated were:

1. Biofilm colonization of all substratum will be described by Noffke *et al*. 's (2001) three stages of "fixation", "smoothing" and "sealing";

2. Mature biofilm will be characterized by a spatially-homogenous bio-mat enclosing all grains, independent of substratum grain size;

3. The longer the growth time, the higher the biomass, as seen in previous studies (Yallop *et al*., 2000; Righetti and Lucarelli, 2010);

4. The longer the growth time, the greater the relative difference between abiotic and biotic entrainment threshold (i.e. increased biostabilization);

5. Smaller sand-size grain sizes will exhibit greater biostabilization than coarser gravel-size sediment; however clumps of non-cohesive sediments glued together by the biofilm are not expected to be seen.

4.3 Methodology

This section presents the set up for the quasi-uniform flow conditions adopted in the Shields flume (see chapter 3, section 3.5) and the relative bed shear stresses τ_b generated (section 4.3.1). In section 4.3.2 the Yalin criterion ε (1972) will be illustrated to explain the engineering technique used to define the erosion at the SS; in section 4.3.3 instead there will be the explanation of the segmentation (image thresholding) method, which allowed addressing the erosion at the LS.

4.3.1 Flume set up

The overall programme is provided in chapter 3 with full instrumentation and methodological details. Provided here is the information specific to chapter 4 data collection. At the end of each week, a box0.2 was removed from the Yalin flume, placed into the Shields flume and tested for entrainment under incremental steps of quasi-uniform flow. In order to define the shear stress τ_b at every flow step, we employed the depth slope equation (see chapter 2, section 2.2.2.3, defined as:

$$\tau_b = \rho_w g R_h S \qquad \textbf{Equation 4. 1}$$

Where τ_b is the bed shear stress, ρ_w is the water density at 22.5 °C (997.74 kg/m^3), g is the gravity acceleration 9.81m/s^2, R_h is the hydraulic radius and S is the slope of the bed. Moreover an equation for the correction of the wall effect (Einstein, 1942) was employed, defined as:

$$\frac{\tau_b}{\rho g H S} = 1 - 0.0017 \frac{U^{1.5}}{b S^{0.75}}$$ **Equation 4. 2**

Where τ_b is the bed shear stress corrected for the wall effect, *U* is the mean cross sectional velocity, *H* is the mean water depth and b is the width of the channel. As with all entrainment threshold studies it is important to consider uncertainty in the experimental set-up; in the present data set this primarily relates to pump control at the lowest discharges of the stability test. Experiments employed between 9-19 flow steps, ranging from 0.52l/s to 10l/s. All flow steps of discharges >= 4l/s provided excellent flow control (*Q*=+/-2%), resulting in a stable water surface hence no variation were recorded compared to the uniform flow set up. However, the lowest flow steps applied were affected by pulsations in the flow caused by slow motion of the impeller system; flows of 0.52 and 0.94 l/s experienced ~25% and 12% fluctuations, whereas the flows up to 4l/s experienced up to +/-3% variation. Assessment of the variation of the flow was difficult because the pump fluctuation was fast, resulting in the impossibility to obtain reliable measurements using a pointer gauge. This problem was resolved in chapter 5, thanks to the usage of the *Jaguar XC* power inverter and the P.I.D. function (see chapter 3, section 3.6.1), which was retrofitted to in order to improve the flow control. For this set of experiments it is important to state that, since the conditions are the same in every test, the comparison among abiotic and biotic sediments threshold is scientifically meaningful even though perfect control could not be achieved.

For all these reasons, in this set of experiments the Meyer-Peter and Müller (1948) equation (equation 4.3) at the reach scale (Robert, 1997) was preferred to identify the hydraulic conditions experienced. It is standard practice to use this equation when the energy slope diverge/converge from the water level slope, which is presented below:

$$\tau = g \rho_w R_h Se$$
$$Se = Sw - Fr^2 (Sw - Sb)$$ **Equation 4. 3**

Where S_e is the slope of the energy, S_w is the slope of the water level, S_b is the slope of the bed, and Fr is the Froude Number, defined as $Fr = U/\sqrt{gH}$, U is defined as $U=Q/A_w$, where A_w is the wet area and Q is the flow. For the hydraulic calculations relative to the different flow steps and experiment see Appendix 4.A. Equations 4.1 to 4.3 were applied for the case of SGS: the depth-slope equation produced the highest value for bed shear stress (τ_b); the Einstein formula (1942) for side wall correction yielded a value between the Depth-Slope equation and the Meyer-Peter and Müller equation (see Appendix 4.A for SGS), which produced the lowest value. Fluctuations in flow through the pump at low flow combined with the long nature of the flume prevented a uniform flow profile from developing in some experiments (in the worst case, the percentage difference between S_e and S_w was up to 25%). In order to not overestimate the value for the shear stress and due to the quasi-uniform nature of our study, the Meyer-Peter and Müller method was preferred and adopted in the rest of the calculations. The bed shear stress τ_b was considered to be constant across the width of the channel and hence over the width of the box: this is a simplification, as it is well known that τ_b is larger in the centre of the flume and lower in the vicinity of the walls, which induce a certain degree of friction. The flow steps were applied for 10 minutes in the case of SGS; however, as will be presented in the result section 4.4.1, after the testing of SGS for up to 10 weeks of growth, it became clear that the variable to investigate in particular detail was the increase in magnitude of the shear stress more than the time of flow application. Hence a larger number of flow steps were introduced to the remainder of the materials and 5 minutes were preferred as the length of flow application. The steps of uniform flow were investigated prior to any of the experimental testing and assumed constant during the testing.

4.3.2 Yalin technique and abiotic threshold

As seen in chapter 3, section 3.5.2, videos were used to analyze the entrainment of single particles according to the Yalin criterion ε (1972) at the SS; this method empirically based allows relating the number of grain detachments from an area to the time of analysis and hence classify the flow step at threshold of motion if

the calculated amount of grains moving match the measured. The equation is presented below:

$$\varepsilon = \frac{N}{At}\left(\frac{\rho_W D^5}{\gamma_s}\right)^{1/2} \quad \textbf{Equation 4. 4}$$

where, ε is equal to 1×10^{-6} and it is the empirical constant obtained by Yalin in 1972, N is the critical number of grains moving in an area A (cm^2) for a time, t (s), ρ_w is the density of the water (g/cm^3), D is the diameter of the grain (cm) equal to the D_{50} and γ_s is the specific weight of a grain in the fluid as obtained from $\gamma_s=(\rho_s- \rho_w)g$ where ρ_s is the density of the material in g/cm^3.

The Yalin criterion (1972) was applied to clean sediments before the start of the erosion experiments. The threshold was met when at least **8 particles** were entrained in both the 1st and the 5th minute of the flow step for SGS and sand substrata; for LGS and gravel substrata, threshold was defined when detachment counts were at least **3 and 2**, as can be seen from table 4.1.

	***A* (cm*cm)**	***T* (s)**	***N***	**Error (particle)**	**Total *n***	***N/n***	**u_c*(cm/s)**	**τ_c (Pa)**
SGS	4.2*3.2	60	8	1	1167	1%	2.95	0.87
Sand	5.0*3.2	60	8	1	1111	1%	3.51	1.23
LGS	5.9*3.3	60	3	0	487	1%	3.66	1.34
Gravel	5.1*2.9	60	2	0	306	1%	4.08	1.66

Table 4. 1. Summary of the variable used in the Yalin criterion (1972). *A* (cm^2) is the area analyzed, *t* (s) the time, *N* the number of grains at threshold according to the Yalin criterion, error is the maximum number of particle miscounted; *n* is the total number of particle in the are *A*, *N/n* the portion of the area which defines the flow at threshold, u_c* the critical shear velocity and τ_c the critical shear stress for every material.

The critical shear stresses in table 4.1 were used as benchmark data to calculate the percentage difference in critical shear stress in the case of biostabilized sediments, in a manner similar to the biostabilization stats provided by Paterson (1997).

4.3.3 Image segmentation for quantifying biofilm areal coverage

Image analysis was conducted for the still images at the LS. By definition, image analysis is the operation necessary to obtain quantified information from images (Francus, 1998). In sediment research, many are the automated procedures for identifying the 'best' threshold (or segmentation) based on the investigation of the distribution of the pixel intensity (see review by Shaoo *et al.*, 1988); often these techniques are based on the localization in the histogram of the pixel intensity for gravel beds of a clear peak (Graham *et al.*, 2005). However it is well known that automated methods often poorly perform on the segmentation of sediments images; hence a manual segmentation backed up visually has been largely preferred by researchers, even though time consuming (Butler *et al.*, 1998). This was the preferred approach taken through this thesis, since finding a common threshold value to apply for every experiment was impossible due to factors such as: i) variation in the colour and transparency of the materials used as the substratum; ii) temporal development of the intensity of the 'green' colouration of the biofilm with either maturity of growth or erosion; iii) distortions of the water surface causing different amount of light scattering.

Therefore, as suggested by Francus (1998), an image technique was carefully chosen herein and evaluated for every specific case analyzed. In order to do this objectively, the image software *ImageJ* (Abramanof *et al.*, 2004) and the *Threshold Colour* Plugin, by G. Landini were employed to insure consistency in the assessment of the erosion. The plugin of *ImageJ* allows to threshold coloured images based on a variety of image spaces (for a detailed review of the different colour spaces Ford and Robert, 1998), such as HSB (Hue, Saturation and Brightness). Hue is a linear transformation of the most common RGB colour space; its advantage lies of the fact that its application is extremely intuitive for human vision (Ford and Robert, 1998). Hue can be referred as the spectrum of colours; the versatility of the HSB space is that it allows choosing among different colours and isolating a particular colour band. In our experiments the biofilm had a very distinctive green colour that could be easily distinguished from the sediments. Slightly more complicated was the individuation of the areas not covered by biofilm in the case of SGS or LGS; due to their transparency a clear differentiation between biofilm was not easy, as seen below.

The thresholding was carried out by:

1) Adjust the brightness of the collected images, by using the “auto” function; this will automatically optimize the brightness based on the histogram of the pixel values (figure 4.1b). The optimization is done by allowing some of the tail values of the histogram to be displaced as black or white, hence a small percentage of the pixels in the image becomes saturated an appears darker (~0 in figure 4.1b,c) or brighter or (~255 in figure 4.1b,c).

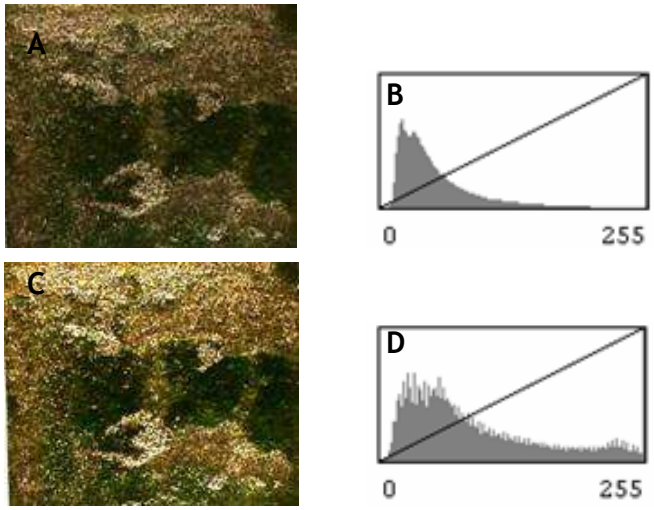

Figure 4. 1. Brightness intensity adjustment using Image J. A) Original picture collected; B) relative histogram of the pixel intensities where 0 represent a dark are and 255 a brighter zone; C) Brightness correction applied and D) relative saturation of the histogram, for which the range has been spread and better visibility was reached. Flow from right to left.

2) Use the *Threshold Colour* plugin, which permitted to use the HSB method (see figure 4.2).

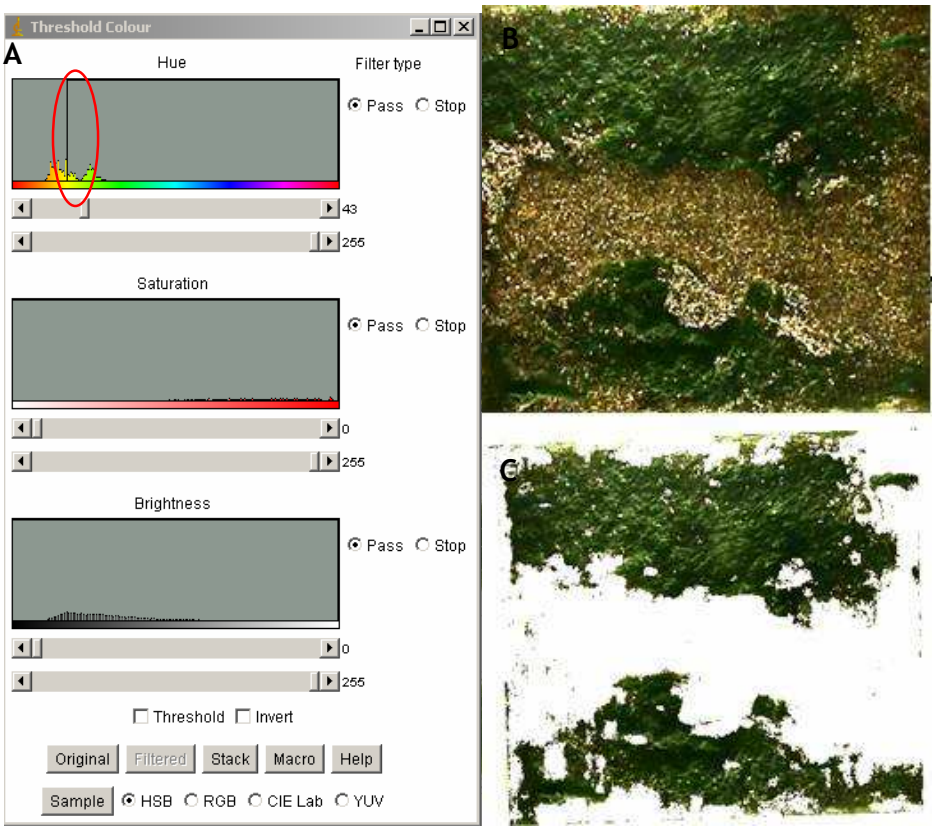

Figure 4. 2. A) Threshold colour plug in with Hue, Saturation and Brigthness modification. The Hue allows differentiating among different colours (e.g. yellow/green). In particular picks among the two colours were identified as good segmentation. B) Original Image of week 3 sand (1.98l/s); C) An example of a successful segmentation using the pick identified in A. Flow from right to left.

This technique was based on the identification of the peak between the yellow and green band. Once this was found, the effectiveness of the threshold was verified using the function of the plugin allowing switching from thresholded to original image. This process was relatively easy for natural sediments because more clear division among spectrum of the colour could be seen, resulting in a thresholding error of not more than 3-5% of the total area. The error was identified looking at consequent flow steps and observing fluctuation of the biofilm area equal to the error value. Instead for the SGS and LGS the process was much more complicated, due to the difficulty in distinguishing among partially covered particles by biofilm. This resulted in a thresholding error 7-9% of the total area. Hence the results presented in section 4.4.4 will be enclosed in these bands.

At different flow steps, biofilm covered pixels were assumed to contain chlorophyll a and hence appear green, therefore proving that biostabilization

was taking place. The resolution (~6 pixels/mm) here is higher than the photogrammetry technique used by Butler *et al*. (1998), where the highest resolution achieved was about 1mm.

In the following sections the erosion of the biotic sediments will be investigated at two different scales: during this work (especially considering the small scale (SS)) strong biofilm colonization has been observed to clump together 2-3 sand grains. However, clumps were never seen to occur for gravel size sediments. Once strong biostabilization was achieved, a biofilm "carpet" was visible over the sediments: this was a composite material (biofilm/substratum) that I will define from now on as "bio-mat". Strong bio-mats would erode under the flow by folding themselves up as a "carpet"; after large areas of bio-mat were eroded, the bed underneath was completely exposed to the flow and eroded. The sediment layer below the bio-mat did not present high cohesion. More details of this process will be found in the following sections introducing the results of the preliminary set of experiments.

4.4 Preliminary experiments results (5 weeks of growth)

The growth methodology and Shields flume description can be found in chapter 3 (section 3.5). The sections below investigate the obtained results, spanning from an assessment of the growth characteristics to the erosion results. In detail, section 4.4.1 will investigate the similarity with the growth characteristics obtained in the Yalin flume and the structure of biofilm growth in the field (Noffke *et al.*, 2001); section 4.4.2 will present the reasoning for choosing 5 weeks as longest time of growth for the preliminary experiment: this time frame was chosen after considering the growth characteristics of SGS up to 10 weeks, for finding the strongest biostabilization. Section 4.4.3 presents the results of the biomass analysis; section 4.4.4-4.4.6 will present the results of the erosion experiments at the SS and LS. The findings will be discussed in great detail in every section.

4.4.1 Representative growth assessment

Reassuringly, the stages of biofilm development observed in the Yalin flume after careful selection of the growth methodology (presented in chapter 3, section 3.4.4) resembled those seen in field studies over cohesive sediments (Noffke *et al.*, 2001; see figure 4.3).

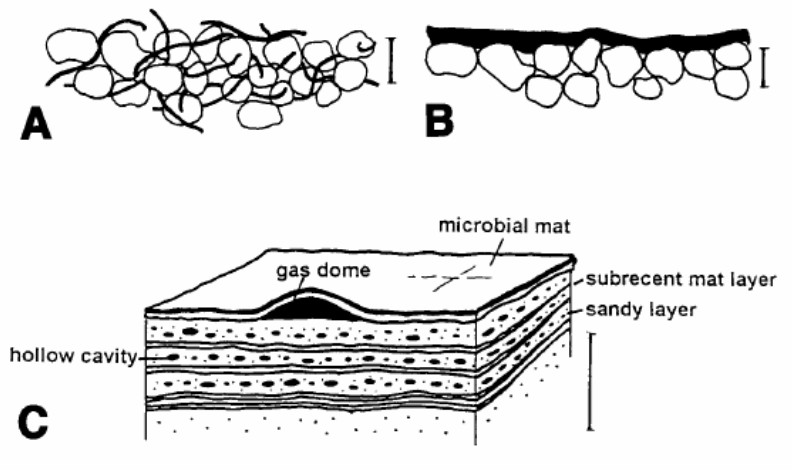

Figure 4. 3. Biostabilization by benthic cyanobacteria. A) The grains are interwoven by cyanobacterial filaments and fixed in their position, increasing the resistance and flexibility of the organic reach sediment (scale 5mm). B) The mucus- reach cyanobacterial cover is reducing the surface roughness of the sand. Hence the frictional forces are reduced, increasing the stability of the deposit (scale 5mm). C) Sediment is sealed by the dense mat layer at a level in which the intra-sedimentary gasses become entrapped. The gas pressure may generate hollow cavities (scale 100mm) (After Noffke *et al*., 2001).

The growth stages equivalent to Noffke's scale are identified visually in the present experimental programme using the following criteria:

(i) Fixation stage; this was defined when the 'majority' of the field of view had been colonized by a thin coating of cyanobacteria. Identification was qualitative, based on visual assessment in which clear was the fact that biofilm was starting to coat the single grain, but just partially, so the surface of each individual grain could still be resolved (see figure 4.4). Importantly, all experiments showed a degree of fixation within 1 week of growth, yet 1-2 weeks was required for pronounced spatial coverage to develop.

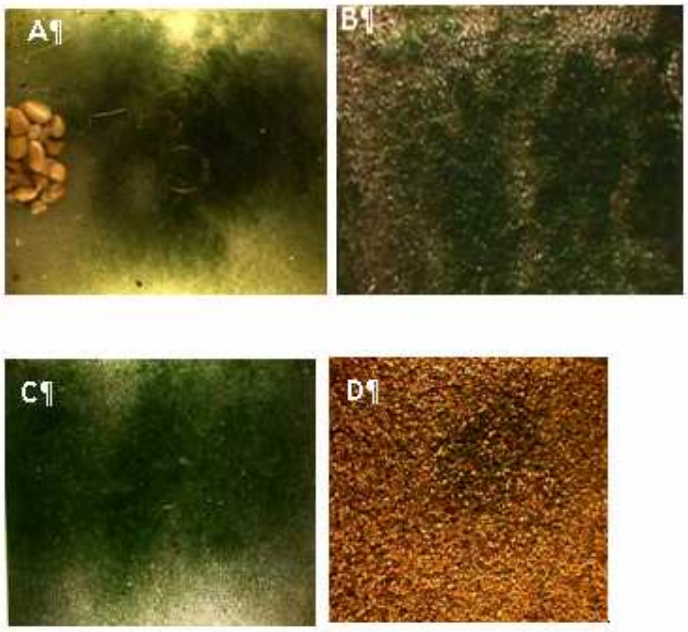

Figure 4. 4. Fixation stage after 1 week of biofilm growth experienced at the LS by: A) SGS; B)Sand; C)LGS; D) Gravel. Scale 0.2m by 0.2m. Flow from right to left.

(ii) Bio-mat stage: this was defined as a spatially-extensive homogeneous coverage of the field of view by a biofilm of length scale equivalent (or greater) to the roughness elements. Given that bio-mat thickness could not be measured directly, visual analysis was employed whereby sand and gravel beds required different characterisations. Firstly, this second stage of growth showed a complete smoothing of the bed surface so as to enclose discrete particles of the sand size sediment (see figure 4.5 A and B). Secondly, for gravel beds, this stage was defined when filaments were easily visible (~2mm length) in protruding from the forelocks of discrete particles. This stage occurred between 3-5 weeks of growth.

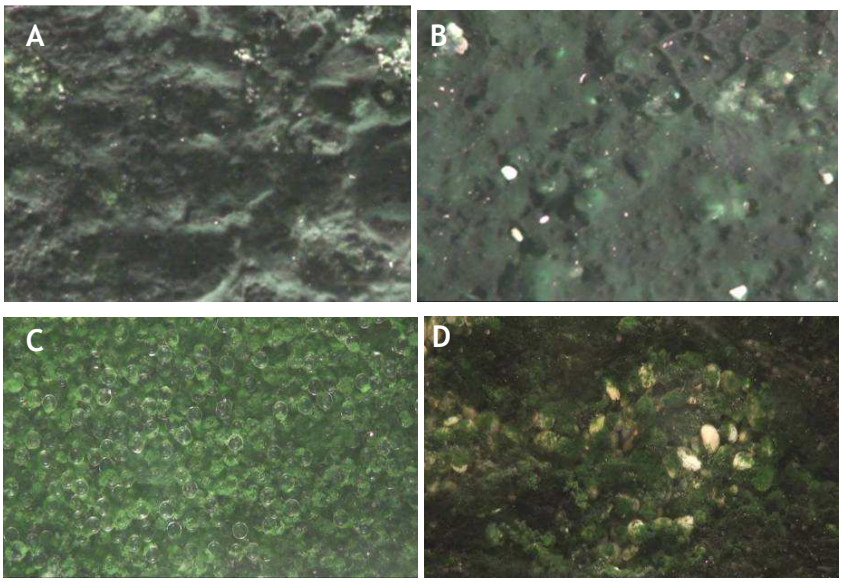

Figure 4. 5. Mature laboratory growth stage (Week 4) at the SS experienced by: A) SGS; B) sand; C) LGS and D) Gravel. Scale: ~50mm by ~30mm. SGS and sand present a clear smoothing of the surface, with grains being embed into the bio-mat and roughness of the bed being decreased; LGS and Gravel show a different trend, with biofilm growing homogeneously on the surface of the grain but no generation a "carpet"; instead streamer were seen growing on top of the grain: this will affect the flow structure around the top of the grain due to the fluctuation of the streamers. Flow from right to left.

(iii) Sealing stage: this was defined when air bubbles were first observed to be under the biofilm. This stage was observed from after as early as 2 weeks of growth and took place intermittently (examples are provided in figure 4.6 for SGS at the LS and Sand at the SS). The process was that the biofilm would grow to a stage in which either the mat was exposed outside the water level during growth (SGS) or small bubbles of air were trapped under the mat (sand). Hence, the mat was more likely to be eroded during growth conditions (e.g. week 3 of growth for SGS). Once eroded, the colonization that took place resulted stronger and smoother (e.g. week 4 of growth SGS): this process was cyclic and repeated itself in time intervals of about 3 weeks. However, this type of process did not take place for gravel size sediment: here a bio-mat was never generated and hence no trapping of air bubbles were experienced.

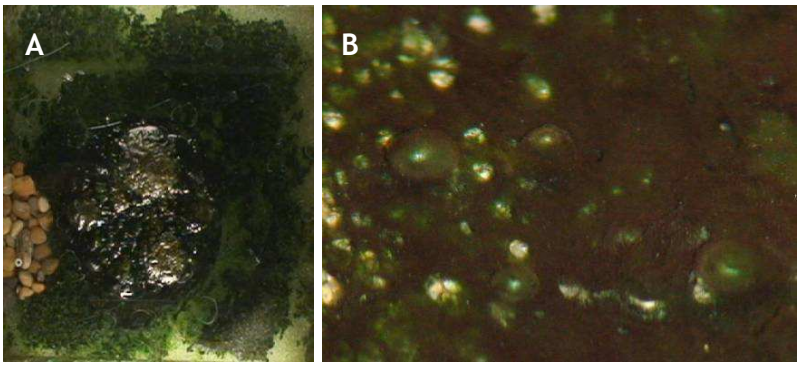

Figure 4. 6. Examples of the sealing stage define by Noffke *et al*. (2001): a) SGS at the LS after 3 weeks of growth: the bubble of air trapped underneath the biofilm is occupying the entire centre of the sample and it is exposed out of the water surface; b) Sand at the SS after 2 weeks of growth it is evident that micro bubbles (about the same sizes of a sand grain) are exposed to the flow and represent a possible weakness of the bio-mat. Flow from right to left.

The distinction of growth-time relationships over different substrata is the main finding of this data set. Given that only a 0.9mm difference in grain size is found between the sand-size and gravel-size fractions tested, such a pronounced distinction in biofilm form at the sand-gravel transition is surprising and therefore requires rationalization. As the reciprocal eco-hydraulic interactions/feedbacks are discussed in chapter 7, the focus of this discussion is specific to the form of cyanobacteria growth and a range of scientific arguments are proposed: *Firstly*, great importance seems to be related to the light intensity used (see chapter 3, section 3.4.4.4). In my experiment biofilm growth was visually very affected by the light source: this represent an important recommendation for further experimental growth (see chapter 5): critical to the present study is that this effect may have been exacerbated by the spot-light system employed in the preliminary runs; hence use of a more diffuse lighting system was sought for chapter 5. *Secondly*, the size of the sediment dictates bed porosity and surface-subsurface flow interaction at the bed surface, where colonization occurs. Simply, the larger the size of a grain, the greater the pore size and porosity (assuming a uniform grain size distribution). Thus, a gravel bed will permit greater vertical exchange of flow at the boundary and increase interstitial subsurface flow in terms of both volume (larger pores = greater conveyance) and velocity (larger pores = relative reduction in side-wall energy losses). This is well-known to increase local downwelling and upwelling above the pore, such that high vertical shear stresses are found here, which may preclude biofilm growth across the pore space (Battin, pers. comm.) and leaving

a biofilm fabric pierced with holes. Importantly, these flow structures would self-perpetuate filamentous growth in that the vertical orientation of shear forces will dictate growth orientation and the boundary for continued nutrient exchange. In a cycle of positive feedback the extension of the filament structure into the fluid flow enhances the vertical orientation of the flow routing into the porous boundary. *Thirdly* the initial colonisation location may underpin subsequent growth dynamics in a manner related to the relative length scales of the grain (D) to the turbulent flow field (l_{turb}) responsible for "seeding" the substratum. To elucidate, if $l_{turb} > D$ then multiple grains will be simultaneously colonized and subsequently affected by locally-homogeneous distribution of nutrients etc. from the fluid flow; this would encourage uniform growth over the locale. Conversely, if $D > l_{turb}$ then only a specific location on a single grain would be seeded from an individual turbulent structure, possibly inducing spatio-temporal heterogeneity across the substrata. Further, the impact of D to l_{turb} relationships would affect growth, in that rough beds are more likely to have a more regular spatial flow structure defined by bed roughness; this is likely to perpetuate sub-grain scale growth. Where the substratum is finer the bed roughness lengths are less, hence flow structures may have more freedom in spatial location leading to time-averaged homogeneity across the patch; this in turn would lead to more uniform growth.

Finally, the use of constant discharge means that the applied shear velocity was slightly lower for the gravel (25-30% that of the abiotic entrainment threshold) than for the sand (35-50% of the abiotic threshold): flow depth was about 6-7 times more than the D_{50} of gravel size sediments and appeared low for the gravel size sediment; this was confirmed by the vertical orientation of streamers growth, which were not bent by the shear force. One consequence of this might have been that the biofilm streamers could reach vertically towards the nutrient source (light) without being affected or bent by the flow and that, as the relative submergence is inversely related to light intensity within the water column, then growth may be higher in 'shallower' locations; this was possible due to the reduction in turbulence correlated to the larger grain size. Hence in coincidence of the top of a gravel grain, the biofilm growth would take place in the form of spongy streamers, grown in slower flow condition and hence less subjected to sloughing and erosion during growth. Therefore the structure of the

biofilm growing on top of the gravel sediments looked not as strong as the one for sand size sediment: in order to obviate to this issue, in chapter 5 a better light system, which did not induce the biofilm to overgrow, and faster flow at growth was applied for gravels, resulting in much stronger biostabilization.

Whilst this data set concludes that laboratory-based experiments can successfully colonize and growth biofilms representative of the field (Noffke *et al.*, 2001), it is concluded that there is clear relationship with growth duration and grain size. Resolving the latter in terms of the four possible explanations posed above into account, the influence of upwelling/downwelling appears most supported by the literature in terms of explaining differential biofilm growth form over different substrata. Thus, chapter 5 will explore the use of detailed flow field data to further the reciprocal Eco-Hydraulic interactions of colonization and growth.

In section 4.4.2 a rational for the length of growth colonization will be offered after growing SGS for up to 10 weeks. The strongest week of colonization was defined as that with the lowest percentage area eroded as will be presented in detail in the next section.

4.4.2 Length of growth colonization: 10 weeks SGS

The first set of experiments was performed using SGS. In order to measure the strongest increase in stability due to the growth of biofilm over sediments, the SGS were colonized for 10 weeks and tested every week in order to find the strongest growth stage. Figure 4.7 present the 10 week of growth and shows the erosion process taking place. In particular the first image represents the initial coverage when extracted from the Yalin flume; the second image is the area coverage after the first flow was applied and the third picture shows the erosion at the end of the last flow (see Appendix 4.A).

Week 1

Week 2

Week 3

Week 4

Week 5

Week 6

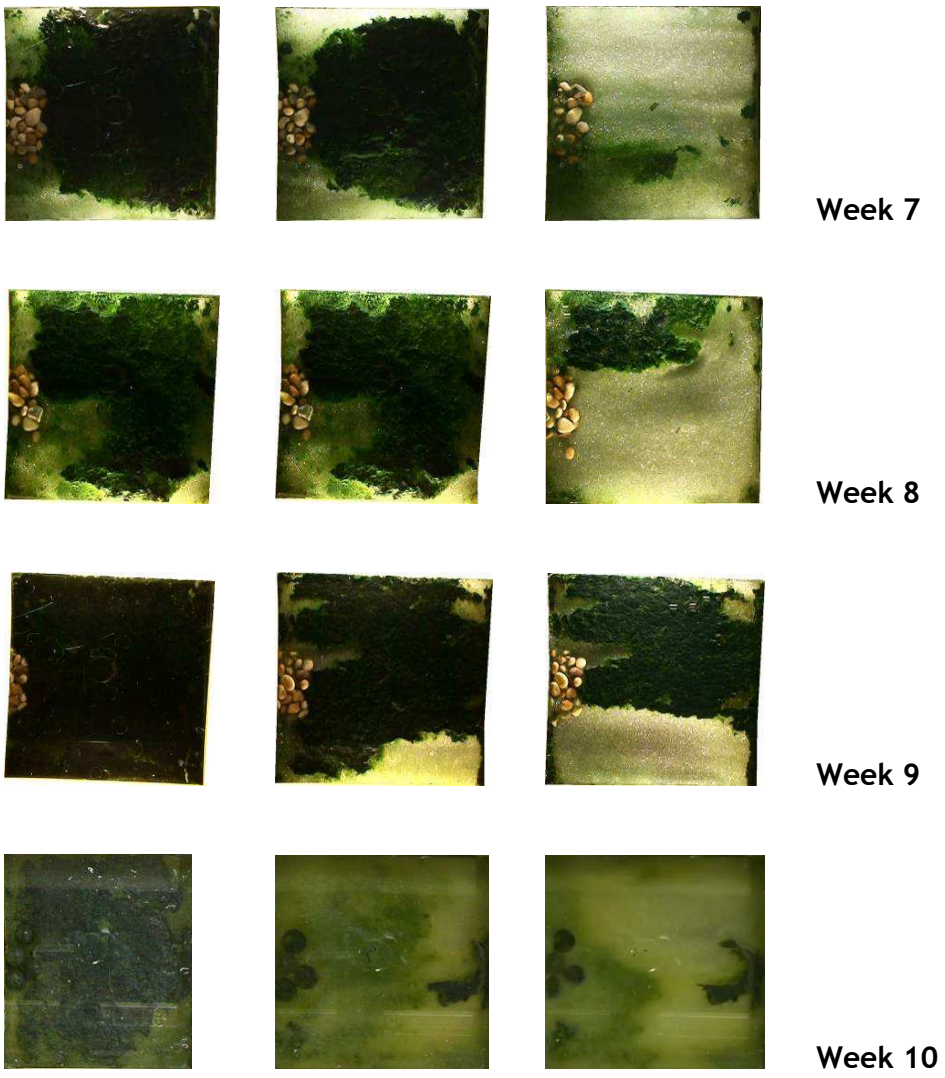

Figure 4. 7. 10 week of growth at the LS used to find the strongest biostabilization stage. 1st image is the original coverage from the Yalin flume; 2nd image is the erosion after the first flow application (0.52l/s); 3rd image is the remaining biofilm after the application of the last flow step (3.40l/s). Flow from right to left.

As can be seen from figure 4.7, the strongest biostabilization experienced was found in week 4 and week 5. After that a recolonization process took place and led to another strong week after 9 weeks of growth. Hence, in order to limit the time for the experimental set-up, all the remainder of the experiments for box0.2 were grown up to week 5 and tested weekly. Interesting to note is that in some cases the bio-mat was covering the whole area at the beginning of the experiment (e.g. week 2 and week 10 of growth) got completely eroded after the first low flow application: this implies the sealing stage of growth (see section 4.4.1) and indicates that in coincidence with these weeks of growth the mat was not anchored to the bed and was prone to be eroded in single sheet.

Another interesting finding was that during the testing of SGS it was seen that the initial assumption, which considered the biofilm as not strong enough to clump non cohesive sediment, was not verified. In cases of strong bio-mat, when the biofilm eroded, clumps comprised by more grains were seen rolling across the box. Even more interesting was that in case of more mature biofilm, hence when the smoothing stage was achieved (Noffke *et al.*, 2001), the way in which the biofilm eroded was similar to a "carpet", as can be seen from figure 4.8 relative to week 7 of growth. The bio-mat was so strong that even when dislodged from the bed was still able to hold and trap sediment. This opened a series of new possible ways in which the erosion of biotic non cohesive sediment can take place. It is well known in face that this phenomenon happens in case of intertidal mats smoothing fine cohesive sediments (Grant *et al.*, 1986; Grant and Gust, 1987). However none before presented the evidence that biofilm could also embed larger sediments. This undoubtedly represent a crucial finding because means that also larger sediments, more typical of river system, could be affected by the biostabilization potential, as will be seen in the result section below. Moreover the highlighted process start to cast doubts on the effectiveness of single particle entrainment models (e.g. Wiberg and Smith, 1987) when biotic sediments are present: these neither account for the clumping of grains, neither for their carpeting by the bio-mat.

Figure 4. 8. Carpet like erosion experienced for week 7 of growth. The bio-mat still traps some of the sediment after being dislodged, proving the strength of the adhesion among biofilm and sediments. Flow from right to left. (Scale 90mm by 60mm).

4.4.3 Biomass

Figure 4.9 presents the weekly relative biomass results (the biomass divided by the dry sample weight) collected over the four different substrata after applying the loss of ignition technique (HIMOM, 2005). A detailed analysis is presented below for different variables:

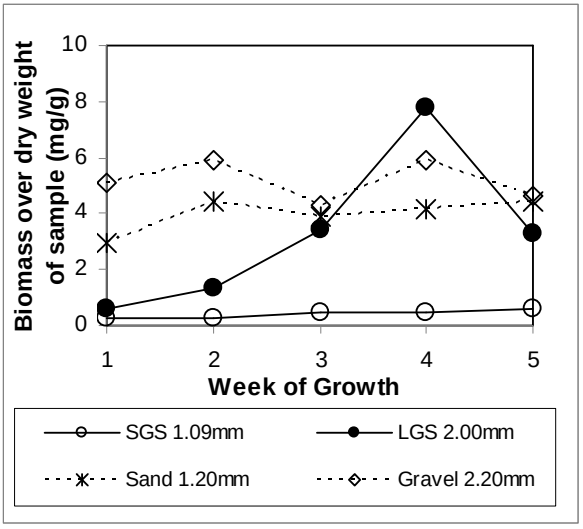

Figure 4. 9. Weekly relative biomass (mg/g), which is biomass (mg) divided by the dry weight of the sample (g), of box0.2 for sand and gravel size sediments as obtained from LOI (HIMOM, 2005).

Absolute data: the maximum biomass varies in absolute weight over an order of magnitude (10-100mg). The relative biomass in figure 4.9 shows an almost constant growth trend for SGS and a sensible increase in biomass for LGS in week 4. Sand and gravel samples present the same range of magnitude, fluctuating around a constant value.

General trend: figure 4.9 presents of a positive relationship between biomass and time of growth. Specifically the increase in biomass with time ranges from +14% for gravel (between week1 and week4) and 92% for LGS (between week1 and week4). This is in accordance with the growth model presented by Noffke *et al*. (2001) for which the growth is incrementing, stepping through the 3 stages

presented in section 4.4.1 (going from 5mm to 100mm length scale). The only exception to this is week 3 of growth for gravel substrata; here the biofilm was entrained over a local area ~cm^2, yet rapidly recolonized over the following week; the reason for premature failure at this location was not obvious.

Growth time: Importantly figure 4.9 shows significant growth over timeframes < 1 week. Three of the substrata (SGS, sand and gravel) clearly show that 53-84% of the overall maximum biomass recorded was already present after 1 week of growth. This trend is most apparent in the natural sediments (76% and 84% of the total grow in week 1 respectively). The exception (LGS) shows only 12% of maximum recorded biomass, indicating that growth is more rapid 2-4 weeks after colonization.

Material size: Coarser gravels indicate slightly higher biomass than finer substrata. Taking the average concentration of the relative biomass in time, it is clear that gravels have ~1.3 times more biomass than sand and LGS have 8 times more than SGS. As seen in section 4.4.1, this might be due to the lower H/D ratio, that allowed more light to reach the biofilm, hence more growth to be allowed. Also, the resulting flow over sand was faster than that over gravels due to the lower roughness, hence permitting the biofilm streamers to reach further into the flow and increase nutrient and light uptake.

Material type is clearly related to biomass, with natural gravel sediments showing approx twice as much average relative biomass (comparing equivalent diameters to each other) than LGS and sand sediments showing almost 10 times more relative biomass than SGS. This might be because the natural sediments have a specific charge and they are comprised by metal particle, which can be used as nutrient by the biofilm (Battin, personal communication).

4.4.4 Biostabilization data: relationships between critical shear stress at entrainment and time of growth – small scale (SS)

Results for the Yalin analysis for the four different materials are presented in figure 4.10, where the percentage increase of the bed shear stress τ_b compared to the abiotic threshold is plotted in time.

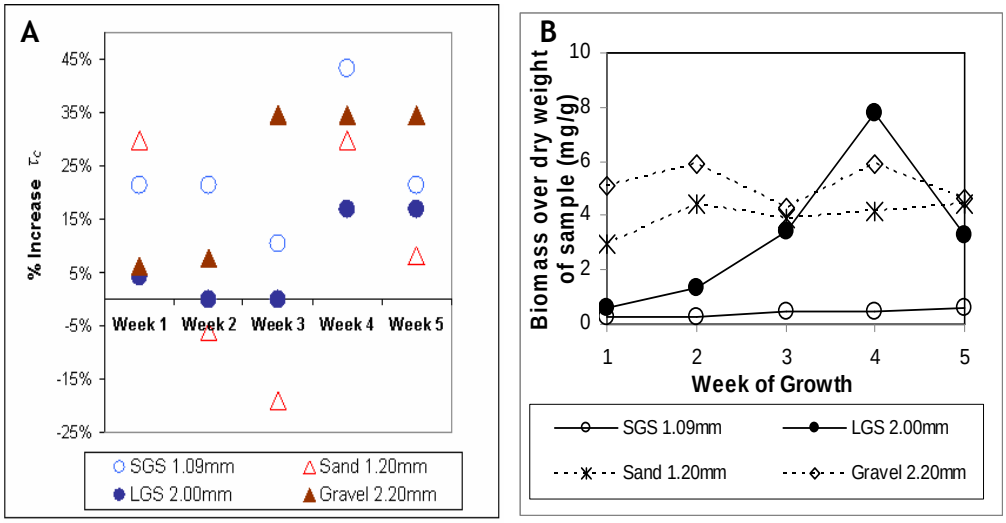

Figure 4. 10. A) Results for the SS for % increase in τ_c compared to abiotic sediments: SGS experienced the largest biostabilization for week 4 of growth with threshold reached after 43% more τb was applied; sand and gravels had a biostabilization of respectively 30% and 35% more than abiotic sediments for mature biofilms and LSG presented the lowest biostability up to 17%; B) Relative biomass (see figure 4.9 for details).

As highlighted in section 4.3.1, fluctuations in the flow generate uncertainty in the bed shear stress τ_b but this cannot be quantified, hence no errors bar can be found in figure 4.10. However, details of the flow variations can be found in section 4.3.1.

Absolute data: The maximum increase in bed shear stress τ_b the maximum value of biostabilization achieved for SGS was equal to 43% and 30% for sand. Gravel presents as well increase stability up to 35%, whereas the lowest value is experienced by LSG equal to 17%.

General trend: A clear finding is evident from figure 4.10: the majority of stages of biofilm growth generate an increase in stability for all the non cohesive sediments; hence biostabilization of non cohesive sediments (even in the range of fine gravel) in a condition of a mature biofilm is significant factor that needs to be taken into account in models of sediment erosion. However the values that have been experienced are an order of magnitude lower than the increase in stability presented in the literature for smaller cohesive or fine sand sediments (Patterson, 1997).

Growth time: biostabilization maxima occur following 4 weeks of growth, an in general larger stability was achieved after a period of growth of 3 weeks. This

coincides with the time necessary to generate the smoothing phase described by Noffke *et al*. (2001; see section 4.4.1). From figure 4.10, the fixation stage (week1) induces a significant effect only in the sand size sediments, whereas gravel size sediments see their stability increased after a mature biofilm is generated.

Material size: SGS was the substratum more responsive to biostabilization, presenting the highest value of biostabilization; this was somehow expected knowing from the literature that biostabilization occurs for fine sands (Paterson, 1997); hence some degree of stability for a sediment size up form the data published in the literature was expected to be seen. The natural sediments present the highest biostabilization potential: this could be due to the fact that the different surface charge of the grains and the metal content might have influenced the biofilm to grow in larger amount (see section 4.4.3) and with a structure different from the SGS due to their irregular shape.

Material type: no specific relation can be extrapolated looking at the material type, since both SGS and natural sediments presented the highest degree of biostabilization.

An interesting finding from figure 4.10 is that in case of sand, for week 2 and week 3 of growth, the Yalin criterion suggested that the area analyzed was at threshold before the critical entrainment for abiotic sediment was reached. This can be explained looking at the LS immediately after the application of the first flow (1.31 l/s) for week 2 and week 3 (see figure 4.11). In chapter 3 it was stated that the SS videos were taken in the centre of the cultured box; week 2 of growth presented a bio-mat colonizing the sample at the beginning of the experiment, which was swept away as soon as the first flow was applied. This generated a general perturbation of the surface sediments, leaving some of them loose and prone to be entrained. This suggests a phenomenon of "bio-destabilization". In case of week 3 of growth the situation is quite different. Figure 4.11B shows that the centre of the box is not the representative area of investigation for the erosion pattern. This is one of the limiting factors arising from the application of the **Yalin criterion: although it allows to clearly defining a critical entrainment threshold value, it doesn't account for the variability and patchiness that can take place spatially during the erosion of**

biotic sediment. In week 3 the video focussed on an area that became scoured, so that faster velocities could take place, inducing sediment erosion to occur even at lower threshold conditions compared to clean sediment. Therefore, in order to compensate for the estimation of the threshold relative just to a portion of the area, the LS was analyzed, to quantify the remaining area covered by biofilm after the application of different flow steps. As seen figure 4.11B, large part of the LS was still biostabilized but this did not come across from the application of the Yalin criterion. The need for a comprehensive analysis of the total area erosion led to the generation of the LS results presented in section 4.4.6.

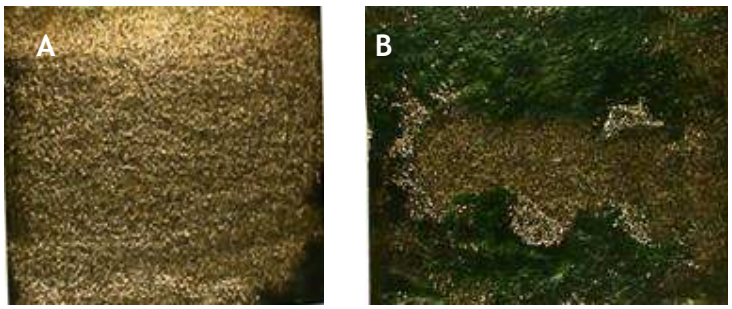

Figure 4. 11. Sand experiment at the LS after the application of the first flow step (1.31l/s): A) week 2 of growth; B) week 3 of growth.

Next section will indicate that no clear relationship can be found among time of growth, biomass and critical shear stress for the different material analyzed.

4.4.5 Critical shear stress from Yalin and relationship with biomass

When time of growth, relative biomass (section 4.4.3) and Yalin critical shear stress τ_c (section 4.4.4) are plotted against each other (figure 4.12) it can be seen that no real trend is evident among the variables. This contradicts some of the findings presented in the literature, for which positive correlations have been demonstrated for biomass and stability of very fine particles (Yallop *et al.*, 2000; Rigehtti and Lucarelli, 2010). Hence we suggest that extra caution needs to be taken in using any biological variable (EPS, biomass, chlorophyll *a*) as a proxy for stability and parameterize these into engineering equations for

sediment transport, as advocated some researcher have already attempted (see Black *et al*, 2002 for a review).

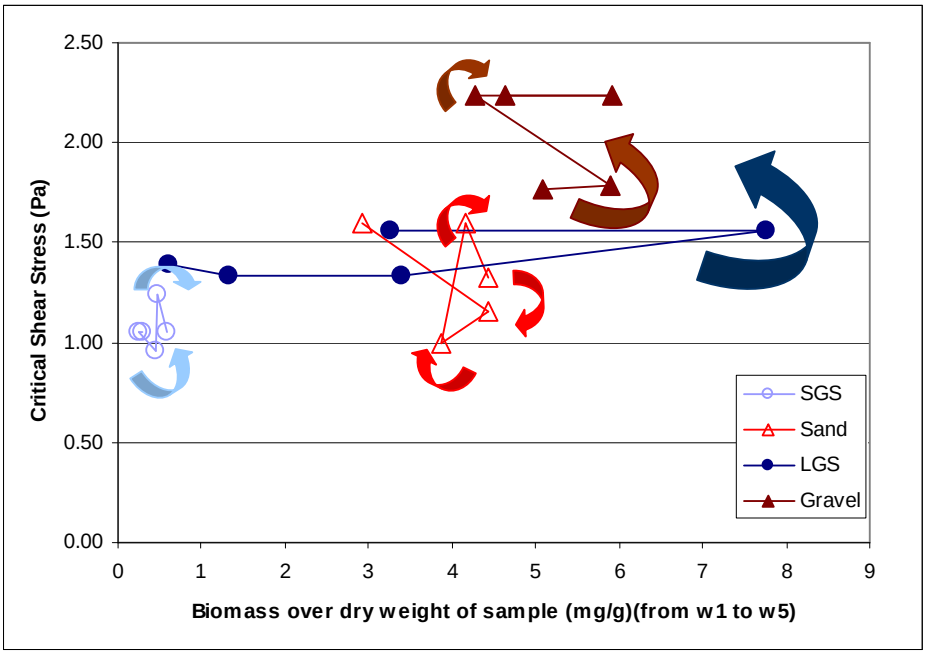

Figure 4. 12. Relative biomass (mg/g) in time (increase growth time from left to right) against critical shear stress τ_c. As it can be seen form the graph no evident relationship exists among time of growth, biomass and critical entrainment threshold. For time direction follow the relavant coloured arrow.

Correlations have been calculated for each of the materials between relative biomass and critical shear stress at threshold τ_c; the results show negative correlation (~-0.40) for natural sediments (sand and gravel), whereas the correlation is positive for artificial sediments (0.11 for SGS and 0.67 for LGS). Apart from LGS, the values are too low for confidently establishing a relationship among entrainment threshold and relative biomass.

Section 4.4.6 will present the erosion results at the large scale (LS), in order to be able to obtain a better evaluation of the spatial processes taking place in the heterogeneous surface of biofilm and sediments.

4.4.6 Biostabilization data: relationships between critical shear stress at entrainment and time of growth – large scale (LS)

Section 4.4.4 has shown that the Yalin criterion is efficient in finding a specific and objective threshold of motion for biotic sediments. This is a major improvement compared to the visual assessment used by researchers to quantify the erosion threshold (Grant and Gust, 1987; Leliveld *et al.*, 2003). However, testing week 2 and week 3 of growth for sand (section 4.4.4) it was evident that the Yalin criterion (1972) might not get the full trend of the stability/erosion because only applied to a ~4% of the total area. In order to obviate to this partial evaluation of the erosion picture, a LS image analysis was carried out on the still images at the beginning and at the end of every flow step, in order to account for the percentage erosion of box0.2 at different flow stages.

Before presenting the results of the LS analysis, an interesting observation was made after carrying out the experiment presented in section 4.4.2. The SGS testing was the first time in which I could assess how biofilm growth affects the stability of the sediment surface, without having any information on the depth of the biofilm colonization. However it was clear to me observing the erosion patterns in the Shields flume that only the top layer of the sediments (~2*D*) looked biostabilized. Once this cohesive layer (where biofim was embedding sediments) was removed, sediments below were clearly at threshold. The behaviour of the non-cohesive sediments used in my experiments is significantly different from the erosion of cohesive sediments; Type I erosion (Sanford and Maa, 2001), for which τ_c increases going further into the bed, was completely absent from my observations. In natural environments, sediment deposits are the result of erosion and deposition cycles, where colonized sediments can be found deeper into the bed compared to my system; this ensures higher biostabilization. Type II erosion (Sanford and Maa, 2003), where τ_c is constant and does not change with the depth of the sample was initially considered as a possible scenario: however, it was very evident to me that as soon as the bio-mat was removed (which is this composite layer of biofilm/sediments present in case of strong biostabilization), the sediments behaved as non-cohesive and lost all the biotic strength. The bed shear τ_b was seen to exceed the critical τ_c for abiotic sediments until a failure of the bio-mat occurred; this was followed by a

very fast erosion of the sediments layers below the surface, which did not present any biostabilization potential. The result was a mix of areas that had been completely eroded (hence with lower elevation compared to the original sample) and areas where the biofilm was so strong that no erosion was evident, as can be seen in figure 4.13.

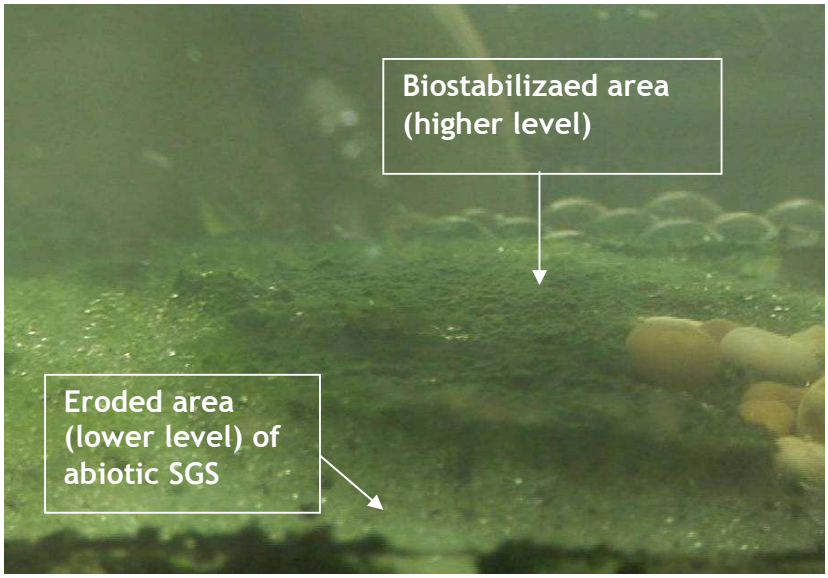

Figure 4. 13. Side view of a typical erosion experiment of box0.2 (SGS), with flow from left to right. The downstream end of box0.2 showed a strong biostabilization and hence this portion of the bed was not eroded; upstream the biofilm growth wsa weaker and, after the surface layer was eroded, the rest of the sediment layers were at threshold so that the bed surface was lower than that of the biostabilized region. (Length Scale 90mm).

Erosion took place differently depending on the areal distribution of strong biostabilization. In order to better understand this concept image analysis at the LS was carried out and the results for the percentage area eroded versus the bed shear stress τ_b for the four different materials are presented below.

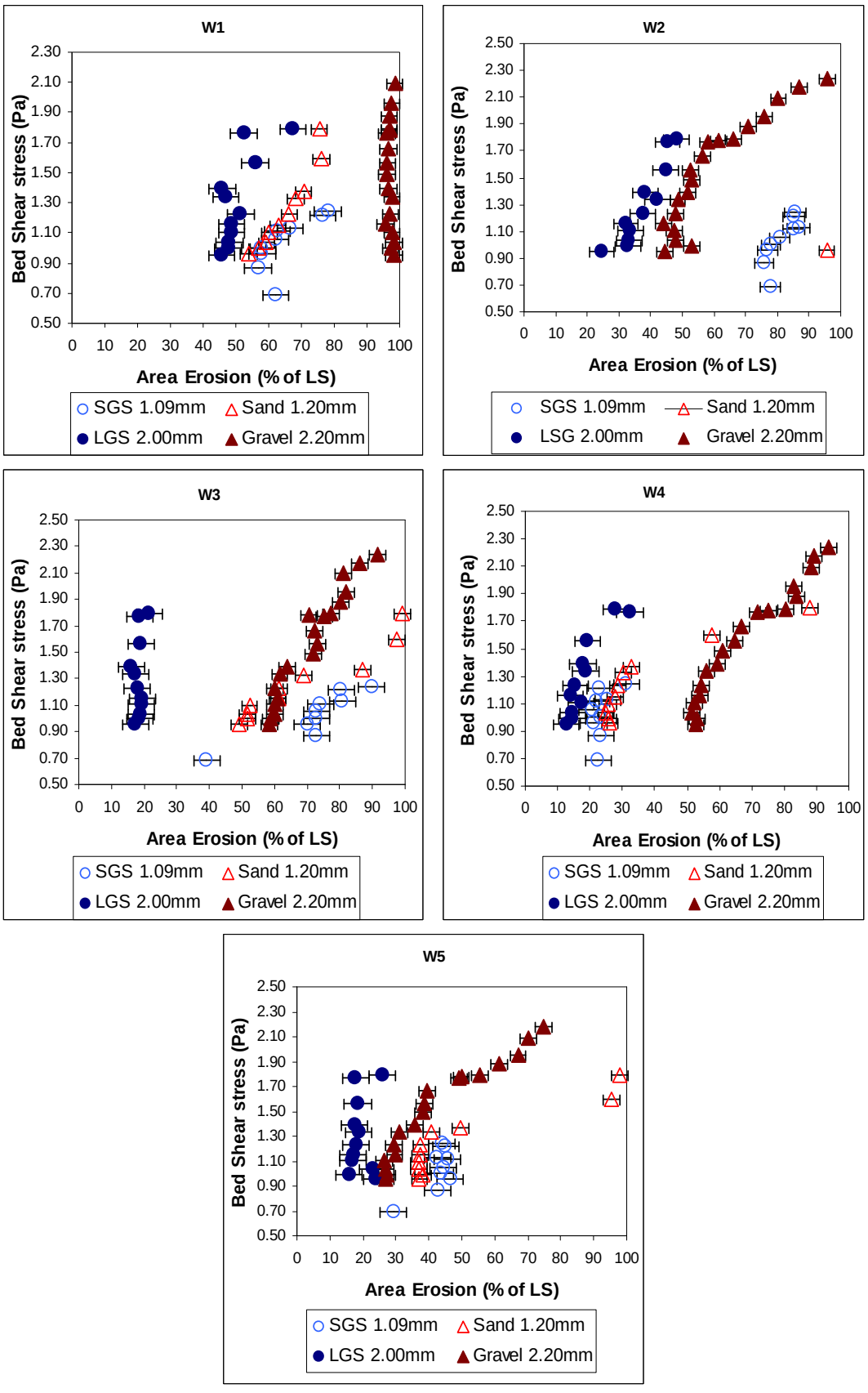

Figure 4. 14. Area erosion (%) of the LS at the end of each flow steps vs the relative bed shear stress for the 4 materials in time. Error bars are up to 9% for glass material and 5% for natural sediments.

The results on figure 4.14 allow identification of key findings of the areal erosion due to increase in bed shear stress τ_b:

Absolute data: once the first flow steps are applied, a percentage of the area is eroded (going from a minimum of ~ 10% for mature biofilm to a maximum of 60% for early fixation stages), yet leaving a significant portion of the box still covered by biofilm and hence biostabilized. This highlights the importance of assessing the erosion at the full scale, especially due to the heterogeneity of the biofilm and the possible patchy erosion of it. Hence the SS an LS should always be coupled in order to understand the full erosion process.

General trend: the initial erosion remains very stable (almost generating a vertical line) when low flow steps are applied; only once the flow steps reach the middle of the range significant erosion (higher than 10-15%) is identified. This is not valid for the case of early biofilm colonization (e.g. gravel in week 1, where no biofilm was found so that the colour of the natural grain prevailed in the segmentation process). If we consider high flow applied to stable bio-mat (e.g. week4 for SGS), the percentage coverage is still high at the end of the experiment (~35%); this suggests that the remaining conditions will be very different in terms of roughness and generated flow structure. This condition can be classified as "patchy erosion".

Growth time: The relationship that is visible from the graph shows that the longer the growth period, the lower the erosion occurring.

Material size: Interesting to notice is that using the Yalin criterion (section 4.4.4) induced us to think that LSG had a lower value of stability compared to the other material. Figure 4.14 shows a different trend at the LS. LGS is in every experiment the material that presents the highest percentage of green pixels throughout the experiments, hence the one having a high degree of biostability.

Material type: no clear trend can be seen according to the different material used.

In terms of the time of application of the flow steps and the assessment of the erosion that these induced, analysis of the images at the beginning and at the

end of the flow steps show that very few differences would take place in the histogram of pixel intensity after the 10 minutes SGS and the 5 minutes for the rest of the experiments. Only in case of the last high flows, a significant degree of erosion between beginning and end of the flow step could be detected. This seems to suggest that the erosion is more related to an increase in τ_b instead of to the time of application of it. However, the author reserves the possibility that the duration of flow application was not long enough to see the time effect taking place. The scope of this project was to primarily identify a threshold of motion that could be easily defined with a hydraulic variable, such as flow or bed shear stress more than time. More research is needed in order to confidently state that time duration of the flow step has a lower effect than an increase in shear stress on the bio-mat. Some progress in this sense can be found in chapter 5, where flow steps were applied for 15 minutes.

In order to compare the results obtained in section 4.4.4 at the SS, in table 4.2 it is possible to find the critical shear stress τ_c according to Yalin and the correspondent area erosion (%) obtained from the segmentation of the LS. In almost all the cases the threshold of entrainment at the SS corresponded to a partial area erosion of the box0.2; in particular for LGS every Yalin threshold corresponded with less then half of the biofilm eroded from the box. Interestingly, for gravel experiments, the percentage of green pixels is lower at the Yalin threshold and goes from 45% to 4%: this could be due to the fact that single streamers attached to the top of the grains could not be resolved at this scale of investigation; instead the segmentation identified solely the sediment colours. However, from the Yalin criterion (section 4.4.4), it was seen that the bed resulted biostabilized, and this could be due to the effect of the spongy biofilm with its streamers on the applied flow field. This is not a new phenomenon: researchers found that biofilm streamers could change the flow characteristics around colonized sediments (Nikora *et al.*, 1998) and either increase or decrease the hydraulic roughness of the bed (Salant, 2011 for a review). This again stresses the importance of the coupling of SS and LS analysis: if used separately a full trend could not be resolved.

SGS	Yalin τ_c (Pa)	% Area eroded
w1	1.05	62
w2	1.05	81
w3	0.96	70
w4	1.24	31
w5	1.05	44
sand		
w1	1.60	76
w2	1.15	***
w3	1.00	73
w4	1.60	58
w5	1.33	41
LGS		
w1	1.39	46
w2	1.34	42
w3	1.34	17
w4	1.56	19
w5	1.56	18
gravel		
w1	1.77	96
w2	1.79	66
w3	2.24	92
w4	2.24	94
w5	2.24	75

Table 4. 2. The Yalin critical shear stress τ_c for the SS is compared to the relative % area eroded at the LS. Mature biofilm for SGS and sand present an erosion at the threshold for the Yalin technique that is less than half the box coverage, similar trend can be seen for LGS and higher values of erosion are identified for gravels, due to the absence of a mat and the impossibility at this scale to resolve the single streamers.

In order to obtain a trend out of the graphs presented in figure 4.14, different fits were applied to the graphs to identify the best mathematical equation relating the % erosion to the shear stress. The regressions used are: i) linear; ii) power law; iii) logarithmic and iv) exponential; the relative expressions of the equations can be found in equation 4.5.

$$\begin{aligned} &Linear: \tau_b = a(Area_{Erosion}) + b; \\ &Power: \tau_b = a(Area_{Erosion})^b; \\ &Logarithmic: \tau_b = a\ln(Area_{Erosion}) + b; \\ &Exponential: \tau_b = ae^{bArea_{Erosion}} \end{aligned}$$

Equation 4. 5

An example of testing the goodness-of-fit of the different forms of regression equations presented in equation 4.5, an example is shown below in figure 4.15

for gravel in week 4. Here it is evident that linear and logarithmic fits generated the highest value of R^2. Therefore these two fits were chosen as the most applicable and more statistical information on their fit are presented below in table 4.3.

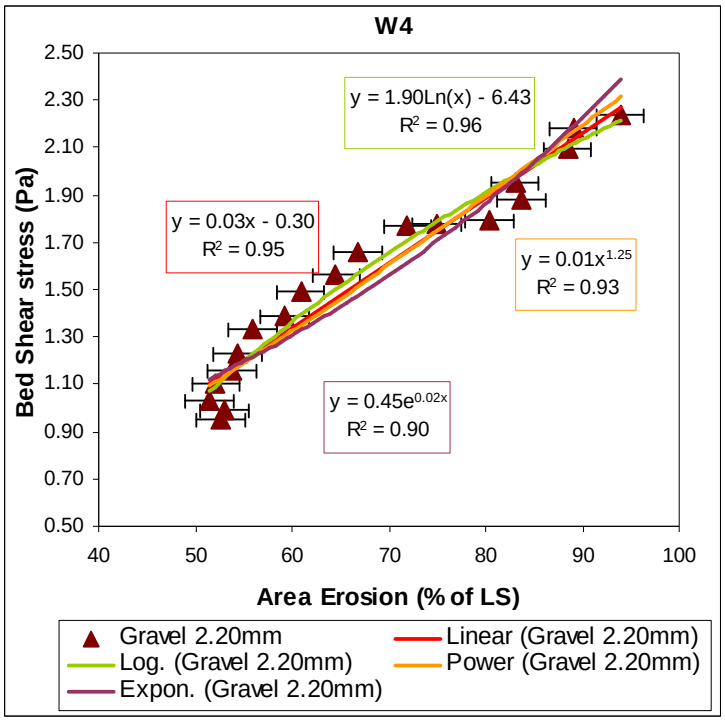

Figure 4. 15. Example of linear, power, logarithmic and exponential regression fits to the gravel results for week 4 of growth. See that the coefficients match those in table 4.3.

Table 4.3 presents the coefficients *a* and *b* found in equation 4.5 for linear and logarithmic regressions, together with the associated *p-values* and R^2.

	Linear						Logarithmic					
w1	**a**	**p**	**b**	**p**	**R2**	**N**	**a**	**p**	**B**	**P**	**R2**	**N**
SGS	0.02	0.03	0.02	0.97	**0.50**	**9**	1.05	0.03	-3.35	0.09	**0.50**	**9**
LGS	0.03	0.01	-0.46	0.41	**0.55**	**11**	1.95	0.01	-6.34	0.02	**0.56**	**11**
Sand	0.03	0.00	-0.96	0.00	**0.92**	**10**	2.19	0.00	-7.87	0.00	**0.90**	**10**
Gravel	-0.05	0.66	6.31	0.56	**0.01**	**17**	-4.82	0.66	23.55	0.64	**0.01**	**17**
w2												
SGS	0.03	0.01	-1.66	0.05	**0.67**	**9**	2.69	0.01	-10.79	0.01	**0.67**	**9**
LGS	0.04	0.00	-0.16	0.42	**0.87**	**11**	1.36	0.00	-3.60	0.00	**0.81**	**11**
Sand	***	***	***	***	***	**1**	***	***	***	***	***	**1**
Gravel	0.02	0.00	0.06	0.71	**0.83**	**19**	1.65	0.00	-5.15	0.00	**0.87**	**19**
w3												
SGS	0.01	0.00	0.21	0.21	**0.81**	**9**	0.65	0.00	-1.73	0.02	**0.77**	**9**
LGS	0.07	0.32	0.02	0.99	**0.11**	**11**	1.19	0.36	-2.17	0.56	**0.09**	**11**
Sand	0.01	0.00	0.34	0.01	**0.92**	**10**	0.96	0.00	-2.76	0.00	**0.92**	**10**
Gravel	0.04	0.00	-1.17	0.00	**0.94**	**19**	2.77	0.00	-10.21	0.00	**0.95**	**19**
w4												
SGS	0.02	0.02	0.59	0.01	**0.49**	**10**	0.60	0.02	-0.85	0.25	**0.49**	**10**
LGS	0.04	0.00	0.48	0.01	**0.82**	**11**	0.96	0.00	-1.46	0.00	**0.87**	**11**
Sand	0.01	0.00	0.81	0.00	**0.82**	**10**	0.61	0.00	-0.88	0.01	**0.89**	**10**
Gravel	0.03	0.00	0.11	0.01	**0.95**	**19**	1.90	0.00	-6.43	0.00	**0.96**	**19**
w5												
SGS	0.02	0.03	-0.02	0.97	**0.52**	**9**	0.91	0.03	-2.38	0.09	**0.53**	**9**
LGS	0.01	0.68	1.06	0.10	**0.02**	**11**	0.26	0.68	0.54	0.77	**0.02**	**11**
Sand	0.01	0.00	0.75	0.00	**0.81**	**10**	0.64	0.00	-1.19	0.01	**0.84**	**10**
Gravel	0.02	0.00	0.53	0.00	**0.92**	**18**	1.05	0.00	-2.37	0.00	**0.96**	**18**

Table 4. 3. Linear and logarithmic regressions and relative coefficients *a* and *b* presented in equation 4.5 plus *p-values* and R^2. Frome the table it is evident that in time the best regression is the logarithmic. However in some cases the logarithmic regression R^2 is as low as R^2 = 0.01. In red are highlighted the *p*<=0.05.

Looking at table 4.3 the best fits can be identified in the logarithmic regression, which has the highest R^2 and lowest *p-values* when compared to the other methods. However the method doesn't work properly in all the situations (e.g. week 1 for gravel has R^2=0.01 and week 3 for LSG has R^2 =0.09). This might reflect the fact that once a catastrophic failure of the membrane occurs or for a very initial stage of colonization, the trend of erosion is different from what seen in the majority of the other cases, resulting in the vertical lines that can be seen in figure 4.14 in correspondence of week 1 and week3 for respectively gravel and LGS.

4.5 Chapter summary

The conclusions from this chapter are:

- According to the Yalin technique, the threshold of entrainment for non cohesive biotic sediments was reached after 43% to 30% more τ_b was applied for sand size sediments and from 35% to 17% for gravel size sediment compared to abiotic sediments;

- Entrainment of sand size sediment when a mature biofilm is present cannot be considered as a single grain pivoting, such as the conventional models of sediment transport assume (Wiberg and Smith, 1987); instead clumps and bio-mats can be seen and need to be better addressed;

- Longer culture ensure generally larger stabilization; in particular week 4 of growth has been considered as the strongest colonization period;

- SGS present the highest biostabilization potential at the SS using the Yalin criterion; however Yalin cannot be used alone for biotic sediment but a combination of scales needs to be used if full assessment of the erosion properties is desired. In many case in fact, even if at threshold according to the Yalin criterion, the LS presented almost 50% of the biofilm coverage still intact. Hence this finding relates the erosion process directly to space and location of the area of erosion. This is something that has not been investigated previously. Researchers instead correlate mass of erosion to bed shear stress, without locating the stability in a bed.

Moreover this chapter has presented the evidence that the Yalin technique at the SS and the segmentation at the LS need to be coupled for the best result to be obtained. From the LS in fact it is possible to obtain new level of information in terms of scale, something that was missing from the Yalin criterion. However, in case of streamer and fixation stage of growth, it is difficult to resolve their presence on natural sediment at the resolution used in the LS (6 pixels/mm) of the biofilm in natural sediment. Hence the coupling of the Yalin at the SS and of

the LS allows a thorough investigation to be carried out and therefore this combined analysis will be pursued also in chapter 5.

CHAPTER 5

Series 1 experiments: length scale 1m

"To study the laws of Nature does satisfy the mind, but it also does serve an utilitarian purpose: …The theory must be applied to the practice…"

duBuat, "Principes d'Hydraulique", 1786

5.1 Introduction

This chapter will present the erosion threshold results over 1m length test beds (box1) after up to 4 weeks of biofilm colonization for the four materials: SGS, sand, LGS and gravel. Based on preliminary data (chapter 4), 4 weeks have been considered sufficient to generate effectively the strongest biostabilization and decision to truncate the data set at this timeframe therefore aligns with the overall objective of this thesis.

Based on the findings and critical evaluation of the results obtained in chapter 4 for box0.2, it was obvious that the following points needed to be addressed in the experimental design of chapter 5 for achieving a more scientifically robust dataset: i) *environmental conditions at growth*, to ensure the highest biostabilization potential for all the materials; ii) *box length scale*, to be more representative of real river scale and to include spatial homogeneity/heterogeneity of biofilm growth; iii) *flow control during testing*, to ensure that low flows applied could be hydraulically controlled within low error bounds. Each associated methodological improvement is detailed and defended in section 5.3.

In addition, resolution of the underpinning process controls of biostabilization in chapter 4 was determined to require additional data collection in this chapter:

1) modification of the flow conditions due to the presence of the biofilm on the sediments: this will be assessed using PIV and will permit evaluating the hydraulic roughness changes at the different stages of growth and the relative average flow condition (see section 5.5.7); 2) possible relationship between spatial erosion and bed shear stress: chapter 4 has suggested that a logarithmic trend between these variables may best fit the data however only by increasing the area of observation (from box0.2 to box1) can these spatial trends be robustly resolved; 3) biological variables relationship to investigate the increase in biostabilization with time: this is an extremely important concept based on the idea that biological information could be used as a proxy for stability in sediment transport equations and has been auspicated by many researchers focussing on field studies (Black *et al.*, 2002). Hence in this chapter both biomass and EPS content (considered fundamental for biofilm adhesive property hence for the increased stability of sediments (e.g. Gerbersdorf *et al.*, 2011)) will be investigated.

The following sections include: the hypotheses (section 5.2). Methodology (section 5.3), subdivided into flume set up for obtaining controlled steps of uniform flow; the identification of the threshold of motion at the SS (Yalin, 1972) and at the LS (image segmentation); protocol followed to investigate the EPS. Section 5.4 will present the results subdivided into: representative growth assessment; biomass and EPS; biostabilization at the SS and LS and PIV investigation of the flow field modification.

5.2 Hypothesis

The hypotheses presented in this chapter follow from careful consideration of the preliminary results (see chapter 4). In particular the assumptions made are listed below:

1. *Colonization*: biofilms would grow in a more natural form reducing the presence of trapped bubble of oxygen (Noffke *et al.*, 2001), identified in chapter 4 as a weakness of the bio-mat;

2. *Biostabilization potential:* it would be higher for every material than in chapter 4, due to the improved growth conditions;

3. *Time of growth and stability*: As seen in our previous dataset and as presented in the literature by many researchers (Yallop *et al*., 2000), it was expected that the longer the growth time, the more the stability;

4. *Scale of growth*: the scale of growth would have a large effect on biostability and bio-mat development;

5. *Biological factors*: Biomass was not expected to vary in trend from the preliminary experiments, a part from LGS and gravel, which herein were exposed to higher flow at growth hence the growth conditions could have changed. EPS were also measured and more EPS were expected to be found for higher biostabilization;

6. *Erosion process:* due to improved growth conditions bio-mat and hence the carpet like erosion would be seen also for larger sediments;

7. *Material:* SGS would present the highest stability for shape, size and material reasons.

5.3 Methodology

This section presents the uniform flow set up in the Ervine flume (see chapter 3, section 3.6) and the relative bed shear stresses τ_b generated (section 5.3.1). Section 5.3.2 shows the calibration of the PIV data, proving that the PIV could resolve within a 10% error the bed shear stresses calculated in section 5.3.1. In section 5.3.3 the information relative to the Yalin criterion ε (1972) will be illustrated (for the equation see chapter 4, section 4.3.2) at the SS; in section 5.3.4 information of the segmentation area and technique at the LS will be given; the technique used is the same as presented in chapter 4, section 4.3.3. Finally in section 5.3.5 the methodology to obtain the EPS results will be shown.

5.3.1 Flume set up

The overall programme is provided in chapter 3 with full instrumentation and methodological details. Specifically, Ervine flume modifications for the present data set intended to reduce uncertainty in the testing of biostabilization compared to the Shields flume data collected in chapter 4. Improvements were: 1) lower pump range (0-15l/s) and *Jaguar XJ* controller with P.I.D. system (see chapter 3, section 3.6) to minimize flow variations to ±1% for every uniform flow step; 2) use of a PIV system for flow field characterization and objective assessment of the temporal development of eco-hydraulic variables during biofilm growth.

Seven flow steps were applied ranging from 1.6l/s to 11l/s; these were designed to assess the full erosion of box1, hence larger shear stress increments (from 0.17Pa to 0.33Pa) were applied compared to those of chapter 4. The steps of uniform flow were investigated prior to any of the experimental testing and assumed constant during the testing and they were applied for a 15 minute period. This timeframe is justified as it permitted enough time to: i) collect 3 series of 2000 PIV images and download them; ii) record 5 minutes video at the small scale for Yalin criterion assessment of entrainment threshold. The UF set up was established filling the 1m testing section with gravel in the range of 4-6mm (see chapter 3, section 3.6.1). The hydraulic variables calculated using the geometry of the bed for the UF set up can be found in Appendix 5.A. The equations used for calculating the bed shear stresses τ_b are the same as equation 4.1 and 4.2 in chapter 4. Improvement to the low flow control also provided better approximation of the bed and water level slope to 1/200; these errors were <±6% for low flow steps (1.6l/s to 5l/s) and between ±9-13% for higher discharges. Based on this accuracy and temporal variability of data, a 1/200 slope has been assumed in all calculations and the Einstein (1942) equation correcting for the wall effect was preferred to the Meyer-Peter and Müller equation used in chapter 4. Further evidence to support this methodological approach is provided in the following section, in terms of good approximation of calculated bed shear stresses compared with measured PIV data.

5.3.2 PIV calibration

To verify that the set up of the PIV was reading the same flow values as the *Portaflow SE,* the system was calibrated for the UF set up presented in section 5.3.1 The camera was mounted to a capture angle matching the 1/200 gradient of the flume and positioned at a distance from the flume's glass side wall which permitted the maximum flow depth to be observed (max FoV of x = 77.6mm y = 62.1mm). Once this was done, a metallic ruler was placed in the centre of the flume perpendicular to the camera and the flow was started and the laser was activated, making sure that the ruler was exactly in the same plane of the beam (see chapter 3, section 3.6.2.3 for pictures of the process and information on the set up); the camera was then focussed on it and a still image of the ruler was captured, which will be used as the calibration file. All experiments employed identical set-up and camera focus, in order to keep the same comparable set up for every experiment.

The resolution of the calibration image was calculated as 16.50pixels/mm. Fundamental for the data collection was the setting up of the "time in between pulses (μs)" (Δt in chapter 3, section 3.6.2.2, set to be equal to the Hertz rate (HZ) in single frame mode), which would dictate the time between consecutive images; physically this is identified by the closing of the camera shutter. In order to find the correct value of Δt for every flow step used in the experiment (see Appendix 5.A), equation 3.2 was applied; this is considered appropriate, since flow and FoV were known. In particular it is good practice to set Δt so that seeding particles would move only of ¼ of the entire length of an Interrogation Area, IA (personal communication with Dr J. Cooper). Pilot data showed that this condition was best obtained for an IA equal to 64*64 pixels (see chapter 3, section 3.6.2.2). Hence the following variables were calculated:

Q (l/s)	*U* (m/s)	*N* images	*T* between pulses (μs)	HZ	Recorded time (sec)	*n* vectors (*nx*ny*) for IA=64, 50% overlap	FoV adjusted (pixels)	FoV adjusted (mm)
1.6	0.30	2000	3264	306	6.5	270 (30*9)	1000*344	60.61*20.85
2.6	0.35	2000	2777	360	5.6	360 (30*12)	1000*424	60.61*25.70
3.6	0.41	2000	2343	427	4.7	420 (30*14)	1000*512	60.61*31.03
5	0.45	2000	2141	467	4.3	540 (30*18)	1000*624	60.61*37.82
7	0.53	2000	1836	545	3.7	660 (30*22)	1000*776	60.61*47.03
9	0.57	2000	1697	589	3.4	780 (30*26)	1000*888	60.61*53.82
11	0.62	2000	1569	638	3.1	870 (30*29)	1000*984	60.61*59.64

Table 5. 1. PIV variables set up: *T* in between pulses is the *Δt* in equation 3.2; HZ is the Hertz rate, matching the Time in between pulses (μs); *n* vectors is the total number of vectors per flow step; FoV adjusted is the dimension in pixels of the resulting field of view taken into consideration. *X* is taken as the downstream direction (length), *y* is the vertical direction (flow depth).

Considering the FoV, it is important to note that of the original 1280 longitudinal pixels only a central portion of 1000 pixels was selected in the final analyzed FoV; this was done to avoid the physical appearance in the images recorded of the "intensifier" (in the shape of a black circle at the edges of each image). The vertical dimension was regulated for every flow step to be only sufficient to resolve each individual flow depth; unwanted areas of the image were masked using the processing software (*DynamicStudio)*, in order to avoid the generation of unwanted vectors and reduce processing time (adjusted FoV is given in table 5.1). The above set up allowed resolving 60mm in the longitudinal direction and 20.6-59.04mm in the vertical.

In table 5.2 the results for the calibrated bed shear stress τ_b over a bed comprised by gravels 4-6mm can be found. Double averaged technique introduced by Nikora *et al*. (2001) was used, which couples space and time average to obtain a single velocity profile. At this point the Law of the Wall (chapter 2, section 2.2.2.3) was applied to the bottom 20-40% of each double averaged profile in order to obtain the roughness z_0 value and the bed shear stress $\tau_{b.}$ Table 5.2 shows that the results from the PIV are in good agreement with those found using the geometry of the flume (always lower than ±10%). Moreover the correlation among shear stresses calculated with the depth-slope equation and those obtained using the PIV is high and equal to 0.98.

Flow (l/s)	Flume *U* (m/s)	Flume τ_b (Pa)	PIV τ_b (Pa)	z_o (mm)	% Error (-)	% Error (+)
1.6	0.30	0.84	0.96	2.06	-7%	7%
2.6	0.35	1.14	1.07	2.86	3%	-3%
3.6	0.41	1.31	1.32	2.77	0%	0%
5	0.45	1.64	1.77	2.81	-4%	4%
7	0.53	1.91	2.04	3.82	-3%	3%
9	0.57	2.23	2.68	2.53	-9%	9%
11	0.62	2.48	2.65	2.58	-3%	3%

Table 5. 2. Comparison of the UF set up bed shear stress τ_b (flume) versus the values for τ_b obtained using the Law of the Wall on the double averaged profiles obtained with the PIV.

What is presented above provided confidence that the measured flow characteristics in the Ervine flume could be used for undertaking good scientific experiments. In section 5.3.3 the set up for the application of the Yalin technique will be presented.

5.3.3 Yalin technique and abiotic thresholding

As seen in chapter 4, the Yalin technique resulted to be a good and objective method to assess locally if biostabilization is taking place, hence it was used for the definition of the entrainment threshold at the small scale (SS) in this chapter. This data was also compared to the large scale (LS) areal thresholding (see section 5.3.3) for a comprehensive analysis of the erosion process. The theory of the technique can be found in chapter 4, section 4.3.2. According to the Yalin technique, in this set of experiments the numbers of particles that need to move from the selected area A to define the flow at threshold of motion are presented in the table below:

	A (cm*cm)	*t* (s)	*N*	Error (particle)	Total *n*	*N/n*
SGS	5.2*2.9	60	**9**	3	1269	1%
Sand	5.2*2.9	60	**7**	2	1047	1%
LGS	5.2*2.9	60	**2**	0	377	1%
Gravel	5.2*2.9	60	**2**	0	312	1%

Table 5. 3. Summary of the variable used in the Yalin criterion (1972) for box1. A (cm^2) is the area analyzed, *t* (s) the time, *N* the number of grains at threshold according to the Yalin criterion, error is the maximum number of particle that can be miscounted; n is the total number of particle in the areas *A*, *N/n* the portion of the area which defines the flow at threshold.

The zero error for gravel size sediments is due to the smaller number of grains in the field of view of the camera, which was not modified from sand to gravel sediments. The camera was left in the same position as for sand size sediments to allow the macro function to work: this function allows zooming in to a smaller area (~4% LS) and it works when the camera is at least 1m distant from the sample; higher positions would have compromised the resolution of the LS and hence were avoided. After the application of the Yalin technique for the four abiotic sediments it was evident that SGS, Sand and LGS were already at threshold for the first flow step applied (see Appendix 5.A). However, choosing lower flow steps was not possible due to the poor control in the flow variability that would have been generated. Hence a value for abiotic sediments read on the Shields curve (see chapter 2, section 2.2.2.3) was used to obtain the clean reference movement for every abiotic material used (SGS, sand, LGS and gravel). To do this, the fitted line to the Shields curve proposed by Soulsby and Whitehouse (1997) was used for the identification of the threshold of motion; this is justified because the curve is a good fit of the Shields curve for intermediate grain sizes (sand and gravel) such as the one used herein (it performs poorly for very fine grains for which $D_*<1$, however this is outwith the size fraction range used in this thesis). The expression of the Soulsby and Whitehouse (1997) curve is presented below:

$$\tau_c = \frac{0.3}{1+1.2D_*} + 0.055[1-\exp(-0.02D_*)] \qquad \textbf{Equation 5. 1}$$

Where D_* is the dimensionless particle size diameter, defined as:

$$D_* = \left[\frac{g(s-1)}{\nu^2}\right]^{1/3} D$$ **Equation 5. 2**

In which s is defined as ρ_s / ρ and ν is the kinematic viscosity of water.

	D_* Soulsby and Whitehouse (1997)	θ Shields parameter (1997)	τ_c (Pa) Soulsby and Whitehouse (1997)
Abiotic SGS	28	0.032	0.52
Abiotic Sand	32	0.034	0.65
Abiotic LGS	51	0.040	1.18
Abiotic Gravel	58	0.042	1.50

Table 5. 4. Based on Soulsby & Whitehouse (1997) calculation this table gives the dimensionless grain diameter D_*, knowing that sand ranges among 1.2< D_* <40 and gravel D_*> 40; the critical Shields parameter θ and bed shear stress τ_b as calculated from an approximation of the Shields curve by Soulsby and Whitehouse (1997) for SGS, Sand and LGS and Gravel.

One important remark about the usage of the Yalin technique is that, without the usage of the glass plate on top of the water surface, the identification of the moving particles was much more complicated than in chapter 4, leading to larger errors in the identification of the movement (see table 5.3). However, it was believed that the elimination of the plate would have allowed better and more realistic hydraulic conditions to be achieved in an experimental set-up with such low flow depths (where use of a glass plate can artificially accelerate flows in a manner similar to an orifice plate). Moreover the Yalin technique validity will always be coupled in this thesis to the LS analysis, in order to back up any finding (see section 5.3.4).

The section below presents the set up used to investigate the erosion of the LS using the same image technique as seen in chapter 4, section 4.3.3.

5.3.4 Image segmentation for quantifying biofilm areal coverage

The erosion at the LS was investigated using image segmentation as presented in chapter 4 (see section 4.3.3 for theory of the technique). The area analyzed with the *Sony* high speed camera (see chapter 3, section 3.5.2) for box1 was located in the centre of the box and was of a size equal to 500mm by 280mm (resolution ~ 4pixels/mm). The still images were collected at the beginning and at the end of every flow step (15 minutes); however, since it was outwith the scope of this thesis to assess the effect of shear stress duration on erosion but more relevant was the increase in τ_b, only still pictures at the end of every flow step will be analyzed. All image set-up, analysis and uncertainty are identical to that outlined and discussed in section 4.3.3.

The section below will introduce the methodology used to assess the quantification of the EPS for the analyzed samples.

5.3.5 EPS analysis

EPS are known to increase the strength of attachment to sediments that biofilm have (Dade *et al.*, 1990); many researchers relate the stability of sediments to the relative content of EPS (e.g. Gerbersdorf *et al.*, 2008; Gerbersdorf *et al.*, 2011). In this thesis it was then necessary to assess the quantity of EPS and try to relate it to the stability of the sediments at different growth stages. In order to evaluate the concentration of EPS in the cultured box1, two different methods were used: i) a *quantitative method,* based on the equivalent glucose concentration of the EPS (μg/ml) and ii) a *visual technique,* using microscopy staining.

An important consideration is that the EPS values that will be presented in this thesis might differ sensibly from those obtained in the field; this is because researchers have experienced that bound EPS decreases when temperature increases (e.g. Gil *et al.*, 2010). In all the experiments presented herein and as seen in chapter 3, section 3.4.4.2, the culturing temperature (28°C) was much

higher than the average of a real river system. Caution needs then to be used in comparing the data in this thesis with results from field studies.

The former method was based on the concept of measuring EPS in terms of equivalent glucose concentration (Daniels *et al.*, 2007); using a spectrophotometer the reading of the EPS were then calibrated against a curve previously obtained using standards. Details of the methodology used, the protocol and standard calibration can be found in Appendix 5.B. Results for this technique can be found in section 5.4.3. This method was used because it is a direct quantification of the amount of EPS present in a sample; the second method shown below, was instead used to verify visually the spatial distribution of the EPS and to back up the results of the quantitative method.

The second methodology used a fluorescent microscope technique, which involves EPS staining as described by de Beer *et al*. (1996). Calcofluor (Fluorescent Brightener 28) was used as the staining chemical, for individuating polysaccharides (de Beer *et al*., 1996). The fixation of the calcolfuor took place by adding to 200mg of sample, a solution of 20 ml PBS with 30 g/l paraformaldehyde. After three washes in PBS, the samples were stained for 4 h in 20 ml PBS with 300 mg/l calcofluor. At this point single grains were glued to a microscope slide and observed under an inverted florescent microscope (with the DAPI function enabled), so that any stained EPS would appear bright blue.

Section 5.4 will introduce to the results of this chapter: section 5.4.1 will present the results of the improved growth set up for box1; section 5.4.2 will describe to the biomass results, whereas in section 5.4.3 the EPS results can be found, both quantitative and visual. section 5.4.4 will show the results related to the application of the Yalin technique at the SS and 5.4.5 to the LS; section 5.4.6 will correlate biomass, EPS and the biostabilization results at the LS to find any possible relation; Finally section 5.4.7 will present the PIV results, for flow statistics for every flow step, change in hydraulic roughness z_0 and bed shear stress τ_b will be shown.

5.4 Series 1 experiments results (4 weeks of growth)

5.4.1 Representative growth assessment

As discussed in chapter 3 and chapter 4 (section 4.3), the growth methodology was improved in box1 set of experiments, in order to obtain the strongest biostability for both sand and gravel size sediments (for more information on the setup see chapter 3.4.4.4). Critically, biofilm growth in this set of experiments took place predominantly in a "mat like" structure independent of grain size; this is distinct from the results obtained in chapter 4 where gravel size sediment indicated filamentous growth. This is visible in figure 5.1 below at the SS and could be due to: i) improved light source conditions, which by being uniform induced a more even growth to take place and no competition among bacteria for light; ii) a higher flow at growth, which insured more firmly attached condition and eliminated the unsecured biofilm at the top of the grains.

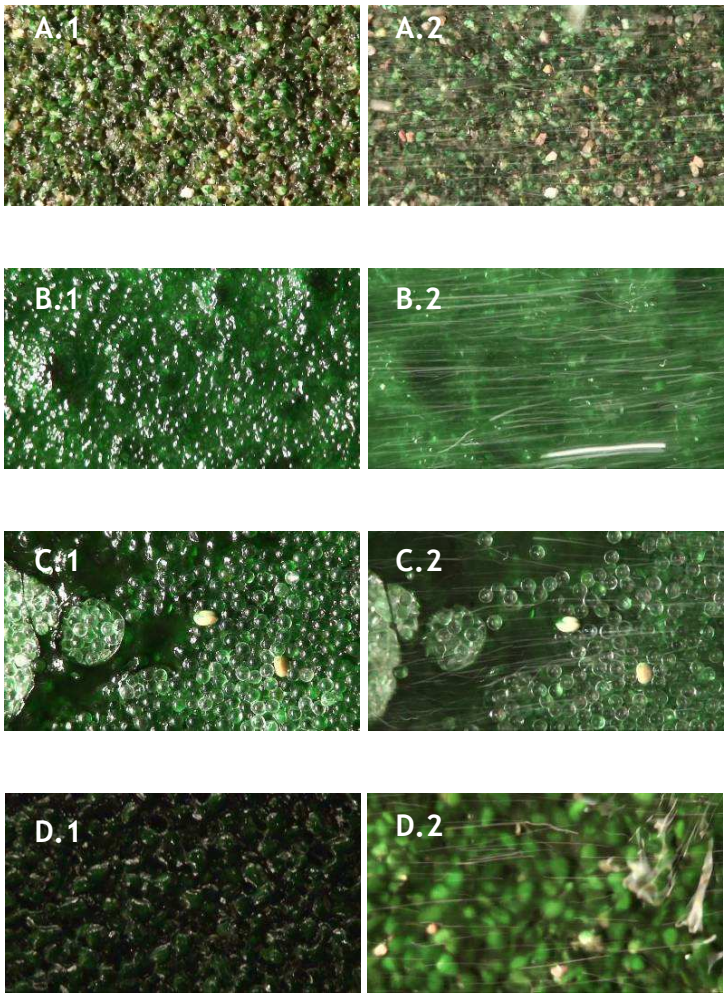

Figure 5. 1. Biofilm growth for box1 at the SS (Scale 52mm*29mm). A) Sand 1 week colonization; B) SGS 2 weeks culture; c) LGS 3 weeks of growth and d) Gravel 4 weeks old biofilm, where .1 is in dry conditions whereas .2 is wet. Flow from right to left and white streaks in the submerged flow image (.2) are light reflections from PIV seeding material.

Secondly, figures 5.2 and 5.3 show that the fixation stage for all sediment substrata occurs within 1 week of inoculation (according to Noffke *et al.*, 2001). For sand size sediments, figure 5.2(a, b) shows that in the first 2 weeks of colonization the growth took place in a very uniform form, allowing a smooth mat to generate. Any further week of growth presented a very patchy and loose bio-mat structure for both the materials (see figure 5.2c, d). This seems to suggest that, once the sealing process took place leading to the erosion of the bio-mat, this occurred in a very heterogeneous manner, leaving patches of areas still coated by biofilm.

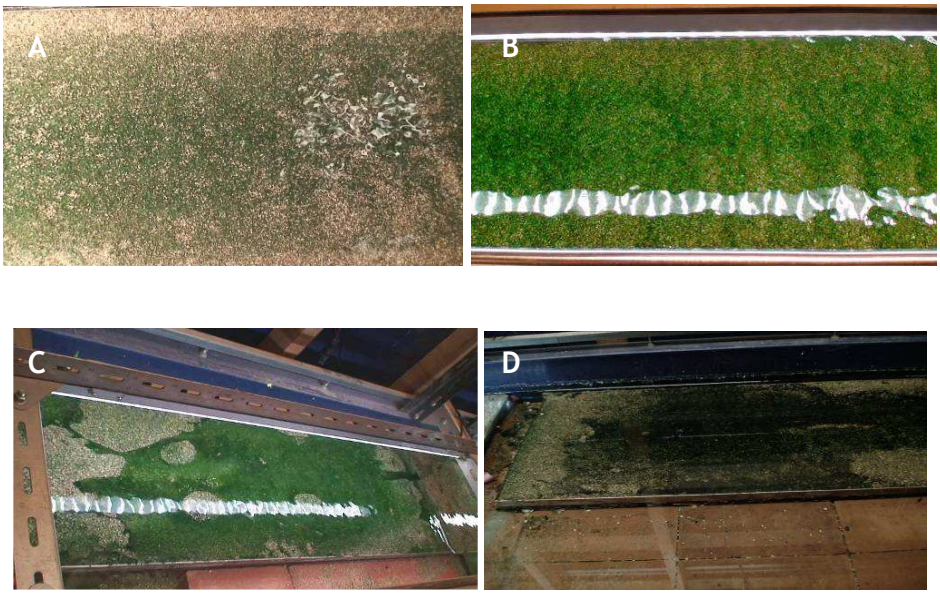

Figure 5. 2. Sand size sediments growth characteristics. A common trend shows that in the first 2 weeks of growth an homogenous growth pattern can be seen in the Yalin flume (A, SGS 1w; B, Sand 2w) whereas for more mature stages of biofilm growth the colonization is patchy and hence less stable (C, Sand 3w; D Sand 4w) (Flow from right to left).

Fore gravel size sediment, figure 5.3_{LGS} and 5.3_{Gravel} shows that after 1 week of colonization the growth over both the gravel size material looked similar to the fixation stage by Noffke *et al.* (2001). In week 2 of growth for LGS the colonization still appears homogeneous, whereas 2 weeks of growth for gravel sample suggested that biofilm erosion takes place at growth conditions, possibly after bubbles exposed the bio-mat to erosion by the flow, and hence left a

patchy growth to take place (figure 5.3 b_{Gravel}); any other stage of growth (figure 5.3 c, d) present patchy biofilm for both the materials.

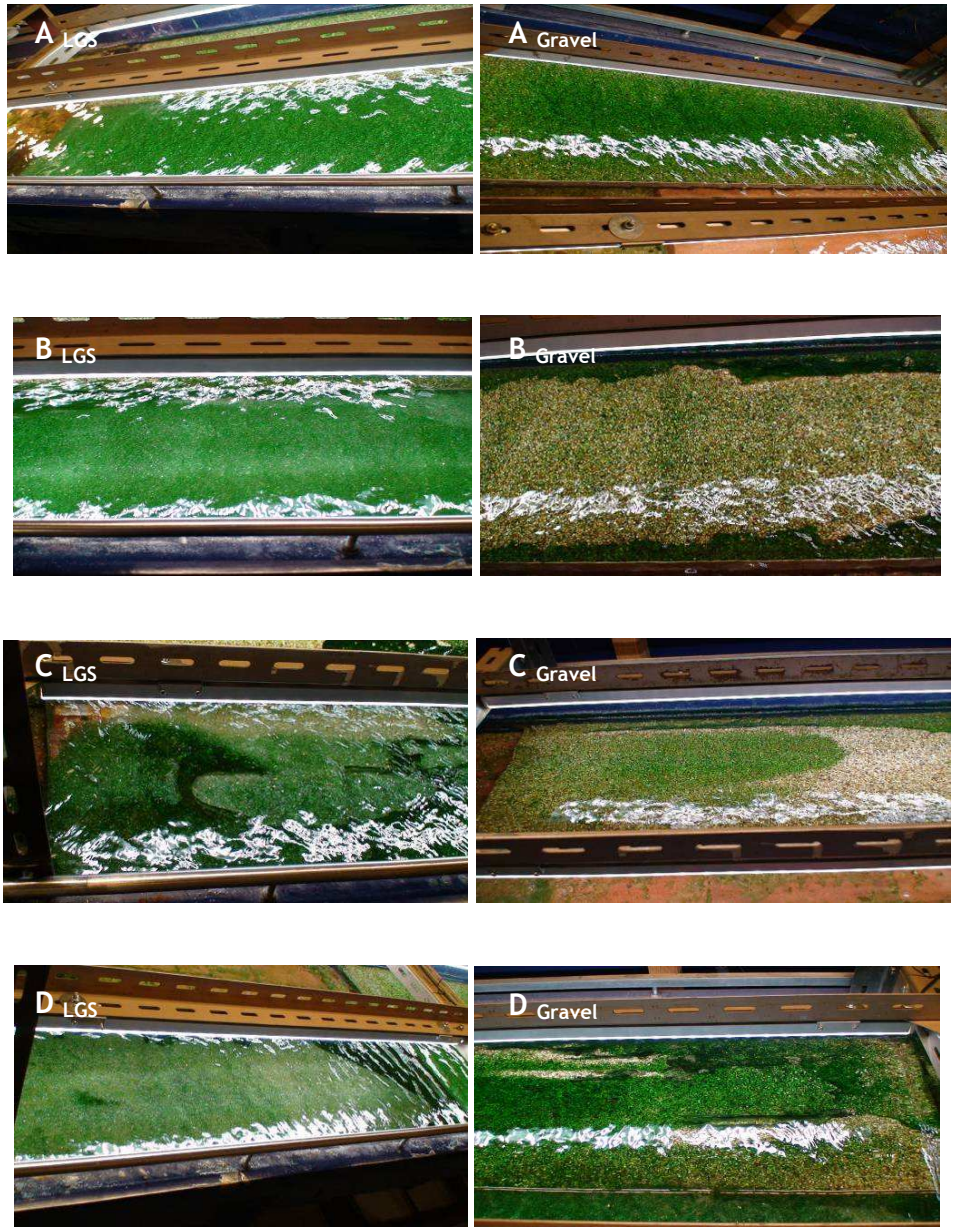

Figure 5. 3. Gravel size sediments growth characteristics. A common trend shows that in the first week (A) both materials show uniform colonization. From 2 weeks of growth (B) the growth pattern changes among LGS and gravel: LGS present uniform biofilm coverage (B LGS) whereas gravel have been eroded during growth condition and appear patchy (B Gravel). Week 3 (C) and Week 4 (D) present heterogeneity for both gravel size materials. (Flow from right to left).

Section 5.4.2 will present the result of the biomass analysis carried out weekly on the samples whereas section 5.4.3 will present the results for EPS.

5.4.2 Biomass

This section, like section 4.4.3 for box0.2, presents the weekly relative biomass results (which is the the biomass value divided by the dry sample weight) collected over the four different substrata, after applying the loss of ignition technique (HIMOM, 2005). Results are presented in figure 5.4 and discussed in detail below.

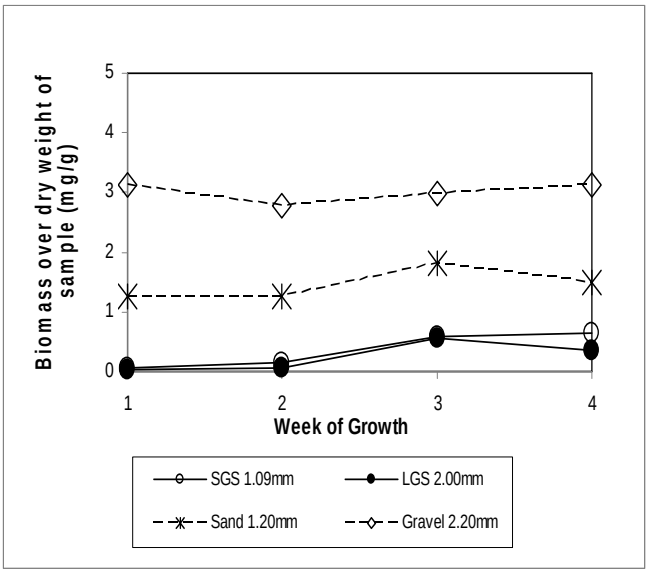

Figure 5. 4. Weekly relative biomass (mg/g), which is biomass (mg) divided by the dry weight of the sample (g), of box1 for sand and gravel size sediments as obtained from LOI (HIMOM, 2005).

Absolute data: for box1 the maximum biomass varies in absolute value over almost an order of magnitude (1-80mg); this range is similar to that measured in chapter 4 despite no filamentous growth being observed in the present data set. However, more detailed comparison of the absolute biomass data clearly shows that typically biomass was lower in the present data set than chapter 4 data; for example, maximum biomass values from figure. 5.4 are ~47-93% of those recorded in the equivalent graph of figure. 4.9, apart from SGS for which the maximum value for box1 was 11% lower than that of box0.2. The general trend seems to suggest that biofilm did not overgrow in this set of experiments, as happened in chapter 4, possibly due to the improved light system. This is unsurprising given that the lighting was redesigned in the present data set to

preclude the local regions of excessive growth symptomatic of chapter 4 and suggests that the experimental set up of chapter 5 was more realistic.

General trend: figure 5.4 shows a positive trend between biomass and time of growth, as seen in chapter 4. Specifically this ranges from +12% for gravel (between week2 and week4) and 94% for LGS (between week1 and week3). The only exception is week 4 of growth for sand and LGS substrata; here the biofilm growth seems to decrease in the mature stage, probably due to a stage of mature sealing and hence erosion taking place during colonization. The results presented here are similar in trend to those presented in chapter 4, clearly indicating temporal development of biofilm growth.

Growth time: Again figure 5.4 shows significant growth over timeframes < 1 week. Sand and gravel clearly show that 69% and 99% of the overall maximum biomass recorded was already present after 1 week of growth; only 8% of the maximum was recorded for artificial sediments. Hence, the "first kiss" of biofilm over the substratum seems to be extremely important in developing biomass on natural sediments: this might be related to the fact that biofilm acquire nutrients directly from the surface of the grains or also due to the charge on the minerals comprising the particles.

Material size: Gravel has average relative biomass 2.1 times greater than sand. This might be due to the fact that biofilm, spreading from the top of the grains down, finds larger pores to fill in case of gravel sediments and can develop due to the low velocity at growth. SGS and LGS have instead very similar biomass.

Material type is clearly affecting the biomass, with natural sediments showing average relative biomass 4 times greater for sand than for glass beads and 12.4 more for gravel compared to LGS. This might be again because biofilm feeds from the nutrients and metal available on the sediment surface (Battin, personal communication).

In the next section the trend of the measured EPS for the different materials in time will be presented.

5.4.3 EPS

This section shows the weekly relative EPS value, which is the absolute EPS divided by the weight of the sample (200mg), collected over the four different substrata using the two procedures presented in section 5.3.5.

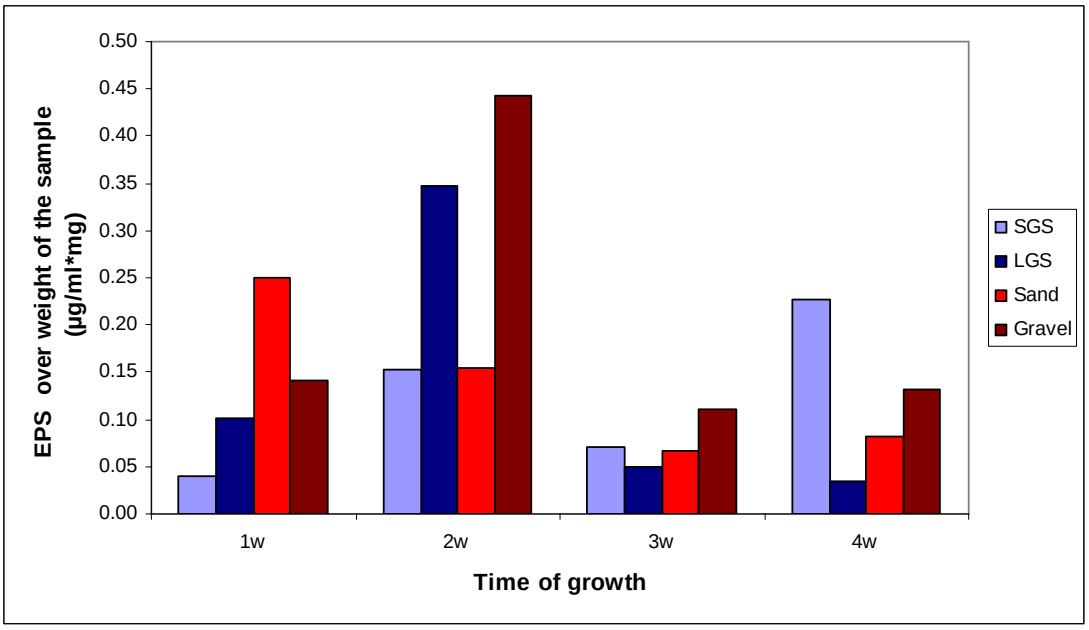

Figure 5. 5. EPS over sample weight (µg/ml*mg) per week of growth over the 4 different materials following the methodology presented in section 5.3.5.

A detailed analysis of the EPS trend is presented below for the different variables:

Absolute data: the maximum EPS relative value varies in absolute concentration of almost an order of magnitude (from 0.03µg/mlmg in week 4 for LGS to 0.44µg/mlmg in week 2 for gravel). Fixation/colonization (after 1 week) results in EPS ranging from 0.04- 0.25µg/mlmg (depending on the substratum), whilst mature bio-mats indicate values between 0.03 – 0.44µg/mlmg.

General trend: Overall trends are temporally complex. There appears an inverse relationship between EPS and time of growth, in that EPS is higher for immature biofilm (week 1-2) than mature biofilm (week 4); this is with the exception of SGS substrata and it is questioned whether this outlier is a robust datum point.

Growth time: figure 5.5 shows a positive correlation of the EPS concentration with time in the first 2 weeks of growth for all substrata, with the exception of sand in week 2. This would be expected during bio-mat development to ensure fixation across the substratum strong enough to resist entrainment and permit development of bio-mat thickness. However, subsequently there is decrease of EPS for all materials in week 3; this then recovers by a moderate increase in EPS between week 3 and 4 (excepting SGS). The difference between maximum and minimum value of EPS goes from 73% in sand up to 90% in LGS and such cyclicity (week 3 to 4) appears related the patchiest condition for every substrata hence the EPS reflects this unstable condition in its low concentration.

Material size: in the majority of the cases gravel material has more EPS than sand size sediment. Gravel experience relative EPS value ~1.5 more than sand in the last 2 weeks of growth and up to ~3 times more relative EPS for week 2 but shows less relative EPS than sand in week 1 of growth; LGS exhibit more than 2 times more relative EPS than SGS in the first 2 weeks, for then showing lower value than SGS for the last 2 weeks of growth. In general then EPS seem to be related to surface area, with more EPS generated on larger sediments.

Material type: natural sediments produce 1.1-1.5 times more average relative EPS than artificial sediments. This might be related to: i) material properties of the glass spheres and their inert nature compared to natural sediments; ii) the higher light uptake that glass materials allow, inducing different biofilm and EPS growth when compared to opaque surfaces; iii) the roughness of the natural sediment compared to the very smooth surface of the beads, which to induce a strong adhesion to the sediment need to be filled in and might also generate greater shear stress so that more EPS will be produce to insure attachment to the surface.

To ensure that the quantitative method of EPS analysis was robustly executed, the staining methodology was also tested; the intention was not to provide detailed comparison of technique, but solely to provide confidence in the quantitative method use. Thus, in figure 5.6 it is possible to see visually the presence of the EPS on SGS after staining with calcofluor was carried out (See section 5.3.5 for information on the technique). Even though the technique was applied to every material, opaque natural sediments did not allow very good

imaging using an inverted microscope (the light was blocked), whereas LGS could be resolved at the desire resolution only in thin circles and no area information could then be obtained. Hence only results for SGS are shown herein because these sediments induced the best visualization and image quality compared to the other substrata, due to the transparency and size of the beads.

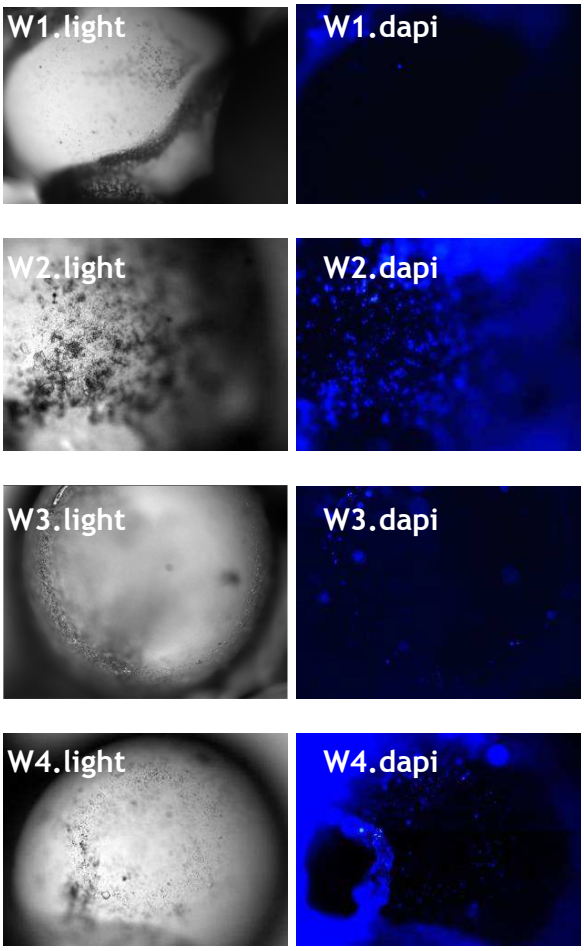

Figure 5. 6. SGS EPS visual assessment: on the left the light image of the sample and on the right the DAPI sequence; here, anything light blue represent the presence of the EPS. Scale 1.24mm by 0.93mm.

From figure 5.6 it is highlighted that even after 3 washes of the stained sample (see section 5.3.5) significant concentrations of bacteria and EPS remain attached to the beads. This shows the strength of adhesion that the EPS allows between bacteria and sediment surface. In particular, according to the results presented in figure 5.6, week 2 and week 4 of growth show the most abundant amount of EPS; this provides confidence in the qualitative method data provided in figure 5.5. Also interesting is that comparison of the the light microscope

image versus the fluorescent (dapi) one, it is possible to notice that EPS is present around the bacteria, acting as a contact point of adhesion.

Section 5.4.4 will introduce to the results of the Yalin technique, as presented in chapter 4, section 4.4.4 and following the set up presented in section 5.3.3.

5.4.4 Biostabilization data: relationships between critical shear stress at entrainment and time of growth – small scale (SS)

Results for the Yalin technique for the four different materials at the SS are presented in figure 5.7, where the percentage increase of the critical bed shear stress τ_c compared to the abiotic threshold is plotted in time.

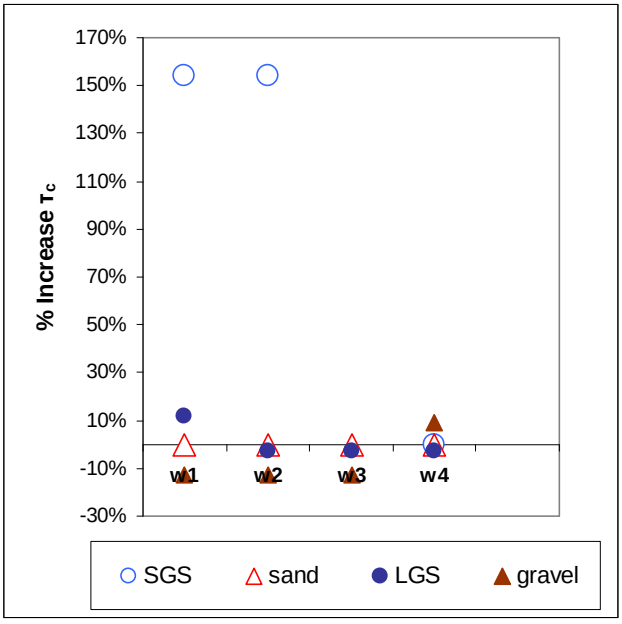

Figure 5. 7. Yalin result of box1 for the four materials in time. N.B. No data are available for week 3 SGS due to failure of the image capture technique during this trial.

Figure 5.7 clearly shows that the first two weeks for SGS are very strongly biostabilized and the threshold of motion occurs after applying a flow ~150% higher than the abiotic threshold; considered in terms of the increment of $\tau_{b,}$ this threshold translates as between 120-150%. However, the majority of data for other materials and durations of growth is more aligned with the lower

bound of chapter 4 data; specifically, figure 5.7 shows up to 11% biostabilization in LGS (week 1) and 9% in gravel (week 4). A reason why the value is towards the lower one presented in chapter 4 is because of the Yalin method and its application for box1 to a larger area: in this case and due to the patchy colonization and erosion, more grains are likely to have been eroded upstream of the interrogation area *A* and hence would have entered into the field of view, increasing the count of moving grains. Sand experiments result always at threshold for the first applied flow. Notably, gravel reached incipient motion before the threshold value obtained with the Soulsby and Whitehouse (1997) equation in the first 3 weeks of growth. This latter point is interesting, and may be a function of the large scatter of experimental values available in the literature for the critical Shield's parameter (Buffington and Montgomery, 1997); for example similar size sediment comparable to the gravel size presented in this thesis showed in the literature Shield's parameter values among θ=0.020 to θ=0.071 (Buffington and Montgomery, 1997).

A clear conclusion from this set of experiments is connected to the limitation of the Yalin method when applied to patchy growth conditions. Hence, it is surmised that Yalin is a good method to identify the incipient motion of strong bio-mats or small colonized areas (e.g. sediment cores) but doesn't account for the spatial heterogeneity and, cannot be used accurately to assess the biostabilization potential in case of a non homogeneous biofilm growth. Hence in the next section the erosion taking place at the LS will be presented, in order to stress even further that this process is related to scale and biofilm growth pattern.

5.4.5 Biostabilization data: relationships between critical shear stress at entrainment and time of growth – large scale (LS)

Section 5.4.4 has shown that the Yalin criterion works well for box1 in finding a specific and objective threshold of motion for biotic sediments only in the case of a strong biostabilization; this is because, if any region upstream the Yalin tested area A shows patchy biofilm and hence no stability, then the particles in

this area will eventually enter the FoV recorded by the camera. Hence in chapter 4 the Yalin technique has been compared and contrasted with an areal erosion assessment at the LS, done through image thresholding of still pictures collected at the end of every flow step. The same process has been carried out in this chapter, with figure 5.8 presenting the results for the percentage area eroded versus the bed shear stress τ_b for the four different materials. It was outwith the scope of this thesis to identify the effect of flow step duration on erosion; instead the importance was given to the resulting erosion induced by the increase in τ_b due to the different flow steps. Appendix 5.C provides a full raw data set of the extent of the erosion taking place at the beginning and at the end of every flow step versus the flow applied.

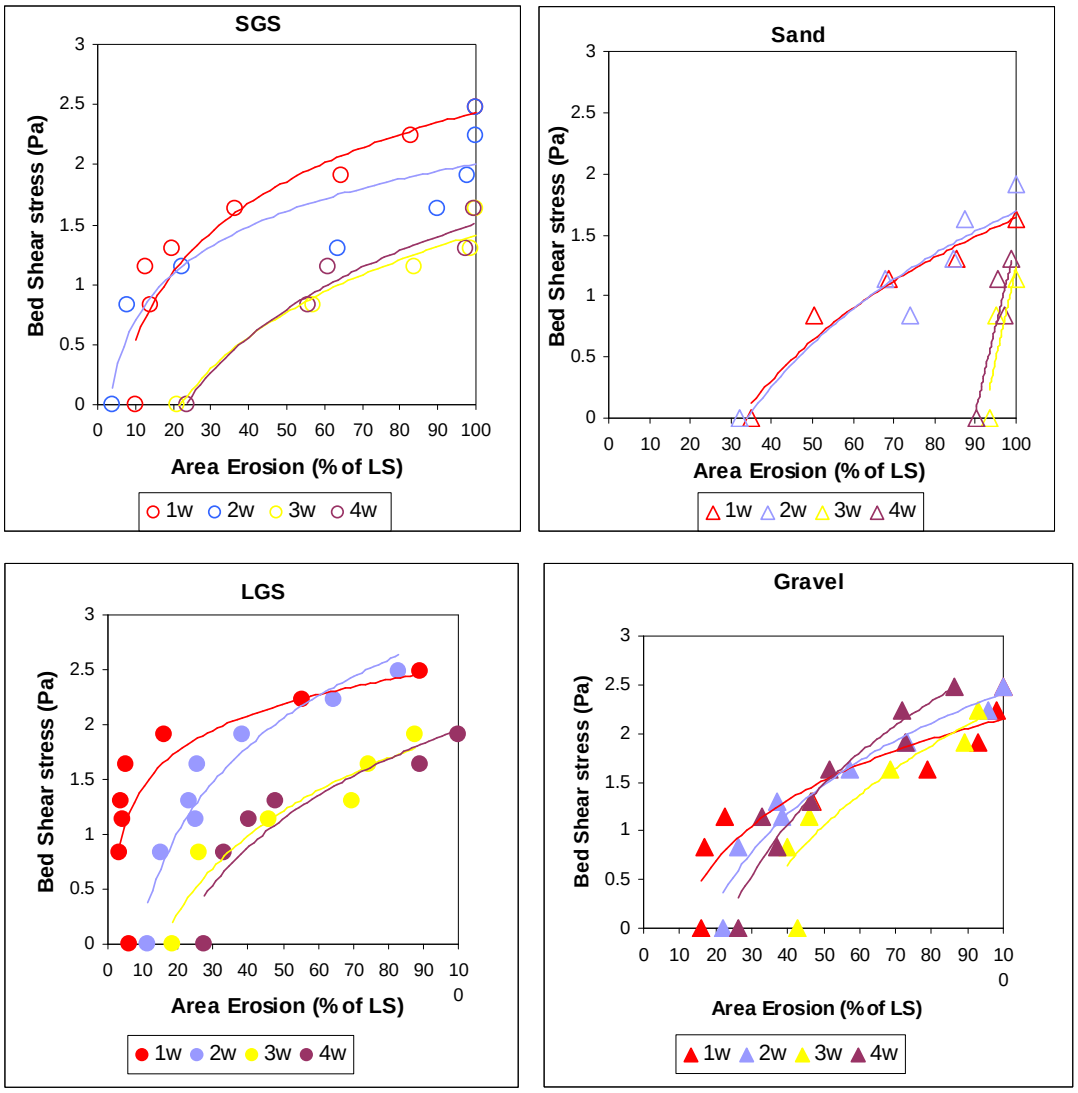

Figure 5. 8. Percentage erosion of the LS at the end of each flow steps vs the relative bed shear stress for the 4 materials in time. Errors are up to 9% for glass material and 5% for natural sediments and have not been added to the graph for clarity of reading. The trend of erosion that takes place for box1 is very well approximated by a logarithmic profile. This was hinted by the results at the LS in chapter 4 (see section 4.4.6). The direct result is that the erosion is exponentially related to the increase in $\tau_{b,}$ which is a finding common to many other cohesive or biotic entrainment thresholds (e.g. Sanford and Maa, 2001).

Figure 5.8 shows that for SGS and LGS the first failure is lower (~10%) in correspondence of the first 2 weeks of growth, ~15-25% for gravel and 50-70% for sand. In case of mature mats for SGS this value increases to ~55% for SGS and ~30% for LGS for mature bio-mat. In case of mature mats over natural sediments, the initial failure has an extent ranging from ~40% for gravels and more than 90% for sand. This shows that longer colonization in case of natural sediments corresponds to lower stability, which is possibly due to the high level of

nutrients available and hence resulting in higher biomass generated, which is more likely to get eroded by the flow.

Table 5.5 shows the coefficients of the linear regression for which τ_b was considered as the independent variable and had the form: $\tau_b = a\ln(\%Area_{erosion}) + b$ (chapter 4, equation 4, section 4.4.6), which can be fitted to the data presented in figure 5.8. The relative R^2 are always higher than 0.73 and in average equal to 0.86, a part for LGS (0.57). This confidently suggests that the areal erosion process is effectively logarithmic and erosion depends on the scale considered (in this case 500-1000 x D_{50}) and on the growth characteristics. P-values show that only in the cases of week 1 LGS, and weeks 3 and 4 for sand should the regression be rejected.

	Logarithmic Trend									
w1	***a***	***B***	***R^2***	***N***	***m***	***S_e***	***p***	***Intercept***	***S_e***	***p***
SGS	0.94	-1.76	**0.88**	8	1.06	0.16	0.00	1.87	0.26	0.00
LGS	0.82	-0.46	**0.57**	8	1.22	0.43	0.03	0.56	0.70	0.45
Sand	1.51	-5.29	**0.96**	5	0.66	0.08	0.00	3.50	0.09	0.00
Gravel	1.08	-2.70	**0.84**	8	0.93	0.16	0.00	2.50	0.27	0.00
w2										
SGS	0.67	-0.97	**0.85**	8	1.50	0.26	0.00	1.45	0.42	0.01
LGS	1.24	-2.73	**0.92**	8	0.81	0.10	0.00	2.21	0.16	0.00
Sand	1.76	-6.33	**0.89**	6	0.57	0.10	0.00	3.60	0.13	0.00
Gravel	1.45	-4.19	**0.94**	8	0.69	0.07	0.00	2.89	0.12	0.00
w3										
SGS	0.97	-3.04	**0.95**	5	1.03	0.13	0.00	3.13	0.15	0.00
LGS	1.12	-3.15	**0.91**	6	0.90	0.14	0.00	2.82	0.18	0.00
Sand	19.10	-86.55	**0.77**	3	0.05	0.03	0.32	4.53	0.02	0.00
Gravel	2.41	-8.47	**0.73**	7	0.41	0.11	0.01	3.51	0.17	0.00
w4										
SGS	1.09	-3.47	**0.95**	5	0.92	0.12	0.00	3.19	0.13	0.00
LGS	1.39	-4.29	**0.84**	6	0.72	0.16	0.01	3.09	0.21	0.00
Sand	15.54	-70.03	**0.85**	4	0.06	0.02	0.08	4.51	0.02	0.00
Gravel	1.98	-6.29	**0.92**	8	0.50	0.06	0.00	3.17	0.10	0.00

Table 5. 5. Coefficient for every material in time of the logarithmic erosion trend, following the equation $\tau_b = a\ln(\%Area_{erosion}) + b$, where R^2 is the goodness of the fit, which is in almost every case higher than 0.73, a part from week 1 of growth for LGS (0.57). *N* is the number of observations, *m* is the *x* coefficient in the linear regression and *intercept* is the intercept of the linear regression; S_e and *p* are respectively the standard error and the p-value on *m* and *intercept*. In red are highlighted the $p<=0.05$. Note that in w3-w4 for sand the value of *a* is very high, due to the very steep erosion and curve seen in figure 5.8.

If the strongest weeks of colonization are considered, which from figure 5.8 are week1 for SGS, sand and LGS and week 4 for gravels, the following values of a and b were found for the different materials: (i) SGS: a=0.94; b=-1.76; (ii) sand:

a=1.51, *b*=-5.29; (iii) LGS: *a*=0.82, *b*=-0.46 and (iv) gravel: *a*=1.98, *b*=-6.29. Interesting to notice is that from the coefficients presented above, the erosion over natural sediments takes place with a higher *a* (ranging from 1.51-1.98), meaning that small increments of shear stress τ_b will induce larger erosion, whereas the area eroded in case of the artificial material is very low in the first 3-4 flow steps (see figure 5.8) for then increasing with a more gentile trend then the natural sediment (*a*=0.82-0.94).

The logarithmic trend can be rearranged to give the percentage erosion of LS depending on the bed shear stress τ_b, as presented below:

$$\%\ Area_{Erosion} = e^{\left(\frac{\tau_b - b}{a}\right)} \quad \textbf{Equation 5. 3}$$

If equation 5.3 is applied to the critical shear stresses at entrainment obtained using the equation of Soulsby and Whitehouse (1997) (see table 5.4) together with the coefficients presented in table 5.5, then the percentage erosion at threshold of motion for abiotic sediment can be obtained as presented below in table 5.6.

		% Erosion at Threshold for Soulsby and Whitehouse (1997)
SGS	**1w**	11.3
	2w	9.3
	3w	38.9
	4w	39.0
Sand	**1w**	51.1
	2w	53.2
	3w	96.1
	4w	94.4
LGS	**1w**	7.4
	2w	23.5
	3w	48.0
	4w	51.3
Gravel	**1w**	48.6
	2w	51.0
	3w	62.6
	4w	50.7

Table 5. 6. Percentage erosion of LS at threshold for Soulsby and Whitehouse (1997), using equation 5.3 and the coefficient vales found in table 5.5.

From table 5.6 almost in every case the biofilm coverage at threshold for abiotic sediments according to Soulsby and Whitehouse (1997) is about 90% for SGS and LGS in the strongest week and about 50% in the case of natural sediments and hence biostabilized. Only for sand (week 3 and week 4) and gravel (week 3) the erosion took place for almost the whole area: this was related to the very patchy growth coverage in this colonizing stage.

This section has clearly showed that biostabilization takes place for non-cohesive sediments and that image analysis can be an alternative to the Sanford and Maa (2001) approach, which relates mass of eroded material and bed shear stress. Ideally, if equation 5.3 was appropriately calibrated in natural environments, it could represent a valuable substitute to invasive assessment of the erosion characteristic of colonized sediment with benthic flumes or CSM; additionally here we used open source software (*ImageJ)* for the image analysis which would keep the analysis cost effective. However the image segmentation technique presented herein is useful to assess the portion of the bed that is biostabilized after a shear stress larger than the threshold for abiotic sediments has been applied, not for quantifying the mass of material eroded. When the "bio-mat" was eroded in fact the sediment was entrained immediately and no biostabilization was experienced for deeper sediment layers. To conclude, this technique is thought to be particularly successful in the case of biostabilization of non cohesive sediments, which might be affected by biofilm colonization only in the first layers at the surface.

Section 5.4.6 correlates the results presented at the LS to the biological analysis that has been conducted and is intended to verify if any direct relationship exists.

5.4.6 Erosion at LS and relationship with biomass and EPS

Whilst outwith the original objectives of this engineering-based thesis, it was considered important to attempt cross-correlation of physical and biological processes for a more detailed interpretation of the underpinning processes for the biostabilization of sediment substrata. Thus, table 5.7 correlates some of

the variables that have been presented so far, which are: i) absolute value of EPS concentration (not divided by the sample weight); ii) absolute biomass; iii) time of growth and iv) Biofilm percentage coverage at threshold according to the Soulsby and Whitehouse (1997), which was for the strongest colonizing weeks ~ 90% for SGS and LGS and ~ 50% for natural sediments. Only for week 3 and week 4 sand and for week 3 gravel the biofilm percentage coverage was lower than these figures. In bold are those values that are considered significant (<-0.8 and >0.8, that we are going to consider representative of the condition of no correlation or positive correlation).

SGS	EPS (µg/ml)	Biomass (mg)	Growth Time	% Biofilm coverage at threshold for abiotic sediment
EPS (µg/ml)	1.00			
Biomass (mg)	0.55	1.00		
Growth Time	0.74	**0.97**	1.00	
% Biofilm coverage at threshold for abiotic sediment	-0.31	**-0.96**	**-0.86**	1.00

Sand	EPS (µg/ml)	Biomass (mg)	Growth Time	% Biofilm coverage at threshold for abiotic sediment
EPS (µg/ml)	1.00			
Biomass (mg)	-0.34	1.00		
Growth Time	**-0.91**	**0.02**	1.00	
% Biofilm coverage at threshold for abiotic sediment	**0.90**	-0.39	**-0.90**	1.00

LGS	EPS (µg/ml)	Biomass (mg)	Growth Time	% Biofilm coverage at threshold for abiotic sediment
EPS (µg/ml)	1.00			
Biomass (mg)	-0.68	1.00		
Growth Time	-0.45	**0.83**	1.00	
% Biofilm coverage at threshold for abiotic sediment	0.47	**-0.92**	**-0.97**	1.00

Gravel	EPS (µg/ml)	Biomass (mg)	Growth Time	% Biofilm coverage at threshold for abiotic sediment
EPS (µg/ml)	1.00			
Biomass (mg)	-0.31	1.00		
Growth Time	-0.29	0.59	1.00	
% Biofilm coverage at threshold for abiotic sediment	0.36	0.47	-0.35	1.00

Table 5. 7. Correlation values among absolute EPS (µg/ml), biomass (mg), growth time, % biofilm coverage at threshold for biotic sediments. Values close to 1 correspond to a good correlation whereas 0 value indicates no correlation and negative values indicate an inverse correlation. In bold the most significant values of the analysis.

General trend: for every material, a part from gravel, there is a strong relationship among the percentage coverage and one of the variables analyzed (EPS, Biomass or Time of Growth). For SGS, sand and LGS the biofilm coverage is inversely correlated to the time of growth: this stresses again the concept that for longer culture time the biofilm grows in a patchier structure (see section 5.4.5).

Percentage coverage and EPS: biofilm coverage is positively correlated to EPS only for the case of sand sediments; however for sand in the last 2 weeks of growth, the coverage is low and so is the concentration of EPS. In all the rest of the cases the value is too low to state any relationship; hence in this study I don't find a direct link among biostabilization and EPS presence, although from looking at the microscope images, it can be stated that EPS represent the key parameter which allows bacteria to attach to surfaces.

Percentage coverage and Biomass: In all cases apart from gravel, the percentage coverage is inversely related to the biomass concentration; in the case of artificial sediment this relationship is very strong (>-0.9). Hence, in a perfect condition as the incubation flume with unlimited nutrient supply, the case of early stage biofilm allowed generating a very strong biostabilization potential. Instead, for more mature bio-mats, hence with more biomass, the biostabilization strength decreased, possibly because the large biofilm accumulation resulted less compact and more prone to erosion even during growth.

Thus, whilst this thesis provides a brief foray into the biological processes thought (from the literature) to be responsible for biostabilization, the outcome of this analysis is that there is no consistent or clear relationship among biological variables, time of growth or biostabilization potential. This clearly shows that is very difficult to relate erosion characteristics to biological variables without a more detailed approach into microscopic processes of biofilm structure, abundance etc.

To stress even more the fact that biostabilization was reached for non-cohesive sediments, section 5.4.7 will present the result on the modification of the flow field after colonization using particle imaging velocimetry (PIV).

5.4.7 PIV results

According to the set up conditions presented in chapter 3, section 3.6.2.2 and following the methodology presented in section 5.3.2 a series of 2000 images were collected for every flow step and they underwent post processing using the software *Dynamic studio*. It should be highlighted that PIV analysis was not intended as the focus of this thesis, rather to provide better understanding of the processes underpinning biostabilization; hence, full analysis of all possible turbulence statistics was considered extraneous to the thesis and this chapter focuses specifically on only three variables; (i) flow velocity in the downstream (U) and vertical components in the centre of the flume (V); (ii) roughness length (z_0) of the bed to infer smoothing/roughening due to biofilm growth, as obtained from the Law of the Wall (see chapter 2, section 2.2.2.3); (iii) bed shear stress (τ_b) as derived from velocity profiles. This produced a large data set that was scrutinized for data quality and relevance to entrainment threshold data provided earlier in this thesis. Specifically two truncations of the data set were applied:

1. For sand size sediments the first flow step employed (1.6l/s) was already at threshold of motion for abiotic sediments, thus degradation of the bed during the experiment resulted in it progressively exiting the FoV by the third flow step employed (3.6l/s); this can be seen in figure 5.9 (A for flow 1.6l/s and B from 3.6l/s). As a zero bed level is critical to velocity profile examination, then only the first 3 flow steps (1.6l/s, 2.6l/s and 3.6l/s) will be analyzed in this chapter.

2. For gravel size sediments the results are presented for the first four flow steps (1.6l/s, 2.6l/s, 3.6l/s and 5l/s). Subsequent to this the quality of the images collected became poor due to increasing turbidity and excessive scatter of the laser by: (i) the addition of seeding material and

wash-off from the side-walls; (ii) entrainment/suspension of biofilm into the flow. For flows higher than 5l/s 5-60% of flow vectors were classified as “wild” and could not be considered representative of the hydraulic conditions taking place. An example of the bad seeding can be seen in figure 5.9C.

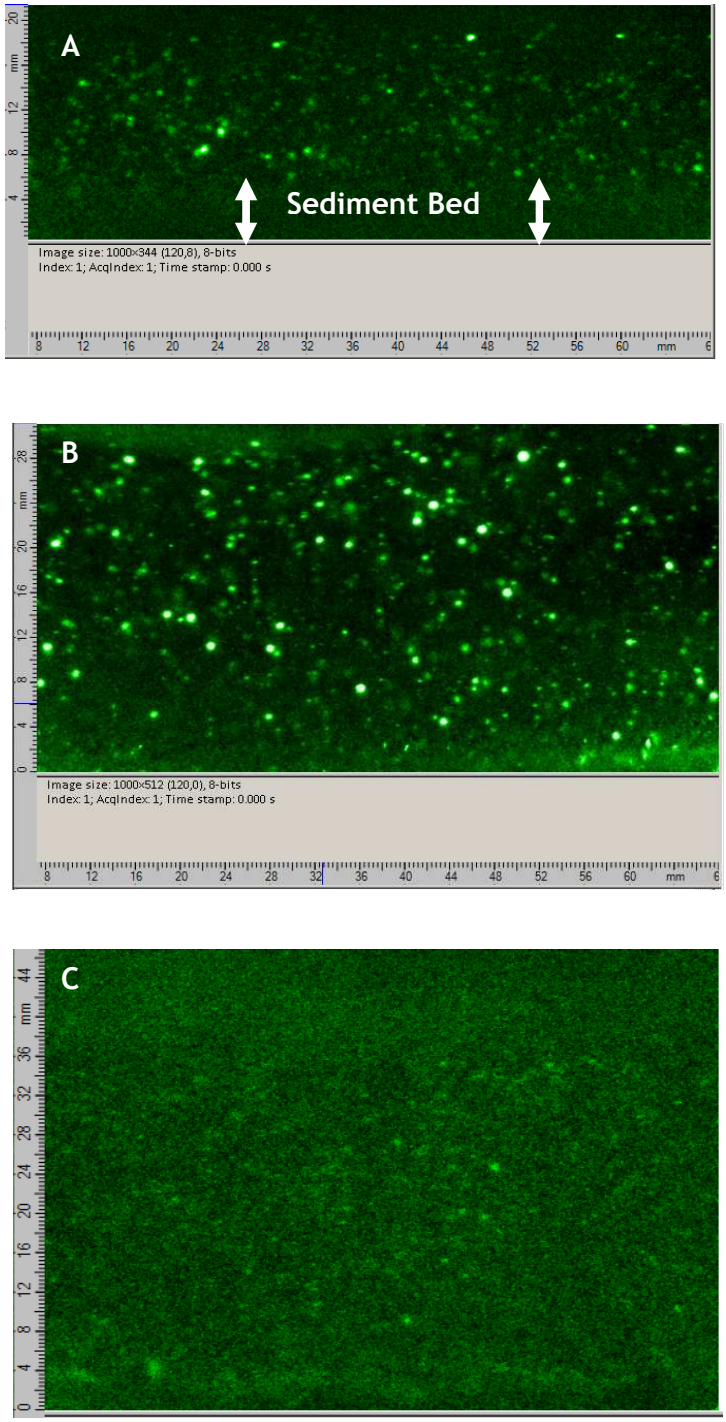

Figure 5. 9. Abiotic SGS: For 1.6l/s and for 3.6l/s. A) the bed is in the FoV (up to 4mm) but erosion is taking place; B) the bed is eroded and hence some seeding particles are outside the FoV; this makes the identification of the zero level of the velocity profile impossible to obtain; C) Example of bad seeding starting from 7l/s for 3weeks of growth gravel.

PIV analysis will offer high resolution, directly-measured data local to the FoV as appropriate to robust analysis of the hydraulic variables. Thus, it is considered more appropriate to employ the PIV-based analysis of bed shear stress in the present chapter, rather than the reach-average estimates employed in the UF-based methodology used in previous sections of this thesis.

In the next section the results obtained from the data processing undertaken according to chapter 3, section 3.6.2.2 will be presented. In particular section 5.4.7.1 will introduce the results for the strongest colonization weeks for every material compared to the abiotic condition. Section 5.4.7.2 will introduce the analysis of the roughness modifications and section 5.4.7.3 will present the bed shear stress τ_b variations induced by the biofilm presence.

5.4.7.1 Comparison of flow characteristics among strongest weeks of growth and abiotic sediments

After seeing the LS results (section 5.4.6), it was evident that stronger biostabilization took place for the fixation stage and lower stability compared to the fixation stage was achieved for the more mature biofilm growth stage. In particular the largest biostabilization potential was experienced for: i) SGS: week 1; ii) sand: week 1; iii) LGS: week 1 and iv) gravel: week 4. In this section, the time average results obtained by post processing the PIV data will be presented and they include: mean longitudinal velocity U, mean vertical velocity V, standard deviation of U or standard deviation of V. Moreover, a spatial average of the data obtained across the FoV is provided for abiotic and biotic substrata, with all raw data of flow statistics for each flow step found in Appendix 5.E. When reviewing the flow field data in this section the cautionary note is reiterated (and later discussed) in that abiotic sands and LGS were already at threshold in the lowest flow step employed, whereas gravels were immobile.

For SGS figure 5.10 and figure. 5.11 show the flow field for abiotic and biotic (1 week) sediments for 1.6l/s and at the higher flow rate (3.6l/s); this latter flow

rate applied a bed shear stress ~150% that of the critical value for abiotic entrainment.

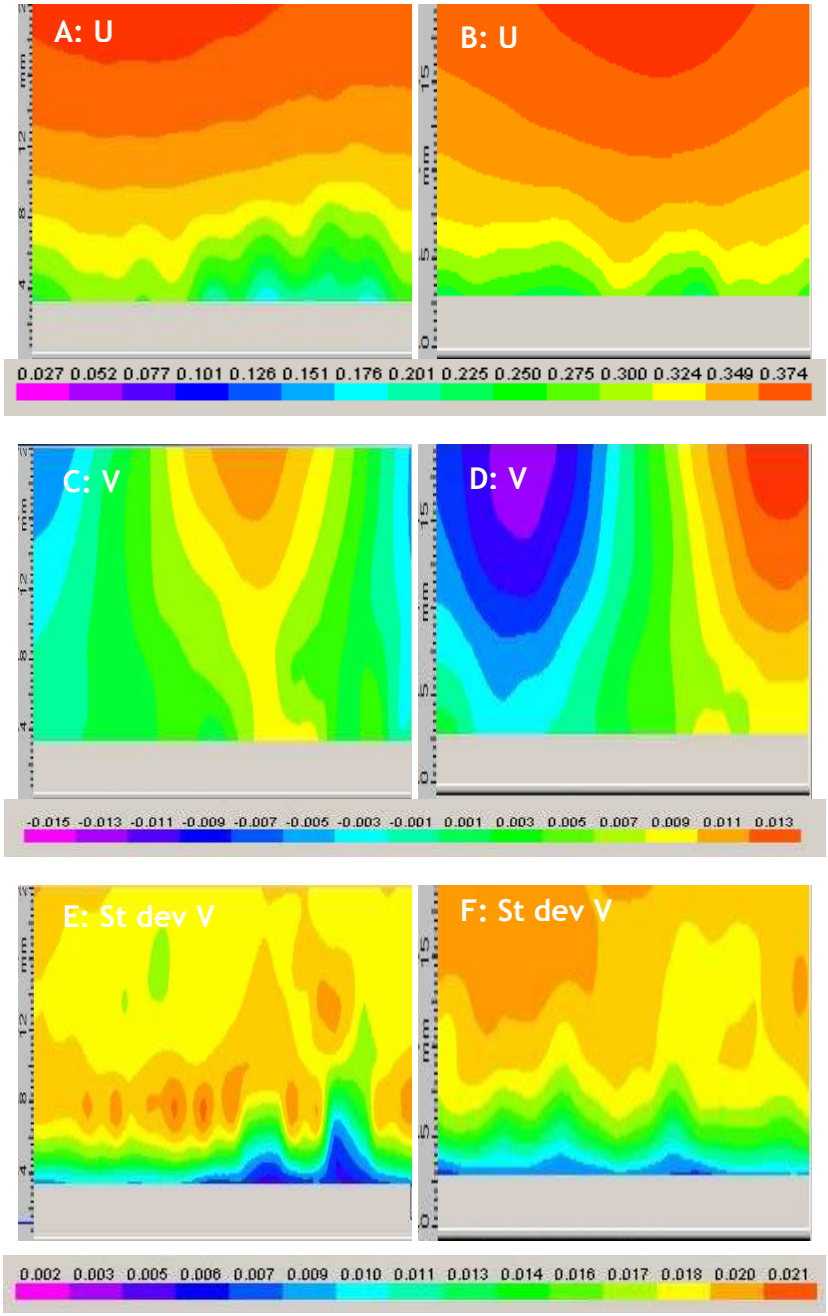

Figure 5. 10. SGS at 1.6l/s: A) *U* abiotic sediments; B) *U* 1 week of growth; C) *V* abiotic sediments; D) *V* 1 week of growth; E)Standard Dev *V* abiotic sediment; F) Standard Dev *V* 1 week growth. (Scale on the x direction equal to 60mm). Note that the grey zones coincide with the presence of a mask to remove the bed from the image-processing region. (Flow from left to right).

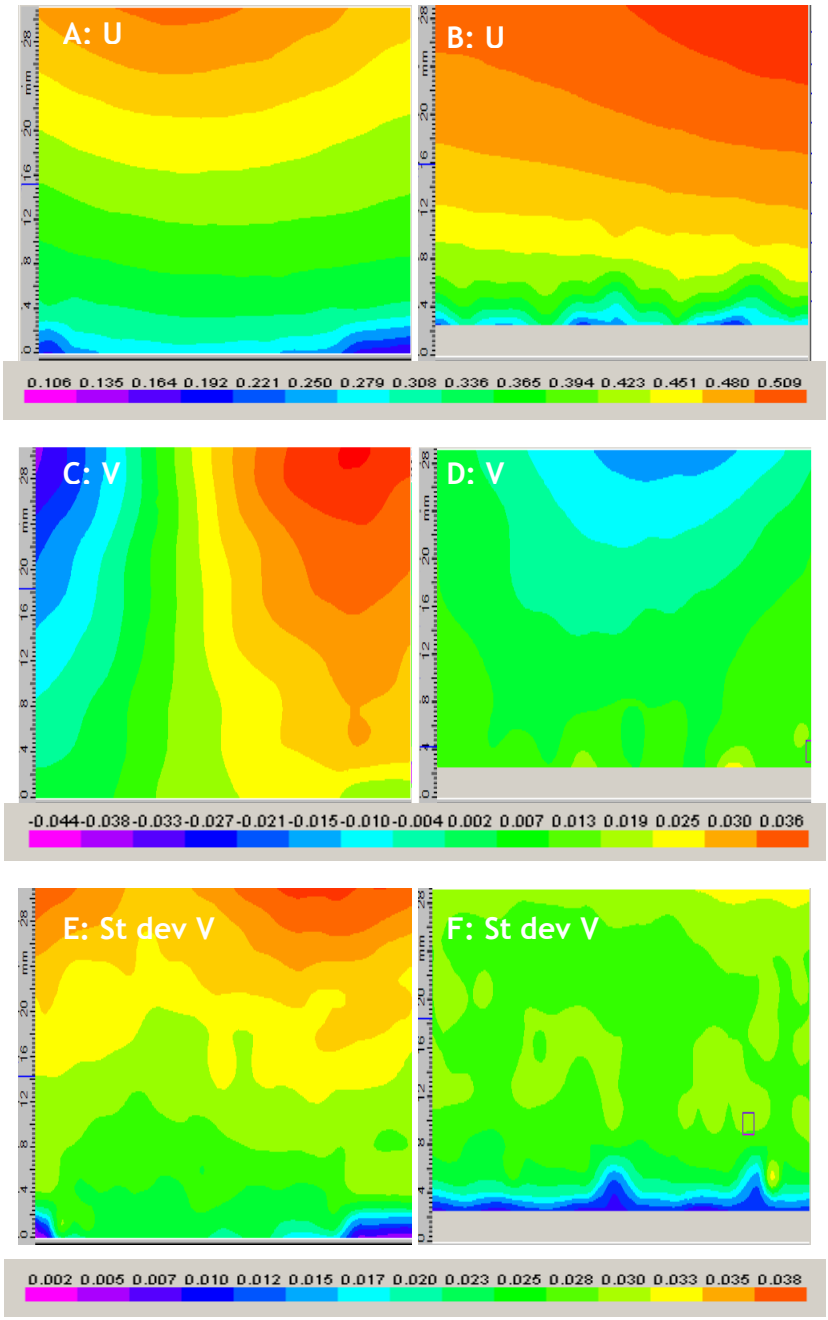

Figure 5. 11. SGS at 3.6l/s: A) *U* abiotic sediments; B) *U* 1 week of growth; C) *V* abiotic sediments; D) *V* 1 week of growth; E)Standard Dev *V* abiotic sediment; F) Standard Dev *V* 1 week growth. (Scale on the x direction equal to 60mm). Note that the grey zones coincide with the presence of a mask and hence the bed was visible. (Flow from left to right).

SGS data in figure 5.10, at low flow, very little difference is observed in the velocity components *U* and *V*, except that the *U* component shows more depth-variability in the near boundary region of the abiotic bed; likely a facet of higher boundary roughness. However, the standard deviation of *V* does provide insight into biotic "clogging" of the pores. Specifically, over the abiotic bed seven highly local regions of high standard deviation are observed ~4mm above the

masked region of the bed which would suggest upwelling/downwelling into local clean pore spaces. Such variability does not occur following biotic growth; instead the standard deviation exhibits lower values more uniformly across the boundary and lower 20% of the depth. In figure 5.11 (and Appendix 5.E), it is clearly visible that the downstream velocity *U* is faster over biotic substrata than for abiotic sediments. Specifically, in case of 3.6l/s flow rate data show that space and time averaged *U* increases from 0.34m/s to 0.41m/s (+22%) after 1 week of growth (figure 5.11). It is logical that this is related to reduced roughness of the bed during bio-mat growth; i.e. clogging of pores and coating of grains. The smoothing reduces the energy losses by overcoming resistance and allows both a faster flow and a decrease of boundary layer turbulence. This is visible from the vertical velocity *V* data (figure 5.11 D-F): firstly, abiotic sediments show well-defined ejections and inrushes of fluid flow (figure 5.11C) in the outer region with velocities ±0.04m/s; the range of velocity reduces in case of the biotic sediments (from -0.026 to 0.010), which corresponds to a decrease in maximum *V* of about ~72% and an increase in minimum of 42%(figure 5.11D), equal to a 56% decrease in range of *V* values compared to abiotic sediments; secondly, the range of the standard deviation of the vertical velocity component *V* significantly reduces (32%) from abiotic to biotic sediments, showing that in the outer layer the variation of *V* was almost uniform. Three explanations are viable here: firstly it is a by-product of bed smoothing and accelerating downstream flow (reducing vertical exchange); secondly, pore-clogging of the bed by the biofilm reduces upwelling/downwelling at the boundary; thirdly, observations note that the biofilm vibrates/flutters under the applied fluid forces acting at the boundary perpendicular to the surface of attachment to, possibly, extract energy and damping the vertical flow field.

In case of sand, results are shown in figure 5.12 for week1 (strongest colonizing week) at threshold of motion for abiotic sediments (1.6l/s) and in figure 5.13 for a higher flow step (3.6l/s), which was ~100% more bed shear stress τ_b than the clean sediment entrainment threshold.

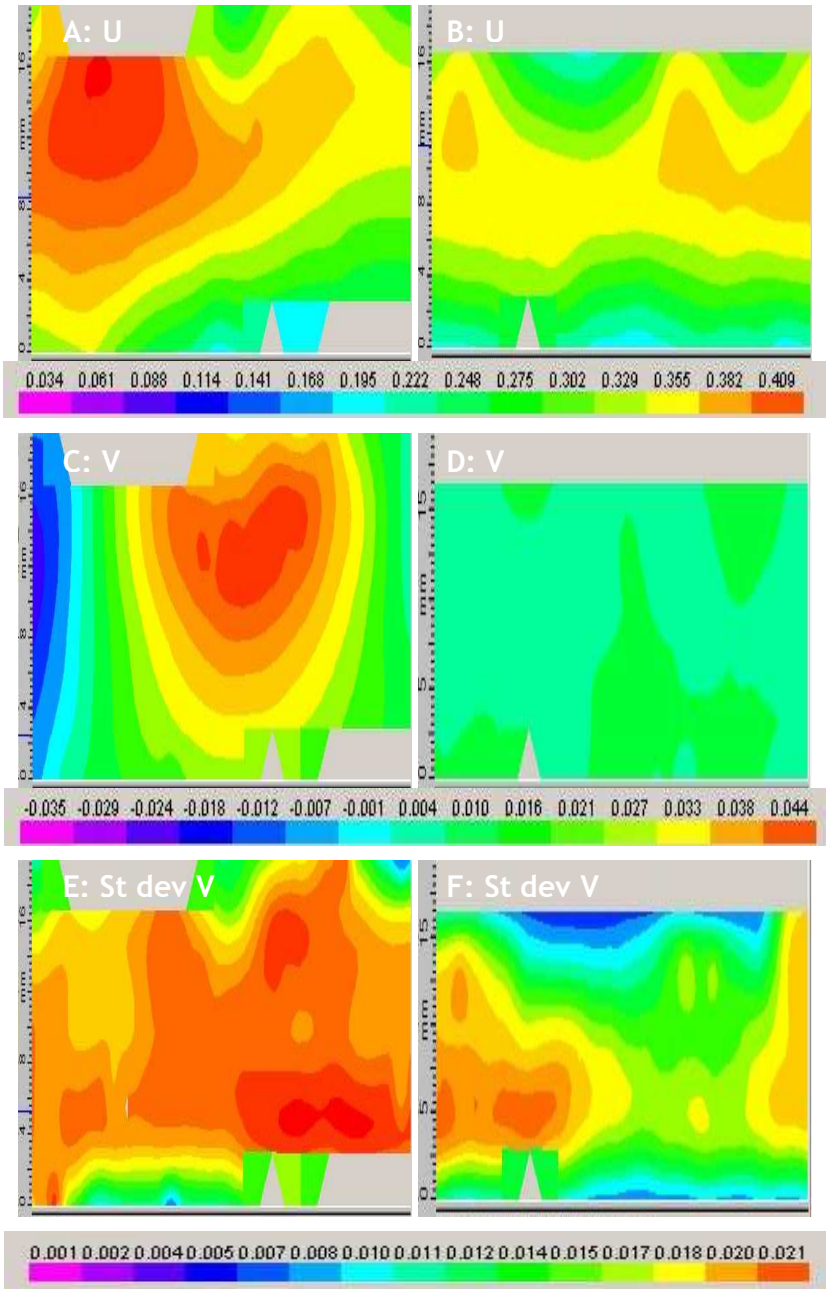

Figure 5. 12. Sand at 1.6l/s: A) *U* abiotic sediments; B) *U* 1 week of growth; C) *V* abiotic sediments; D) *V* 1 weeks of growth; E) Standard Dev *V* abiotic sediment; F) Standard Dev *V* 1 week growth. (Scale on the x direction equal to 60mm). Note that the grey zones coincide with the presence of a mask and hence the bed was visible. (Flow from left to right).

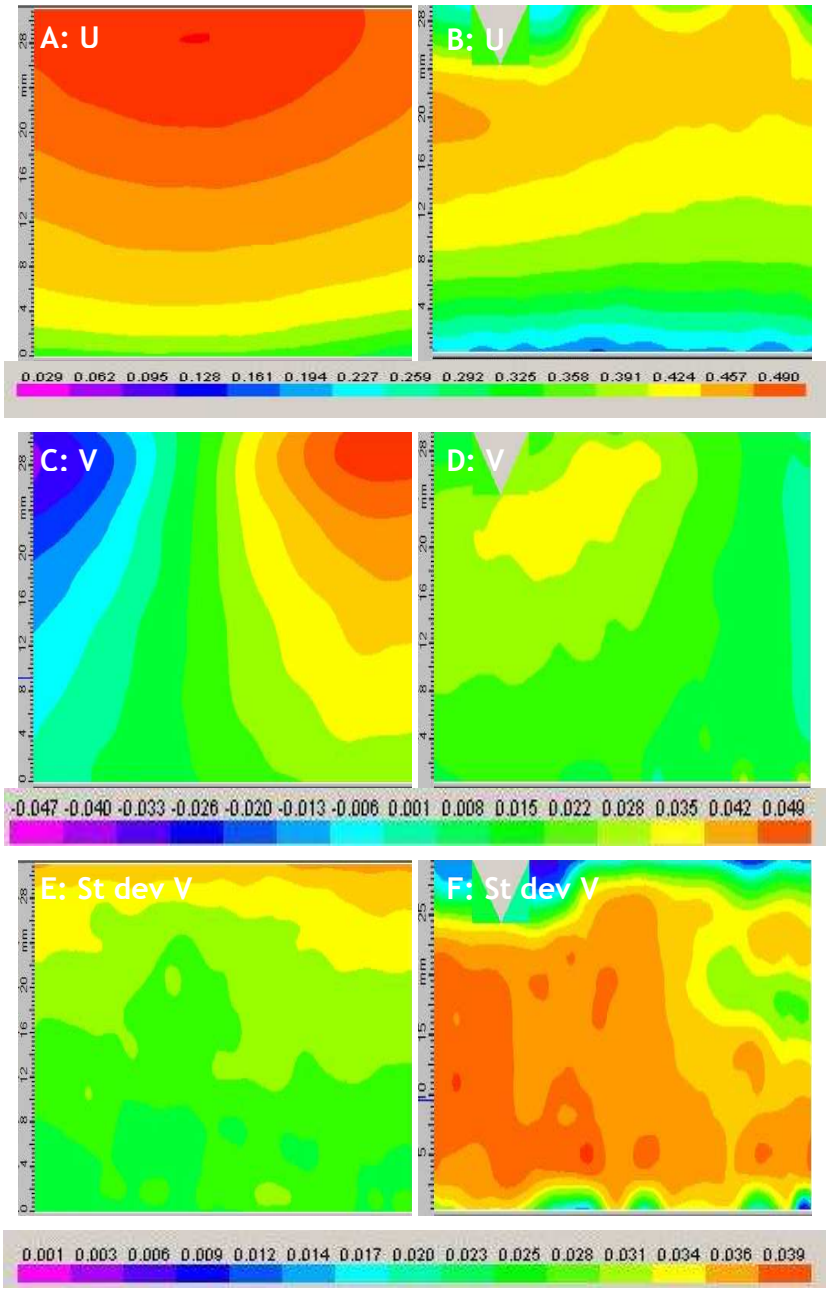

Figure 5. 13. Sand at 3.6l/s: A) *U* abiotic sediments; B) *U* 1 week of growth; C) *V* abiotic sediments; D) *V* 1 weeks of growth; E) Standard Dev *V* abiotic sediment; F) Standard Dev *V* 1 week growth. (Scale on the x direction equal to 60mm). Note that the grey zones coincide with the presence of a mask and hence the bed was visible. (Flow from left to right).

Sand data show for both 1.6l/s and 3.6l/s slower average values of *U* (respectively a decrease of 8% and 22%) and the outer layer becomes more homogeneous in case of the biotic sediments (figure 5.13B), with the bands of similar velocity getting wider compared to abiotic sediments. These data are interesting, as they are counter to those found in the SGS data; thus, the higher biomass of biofilm grown over sands may be increasing hydraulic roughness due

to different “bioform” (i.e. the macro-scale architecture of the biofilm). Based on the biomass information, it may also be that thickness of the mat may therefore be greater over sand so as to enhance fluttering and energy extraction from the flow; however, intuitively less variability in *U* would also reflect (to some degree) reductions in the fluctuation of V (figures 5.12D and 5.13D).

The most interesting finding is again the homogeneity of *V*, with a decrease in range values of *V* of 92% for 1.6l/s and 65% from 3.6l/s. These values are higher than the 56% reduction in range of V found for SGS, showing that the key effect over natural sediment is the homogenization of the vertical velocity *V*. This could be possibly due to the extraction of turbulence induced by the vibrating membrane on the boundary layer or by the extraction of energy due to the contact with the biofilm growing on top of the sediments and vibrating in the flow. Both the cases presented seem to suggest that for sand size sediment the presence of a strong biostabilization potential homogenize the vertical velocity, which suggests that less turbulence is generated.

The same type of analysis was then carried out for coarser substrata. Specifically, LGS for 1 weeks of growth is discussed below, which provided the maximum biostabilization. Figure 5.14 presents the flow field at 1.6l/s, which was already at threshold for abiotic sediments, whereas figure 5.15 presents the subsequent results at a higher flow rate (3.6l/s), which was equal to ~10% more τ_b.

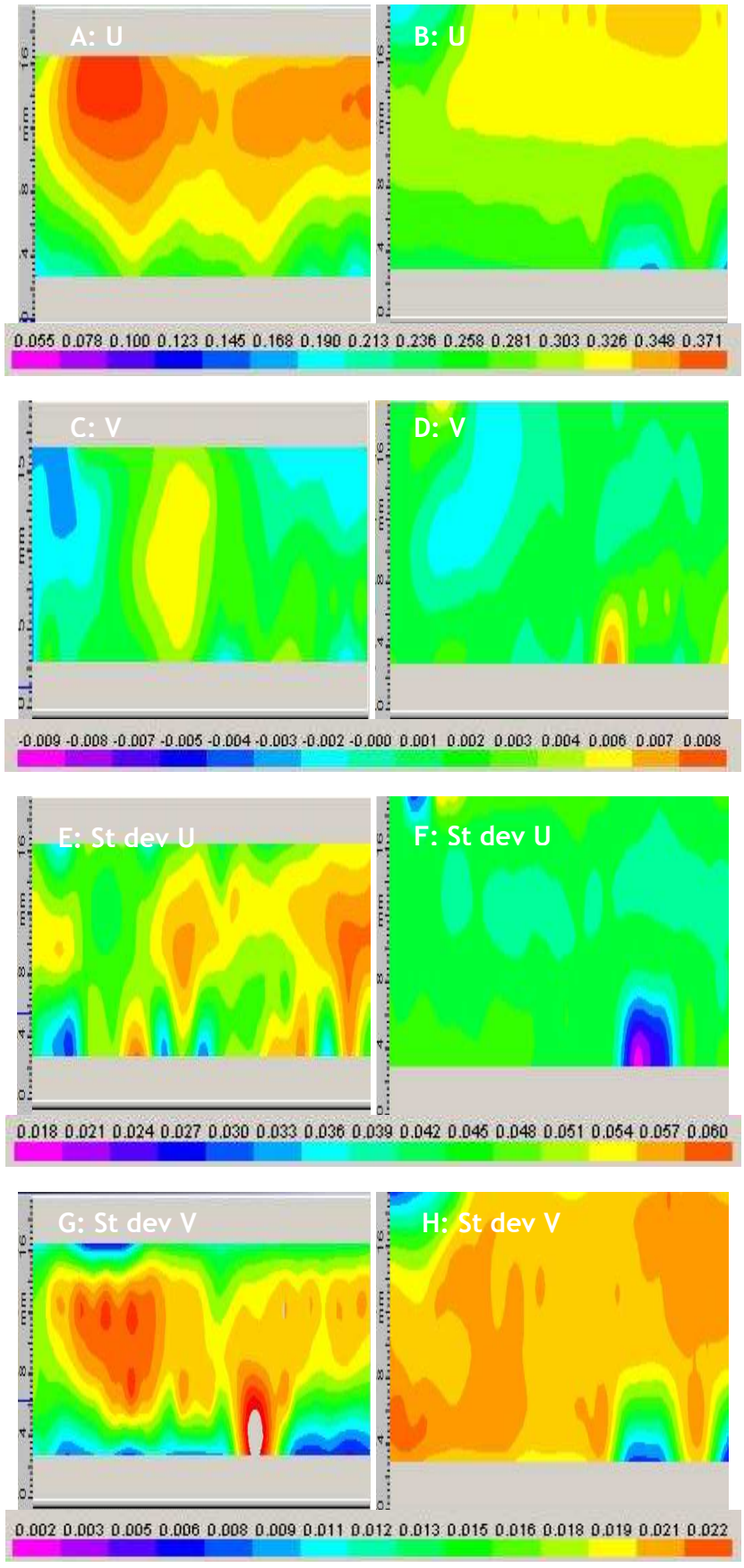

Figure 5. 14. LGS at 1.6l/s: A) *U* abiotic sediments; B) *U* 1 weeks of growth; C) *V* abiotic sediments; D) *V* 1 weeks of growth; E)Standard Dev *U* abiotic sediment; F) Standard Dev *U* 1 week growth; G)Standard Dev *V* abiotic sediment; H) Standard Dev *V* 1 week growth. (Scale

on the x direction equal to 60mm). Note that the gray zones coincide with the presence of a mask and hence the bed was visible. (Flow from left to right).

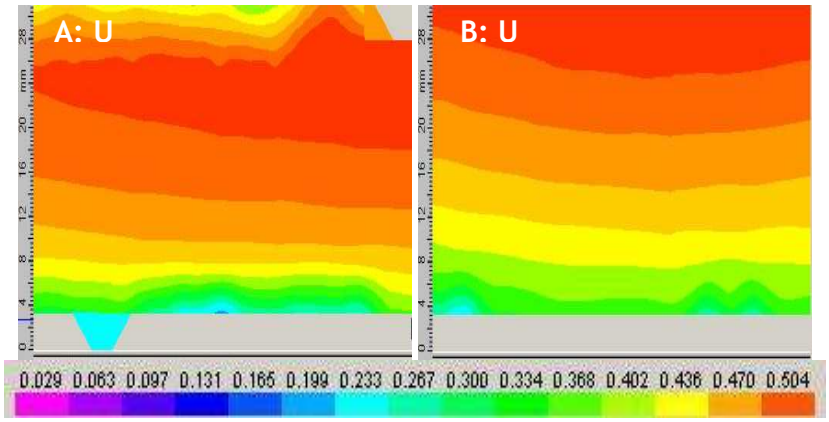

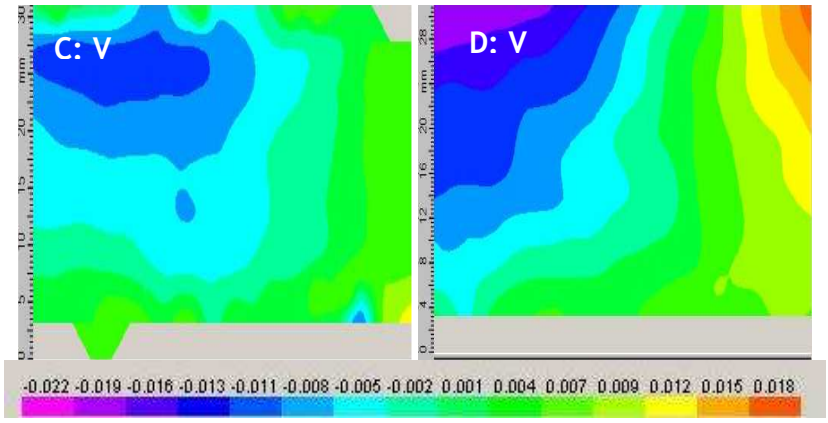

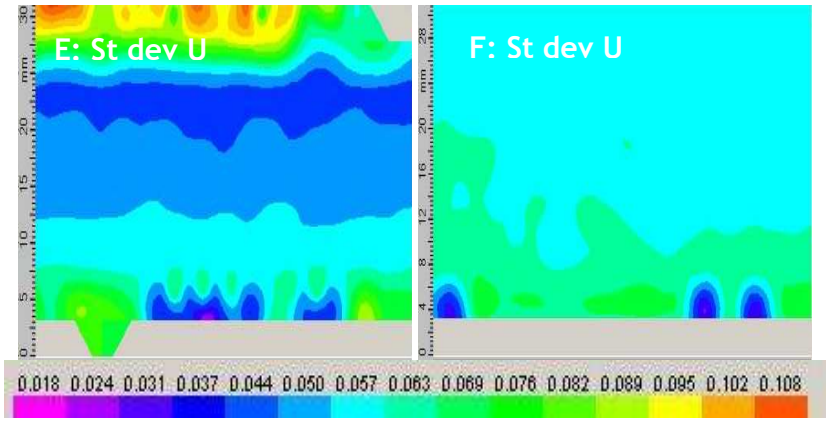

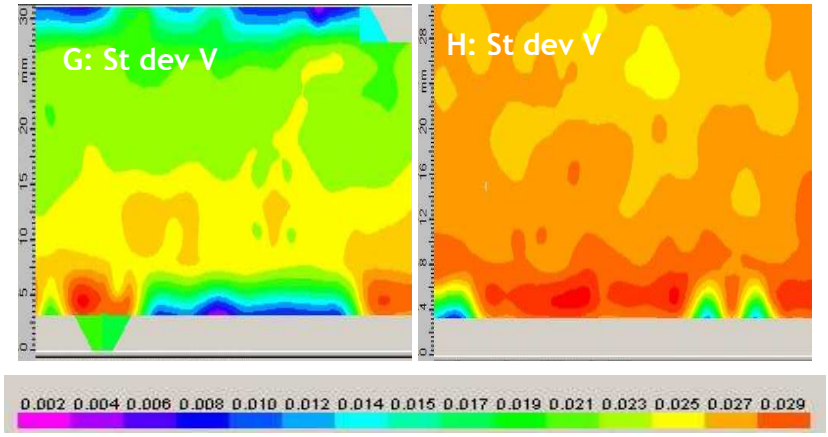

Figure 5. 15. LGS at 3.6l/s: A) *U* abiotic sediments; B) *U* 1 weeks of growth; C) *V* abiotic sediments; D) *V* 1 weeks of growth; E)Standard Dev *U* abiotic sediment; F) Standard Dev *U* 1 week growth; G)Standard Dev *V* abiotic sediment; H) Standard Dev *V* 1 week growth. (Scale on the x direction equal to 60mm). Note that the gray zones coincide with the presence of a mask and hence the bed was visible. (Flow from left to right).

LGS data show for *U* a trend similar to that of sand sediments. Importantly, figure 5.15 (3.6l/s) was affected by partial entrainment of the biotic substratum, thus resulting in little distinction between the abiotic and biotic data; hence, analysis herein focuses on the 1.6l/s biotic growth. At this lower discharge, the average downstream velocity *U* (see Appendix 5.E) is slower over biotic sediments than abiotic one for 1.6 l/s (8% less). Again, the range of *U* values is reduced in figure 5.14B, showing that the presence of the biofilm homogenizes the downstream flow velocity (either by membrane vibration and/or as a facet of damping of the V component of the fluid flow). Looking at the vertical velocity *V*, 1.6l/s (figure 5.14C, D) show a reduction in the range of the velocities from abiotic to biotic conditions (17%); whereas no great difference can be seen for 3.6l/s flow step. This value is lower than the reduction of *V* experienced for SGS (56%) and sand (from 65% to 92%). The standard deviation of V is slightly increasing for biotic sediments compared to abiotic condition (see figure 5.14H and 5.15H): this could be because erosion was taking place in some regions of the FoV. More interesting was the result obtained for the standard deviation of *U* (figure 5.14 E, F and figure 5.15 E, F). The standard deviation of *U* for 1.6l/s decreases of 14% from abiotic to biotic sediments. This can be explained again due to the more limited range of values of U experienced for biotic sediments.

Similarly, figure 5.16 and figure 5.17 show equivalent data for gravel beds at 4 weeks of growth at 1.6l/s and 5l/s, which was the threshold of entrainment for abiotic gravels (~10% more τ_b).

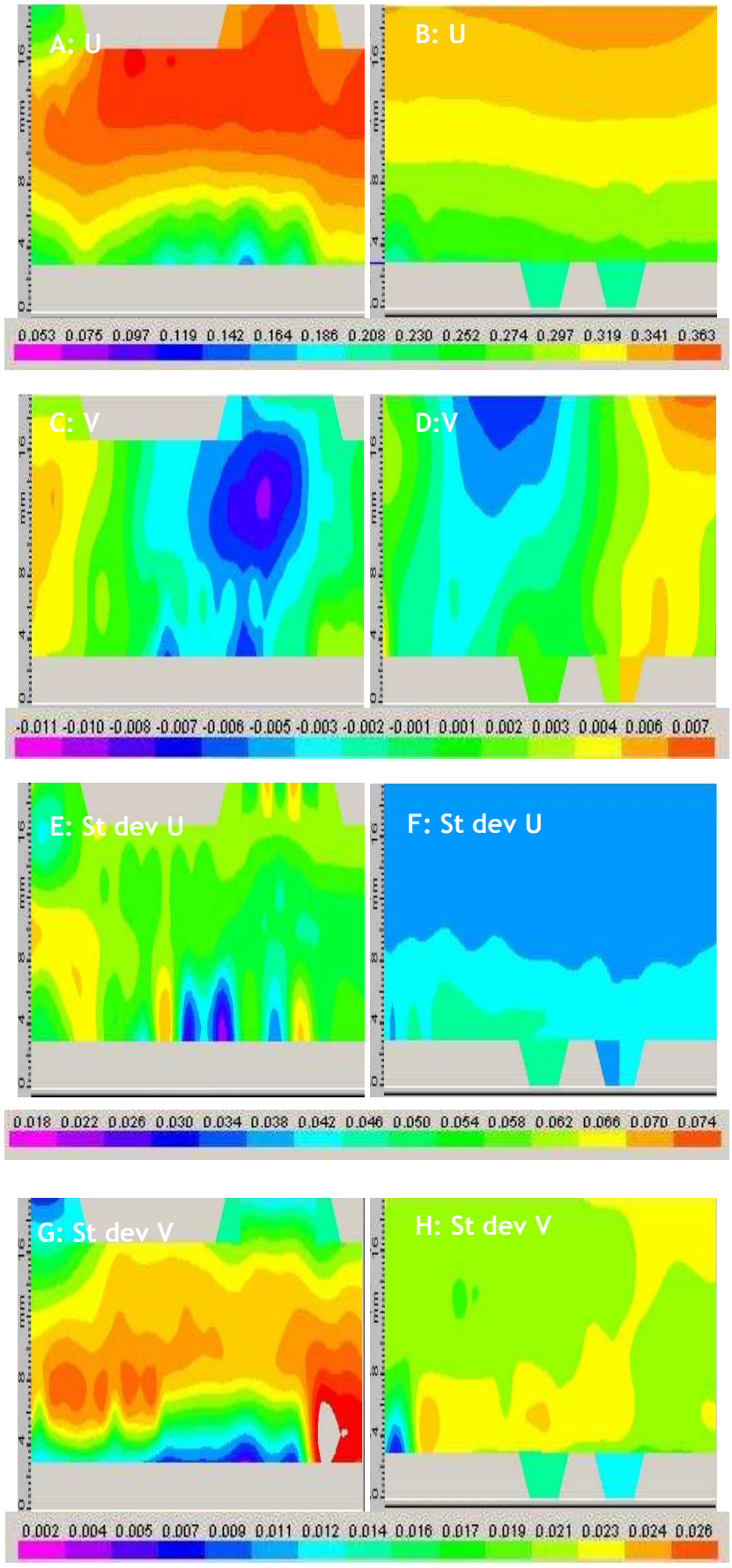

Figure 5. 16. Gravel at 1.6l/s: A) *U* abiotic sediments; B) *U* 4 weeks of growth; C) *V* abiotic sediments; D) *V* 4 weeks of growth; E)Standard Dev *U* abiotic sediment; F) Standard Dev *U* 4

week growth; G) Standard Dev *V* abiotic sediment; H) Standard Dev *V* 4 week growth. (Scale on the x direction equal to 60mm). Note that the gray zones coincide with the presence of a mask and hence the bed was visible. (Flow from left to right).

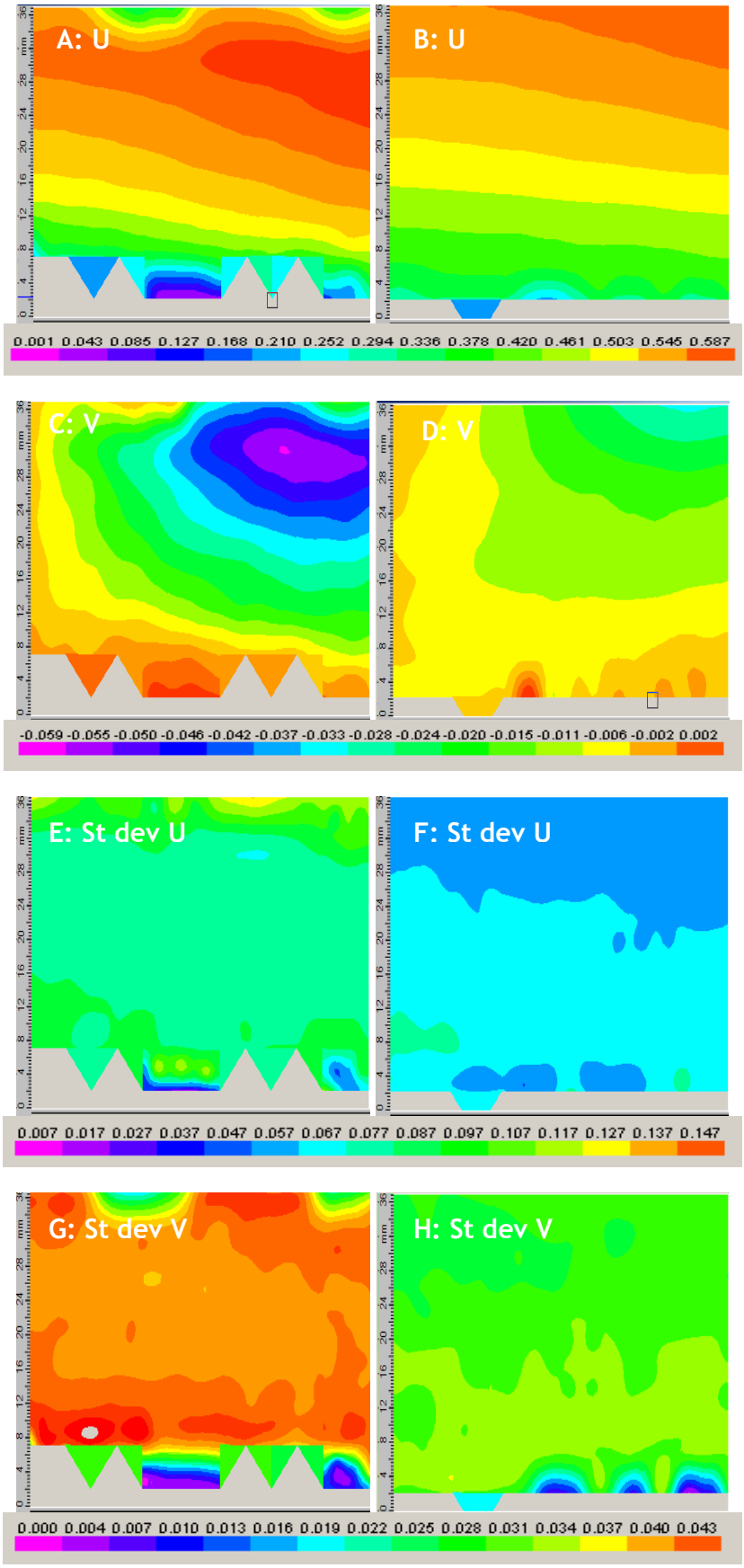

Figure 5. 17. Gravel at 5l/s: A) *U* abiotic sediments; B) *U* 4 weeks of growth; C) *V* abiotic sediments; D) *V* 4 weeks of growth; E) Standard Dev *U* abiotic sediment; F) Standard Dev *U* 4 week growth; G) Standard Dev *V* abiotic sediment; H) Standard Dev *V* 4 week growth. (Scale on the x direction equal to 60mm). Note that the gray zones coincide with the presence of a mask and hence the bed was visible. (Flow from left to right).

Gravel data. Looking at Appendix 5.E, a decrease in *U* over biotic substrata is ~5% in both discharges applied. Although this change in spatially averaged velocity is not very large, it is evident from the figure 5.16B and figure 5.17B that the bands of flow velocity in the case of biotic sediment become wider showing reduced standard deviation (29% lower for 1.6l/s and 22% for 5l/s) of the downstream flow velocity. The vertical velocity range *V* range, especially for the threshold condition 5l/s, reduces over biotic sediments by up to 10% (this is similar to the 17% value of LGS). Finally, looking at the standard deviation of V it is again very clear that the range of values is smaller than that of abiotic conditions and in particular from Appendix 5.E it is clear that for 5l/s there is up to a 32% decrease of the standard deviation over biotic sediments.

SUMMARY: When considered overall, the PIV results show that biofilm development over a non-cohesive coarse substratum causes the following:

- Reduction in the mean downstream velocity (*U*) by 5-22%; this is intriguing, as biofilm is seen to smooth the bed surface which would be expected to show acceleration. As this effect is seen in the natural materials of sand and gravels, it may be a facet of higher biomass and thus development of thicker and/or rougher bio-form (architecture of the biofilm surface) due to nutrients being present on natural grains and larger pore spaces (e.g. LGS) possibly enhancing the vertical aspect of growth. This would increase very local flow path lengths over the biofilm surface to augment boundary resistance in a manner observed by Battin *et al*. (2003) in biofilm surface "sinuosity". In addition, the observations of biofilm "flutter" are noted in these beds and, due to the physics of constructive wave interference, such oscillations may extract energy locally from the flow field.

- The exception to the above is SGS, which indicates a small degree of acceleration (+22%) in the *U* component of the flow field. As biomass is

low and pore sizes small, this may represent development of just a very thin and very smooth biofilm with pore clogging. This manner of smooth, homogeneous mats would reduce boundary resistance to accelerate flow; however, it is noted that some degree of membrane flutter can still be noted here and may act to self-limit the acceleration capability of the flow.

- The widening of the band of similar downstream velocity (i.e. the standard deviation of *U*) is also noted and will directly affect the bed shear stress, according to the fundamental definition $\tau_b=\mu\delta U/\delta y$, where for which smaller δU will induce lower values of τ_b. Thus, further review is undertaken in section 5.4.7.2.

- Clear evidence that vertical velocities are reduced by up to 72% following biofilm development. This reflects: (i) pore clogging so as to reduce upwelling/downwelling at the boundary; (ii) wave interference processes as membrane oscillations deflect the membrane vertically so as to "damp" vertical velocities. Crucially, it does seem that the boundary effects are not constrained to the inner region of the flow, but also impact the outer region flow structures to reduce vertical flow exchange in the upper layers of flow. This has important implications for nutrient exchange between fluid layers and between substratum-flow for river systems, as the flow is essentially more "laminar".

- Emerging trend for reduced standard deviation of downstream flow field component pertaining to a more homogeneous flow field. This also means that over a biotic bed the ejection and sweeps are more likely to be attenuated and follow a similar trend to that of a smoothed bed (Hardy *et al*. (2009); chapter 2, section 2.2.2.2), where the angle of the burst is reduced.

- Generally a strong relationship between biofilm development and lower range of standard deviation of the *V* component is found (reductions of up to 32%). This indicates damping of flow turbulence in the vertical, which is considered reflective of one or more of the following processes: (i) biological clogging of pore spaces reducing surface/subsurface exchange;

(ii) biofilm "fluttering" perpendicular to the plane of attachment, thus extracting energy and damping vertical flow fluctuations.

Given the above, Law of the Wall analysis was applied to the flow data to ascertain whether the boundary was smoothing during growth (z_0) and provide local shear stress data τ_b (considered more accurate than depth-slope averages employed in section 5.3.1).

5.4.7.2 Roughness values obtained applying the Law of the Wall

The double average technique of Nikora *et al.* (2001) was applied to our dataset: this, by averaging in time and in space, allows creating a single velocity profile representative of the hydraulic conditions taking place in the entire FoV analyzed. The time averaging technique, if applied over a long period of time (e.g. minutes, as in the conventional pulsed PIV systems) could mean that at threshold the flow structure around a biofilm eroding might be lost. In my case, since I was using a time resolved PIV I did not experience this problem and the time average was performed over time intervals smaller than 10 seconds. At this point the Law of the Wall (see chapter 2, section 2.2.2.3) was applied to each space and time averaged velocity profile. Values of the hydraulic roughness z_0 and of the bed shear stress τ_b at every flow step could be acquired, as shown in table 5.8. Importantly, the double average approach eliminates the time-variability of any membrane fluttering of the z_0; hence simplifies the hydraulic analysis herein.

SGS z_0 (mm)

Flow (l/s)	Clean	w1	w2	w3	w4
1.6	**1.16**	**0.36**	0.26	2.10	0.09
2.6	1.79	0.63	0.18	1.89	0.28
3.6	**3.48**	**0.44**	0.73	0.02	3.31

Sand z_0 (mm)

Flow (l/s)	Clean	w1	w2	w3	w4
1.6	**2.99**	**0.41**	1.08	1.19	0.00
2.6	0.85	0.50	1.11	1.61	4.08
3.6	**1.74**	**3.31**	1.61	0.94	4.88

LGS z_0 (mm)

Flow (l/s)	Clean	w1	w2	w3	w4
1.6	**1.35**	**0.59**	2.09	0.00	1.35
2.6	1.92	1.21	2.58	1.61	3.14
3.6	**5.81**	**2.39**	4.24	6.28	6.55
5	0.94	4.99	4.65	2.27	1.54

Gravel z_0 (mm)

Flow (l/s)	Clean	w1	w2	w3	w4
1.6	**2.80**	1.16	0.87	2.25	**0.17**
2.6	5.72	4.73	3.87	2.55	0.60
3.6	9.33	5.58	7.55	4.76	1.21
5	**12.96**	4.80	7.19	3.67	**5.51**

Table 5. 8. Hydraulic roughness z_0 (mm) calculated from the law of the wall for double average flow information at every flow step. Shaded cells show increases in roughness value; observations note that these occurred where the PIV FoV was localised over an unstable small area of substrata where entrainment threshold had been exceeded. In red, the strongest biostabilization conditions.

Looking at table 5.8, it is evident that each bed shows more than an order of magnitude of smoothing during biofilm growth, with minimum roughness values showing perfect smoothing (z_0 ~ 0mm) for all biotic substrata. The differences between %-change data were similar for all substrata, so no clear material difference could be found. However, examining table 5.8 in detail does suggest that the absolute values of z_0 tend to remain higher for biotic coarser substrata, in particular gravels; this is either a facet of the relative thickness of biofilm to initial roughness length (as highlighted earlier in chapter 5) or a function of bio-form being rougher over gravels due to maybe different growth orientations over the larger pores. Critically, in analysing table 5.8 it should be remembered that PIV data FoV was less than the area of planform observation used for areal erosion examination. Thus, the spatial patchiness of biotic substrata stability becomes important, and shaded cells in table 5.8 reflect data sets where PIV data appears localised to an unstable patch. Here entrainment threshold may have been exceeded and roughness lengths were therefore unreflective of biotic

coating. Therefore, analysis of this section considers the strongest biostabilization weeks (highlighted in red) as presented in section 5.4.7.1. Hence:

Hydraulic roughness z_0: In general two key points are highlighted from table 5.8. Firstly, all strong biotic beds with high biostabilization potential indicate roughness values less than abiotic beds for flows up to and including entrainment threshold. In particular the strongest biostabilized beds showed hydraulic roughness 56%-94% less than that of the equivalent abiotic substrata. In the case in which the roughness was increased compared to abiotic condition (see shaded cells in table 5.8) it is clear that for this flow rate the sample was for large part eroded and hence subject to transport that might have caused the high roughness to occur. Secondly, coarser substrata (a part from gravel in week 4) indicate slightly less smoothing than finer substrata which is indicative of the relative dimension of the sediment to the biofilm coating (i.e. for a sand grain a biofilm coating is "thick" relative to the size of the grain, and vice versa for gravel).

In the next section, the same analysis carried out for z_0 will be applied to the bed shear tress τ_b.

5.4.7.3 Bed shear stress values obtained applying the Law of the Wall

The double average technique of Nikora *et al*. (2001) coupled to the Law of the Wall (chapter 2, section 2.2.2.3) was applied to each space and time averaged velocity profile. Values of the bed shear stress τ_b are shown in table 5.9. Important to note is that these value are more precise than the depth average analysis presented before and hence will generate a better insight into the flow modifications induced by the biofilm presence on the bed.

SGS τ_b (Pa)

Flow (l/s)	clean	w1	w2	w3	W4
1.60	**0.95**	**0.62**	0.80	0.79	0.35
2.60	1.13	1.19	0.80	1.55	0.56
3.60	**1.38**	**0.98**	1.29	0.21	1.81

Sand τ_b (Pa)

Flow (l/s)	clean	w1	w2	w3	w4
1.60	**1.55**	**0.60**	0.99	0.89	0.01
2.60	0.91	0.78	1.00	1.47	2.00
3.60	**1.41**	**1.53**	1.20	1.03	2.57

LGS τ_b (Pa)

Flow (l/s)	clean	w1	w2	W3	w4
1.60	**0.79**	**0.47**	1.22	0.02	0.94
2.60	2.02	0.83	1.87	1.13	2.22
3.60	**3.39**	**1.58**	2.52	3.36	3.39
5.00	1.17	2.08	2.16	1.95	1.95

Gravel τ_b (Pa)

Flow (l/s)	clean	w1	w2	W3	w4
1.60	**1.71**	0.77	0.54	0.55	**0.31**
2.60	3.53	2.47	1.80	0.84	0.64
3.60	4.79	2.62	3.45	1.87	0.82
5.00	**5.51**	3.28	3.30	2.37	**2.31**

Table 5. 9 Bed shear stress τ_b values (Pa) calculated from the law of the wall for double average flow information at every flow step. Shaded cells show increases τ_b value; observations note that these occurred where the PIV FoV was localised over an unstable small area of substrata where entrainment threshold had been exceeded. In red, the strongest biostabilization conditions.

Bed shear stress τ_b: generally values of the bed shear stress resulted decreased compared to abiotic values at the same flow step; there was very little difference in the order of magnitude of shear stress reduction between material types; however the following hierarchy was noted at the lowest flow step (1.6l/s) SGS (34%) < LGS (41%) < sand (61%)< gravel (82%). This explains what has been seen in section 5.4.7.1, with the bands of similar velocity becoming wider and wider over biotic sediments and hence reducing the bed shear stress τ_b. Moreover, the reason why the decrease in bed shear stress τ_b is more evident for natural sediments depends on the fact that these are a rougher abiotic substrata compared to spheres and the presence of the bio-mats allowed to decrease significantly the irregularities of this surface and decreasing the resulting turbulence.

This again shows that the biofilm presence induced lower shear stress for colonized sediments in the case of strong colonization: the effect could be due

to the bio-mats, which because of their large density and consistency might have been allowed to flutter in the flow and hence to extract energy from it. More in depth analysis of this effect will be investigated in chapter 6 and chapter 8, where mechanical investigation of the bio-mat properties will be taken into consideration in the first chapter and a model considering the interaction of flow, sediments and bio-membrane will be suggested in the latter.

5.5 Chapter summary

Looking at the Hypothesis stated in section 5.2 it is possible to state that:

1. *Colonization*: it is evident that testing of larger-scale boxes (1m) with improved environmental set-up provides more natural bio-mat growth across all substrata (compared to that of chapter 4); thus, under the low shear stresses employed during growth in the present thesis bio-mats are the dominant biological growth form over sand and gravel beds. Specifically scales of 500-1000x grain diameter are considered appropriate for analysis of grain-scale entrainment analysis, as this scale permitted observation and analysis of spatial heterogeneity of biostabilization (which is evident in the field, Paterson personal communication); this permitted consideration of areal patchiness influence on entrainment threshold definition and indicated reduced growth time to maximum biostabilization of samples.

2. *Biostabilization potential:* was higher than what experienced in chapter 4 also for gravel size sediments; in particular it was clear that biostabilization depends on scale of growth (see section 5.4.5) and is strictly related to the time of growth and the relative patchiness that could depend on it. Strongest stability was found for SGS, sand and LGS in the first 2 weeks of growth, whereas for gravel sediment the strongest week coincided with week 4 of growth. This clearly indicates that river systems of even short periods of low/constant flow will be susceptible to biofilm development and significant biostabilization potential.

3. *Biological factors*: no clear relationship could be found between biofilm coverage (and hence biostabilization) and biological factors such as biomass and EPS (See section 5.4.6). As a detailed biological analysis of other variables (e.g. abundance, biological architecture) was outwith the scope of an engineering thesis, further research by microbial ecologists is recommended.

4. *Entrainment threshold definition:* In section 5.4.5 it is shown that the bed shear stress τ_b can be related to the percentage erosion of the box by an exponential relationship depending on time. If equation 5.3 was appropriately calibrated in natural environments, it could represent a valuable substitute to invasive assessment of the erosion characteristic of colonized sediment (e.g. benthic flumes or CSM). Moreover chapter 5 together with chapter 4 have demonstrated that the Yalin technique is effective in case of small samples but becomes less effective if the scale of culture is larger and hence patchiness takes place. This is because the techniques focuses on a very small scale and does not account for the behaviour of the remaining sample.

5. *Flow velocity & turbulence:* no clear change in the downstream velocity U was experienced in strong biotic beds, apart from SGS, for which the clogging of the pores might have meant a complete smoothing of the bed and hence a faster velocity. Interesting is that the standard deviation of U and V result lower over strong biotic beds than abiotic sediments. This is a result of the homogenization of the flow field and hence of the reduction of the turbulence (damped) due to biofilm growth (clogging and fluttering speculated).

6. *Roughness*: strong biostabilized bed have indicated to reduce significantly the hydraulic roughness of the substratum in a range going from 56% up to 94% less than the equivalent abiotic substrata; this has great importance on the turbulence generating on top of the bed.

7. *Shear stress at boundary*: The bed shear stress τ_b was clearly reduced as well due to the smoothing of the bed and thanks to the more homogeneous velocity field experienced over strong biostabilized beds. In

particular the reduction went from 34% for SGS 3.6 l/s to 82% for gravel 1.6l/s. The Law of the Wall has shown to be a much more detailed method to apply on space and time averaged velocity profile if detailed flow characteristics are wanted. However, this is quite a lengthy process of data collection and analysis and it could not be applied for all the flow steps analysed (see section 5.4.7); hence the depth-slope equation was a good quick approximation of the flow characteristics, which could yield preliminary results on the erosion characteristics.

Thus, the findings of chapter 5 show that bio-mat development clearly alters flow and sediment dynamics of an environmental boundary and discussion of these interactions and processes are elucidated further in chapter 7 (with reference to the literature). One factor implicit to this is the conclusion of inapplicability of conventional models of sediment transport (based on the concept of single particle moving) for predicting the entrainment threshold of bio-mat/carpeted sediments (where the entrainment dynamics and nature of the shear stress are both moderated by the bio-mat). When this difference of entrainment mechanics is considered alongside the failure of chapter 5 data to resolve the biological controls on biostabilization, there appears need to further review the bio-mat internal strength. At a macro-scale (cm-scale) level, this seems an engineering "material" consideration, appropriate to the present thesis. As no assessment of the mechanical characteristics of bio-mat failure appears present in the literature, it is possible that definition of elastic strength may be beneficial to implementation of mathematical modeling such that entrainment threshold/erosion could be associated to the strength of the membrane, which was defined as a composite material comprised of biofilm and embedded sediments. Membranes were evident at strong biostabilization stages and they sheltered and protected the sediment below, until the point in which the shear stress induced a break in the mat; what followed was a "carpet" like erosion, which left the previously covered sediments free to be eroded. This argument is therefore developed in chapter 6, based on quantifying the additional elastic force acting on a single grain due to the presence of the biofilm and EPS. Integration of chapter 5 and chapter 6 information will be given in the Discussion chapter (chapter 7)

and a suggestion for a model accounting for this force will be made in the Future Recommendations (chapter 8).

CHAPTER 6

Biofilm Mechanical Properties

"A scientist discovers that which exists.

An engineer creates that which never was."

Theodore von Karman

6.1 Introduction

This chapter investigates the importance of the biofilm "material" from a mechanical point of view. Although biofilms are prevalent in almost all moist and wet environments, very fragmented and situation bound information are available on the properties of cell-cell cohesion and biofilm adhesion to different surfaces. This makes the modelling of biofilm erosion and sloughing fraught with uncertainties. The majority of previous studies focus on the nano and micro-scale properties of biofilm (See section 6.2 for a review) in waste water treatment application. In the case of large bio-mats in marine and riverine environments very few papers investigate the bulk property of biofilm at the cm^2-m^2 scale (section 6.2).

Thus, in this chapter the focus was on measuring the bulk properties of biofilm-only and biofilm coating sand size sediments, in a way that was believed useful to increase our knowledge on the processes of erosion of these bio-mats under shear flow. In chapter 4 and chapter 5 it has in fact been demonstrated that for sand size sediment the erosion of mature bio-mats takes place as a "carpet"; this induce to think that the mats have an elastic strength, which will fail at a certain point under the fluid shear. This failure mechanism is very similar to what takes place during a traditional tensile test. Hence in this chapter it will be

demonstrated that the cohesive strength (section 6.3- section 6.6) and Young's modulus of elasticity of moist bio-mats can be measured using tensile testing, with the condition that strong filamentous bacteria need to comprise the biofilm. Tensile testing has never been used to investigate the bulk property of a self sustaining biofilm; due to its fragile nature many researchers have deemed this extensively used engineering technique as inappropriate (Aggarwal *et al.*, 2010). Only one team (Ohashi *et al.*, 1999) has successfully used this method for obtaining bulk property of a fragile biofilm but growing this on tubes and testing the strength of the adhesion at the junction (see section 6.2). I instead showed that, if the structure of the biofilm is strong, which means having filaments entangled and creating more strength, then tensile testing can be used to acquire measurements of the Young's modulus of elasticity (*E*). This innovative way of testing bio-mats is straightforward because it allows use of a commercial load cell without the need to customize any porously built testing equipment; yet it can improve dramatically our knowledge on the material properties, which are desperately required for parameterising new mathematical models of bio-mat breakage.

To my knowledge the testing of bulk biofilm properties at a large scale using a commercially available instrument (*Tinius Olzen 5N Tensile Tester)* has never been attempted before in research; this is why the results in this chapter have been recently published in the journal of B*iotechnology and Bioengineering* (Vignaga *et al.*, 2011). The results presented herein aim to modify many of the available engineering models of sediment transport for sand sizes and smaller, as will be briefly presented in chapter 8 in the future refinements section.

However, for fine gravel size sediments, which do not experience the formation of bio-mats, I intended to raise the awareness that biofilm presence might anyway affect the behaviour of such sediments size. In fact biofilm can change the non-cohesive properties of the sediments due to its adhesive nature. By using a very simple adhesion test (see section 6.7) I will show that under fluid shear gravel might experience an increased cohesion due to the colonizing biofilm. This has the scope to induce researchers to evaluate for the first time the possible effects that biofilms might have on larger sediments, a topic that has been completely neglected in the literature up to now.

6.2 Mechanical and elastic properties of biofilms

Biofilms can be both positive, such as in bioremediation (Paul *et al.*, 2005; Fernández-Luqueño *et al.*, 2011), metal immobilization (Cox *et al.*, 1999; Van Hullebusch *et al.*, 2003) and biostabilization of mobile substratum (e.g. Paterson 1997; Black *et al.*, 2002), or negative, for example, in biofouling of infrastructure or ship hulls (Little *et al.*, 1997; Schultz and Swain, 1999; Teng *et al.*, 2008; Andrewartha *et al.*, 2010). Wastewater treatment is a prime example of the importance of biofilms. In this field the mechanical properties of biofilm have largely been investigated by researchers in order to avoid sloughing and erosion, in order to keep the cost of the water-treatment plants low. The mechanisms that induce biofilm detachment are complicated to define and to model (Stoodley *et al.*, 2001; Ahimour *et al.*, 2007). This is because it is difficult to obtain mechanical properties of biofilms without disrupting the inherent structure of the microbial assemblages. As particular attention is afforded to analysis at scales of specific engineering relevance (Poppele and Hozalski, 2003; Aggarwal *et al,* 2010), the majority of papers consider detachment mechanics at the micrometer scale (e.g. Poppele and Hozalski, 2003; Ahimou *et al.*, 2007; Aggarwal *et al,* 2010) as appropriate to the detachment scales of 25-200μm found for wastewater treatment applications (Zahid and Ganczarczyk, 1990). Many of these experimental studies have used a well know bacterium *Pseudomonas aeruginosa,* which forms biofilms with a consistency akin to that of a weak gel (Körstgens *et al.*, 2001; Poppele and Hozalski, 2003 and Aggarwal *et al*. 2010). The inherent fragility of those biofilms has led researchers to design delicate and sensitive analysis techniques to measure the cohesive strength at the micro-scale. Thus, methods successfully utilised at this scale include the micro mechanical technique (Yeung and Pelton, 1996); micro-cantilever method (Poppele and Hozalski, 2003); atomic force microscopy (Ahimou *et al.*, 2002; Ahimou *et al.*, 2007); and fluid dynamic gauging (Möhle *et al.*, 2007).

However, biofilms in aquatic environments (such as rivers, estuaries and coastal waters) more firmly colonize sediments by forming strong bio-mats that roll and tear in a fabric or carpet like manner over scales of many centimetres (chapters 4 & 5; Neuman *et al.*, 1970; Grant *et al.*, 1986; Walker and Grant, 2009). The failure mechanism and the fact that cm^2 of detached biofilm and heavy

sediments remain intact suggest that it is actually the 'bulk' properties of the biofilm that are crucial to cohesive strength analysis; this implies that biofilms may be amenable to direct measurement of their strength by uniaxial tensile testing. The benefit of tensile testing over other techniques is that it is a very traditional and established engineering technique that directly relates stress (σ) and strain (ε). This latter point is important, as stress-strain would yield tensile strength and Young's modulus (E) of elasticity; i.e. parameters suitable for correcting existing engineering equations for biotic interaction (Black *et al.*; 2002). Thus, table 6.1 shows five past studies that specifically implement tensile testing of biofilm for a range of scales; of these, only the papers by Ohasi amd Harada (1996) and Ohasi *et al.* (1999) are at scales >1mm^2 and therefore relevant to the present thesis. Specifically, Ohashi and Harada (1996) applied a compression test to the biofilm; yet, compression is unlikely during shear-based erosion of biofilm in marine and riverine environments, where fluid drag and lift forces would most likely lead to tension at failure and it has been shown to yield larger values than any other testing technique (Aravas and Laspidou, 2008). Thus, only one team of researchers have quantified the cohesive bulk properties of a biofilm by traditional tensile testing (Ohashi *et al.,* 1999). This study separately cultured aerobic and denitrifying biofilms of slightly different bacterial structure in tubes 4.76mm in diameter. Their uniaxial tensile test artificially induced biofilm detachment at a specific location, resulting in tensile strength of 500-1,000Pa. Whilst this is directly relevant to providing a measure of cohesive strength it is highlighted that Ohasi *et al.*'s (1999), research is still at the sub-cm scale and necessitated of a surface to sustain the sample during the testing, crucially modifying the adhesive properties of the biofilm. Thus, the present thesis extends tensile testing to self sustained moist samples at cm scales, more relevant to biostabilized sediments in natural aquatic and marine environments and compares the properties of biofilms alone with biofilm/sediment composites.

Bacterial species	Method or device	Scale (mm^2)	Result (Pa)	Reference
Denitrifiers and Anaerobes	Tensile test device	~1	500-1,000	Ohashi *et al.* (1999)
Denitrifiers	Centrifugation and plate drop method	2500	0-8	Ohashi and Harada (1996)
Sludge Flocs, *P. Aeruginosa*	Microcantilever	0.002	395-15,640	Poppele and Hozalski (2003)
P. aeruginosa and *S. epidermidis*	Microcantilever for intact biofilm	0.1	59-18,898	Aggarwal *et al.* (2010)
S. epidermalis	Microcantilever for intact biofilm	0.05	780-4,550	Aggarwal and Hozalski (2010)
Cyanobacterium (*Phormidium* sp.)	Tensile Tester	200	1,288-20,056	This study (2011)

Table 6. 1. Tensile strength values available in the literature and relative experimental techniques employed and scale (mm^2).

The importance of evaluating the cohesive strength of biotic sediments at cm^2-m^2 scales appropriate for sediment erosion is well known among field-based researchers that work with colonized cohesive sediment. For example, the Cohesive Strength Meter (CSM, Paterson, 1989; Tholurst *et al.*, 2000; Vardy *et al.* 2007; See chapter 2), is now extensively used in the field for this purpose. Alternatively, the ingenious Magenetic Particle Induction (MagPI- magetic particle induction), based on the magnetic attraction of artificially produced fluorescent ferrous particles, is being explored for assessing stability in biogenically coated sediment systems (Larson *et al.*, 2011). However, it is difficult to translate the proxy measurements of strength (e.g. water turbidity variations or magnetic force) into established engineering variables and thus calibrating a mechanical model of bio-mat failure where stresses are applied in shear rather than normal to the bio-mat surface.

In chapter 4 and chapter 5 it was shown that that the bacterial species that we selected produces strong mats comprising entangled filaments in a dense EPS matrix. Removing large portions of the bio-mats from the surface of the sand size sediment surface was possible and, in many cases, grains of sediments were still embedded into the mat after extraction. This suggested that the bio-mat was strong enough to be tensile tested and the methodology and results of these tests are presented in the following sections.

6.3 Methodology (5N-100N *Tinius Olsen* H1KS tensile tester)

6.3.1 Bacterium, inoculation, and colonization

In line with chapters 4 and 5, a phototrophic cyanobacterium *Phormidium* sp. (See chapter 3, section 3.4.1) was cultured fully-submerged in a fluid medium of full strength BG-11 (with $NaNO_3$) nutrient (Ripkka *et al.,* 1979). Table 6.2 shows that two different types of specimens were grown: biofilm-only and biofilm grown over sediment. **Biofilm-only (BO)** was cultured into in non agitated conditions for 2-3 weeks in an incubation chamber. A constant water temperature of 28°C and a light intensity of 25 µmol m^{-2} s^{-1} were maintained throughout. This produced thin sheets of bio-mat, floating in the nutrient solution. **Biofilm grown (BG)** over sediment samples were cultured for up to 8 weeks under constant unidirectional flow conditions applied over non-cohesive granular substratum of spherical glass **beads** with D_{50}=1.09mm (BG**B**) or **sands** (BG**S**) with D_{50}=1.2mm[1]. Experimental conditions were identical to those outlined in chapter 3, section 3.4.4 and resultant composite-sediment growth assemblages were comparable to Noffke *et al*. (2001), with initial mat development taking 2-4 weeks.

	Width (mm)	Length (mm)	Thickness (mm)	Flow Conditions	Growth period	Measurement Method	Light Int. (µmol m^{-2} s^{-1})	Load Cell
BO1	6.00	28.00	1.02	Non agitated	2/3 weeks	Caliper	25	5N
BO2	12.00	16.00	0.60	Non agitated	2/3 weeks	Caliper	25	5N
BO3	6.00	22.00	1.02	Non agitated	2/3 weeks	Caliper	25	5N
BO4	14.00	29.00	0.51	Non agitated	2/3 weeks	Caliper	25	5N
BGB1-C	8.90	12.75	1.12	Flowing	¾ weeks	Sony HDR-SR5E	120	5N
BGB2-C	18.30	28.95	2.14	Flowing	¾ weeks	Sony HDR-SR5E	120	5N
BGB3-C	5.35	15.76	2.00	Flowing	¾ weeks	Sony HDR-SR5E	26	100N
BGB4	2.58	9.36	0.90	Flowing	2/3 weeks	Sony HDR-SR5E	26	100N

[1] It is important to note that gravel beds are considered separate (Sec. 6.7) to the main body of research in this chapter; in justification, chapters 4 & 5 indicate that extensive bio-mats are not present in these beds, precluding sample extraction for ex-situ tensile testing.

BGB5	6.73	12.72	2.10	Flowing	7/8 weeks	Sony HDR-SR5E	26	100N
BGB6	9.13	10.38	1.45	Flowing	7/8 weeks	Sony HDR-SR5E	26	100N
BGS1-C	6.35	12.29	3.42	Flowing	¾ weeks	Sony HDR-SR5E	120	5N
BGS2-C	8.33	13.44	2.36	Flowing	¾ weeks	Sony HDR-SR5E	120	5N
BGS3-C	6.10	14.10	2.70	Flowing	¾ weeks	Sony HDR-SR5E	120	5N
BGS4	6.98	13.64	1.61	Flowing	6/7 weeks	Sony HDR-SR5E	26	100N
BGS5-C	6.69	14.50	2.67	Flowing	7/8 weeks	Sony HDR-SR5E	26	100N
BGS6-C	9.65	16.70	2.86	Flowing	7/8 weeks	Sony HDR-SR5E	26	100N

Table 6. 2. Biofilm only (BO) and biofilm grown over a substratum (beads (BGB) or sand (BGS)) specimen's type (biofilm only/composite), dimensions, growth conditions and load cells used for the tensile tests.

6.3.2 Tensile tests

All samples (BO; BGB; BGS) were carefully extracted from the culturing medium and cut into sub-samples (~20mm in length by ~10mm in width) approximately rectangular after the excess surface water was removed using absorbent paper. In the case of biofilm grown bed surface; due to growth characteristics samples naturally self-restricted to removal of the surface-layer only, with the result that some of the specimens presented grains attached to the bio-mat. These samples are classified as **composite** biofilm/substratum and will be identified with the suffix **-C** (see table 6.2). Specimens longer than ~20mm could not be generated because the weight of the grains attached induced their failure. For each sample, the shorter edges of the samples were glued (using cyanoacrylate based adhesive on both side of the sample) onto paper strips and clamped into a *Tinius Olsen H1KS* tensile test machine as shown in figure 6.1.

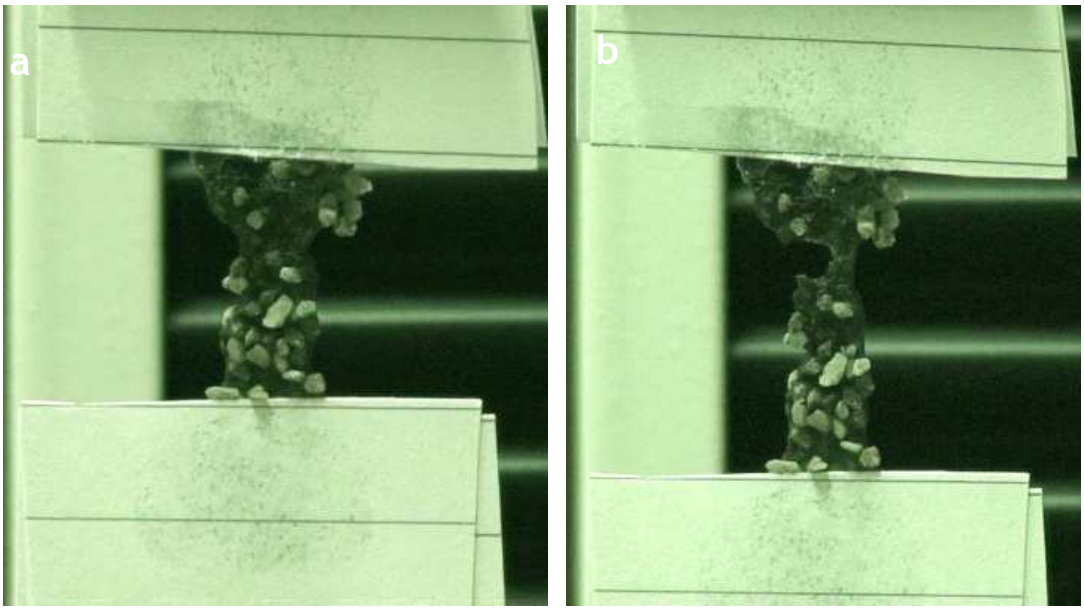

Figure 6. 1. Tensile tests for composite biofilm/sand BGB3-C under low applied force (a) and during failure under higher forces (b). This shows high adhesion as no particles detached from the bio-mat under testing.

Ideally the load testing would have been done using the most sensitive load cell available, which in our case was a 5N cell. Unfortunately, this cell broke during the period of our experiments and we resorted to a less sensitive 100N cell; however the trend experienced clearly indicate that this gave equivalent results (see section 6.5) and this is considered a useful finding in itself, in that expensive sensitive loads cells are not a prerequisite for biofilm testing. Using this load cell, initially a low constant displacement of 1.67 μm/s was applied to BO1-2 (strain rate of 0.06-0.10m/s) in order to measure force variations in great detail; since bio-mats have never been tested before the aim was to achieve as much information and as great resolution as possible during the testing in order to capture even the smallest fracture in the specimen. Throughout the remainder of the experiments a constant displacement of 8.33 μm/s (strain rates of 0.29-0.89 m/s) was then used in order to minimize drying of the sample whilst still permitting very detailed analysis of force variations during elongation. The rates selected were 3 orders of magnitude lower than Aggarwal and Hozalski (2010). Biofilm dimensions (length, width and thickness) were also measured using ruler/callipers (BO1-4) or a *Sony HDR-SR5E* camera (BGB1-6, BGS1-6) with recorded data accurate to ±0.03mm; this data is presented in table 6.2. All tensile tests (except BO2) were executed within a timeframe of < 60 minutes

after their extraction from the fluid medium; this ensured that the biofilm remained 'moist' during testing.

The tensile force, F, and relative elongation (Δl) were recorded during the tensile test. The initial cross-sectional area, A, was calculated from table 6.2, multiplying the thickness by the width of each sample and this was used to obtain the engineering stresses assuming that the cross section would not change until failure. The engineering stresses (σ) and strains (ε) before failure have been calculated using the equations,

$$\sigma = \frac{F}{A} \qquad \textbf{Equation 6. 1}$$

$$\varepsilon = \frac{\Delta l}{l_0} \qquad \textbf{Equation 6. 2}$$

where Δl is the elongation and l_0 is the initial length of the specimen. The cohesive strength was taken to be the maximum stress achieved in the test before failure. Young's modulus, E, is given by,

$$E = \frac{\sigma}{\varepsilon} \qquad \textbf{Equation 6. 3}$$

and is commonly used as a proxy for the stiffness of biofilm material (Aravast and Laspidou, 2008). This was approximated by the gradient of the best-fitting (least-squared) straight line though the elastic component of the stress-strain curves.

6.4 Hypothesis

The mechanical properties of bio-mats (BO, BGB and BGS) were investigated using tensile testing. Three hypotheses have been made for those experiments:

- *Elasticity of the material*. Bio-mats have been expected to behave as an elastic material (with a linear proportionality among force applied and elongation) in line with the finding of others (Klapper *et al.*, 2002; Klapper and Alpkvist, 2007; Shaw *et al.*, 2004). I anticipated that the strength of biofilm-only (BO) specimens and the relative cell-cell cohesion would be higher than the composite biofilm-substratum; i.e. bonding to the surface is weaker than bonding between filaments.

- *Cohesive strength*. *Phormidium sp*. cohesive strength would be comparable in magnitude to the higher ranges published in the literature (see table 6.1 and experiments on return activated sludges (RAS) by Poppele and Hozalski (2003)). This is logical, as the ESEM data (see chapter 3, section 3.4.1) show cyanobacteria to have highly filamentous structure embedded into the EPS matrix; this should augment mechanical strength, compared to the more gel-like biofilm considered in previous literature.

- *Tensile Test limitation*. Tensile testing would only be viable where bio-mats were well-developed; based on chapter 4 and 5 data, this would limit analysis to sand size (and finer) substratum. Yet, given that biostabilization has been shown to occur for gravel beds, a bespoke analytical technique should be explored to quantify biofilm-gravel adhesion strength via similar ex-situ testing.

6.5 Tensile tests results

In figure 6.2 we present the raw data trend derived from the tensile tests of BO specimens and BG samples; this plots the force (N) to elongation (mm) relationship for all the specimens sampled and is preferred (to normalized stresses) in situations considering multiple membrane failures. Subsequently table 6.3 presents the normalized stresses and the Young's moduli of elasticity calculations to analyze if there is a consistency in the material properties within different material types.

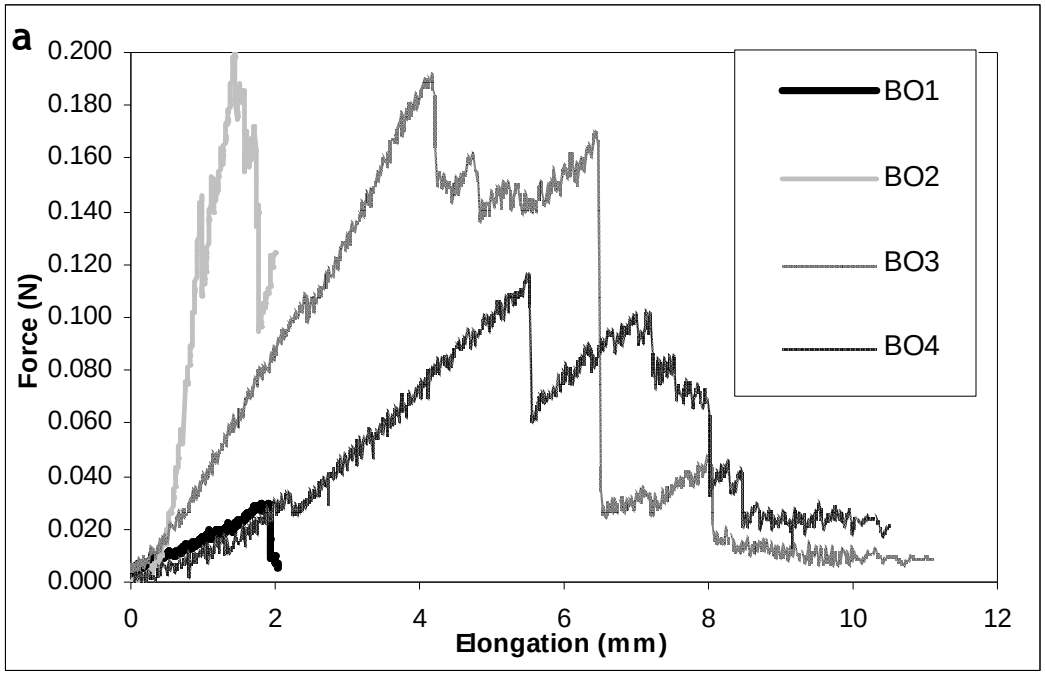
a
0.200
0.180
0.160
0.140
0.120
0.100
0.080
0.060
0.040
0.020
0.000
Force (N)
0
2
4
6
8
10
12
Elongation (mm)
BO1
BO2
BO3
BO4

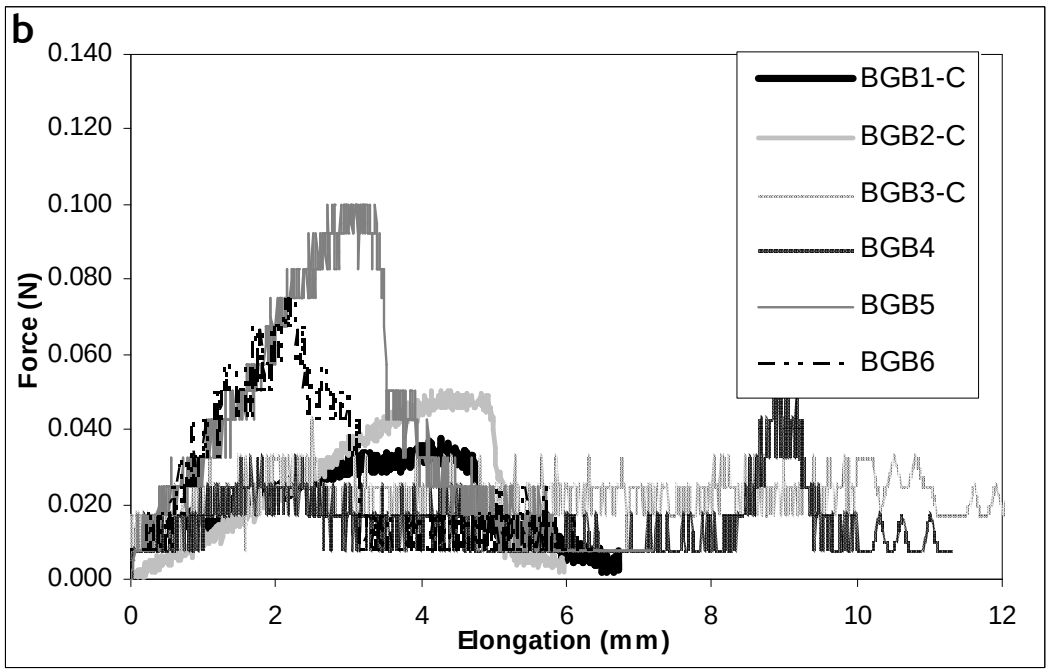
b
0.140
0.120
0.100
0.080
0.060
0.040
0.020
0.000
Force (N)
0
2
4
6
8
10
12
Elongation (mm)
BGB1-C
BGB2-C
BGB3-C
BGB4
BGB5
BGB6

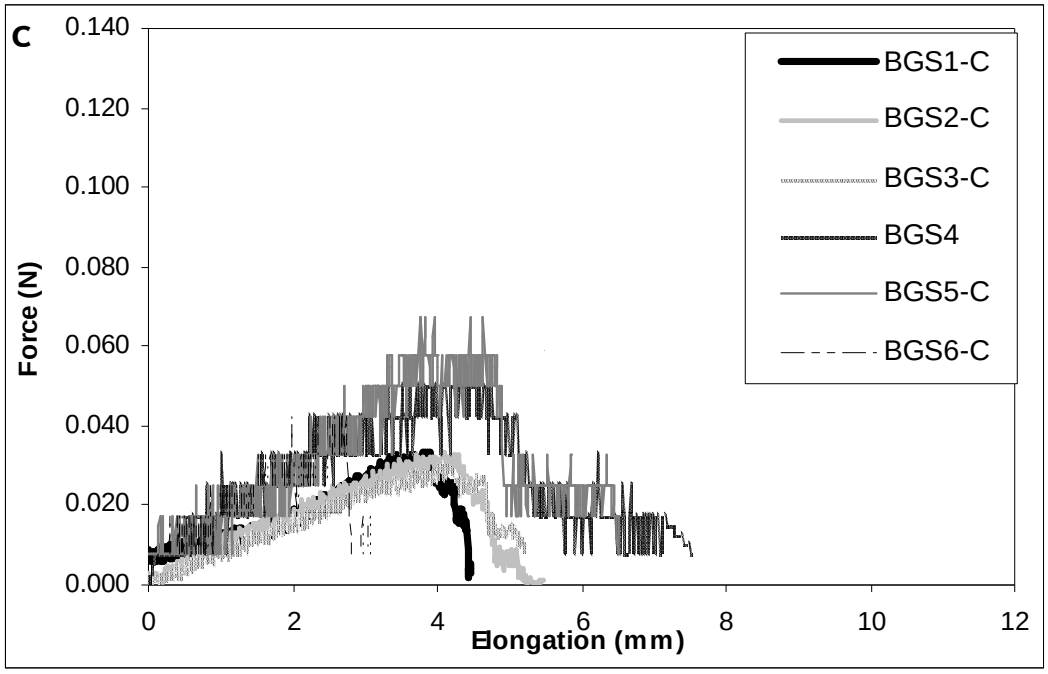

Figure 6. 2. Force (N)-Elongation (mm) graphs for: a) Biofilm only samples (BO1-4); b) Biofilm grown over beads samples (BGB1-BGB6) and c) Biofilm grown over sand samples (BGS1-BGS6). In case of the usage of the 100N load cell (see table 6.2), although the data present lower accuracy in the resolution, a clear initial elastic trend is visible.

In terms of the failure mechanics, figure 6.2a shows that BO samples exhibit multiple failures (except BO1). Typically the maximum force applied during the test is associated with the first failure, which then weakens the biofilm such that subsequent failures occur with lower applied force. Crucially, this type of failure is distinct from that shown by BG samples, which demonstrate a single catastrophic failure event (see figure 6.2b and figure 6.2c). This leads us to think that BO has a higher cohesion among cells because it is not affected by any discontinuity (which represents a weakness) in its surface as for composite materials. Hence BO therefore stretches, almost like a relatively homogenous fabric to present high mechanical resistance. Once one failure has occurred, subsequent failure is a facet of the additional weight of the failed component action on the reduced area of attachment of the remaining bio-mat; hence it is logical that a subsequent failure occur for lower forces because the specimen has been already weakened by the first failure, yet the cohesion among the remaining cells is still strong enough to remain intact. On the other hand a biofilm grown over a substratum has the strong, cohesive cell-cell bonds and intertwining of filaments interrupted by the sediments. Here this represents a weakness of the composite material, which is more prone to tearing and, once

tearing begins, the additional weight of the failed grain and biofilm composite is sufficient to continue the tearing process in one single failure process.

Regarding the quantification of material strength, the maximum force recorded at first failure data, F_{max}(N), and cohesive strengths given by the engineering stress σ_{max}(Pa) are presented in table 6.3 for BO, BGB(-C) and BGS(-C) samples. The cohesive strength of BO samples range from 4,132Pa (BO1) to 20,056Pa (BO2); however, sample BO2 was affected by drying time slightly in excess of the prescribed 60 minute threshold and the associated uncertainty means that it is more appropriate to consider BO3 values as the maximum strength recorded (15,098Pa). Importantly, this compares well to biofilm samples grown over the glass beads (BGB4-6, which indicate equivalent strengths of 5,667Pa-14,018Pa) and over the sands (BGS-4, at 3,886Pa). However if we consider the composite samples (-C) where grains are still embedded in the biofilm, then samples with glass beads (BGB1-3-C) have strengths only 1,288Pa – 3,034Pa and sands (BGS1-3-C and BGS5-6C) show 1,339Pa – 3,283Pa. Thus, it becomes clear that the material strength of composites is up to 10 times lower than BO samples.

Three findings are therefore notable: firstly, the cell-cell cohesive strength of the bio-mat appears the same, independent of whether it grows over a substratum of glass beads or suspended in a fluid medium; secondly, the adhesion of biofilm-to grain clearly weakens the mechanical properties of the material; thirdly, bio-mats grown over natural sands appear to be naturally weaker due to geochemical properties of the sand surface. The significant benefit of the data set presented is that these findings are appropriately validated and quantified.

	F_{max} (N) [a]	σ_{max} (Pa)[b]	Max Strain	E (Pa)[c]	R^2	Property[d]
BO1	0.030	4,132	0.06	50,627	0.98	Cohesion
BO2	0.146	20,056	0.06	316,979	0.84	drying/cohesion
BO3	0.108	15,098	0.11	139,106	0.99	Cohesion
BO4	0.033	4,674	0.07	54,590	0.92	Cohesion
BGB1-C	0.019	1,921	0.07	8,706	0.65	cohesion/adhesion
BGB2-C	0.050	1,288	0.14	8,692	0.99	cohesion/adhesion
BGB3-C	0.033	3,034	0.07	17,254	0.36	cohesion/adhesion
BGB4	0.033	14,018	0.16	49,912	0.63	Cohesion
BGB5	0.100	6,179	0.21	24,828	0.97	Cohesion
BGB6	0.075	5,667	0.21	24,428	0.93	Cohesion
BGS1-C	0.034	1,339	0.31	3,475	0.95	cohesion/adhesion
BGS2-C	0.033	1,690	0.30	5,207	0.97	cohesion/adhesion
BGS3-C	0.031	1,599	0.29	5,191	0.97	cohesion/adhesion
BGS4	0.050	3,886	0.24	11,257	0.83	Cohesion
BGS5-C	0.068	3,283	0.26	9,111	0.89	cohesion/adhesion
BGS6-C	0.043	1,538	0.11	9,156	0.85	cohesion/adhesion

[a] F_{max} (N) is the maximum force experienced before break;
[b] σ_{max} (Pa) is the maximum engineering stress achieved before alteration of the sample relative to the maximum strain (Max Strain);
[c] E (Pa) is the Young's modulus of the elastic trend;
[d] Properties underlines if during the test adhesion was also a variable due to the presence of grains attached to the specimen.

Table 6. 3. Cohesive strength results for biofilm only (BO) and biofilm cultured over a substratum (beads (BGB) or sand (BGS)) in the initial elastic trend before failure of the sample.

In figure 6.3 we have related the strain (ε) against the maximum engineering stress (σ_{max}Pa). Interestingly BO samples experience much higher cohesive strength, but show limited elongation. This seems to suggest that the internal bonds for BO are stronger than any other composite material, increasing the stiffness of the sample. A similar behaviour can also be seen for BGB samples: the internal strength is comparable to the lower range of BO values but the elongation is 2 to 3 times higher.

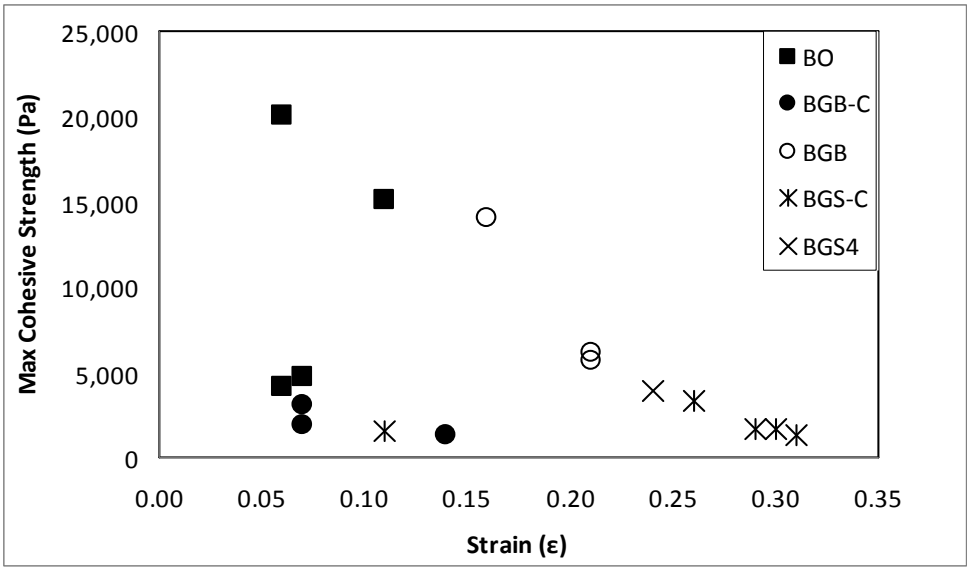

Figure 6. 3. Strain (ε) plotted against the maximum cohesive strength σ_{max}(Pa) for biofilm only (BO, ■), composite biofilm and beads (BGB-C, ●), Biofilm grown over beads (BGB, ○), composite biofilm and sand (BGS-C, *) and Biofilm grown over sand (BGS4, X).

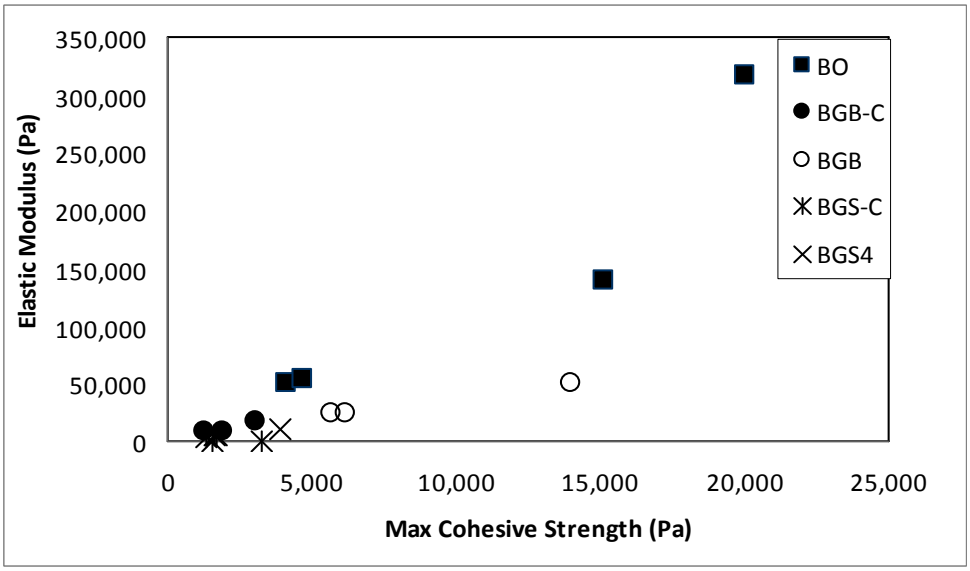

Figure 6. 4. Maximum cohesive strength σ_{max} (Pa) against the elastic modulus (E) (Pa) for biofilm only (BO, ■), composite biofilm and beads (BGB-C, ●), Biofilm grown over beads (BGB, ○), composite biofilm and sand (BGS-C, *) and Biofilm grown over sand (BGS4, X). The proportionality among BO is 7 times higher than BGS-C samples, 5 times higher than BGB and 3 times higher than BGB-C.

In figure 6.4 the elastic moduli are compared to cohesive strength; here there is a direct positive relationship between the two variables and this is not surprising, since Young's modulus of elasticity has been used as a proxy for biofilm stiffness (Aravas and Laspidou, 2008). Hence a direct proportionality as

presented in figure 6.4 can be explained. However, when comparing the different samples tested, it is possible to see that the proportionality of σ_{max}(Pa) and Young's modulus (see figure 6.4) in BO specimens is 5 times higher than BGB, 3 times higher than BGB-C and 7 times higher than in BGS-C samples. Specifically, table 6.3 shows that BO specimens have a Young's modulus (from 50,627 to 139,106Pa, ignoring the outlier of BO2) greater than the biofilm cultured over a substratum but with no grains attached; this is up to 3 times greater than BGB4 (49,912Pa) and 12 times greater than CBS4 (11,257Pa). Given that the substratum type does not appear to affect the time frame of bio-mat maturity for strength to develop, the lower Young's modulus for sand-based composites (compared to beads) must be linked to weaker biofilm adhesion onto the sand surface and/or different biofilm structure during growth over an opaque medium.

In terms of mechanical properties, BO would be expected to have denser biological material and thus one might expect the increased stiffness due to the complete absence of weak points. The fact that the less stiff composite can undergo a greater deformation before failing (figure 6.3) despite being ostensibly the same biological material lends weight to the idea that the organisation of filaments and EPS is different.

The main finding of this study is that our biofilm behaved as an elastic material. This is in accordance with what experienced by many other researchers, which found that biofilms of different composition and age behave as elastic materials (Ohashi et al., 1999; Aggarwal et al., 2010; Aggarwal and Hozalski, 2010). Moreover a wide range of moduli have previously been published (Stoodley *et al.*, 1999; Körstgens *et al.*, 2001). Our results derived from the uniaxial tensile test (table 6.3) were, for the most part, within the range of previously reported moduli, providing confidence in our data set; desiccation of BO2 has been highlighted in earlier sections and is not considered in the analysis herein (Aggarwal *et al.*, 2010; Ahimur *et al.*, 2007).

6.6 Adhesion strength for Gravels: a proof of concept

Chapters 4 and 5 clearly show that extensive bio-mat was not formed in gravel beds; thus, extraction of the 20mm composite sample for tensile testing was impossible (as proposed in Hypothesis of this chapter). However, since biostabilization has been shown to occur for gravel-sized beds (chapters 4 and 5). Hence there is good justification for attempting to quantify the mechanical properties and strength of these composites by some other technique.

In earlier sections of this chapter it has been highlighted that during the extraction of specimens from the surface of the bed a complication can be found in relation to the adhesion of particles to the bio-mat and their weight (*W*), which might induce failure of the sample. Thus, if the self- weight of the particle is serving as a displacement force in the direction of gravity then it would be operating counter to the adhesive force (F_a) of the biofilm, which is trying to resist failure by displacement. Given that particle size and density is known, particle self-weight can be calculated; hence, an experimental set-up whereby the composite gravel-biofilm is attached to the lower surface of a plate permits analysis of failure by self-weight (see figure 6.5a). However since a bio-mat was not present, the analysis focussed only on the single grain behaviour. The data hence needs to account for the area of attachment of the grain in order to achieve a meaningful value of the shear stress standed as demonstrated in figure 6.5b. By knowing the volume of the sphere and the density of the glass (ρ_{glass}=2500kg/m^3) it was then possible to determine *W*, the weight force defined as the mass of the beads by the acceleration *g* (9.81m/s^2). The area of attachment was considered as the one of a sphere cap (traditionally defined in geometry as S_{cap}=2πrh) having different heights (*h*), showed in figure 6.5b by the red line (with height h of the cap chose to span on a range going from 1/20r<*h*<1/4r). This was done because it was impossible to infer through the recorded video the exact area covered by the biofilm; hence different degrees of biofilm adhesion were inferred and compared. Doing so it was possible to obtain the shear stress the biofim was subjected to by dividing the force *W* (*W*= 0.103*10^{-3}N) by the attached area. Whilst this theoretical methodology provides a value of shear stress, two points are highlighted: (i) the structure of the sample tested is clearly still composite, however here the failure was not

investigated because no grains were seen falling from the plate; this method hence implies the increased adhesive properties of large sediments; (ii) data stemming from this methodology should not be considered directly comparable to tensile test data for sand size sediments.

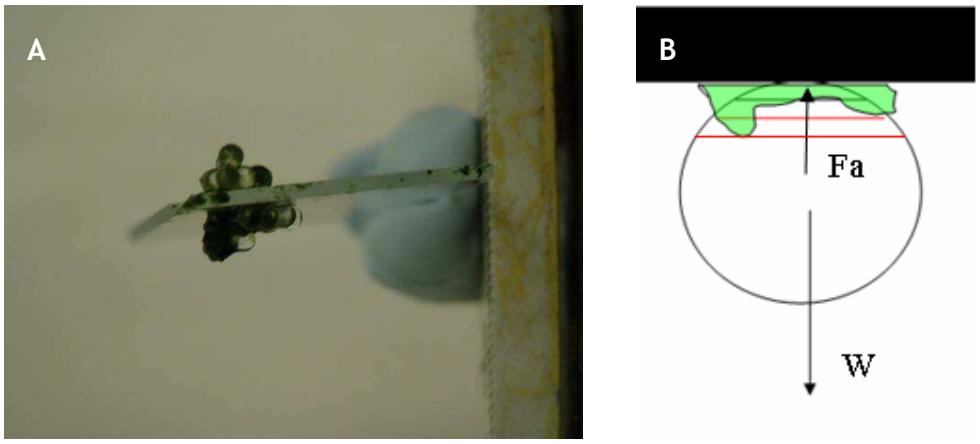

Figure 6. 5. a) Glass beads D_{50}=2mm attached to the microscope slide after being removed from the 1 week old colony; b) diagram of a single bead exposed to the weight force (*W*) and resisting through the adhesion force generated by the biofilm (*Fa*)

To execute the self-weight experiments for gravels, three glass bead tests were undertaken using LGS colonized for 1 week in environmentally-controlled flume experiments (equivalent to those outlined in chapter 3, section 3.4). Once the growth was reached, a microscope slide was vertically inserted through the biofilm/beads surface of the just drained. Figure 6.5 shows that some grains stuck to the slide and could be removed for ex-situ self-weight testing. A *Sony HDR-SR5E* video camera was used to record if any particle would detach. In line with the < 60 minute ex-situ drying time threshold employed in section 6.3, experiments were stopped at 60 minutes if failure had not been observed.

For all three repetitions, failure was not induced. Results are shown in table 6.4 and clearly show that shear stresses of at least 65Pa can be resisted by biofilm-gravel composites, thus confirming biostabilization in terms of increased adhesion, even among gravel size sediments. Given the possible variants of cap size of the sample, resistance of shear stresses may be as high as 327Pa approximating to the lower ranges of previous literature (table 6.1) for adhesion to flat surfaces.

H	*H(m)*	τ=*W*/A (Pa)
1/4 r	0.000250	65.40
1/8 r	0.000125	130.80
1/12 r	0.000083	196.20
1/16 r	0.000063	261.60
1/20 r	0.000050	326.00

Table 6. 4. Possible values of the shear stress a single glass bead would be subjected to if the cap height (h) ranged from 1/20r<h<1/4r.

Whilst this data is bespoke and invalidated; it has been included in this thesis to indicate that increased adhesion can be seen also for gravel size sediments; hence this support the fact that biostabilization of gravels was observed in chapters 4 and 5. That biostabilization has been suggested for this coarse size fraction is highly significant in river science, as the literature has previously only considered biotic gravel in relation to the change in flow field characteristic induced by epiphelic biofilm (e.g. increase or decrease in hydraulic roughness). In reality here we have seen that the microbes adhering to the surface of larger grains can act as glue, which becomes even stronger once dried out. Many are the implication of this finding: (i) smaller particle and pollutants can easily be trapped into the colonies of micro-organisms living on top of the gravels. Hence transport of pollutant cannot be associated only to the presence of fine substratum but should also be considered linked to larger gravel size; (ii) sediment transport of biotic gravel might be affected by the presence of the bacteria in particular in environment experiencing cycles of wet and dry condition. This might mean that some of the gravels reach a higher stability once drying out because of the bacteria that they have been colonized by. Thus, despite recognised limitations in the mechanical testing undertaken here, the argument above gives scope to carry out more future research on the behaviour of biotic sediments, their entrainment threshold and the potential “trapping of pollutants” effect that biotic gravels might exhibit.

6.7 Discussion

- *Elasticity of the material*. My data implies that the bio-mat at the cm scale behaves as an elastic material. I are therefore the first to show that tensile testing can be undertaken at a scale relevant to the engineering appliocations of this work (Poppele and Hozalski, 2003; Aggarwal *et al.*, 2010). Table 6.1 presented the evidence that tensile testing has been applied by other researchers, but in no case a scale such as the one presented herein was investigated. The stiffness of the material also showed that tensile testing can be undertaken on strong filamentous mats; this depends on the fact that in some cynobacterial biofilms, where the filaments become more systematically intertwined into rope-like structures (Garcia-Pichel and Wojciechowski, 2009), then an increase in mechanical strength will be achieved, as seen in our experiments. For those types of biofilm/bio-mats and looking at the characteristics of the bio-mat erosion seen in chapter 4 and chapter 5 together with the findings in literature, for which bio-mats appear to rip off in sheets in response to applied shear stresses (Neuman *et al.*, 1970; Grant *et al.*, 1986; Walker and Grant, 2009), it is evident that the tensile strength will be important in developing quantitative models of the failure mechanism. The mechanical investigation *ex - situ* offers information that can be used in engineering models of sediment transport (see chapter 8), once a clear calibration of the erosion process under shear is carried out. This is what is currently needed for the future: the results presented herein give me confidence that a more in depth research on the coupled effect of flow erosion and bio-mat mechanics would further our ability to predict erosion of biotic sediments.

- *Cohesive strength*. The maximum tensile strength measure for our biofilm only specimens (BO1-BO4) ranged from 4,000Pa to 20,000Pa, which is similar to that previously measure for activated sludge flocs using a micro cantilever (Poppele and Hozalski, 2003). These values are higher than for other biofilms reported in the literature and may be because the moist biofilms typically comprise filamentous bacteria in a matrix of EPS (see chapter 3) and reside in high shear environments. Most previous studies report the tensile strength of *Pseudomonas aerouginosa* biofilms.

- *Tensile Test limitation.* The first limitation of this technique is related to the fact that it is conducted ex-situ and hence a certain degree of exsiccation might be experienced (Aggarwal *et al.*, 2010). However, in order to develop a model to couple fluid shear and mechanical strength of the bio-mats we intend to generate calibrated data from flume experiment. This has been partially done in this thesis but a more in depth and wide analysis, which opens to other types of species forming bio-mats in the field (e.g. diatoms) need to be undertaken in the near future. Moreover, in case of larger sediment sizes (e.g. gravels) which do not form bio-mats then tensile testing is not applicable. In this thesis a very basic proof of concept experiment has been presented to show that even larger size sediment can be affected by the biofilm colonization and might present new adhesive forces. Even thought the analysis presented herein is basic and simple, it goes to show that more research needs to be opened in the analysis of elastic forces generated by the presence of biofilm on gravel size sediments at the grain to grain scale. One suggestion could be the usage of the micro-cantilever method (Aggarwal *et al.*, 2010) of the MagPI technique (Larson *et al.*, 2009), in order to investigate the elastic forces that can generate among grains. Once this is done, traditional models of sediment transport (e.g. Wiberg and Smith, 1987) could be modified adding in the biotic component (see chapter 8).

6.8 Chapter Summary

Chapter 6 have indicated that tensile testing of bio-mats (biofilm-only and composite material) can be performed with strong biofilm (such as cyanobacteria) and can provide some interesting mechanical properties of moist biofilms. Those properties, once calibrate against shear erosion by flow, could represent a very valuable information for modelling the “carpet like” erosion seen in the laboratory (see chapter 4 and chapter 5) and in the field (Neuman *et al.*, 1970; Grant *et al.*, 1986; Walker and Grant, 2009). Our aim is to compare the values of tensile strengths (chapter 6) and critical shear erosion (chapter 4 and chapter 5) which lead to the break of the biotic membrane and implement

these findings into an initial mathematical model (see chapter 8) which takes into account the mechanical and elastic properties of the bio-mats.

Finally, if we consider the gravel size sediments, section 6.6 has suggested that biofilms and EPS matrix can have an effect for larger sediments adhesion.

Chapter 7 will include all the information generated in previous chapters to present a well rounded discussion on biostabilization of non-cohesive sediments

CHAPTER 7

Discussion

"ipsa scientia potestas est"; Knowledge itself is power.

Sir Francis Bacon

This thesis has brought evidence that the stability of fine gravels can also be affected by biofilm colonization; moreover it has confirmed that biostabilization of non–cohesive sediments in the coarse sand size range can occur, as first suggested by Yallop *et al*. (1994). This phenomenon takes place and should be considered and incorporated to an extent into mathematical models predicting sediment erosion. In particular, I present below an in depth discussion of the results presented in this thesis compared to the Aims stated in chapter 1.

7.1 Lab-culturing and environmental conditions

Biofilm colonization of sediment substratum in a flume environment was successfully generated in this thesis. The growth generated presented similar structure to that of natural environments, with fixation and sealing stages (Noffke *et al.*, 2001) clearly recognized: this gave me confidence that the culturing methodology adopted was appropriate. Moreover as seen in chapter 5, the improvement of the growth conditions (LED lights and higher flow during colonization for gravel sediments) enabled the generation of bio-mats over every sediment size. Bio-mats are important because they have been shown to significantly increase the stability of fine sediments in the field (Grant *et al* 1986; Grant and Gust 1987). Therefore it is clear that using the "manipulative approach" (Rice *et al.,* 2010a) through flume experimentation allows regulated control of specific variables (e.g. flow, nutrients, temperature, light) that might affect the biostabilization potential. This allows me to understand the relevance

of each of these variables, which cannot be separated in the complex natural environment.

In particular in chapter 4 and 5 I have demonstrated that the environmental conditions are fundamental for the development of strong bio-mats. Researchers have shown in literature that the most important physical factors affecting biofilm growth in a river system are: 1) temperature; 2) light intensity and 3) current velocity (Biggs *et al.*, 1998; McCabe and Cyr, 2006; Dorigo *et al.*, 2009). My results from chapter 4 and 5 clearly show that biostabilization conditions are highly related to *light, flow and time of growth* (with the temperature kept constant at 28°C).

For SGS, changing only the light conditions, meant that a very different behaviour in chapter 4 (24h illumination with spot lights) was experienced compared to chapter 5 (12h illumination with the LED lights): in fact the highest stability in chapter 4 was achieved after 4 weeks of growth, whereas in chapter 5 this occurred in the first week. The higher PAR radiation (120 μmol m^{-2} s^{-1} in chapter 4 modified to 26 μmol m^{-2} s^{-1}in chapter 5) generated in the preliminary experiments might have induced the biofilm to overgrow, so that more biomass was exposed to erosion, generating a patchy and not very strong biofilm cover. For my findings to be applied to the river systems more research has to be undergone looking at the spatial variability of biofilm community related to seasonality, light and nutrient supply. A small number of researchers (Biggs *et al.*, 1998; Dorigo *et al.*, 2009) have begun investigating these aspects, approaching the matter from a biological point of view; however very few studies exist from the engineering or geomorphologic point of view. As afore mentioned engineers focus more on the effect that hydrodynamics have on the development of biofilm, offering less insight on the relevance of other fundamental environmental conditions. This is something that needs to be carefully addressed if the "best science" wants to be produced. In order for this to happen, collaboration among disciplines is strongly advised to pull together the expertise of scientist and engineers.

When considering hydrodynamics and its effect on the growth of biofilms, it is clear from the literature that what has been done so far is qualitative (Battin and Sengschmitt, 1999). Battin (2000) suggested that hydrodynamics extensively

affects biofilm activity; in terms of the development of biofilm under flow condition Battin *et al*. (2003) found a clear relationship among the overlying velocity during growth and the final structure of the biofilm: in particular slower velocity induced thicker and higher sinuosity biofilms, compared to those grown under faster velocities. This is very similar to what has been seen in chapter 4 for gravel sediments: here it was evident that under flow conditions that induced bed shear stress τ_b to be 25-30% the threshold value for abiotic sediment, a spongy and loose biofilm with streamers was generated, which had a very low biostabilization potential (17-35% for gravel/LGS compared to the 30-43% of SGS/sand according to the Yalin criterion (1972)). Instead in chapter 5, once the flow was increased (τ_b 35-50% the threshold for clean sediment), then the biofilm grew in a mat like form even over gravel sediments, with more then 50% of the box area still biostabilized during threshold condition. The importance of the hydrodynamics on the development of biofilm is expressed also by the findings of Moulin *et al*. (2008), who stated that the development of dense or porous mat was only dependent on the different flow conditions applied over the substratum and generated almost the same amount of biomass. In our case the presence of bio-mats, the strongest biostabilization stage, even over gravel size sediments in chapter 5 is a novel and important finding: gravel were in fact not considered as sediments that could be biostabilized due to their size and weight. Bio-mats developments over these larger sediments might depend not only on the hydrodynamic but also on the improved light conditions in chapter 5. More in-depth analysis is needed to determine which variable is responsible for the strongest biostabilization. Another important point for future work into the biostabilization potential is that a smaller growth timescales (less than a week) is required to give more resolution.

To conclude it is very complicated to relate biological variables to stability (e.g. biomass, EPS content), without taking into account the hydrodynamic field and environmental conditions, both of which strongly affect the growth of biofilms. Hence I believe it is almost impossible to relate biomass to stability equations since the results would be situation bound and have limited applicability (Gerbersdorf *et al*., 2011). Hence the future is to relate hydrodynamic conditions to biological variables and find relationships among flow, biofilm growth and sediment stability. Ideally, these relationships should be tested in

the field for which I suggest designing an *in situ* flume, wide enough for testing non-cohesive sediments and less susceptible to side wall effects. To be realistic the erosion should take place in the stream flow direction by controlled increases of the flow in the flume (e.g. by means of a pump) and the shear stress should be measured from instantaneous velocity data. This information should be combined with data on biological variables of the site prior to the erosion testing, in order to correlate flow with biofilm strength and sediment stability in a thorough way.

7.2 Biostabilization potential over non-cohesive sediments

As seen in chapter 2, Paterson in 1997 reviewed the biostabilization potential for cohesive and fine non-cohesive sediments. Section 2.4.4 presents the percentage increase in biostabilization compared to abiotic sediments. From this review it is evident that the biostabilization potential of cohesive and fine non-cohesive sediments can increase the stability of the sediments from a minimum of 100% to a maximum of 960%. Many of the studies presented in the literature about biostabilization (e.g. Grant and Gust, 1987; Dade *et al.*, 1990; Lelieveld *et al.* 2003) have used the bed shear velocity u^* as a comparative measure among abiotic and biotic sediment; however, this unit of measure is unusual in engineering-based sediment transport models (such as Shields), where bed shear stress τ_b is preferred. Because of this the data presented in chapter 4 and 5 has instead been related to the more commonly used engineering form; bed shear stress τ_b (Black *et al.*, 2002), which depends on the shear velocity u^*, following the relation $\tau_b \propto u^{*2}$. Keeping this in mind, the values of biostabilization that I have experienced in this thesis using the Yalin criterion (1972) showed between 17-43% higher bed shear stress τ_b is required to generate threshold conditions in box0.2 and in case of the strongest biostabilization (week 1 for SGS) in chapter 5, 150% more τ_b. My results are an order of magnitude lower than those found for cohesive and fine non-cohesive sediments: this might be due to the fact that: i) the nature of the single species bacterium; in real river systems evidence has been shown (Lubarsky *et al.*, 2010) that mixed assemblages (bacteria and

diatoms) might induce higher degrees of stability compared to biofilms composed of only one organism; ii) the size and shape of the materials combined to the specific growth set up used herein do not allow the generation of a homogeneous biofilm/sediment composite material, that physically smoothes the substratum by producing a “carpet” which embeds the sediments, sheltering them from the flow iii) the more porous bed herein compared to cohesive sediments induces up-welling of the flow, so that strong bio-mats cannot be generated and instead more channels are formed in the biofilm, making its structure loose; iv) visually during incubation in the flume I observed, that the preferential initial location of bacterial attachment and growth coincided with the crest of grains, where I speculate that nutrients are more abundant; the growth then spreads down into the bed, where nutrients are more limited and flow conditions might impede the pore filling by the bacteria, in order to generate a uniform mat.

Hence comparing the behaviour of our sediments sizes (sand and gravel) to published work for smaller size sediments, it seems clear that roughness plays a fundamental role in generating strong bio-mats. This is supported by the findings presented in chapter 6, where the mechanical strengths of bio-mat grown over sand size spheres (BGB samples) were compared to that of bio-mats grown over sand sediments (BGS samples). Here it was shown that biofilm growing over smoother beds (SGS) would present higher tensile strength than samples generated over sand. This might be due to the fact that lower discontinuity is present in the bio-mat grown over a smoother bed and hence more stability is insured.

Crucially, the reduction in sediment transport is related to the modification of the bed roughness due to biofilm growth and the relative cohesive properties induced by the EPS presence on the surface of the grains, influencing the flow structure above the biotic bed, which significantly changes after the biofilm has clogged the pores when compared to the original abiotic bed. The next section analyzes this process in depth.

7.3 Eco-Hydraulics of biotic non –cohesive beds using the non-invasive PIV technique

As seen in chapter 2, much of the engineering literature on eco-hydraulics has focused on the effects of biofilms cultured over immobile rocks and the modifications to the flow induced by them (see Nikora *et al*. 1997, 1998, 2002; Graba *et al*., 2010; Salant, 2011). However, there has been no work done to my knowledge so far investigating the relationship and interactions between biofilm growth, flow modification and sediment entrainment. Following the procedure outlined by Moulin *et al*. (2008), PIV for non- invasive flow evaluations was used, in order to determine the changes in flow characteristics and hydraulic roughness depending on the different stages of biofilm growth.

Looking at the roughness variation induced by the biofilm growth (chapter 5, section 5.4.7.2), my data shows that each bed underwent more than an order of magnitude of smoothing during biofilm growth, with minimum roughness values approximating perfect smoothing (z_0 ~ 0mm) at least in one of the colonizing weeks for all biotic substratum. In particular, all the strongest biostabilization weeks (week 1 for SGS, sand and LGS and week 4 for gravel) had z_0 ~ 0mm at the beginning of the erosion experiment. This phenomenon is in line with the findings of Godillot *et al*. (2001), who saw that thick *Periphyton* mats could create a smoother and uniform surface, which reduced roughness, bed shear stress τ_b and induced dampening of the turbulence (Black *et al*., 2002). Similar results were obtained by Graba *et al*. (2010), whereas Nikora *et al*. (2002) presented a 16-21% increase in z_0 when the biofilm was well developed. This is a crucial finding since in chapter 5, with the most realistic growth condition, my highest biostabilization potential was obtained in correspondence of the fixation stage (week 1 of growth for all the materials, a part form gravels): this suggests that the more mature the biofilm becomes, the more complex and less adhesive the bio-mat structure; making it more prone to erosion and patchiness. In fact many researchers saw that more mature biofilm result in low homogeneity (Nikora *et al*. 1997, 2002; Laboid *et al*., 2007).

When considering the bed shear stress variation from abiotic to biotic beds, this thesis has shown a general decrease in τ_b, where the following hierarchy was

noted at the lowest flow step (1.6l/s): SGS (34%) < LGS (41%) < sand (61%) < gravel (82%) when comparing abiotic conditions at the same flow step. Thus, natural materials demonstrate very slightly greater reductions in shear stress, possibly as a product of greater biomass which would develop a thicker mat and clog the larger pores. This is in contrast with the findings of Nikora *et al*. (2002) and Laboid *et al*. (2007), whom found that an increase in turbulence intensity and shear velocity u^* were evident after biofilm colonization. This thesis stresses the importance of the bio-mats presence and the resulting pore clogging and smoothing of the bed: ensuring a more stable condition for biotic non cohesive sediments.

Unlike Godillot *et al*. (2001) and Graba *et al*. (2010) when smoothing of the bed was evident, my experimentation did not show an increase in downstream flow velocity *U* (despite SGS, with a 22% increase in U for the strongest week of growth), instead, the common trend experienced by natural sediments and LGS was a slight reduction in the mean downstream velocity (*U*) by 5-22%. An important point to be stressed about these experiments is the widening of the band of similar downstream velocity (i.e. the standard deviation of *U*), which explains the decrease in bed shear stress τ_b, according to the fundamental definition $\tau_b=\mu\delta U/\delta y$. Moreover a reduction in the vertical velocities (up to 72%) following biofilm development was experienced; this might be due to the pore clogging so as to reduce upwelling/downwelling at the boundary or even more interestingly if the bio-mat vibrates or "flutters" into the flow, then wave interference processes will "damp" the vertical velocities, resulting in lower turbulence generation. This phenomenon has been seen previously in the literature by Paterson (1989), who described the interface between flow and colonized sediments as the skin of a drum; this will vibrate under the flow until a critical τ_b is applied and the skin reaches the breaking point and releases the sediments. This concept has been qualitatively presented by Black *et al*. (2002): the results presented in this thesis offer a clear quantification of the turbulence reduction (decrease in the standard deviations of *U* and *V*) and a more uniform flow field generation.

The roughness modification process and bed shear stress alteration make the investigation of the biotic erosion process very complicated, especially in natural conditions, where hydraulic and environmental information are complex. If the

effect of biofilm on flow above colonized sediments is considered important, then a lot of care needs to be taken when interpreting the results of *in-situ* devices for the assessment of biotic sediments erosion (e.g. the CSM: Patterson (1989); benthic flumes: Tolhurst *et al*. (2000), Aberle *et al*. (2003)). However, these instruments may underestimate the biofilm modification of the flow field (e.g. a vertical jet fired into the biotic bed in the CSM is different from the longitudinal shear stress τ_b inducing erosion; in the same way, the constrains due to the small width of the benthic flumes and their low efficiency to investigate bedload; making these instruments in my opinion unsuitable for larger non-cohesive sediments erosion). On the other side, if cores are sampled from the field, transported and tested in flumes, physical modifications of the sample's characteristics are likely to occur, as implied by Tolhurst *et al*. (2000).

I therefore, believe that the best method to ascertain the complexity of biostabilization is to carefully control the relevant environmental variables at their relevant scales, i.e. through experimentation in a flume laboratory (See section 7.1), as presented in this thesis. Although this work was performed using a single bacterial species, under optimum growth conditions, it still has importance and relevance as a proof of concept. Further work should extend this to experimentation under more realistic conditions, with multiple microbial organisms. Therefore in chapter 8, section 8.2.1, it will be shown that culturing biofilm onto artificial sediments from real river water is possible and offered interesting preliminary results on biostabilization. However, it is important to remember that engineers likely have limited knowledge about the biotic component of biostabilization; as stated by Rice *et al*. (2010a) and as interdisciplinary research remains relatively rare the "best-science" landmark is sadly rarely reached. This is why in my opinion, only through a joint effort on the subject can real progress be gained.

Finally in chapters 4 and 5 image analysis at the large scale (LS) has been introduced as a new method to address the erosion threshold for non-cohesive sediment, without any invasive measurement. This is extremely important, in particular for non-cohesive sediments, since their stability takes place only for the first few layers of sediments at the top of the bed; in fact, once the biofilm or bio-mat is eroded, the bed underneath is no longer stabilized, hence subject to erosion. In the method presented herein, it is not necessary to collect data of

the eroded mass of sediments, since a visual segmentation of the area covered by biofilm is sufficient. This has been shown to be an efficient way to assess erosion, so that an exponential relationship could be successfully fitted to my data that links bed shear stress τ_b with the erosion rate (equation 5.3). Ideally, if equation 5.3 was appropriately calibrated in natural environments, it could represent a valuable substitute to invasive assessment of the erosion characteristic of colonized sediment with benthic flumes or CSM; additionally the use of open source software (*ImageJ)* for image analysis will keep the analysis cost effective. Therefore I believe the approach based on the eroded mass in suspension (e.g. Sanford and Maa, 2001) can be substituted to a specifically calibrated visual analysis for non-cohesive sediments where the bedload component prevails.

7.4 A standardized criterion of motion for biotic sediment

The Yalin criterion (see chapter 4, section 4.3.2 for theory) was implemented with the aim of introducing a standardized method with empirical basis, to assess the entrainment of biostabilized sediments. It is widely accepted that the implementation of the commonly used Shield's curve might lead to a certain degree of uncertainty, because Shields' (1936) criterion of motion was based on the visual assessment of sediment entrainment, defined as "small degree" of transport; other researchers stated qualitatively that the threshold of motion was reached when "weak movement" (Kramer, 1935) or "general bed movement" (Chepil, 1959) or "scattered particle movement" (Rathbun and Guy, 1967) would take place, inducing even further subjectivity in the identification of the incipient motion. Only with Neill and Yalin (1969) and later Yalin (1972) the first objective motion criterion was developed, based on the concept that at threshold a small degree of sediment transport occurs (Miller *et al.*, 1977), which can be experimentally quantified.

A lot of subjectivity in the identification of the threshold of motion can be found in the literature when considering biotic sediment, which is an even more complicated subject because biofilm can clump sediment together, generating

different densities and sizes. Hence very different techniques have been used to assess the entrainment of colonized sediments (e.g. Grant and Gust 1987, Leliveld *et al*. 2003), making the results difficult to compare. This thesis has shown that for small samples (such as box0.2, of a similar size than cores sampled from the field and tested in flumes) the Yalin criterion is a good and objective method for the identification of the incipient motion. The Yalin criterion could represent a very valuable tool across the research community to stipulate a common way of investigating the incipient motion threshold in case of biotic sediments. Researchers such as Grant and Gust (1987) have stated that the threshold of motion for colonized sediments was reached if 10 or more grains moved at one time over the area of a core, sampled *in-situ*; in their case if the Yalin criterion was to be applied, considering the geometry of their cores (diameter equal to 75mm) and assuming quartz as the density of the sand (D_{50}=189μm) and water temperature at 22°*C*, the number of particles that should have moved in one second form half of the core area at the same time to define the sample at threshold was equal to 18 (only half of the core would be considered so that the highest camera resolution could be reached). In case of the work presented by Lelieveld *et al*. (2003), considering the geometry of their core (130mm), water at 22°C and sediment (D_{50}=169μm) density such as quartz, the number of particles that should move acceding to the Yalin criterion at the same time from half of the core area to define the motion at threshold should be 73; however in their study Lelieveld *et al*. (2003) considered as a first stage of erosion the condition in which 20 grains were moving simultaneously. These are just two examples on how the subjectivity of the visual assessment could be resolved by implementing an engineering technique, which is extensively used in sedimentary research to assess the entrainment threshold of sediments (e.g. Miller *et al*. 1977; Paphitis and Collins, 2005; Haynes and Pender, 2007).

However, as it has been evidenced in chapter 5 for larger samples, the Yalin technique will work well only for a small and strongly biostabilized sample, not affected by patchy biofilm growth. In fact, if patchiness is experienced, some particles eroded upstream might enter the area investigated and hence lead to consider the flow at threshold, even though the FoV is clearly biostabilizaed (due to extensive green pixels presence). To obviate this problem, the image

analysis at the LS was instead preferred for non-cohesive sediments (see section 7.3).

7.5 Biofilm mechanical properties and mathematical models for incipient motion

Chapter 6 has clearly presented the evidence that bio-mats (biofilm only or composite biofilm/sediment) have mechanical strength high enough to allow performing tensile testing and acquiring information on their elasticity. Tensile testing, a conventional engineering technique used for direct measurement of material stiffness and elasticity, had been ruled out for the investigation of biofilm cohesive strength by researchers in biotechnology for many years because the biofilm usually tested in the literature (e.g. *Pseudomonas aeruginosa*) were gelatinous and could not withstand their own weight (Körstgens *et al.*, 2001; Poppele and Hozalski, 2003 and Aggarwal *et al.* 2010).

In this thesis I have demonstrated that, if the biofilm used is composed of a strong material (generated by entangled filaments of cyanobacteria that creates almost a rope structure (Garcia-Pichel and Wojciechowski, 2009), then tensile testing can be applied to obtain Young's modulus of elasticity (E) and cohesive strength information of moist bio-mat samples. Knowing E can have a fundamental importance in the introduction of models based on the mechanical strength of bio-mats coating sediments (see chapter 8, section 8.2.3): a first theoretical definition of a model coupling biofilm mechanical strength and flow will be presented. In this way, we can obviate to the clear inapplicability of traditional abiotic models of sediment transport when biofilm coats the sediment (Black *et al.*, 2002): those models (e.g. Wiberg and Smith, 1987), which account for the equilibrium of forces on a single grain, do not consider the biological force and hence are inappropriate when micro-organisms biostabilize the sediments. In chapter 8, section 8.2.2, I will also present a theoretical model where the biofilm force is considered in the forces balance of the equilibrium balance of the Wiberg and Smith (1987) model. Assuming the biofilm acts as an elastic spring, where the constant of elasticity k can be obtained out

of tensile testing or techniques such as the MagPI (Larson *et al.*, 2009) and the Micro-Cantilever (Aggarwal *et al.*, 2010), which provide adhesive information at the grain to grain scale, I was able to modify this for sediment transport by including the biofilm in the equation in a theoretical form.

Moreover in chapter 6 it has been shown that gravel sized sediments (LGS) coated by biofilm show adhesive properties, which increase while drying. All the information pertaining to the mechanical behaviour of colonized non-cohesive sediments are novel; however more research is needed to understand the effect that biofilm adhesion has on the stability of larger biotic sediments in wet and under fluid shear conditions.

7.6 Conclusion

This chapter summarizes the findings of this thesis:

- Biostabilization was for the first time in literature seen to occur for fine non-cohesive gravel sediments and confirmed for coarse sand size sediements;

- Flume culture and testing of biostabilization at a relevant scale to that of a river system is a valuable option that could lead to a more comprehensive understanding of the subject;

- In order to fully understand the processes that induce the erosion of biotic sediments it is required to: 1) know the hydraulic modifications on the flow induced by the biofilm (e.g. PIV); 2) consider the mechanical forces (elastic) that gets generated due to the biofilm presence; 3) merge all this information for generating predictive entrainment models for biotic sediments (two examples will be given in chapter 8, section 8.2.2 and 8.2.3);

- In future more realistic culture of natural river biofilm, directly collected from a river system and flume cultured for biostabilization experiments is

strongly advised, so that the growth achieved in the laboratory can be comparable to that of a river system (a proof of concept has been undertaken in chapter 8, section 8.2.1). If a comprehensive and realistic scenario is wanted the only way of achieving this is if different disciplines comes together and share their expertise for the best science to be generated. Finally (section 8.3) an ideal combined tensile testing-flume facility for measuring the mechanical strength of the biofilm in more natural conditions will be presented; this is only a hypothetical facility that could be quite costly to built but very effective in its purpose.

CHAPTER 8

Conclusions and Future Research Recommendations

"The wise finds pleasure in water"

Confucius, 551 BC - 479 BC

8.1 Conclusions

This thesis has presented a series of key points, which are summarised below:

1. *Flume experiments:* can be representative of biofilm growth at scales comparable to that of real river systems. Herein, by inoculation a bacterium onto sediments in an environment where variables such as light, temperature, nutrients and flow were controlled, I achieved all stages of natural biofilm growth (Noffke *et al*., 2001). Hence the methodology that I have used has great scope if resolve of the unanswered questions arising from the interaction of biofilm with sediments want to be resolved.

2. *Bio-mats*: have been identified in the literature as responsible for increase in sediment stability (e.g. Grant and Gist, 1987); the project presented herein has shown that with the right culturing set up, bio-mat can be grown also over larger sediment (sand and fine gravels), which are more typical of riverine environments. These sizes have been largely ignored in the study of biostabilization so far.

3. *Eco-Hydraulics*: the interaction among bacteria and flow has shown three main hydraulic modifications: i) roughness z_0 can decrease up to 94% when biofilm coat non-cohesive sediments in relatively low flow conditions; ii)

bed shear stress τ_b over mature biofilm will be reduced up to 82% as a facet of biofilm smoothing of the bed and bio-mat "fluttering" in the flow; iii) turbulent damping was clearly evident from the PIV data: this will affect the flow field and induce decrease in the shear force and hence modification on the biofilm structure during growth.

4. *Biostabilization and areal relationship*: this thesis shows that entrainment threshold of biotic sediments can be analyzed most beneficially by using the Yalin criterion (1972) at the SS, while at the LS an areal image analysis should be employed. In this way erosion can directly be related to the bed shear stress τ_b by an exponential relationship and can have great advantage if applied in the field, because non invasive.

5. *Biostabilization extent*: in accordance with the literature (Paterson, 1997), biostabilization is greater for fine substratum (up to 150% more stability was shown in this thesis for SGS) than in gravel sediment. However, all the sizes used in this project have shown an effect due to biofilm colonization: this is of great importance for sediment transport models, which very rarely account for the presence of biotic forces (Righetti and Lucarelli, 2007; Borsje *et al.*, 2008). In the section below a model accounting for the presence of the biofilm force at the grain to grain scale (modification of the Wiberg and Smith model (1987)) will be presented as a recommendation to be carried out in the future.

6. *Failing mechanic of bio-mats:* I have shown herein that bio-mats comprised by cyanobacteria are so strong that can be tensile tested; the results presented on the cohesive strength of composite biofilm/sediments can be used in mathematical models, which should consider not the forces action on the single grain but the complex interaction of sediment and flow with biofilm. In section 8.2.3 a very preliminary and theoretical model will be presented for this reason.

7. *Biological variables:* no direct correlation could be seen among biological variables (e.g. biomass, EPS) and biostabilization, as largely advocated by many field scientists (Black *et al.*, 2002).

8.2 Future research recommendations

As with any novel research investigation, this thesis has raised a number of fascinating research questions considered beyond the scope of the PhD. Whilst a plethora of research avenues could be explored, this thesis recommends that three main directions are crucial for advances in this discipline: (i) field-based samples of complex multi-species biofilm to be cultured for biostabilization analysis; (ii) modification of traditional models of sediment entrainment for discrete particle detachment from biotic substratum; (iii) understanding and modelling the effect of oscillations in mature bio-mats and consequences for induced turbulence damping. The rationale for each recommendation is provided below, underpinned by appropriate pilot data where available.

8.2.1 Field-based biofilm (multi-species)

It has been established in chapters 4 and 5 that a single species cyanobacterial bio-mat significantly biostabilizes sediments at the flume scale; however, the representativeness of these experiments to natural multi-species biofilms in field situations remains a valid question. Whilst colonization of stable substratum from river water has been undertaken by e.g. Battin *et al*. (2003) and Nikora *et al*. (2002), the only previous study on sediment biostabilization in rivers was undertaken by Gerbersdorf *et al*. (2009). Whilst her work uses natural biofilm, the tests are performed at too small a scale (laboratory bench scale) to be representative assessment of river beds and fail to consider the effect that live unidirectional flow (i.e. tangential shear force over the substratum) has on entraining biotic sediments. Thus, this section specifically provides pilot data to overcome these deficiencies such that data on the colonization and biostabilization of flume-based sediments (similar to previous chapters) using natural river water is provided. This methodology ensured: (i) a natural multi-species biofilm; (ii) colonization by organisms settling out from the flow column onto the substratum; (iii) nutrient supply from the river water only, i.e. no

artificial enrichment. As it is considered outwith the scope of a Civil Engineering thesis to undertake DNA analysis for biofilm composition, my overall aim was to show, from detailed analysis of the biofilm mechanical properties (and its influence on flow and sediment dynamics) that natural river biofilms can be grown in flume-based conditions for direct analysis of their biostabilization capabilities. Importantly, for this aim to be fully realized, the biostabilization capability had to be of magnitude significant enough to be outwith the uncertainty of experimental error.

Specific hypotheses in these tests were that:

- Diatoms and/or cyanobacteria would be present in natural river water such that colonization and growth would result in biostabilization, possibly with bio-mat development (see Paterson, 1997);

- Biostabilization would take longer to develop using natural river water than that observed in chapter 4 and 5 via direct inoculation onto the substratum. Justification is three-fold: (i) lower water temperatures of natural water sample reduce the rate of growth of organisms (compared to the heated water conditions in chapter 4 and 5); (ii) nutrients are limited to those present in the extracted water sample; (iii) natural selection and competition processes between species may reduce overall growth rate.

8.2.1.1River investigation for site selection

Crucial to this section was the field sample location, hence field investigations throughout lowland Scotland were undertaken. A detailed desk-based survey of Ordnance Survey (O.S.) data initially refined the search are to the South-East and South-West of Scotland, where mid-reach river gradients were most similar to the flume-bed gradients employed in earlier chapters. After an initial reconnaissance survey of a number of channels, three river systems were considered suitable for further analysis as they fulfilled the following criteria: i) visual presence of biofilm in the river, possibly cyanobacteria or diatoms as

crudely identified by colour/chlorophyll presence and microscope analysis; ii) a sediment substratum in the non-cohesive size range of sand/gravel, directly measured from calliper-based (*Powerfix*, resolution 0.01mm) b-axis measurement of 400 grains as per Fripp and Diplas (1993) and Rice and Church (1996). Sieve analysis would have been a better technique for size identification; however I was not granted the permission to collect large sediment samples by the relevant authority (Scottish Environmental Protection Agency). Therefore I collected only a few hundreds randomly selected sediment grains from the centre of the sample for calliper analysis; iii) a non-urban area, i.e. no obvious pollution effects on biofilm growth in terms of physical disruption or nutrient availability. Specifically, the river systems were: (1) the Eden River (St. Andrews) in the East of Scotland, a well known location that has been previously studied for biostabilization in tidal reaches (E.g. Spears *et al,* 2008); (2) the Devon, in the central belt of Scotland; (3) the Camps Water, in the West of Scotland. Appendix 8.A summarises the characteristics of each river and indicates that all reaches have appropriate substratum and biofilm for testing, thus fully justify the need for biofilm research in river systems. As the timeframes of this pilot research dictated that only one sample location could be used, the following rationale was employed to justify our choice of Camps Water: (i) it has a grain size of coarse sands, demonstrated in chapters 4 and 5 to offer the greatest biostabilization potential; (ii) it is a freshwater location, far from influence of tidal waters or species; (iii) it is subjected to regulated flow cycles from the upstream reservoir which include artificial water releases (freshets) during which the biofilms present would have to have resisted entrainment by higher flow (Stoodlye *et al*., 2002); (iv) there is no existing data for this river. Thus, 300l water was abstracted from Camps Water and utilized to colonize a flume-based coarse sand substratum; all appropriate permissions for river water extraction were granted from the Scottish Environmental Protection Agency (SEPA, East Kilbride office).

8.2.1.2Experimental procedure

As these trials were temporally extensive and tangential to the main research program of the thesis, hence the test flume employed was distinct from those used in chapter 4 and 5. Full details of the facility and set-up can be found in Appendix 8.B. Importantly, a non cohesive artificial sand was employed commensurate with field data (Appendix 8.A) and chapter 4 and 5. Whilst these glass spheres (D_{50}=0.85mm) were slightly smaller than the field sediments this is appropriate given that: (i) biostabilization effects of chapters 4 and 5 are greatest for this size fraction; (ii) beads are inert, hence biostabilization processes stem solely from biology and nutrients in the river water; (iii) model development is easier for regular, spherical grains as the surface area is known; (iv) the test flume used drew a maximum flow of only 4l/s, hence a smaller grain ensured entrainment threshold was possible in this facility; (v) the test flume was narrow (81mm width) and it was important to maximize the number of grains per width, so at D_{50}=0.85mm ~100 grains comprised the test width and this was considered appropriately representative for biofilm attachment and growth. Uniform flow conditions were employed throughout 10 weeks of growth at shear stresses 86% of the critical threshold of abiotic glass beads (τ_b = 0.70Pa for abiotic beads). Entrainment threshold, biomass and EPS analysis was undertaken in a similar manner to chapters 4 and 5.

8.2.1.3 Results and discussion

The growth achieved after 10 weeks was relatively homogeneous across the test bed and of colour and structure equivalent to the field site (see Appendix 8.A-8.C for images). Whilst biofilm covered the sediment, a mature bio-mat did not form in the laboratory. This form was akin to the field sample location and it is concluded that natural biofilm can be grown in a representative way via inoculation from real river water in a recirculating flume system. The benefits of this finding are undoubted as it permits natural biofilm response to a range of controlled environmental variables to be assessed, and is therefore advocated as a technique for future research at the mm-m scale.

Using the Yalin Criterion, the natural biofilm increased the critical shear stress of entrainment (τ_c) by 21%, compared to that of the abiotic sediments (see Appendix 8.C). Crucially, this magnitude of change is significant enough to be outwith experimental uncertainty (higher than the 15% uncertainty in shear stress estimation caused by fluctuations in the pump and instrument precision), supporting flume-based analysis of field-derived biofilm. Yet, the biostabilization strength is significantly lower (by around 50%) than the cyanobacteria data; this could be a function of species and reduced coverage by way of a biotic coating (rather than a mature bio-mat *per se*). From the present pilot data, it would be interesting to isolate the controls on biofilm form to establish the significance of biostabilization potential of coatings (compared to bio-mats) and to link the biostabilization potential to specific species or combinations of those.

Areal coverage of biofilm (Appendix 8.C) showed that 84% of the test area remained covered at the biotic threshold of entrainment and 35% remained covered even at the maximum applied shear stress (+27% above abiotic threshold). Thus even though a mature bio-mat was not developed, the biofilm coating was sufficient to cause patches of locally stable sediment. Resolving the specific controls on spatial heterogeneity will require simultaneous examination of grain-grain interactions and larger scale interactions (such as turbulence length scales to be resolved and compared to bio-mat patchiness). Whilst some examination of upscaling has been undertaken from chapter 4 to chapter 5 of this thesis, grain-grain scale interactions are not considered under fluid flow conditions and therefore only chapter 6 data tends towards grain scale resolution of process. Specifically, this could be developed further towards validation data of a biotic force component acting on single grains, which could be used to modify traditional models of sediment transport (e.g. Wiberg and Smith, 1987); thus, a proposal is made in section 8.2.2 as to how to further this research.

The value of biomass obtained through loss of ignition (Himom, 2005) showed that 10 weeks of colonization led to 17.70mg of biomass (see Appendix 8.C); this is of the same order of magnitude of the strongest biostabilization data obtained in chapter 4 and 5 and provides confidence that single and multi species colonization is equitably viable and comparable using flumes.

EPS values were very low, 3.8µg/ml; this is 48% the value of the EPS for week 1 in SGS, which presented the strongest biostabilization potential among all the experiments (see chapter 5, section 5.4.3). Given that chapter 5 data for SGS suggested an inverse relationship between EPS and biostabilization, this might suggest strong biostabilization potential of the natural biofilm. Hence these findings require to be verified at a scale comparable to the one of a real river system.

Thus, in summary these data (considered alongside research of Gerbersdorf *et al.*, 2009; Battin *et al.*, 2003 and Nikora *et al.*, 2002) have concluded that the experimental flume-based techniques provided in this pilot study and wider thesis are appropriate to analyzing the biostabilization potential of natural river systems. Crucially, this flume-based methodology is highly beneficial as it permits future studies to physically model the field situation in a way that individual environmental variables can be isolated and examined as to their significance on biostabilization process.

8.2.2 Modification of a traditional model for sediment transport including biofilm force.

In the light of what seen for chapter 4, 5 and 6, it seems clear that the traditional models of sediment transport based on the concept of a single particle pivoting under the forces action on it is not applicable in the case of biotic sediment. This depends on a number of reasons: i) chapter 4 has specifically showed that in case of strong biostabilization, clumps of non cohesive sediments instead of single grains can be seen for sand size sediments; ii) in case of gravel sediments, chapter 4 and 5 demonstrated that biostabilization can occur and chapter 6 has crudely evidenced that gravel size sediments can experience increased adhesion properties due to biofilm colonization (See section 6.6); iii) in case a bio-mat is generated over the substratum, the erosion is far from being similar to pivoting of single sediments, looking instead more like a “carpet”, rolling and tearing. This particular case will be considered in section 8.2.3 of this chapter, where a new model of erosion

for carpeted sediment, which includes the biofilm material, will be briefly presented.

For all these reasons it is fundamental that engineers start to consider the effect that biofilm might have at different scale (grain to grain, large bio-mat ~cm^2 to m^2) and parameterize this effect into traditional and commercial models of sediment transport. Although the achievement of this point was outwith the scope of this thesis, the author has attempted a modification of a commonly used model of sediment transport (Wiberg and Smith, 1987) by introducing the biofilm force in light of the results obtained in chapter 6 for the mechanical properties of the material. In particular it is common sense to consider the biofilm as an elastic force (see chapter 6 for results and for a detailed review). Hence an elastic force (expressed using the Hooke's law, as suggested by Alkvist and Knapper, 2007) has been introduced in the balance of force that could affect the entrainment of a biotic particle. The modification of the model and speculations on its behaviour can be found below (for the detailed derivation, see Appendix 8.D). The model was not calibrated due to lack of time at the end of this project: a recommendation is that in future research the validation of this theoretical model is carried out using results obtained from naturally colonized sediments (as seen in section 8.2.1), in order to obtain the most representative result.

Wiberg and Smith (1987) created a model (WSM), which yields the mathematical expression of a critical shear stress τ_c for single grain entrainment, based on the balance of rotational forces acting on it. The WSM uses the law of the wall velocity profile to calculate forces on a particle. The forces that are taken into consideration are: Gravity (F_G), Buoyancy (F_B), Lift and Drag over the particle (F_L and F_D), Resisting force (F_R). $F_{G'}$ is defined as the difference between the gravity and the buoyancy force (see Wiberg and Smith, 1987). A sketch of the acting locations of the considered forces is presented below, where β is the slope of the bed and Φ is the particle angle of response, also called pivoting angle.

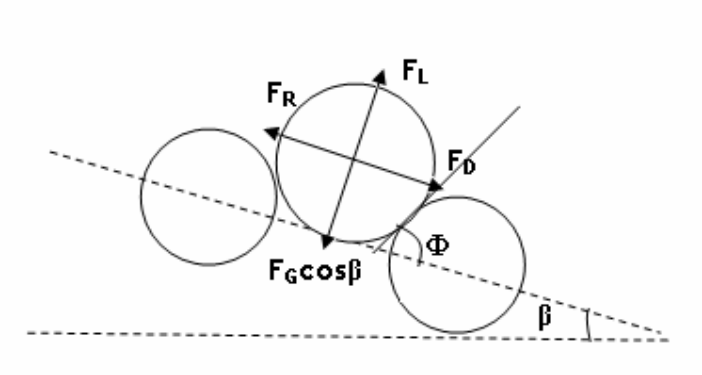

Figure 8. 1. Forces balance on a particle at the surface of a bed (After Wiberg and Smith, 1987).

The biofilm resistance can be expressed as an **elastic force (F_e),** defined following the Hooke's law so that $F_e=K(dL)_{cr}$, where k is the constant of elasticity (equal to the spring constant) and dL is the elongation of the biofilm before breaking an "cr" represent the length at break of the biofilm among two grains (see figure 8.2). The direction of application of the biofilm/spring is highlighted in shown in figure 8.2 and it is opposite to the drag component.

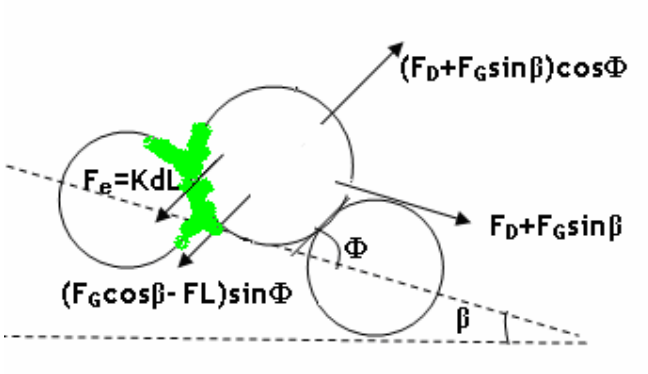

Figure 8. 2. Force moment balance diagram for the entrainment of a single-sediment grain including the elastic force due to the biofilm Fe. Fe direction of application is highlighted in the diagram by the red arrow (modified after Bridge and Bennett, 1992).

Considering all the forces that come in to play and including the biofilm component, the equation below can be derived (see Appendix 8.D for its derivation):

$$\tau_c = \frac{2}{\alpha}\frac{1}{C_D f^2\left(\frac{z}{z_0}\right)}\frac{(\cos\beta tg\Phi - \sin\beta)D}{\left[1+\frac{F_L}{F_D}tg\Phi - \frac{KdL}{F_D\cos\Phi}\right]}$$

Equation 8. 1

Where C_D is the drag coefficient, U is the temporal mean velocity at height z over the bed, z_0 the zero velocity level of the logarithmic profile.

Equation 8.1 differs from the Wiberg and Smith (1987) model only for the term that has been circled in red, which depends on the elastic properties of the biofilm. If we assume that F_L can be neglected, as has often been done, although not quite correctly, in the past (e.g. Egiazaroff, 1965) in order to simplify the analysis we can speculate that:

1. $\frac{KdL}{F_D\cos\Phi} = 0$: equation 8.1 becomes the Wiberg and Smith original one, for abiotic sediments.

2. $\frac{KdL}{F_D\cos\Phi} > 1$: The elasticity force wins over the drag force. This result in the highest biostabilization for the sediment and requires a higher shear stress for erosion.

3. $\frac{KdL}{F_D\cos\Phi} = 1$: The drag force is equal to the elasticity force. The shear stress required to entrain a sediment particle is smaller than the one in point 2.

4. $\frac{KdL}{F_D\cos\Phi} < 1$: The drag force is larger than the resistance due to the biofilm. The shear stress at erosion is smaller than Point 3 but larger than the one obtained for the unmodified model of Wiberg and Smith (1987) for abiotic sediments.

However, in order to be more realistic in the application of the model, the lift force F_L is included in the following worked example, considering the case of a

strong biofilm under two different flow conditions. The worked example was generated to demonstrate the magnitude of the different variables in equation 8.1. I have selected the case of SGS for week 1 of growth for the flows 1.6l/s and 5l/s (see Appendix 5.A). The calculations of the forces followed the definitions presented in Wiberg and Smith (1987), apart from the case of F_L which was approximated to be $0.85F_D$, as suggested by Chepil (1958) for flows with R_{ep}<5000. Table 8.1 shows the values of the parameters used and their sources. The assumption is that the bed shear stress represents the threshold value: in this way is then possible to obtain a quantification of F_e. A value of *dl* was measured using ImageJ before the breaking point (n=1) and it is only used as a rough guide to detect the value of *k*, the elastic constant.

SGS	**1.6l/s**	**5l/s**	**Note**
C_D	2.08	1.80	Brown and Lawler (2003)
R_{ep}	28.54	36.59	
U_b **(m/s)**	0.03	0.07	Velocity acting on the particle obtained from the PIV profile
Φ **(°)**	36.30	36.30	Li and Komar (1986)
β	0.005	0.005	
α	0.75	0.75	
F_D **(N)**	3.27E-07	2.29E-06	Wiberg and Smith (1987)
F_L **(N)**	2.78E-07	1.95E-06	Chepil (1958)
F_e **(N)**	4.21E-07	2.99E-06	
dL(max) mm	0.71	0.71	As measured from ImageJ analysis of SS (n=1)
k	0.00059	0.00421	
$F_L/F_D*tg\Phi$	0.62	0.62	
$F_e/F_D cos\Phi$	1.60	1.62	

Table 8. 1. Worked example for the magnitudes of variables in equation 8.1. The calculations were computed for SGS at flow 1.6l/s and 5l/s (Appendix 5.A for flow characteristics). The calculations are presented as if τ_b was the critical value at threshold.

Thus, a theoretical model for incipient motion of single particle, the Wiberg and Smith (1987) model, based on the balance of forces acting on a grain, has been modified introducing a term for biotic force (circled in red). This term sees the elastic force on the top, divided by the component of the drag force acting on the same axis. Hence, speculating on the value of this term shows that if biostabilization takes place (hence the elastic force is higher than the drag force), then the critical shear stress required for induce erosion increases significantly (as seen in chapter 4, chapter 5, & section 8.2.1). However, even if the force of the biofilm is smaller than the drag force acting on a particle,

equation 8.1 still shows that the shear stress required for entrainment will be higher than for the abiotic prediction of unmodified Wiberg and Smith model. Put simply, this means that any biotic colonization which offers a degree of adhesion will modify the stability of a sediment particle in a manner so as to require a higher bed shear stress to be eroded.

Whilst the recommendation to pursue this line of research development in the future is fundamental to reducing uncertainty in sediment transport predictions made by current abiotic commercially available models, this method of biotic model correction is particular to discrete particle entrainment and should not be considered in any circumstance where bio-mats are present and the mode of failure is flocs or carpets; in light of this statement, a tentative alternative is highlighted below.

8.2.3 Erosion model based on an elastic membrane coating the sediments

As an alternative to discrete particle entrainment model correction proposed above (section 8.2.2), where a bio-mat is present it will be this that dictates the nature of the boundary fluid and sediment dynamics. In chapter 4 and 5 the bio-mat was clearly seen oscillating under unidirectional flow application; here, PIV data showed turbulence damping in response to fluttering extracting energy from the flow and entrainment data showed floc and carpet detachment modes. Similarly, chapter 6 showed composite biofilm/sediment mechanical strength and future modelling of biostabilization processes would be well served to consider strong bio-mat behaving more like a composite elastic membrane (See figure 8.3) than single individual grains. Whilst the numerical analysis of this modeling is complex, the theory would be that the bio-mat is more strongly anchored in some locations than others, thus as the flow increases (or as gas bubbles form under the mat) the weaker connections will progressively fail and the distance (L) between the anchor points will increase. Thus, the oscillations in the elastic membrane will become increasingly pronounced (in the vertical) and unstable in high flows; this will lead to failure of the mat beyond a

particular threshold, which will rip releasing clumps of biofilm/sediment. In this case, it is the horizontal length-scales over which oscillations occur which should be considered more important for incipient motion than the roughness length scales (such as z_0) used in conventional abiotic sediment transport models. In this case, the initial case for model development is therefore restricted to purely an Eco-Hydraulic problem (as sediment is not exposed at the boundary and therefore cannot influence flow), such that the mechanical feedback between the membrane motion, shear stress and turbulence damping are critical. However, the data provided in this thesis should be appropriate to validating such an approach to biotic hydraulic and sediment model development in the innovative way proposed.

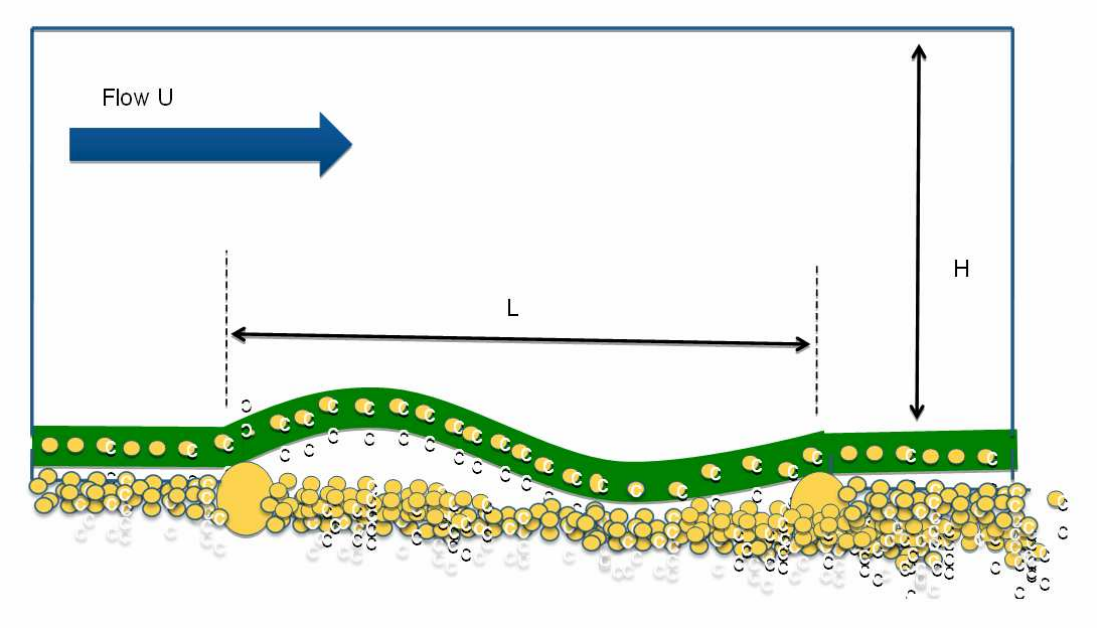

Figure 8. 3. Representation of the flow conditions in a flume causing the composite bio-mat and sediment on the bed to oscillate.

8.3 Ideal combined tensile testing-flume facility

As presented in chapter 6, tensile testing could represent a very useful technique to investigate the mechanical properties of bio-mats. However in this thesis I had to extract the samples from the culturing location and this process

could result in modification of the original physical properties of the material (e.g. drying).

Hence, ideally a test directly carried out in a flume, avoiding any extraction and performed in wet conditions would provide the most representative result. This could be done if a flume was equipped with a horizontal tensile testing facility, which means that a region of the flume bed could be equipped with a plate connected with a load cell (possibly 5N, in order to obtain very detailed analysis). The plate could be allowed to move at a set displacement rate (in the same way as a tensile tester). Ideally the bed material should be fixed on the movable pate and on the upstream region of the flume, so that no disruption could be caused by the dislodgement of sediments on the surface and biofilm could just grow and "carpet" the immobile bed. This test cannot be carried out under real flow conditions, because the weight of the water column could break the biofilm while testing; however, if the flume is carefully and slowly drained, then the horizontal tensile test could be carried out when the bio-mat is still in wet conditions, ensuring that the test is measuring the real biofilm properties.

This method, which could be quite costly (e.g. load cell of high accuracy immerse in water; a flume facility with a plate that can be displaced at a controlled velocity), would be the most representative way of testing bio-mats without extracting them.

In my opinion this facility could also be exported to the field, if a plate (that has can be separated in the centre) is left to be colonized *in situ* and then transported to the flume for testing. The transportation could create some disruption in the sample but this can be minimized by keeping the sample constantly wet; moreover, since the sediments should be glued onto the plate, no dislodgment or settlement of the substrata should occur, so that only the biofilm strength could be analyzed.

8.4 Closing Statement

This thesis has provided novel data sets on: (i) biostabilization of non-cohesive sand/gravels; (ii) Eco-Hydraulics over bio-mats; (iii) biomechanics of composite biofilm-sediment mats. Not only has quantitative, robust measurement of each of these processes been provided for a range of spatio-temporal conditions, but numerous variables have been specifically isolated and examined to attempt to resolve the underpinning relationships responsible for biostabilization. Crucially, this thesis has provided unequivocal evidence that biofilms can be successfully be cultured and colonized in a laboratory flume at the scale representative of growth in the field; this finding should not be understated, as it yields significant potential for researchers (engineers, geoscientists and biologists) to start to control and unravel biostabilization in far more detail. However, due to the complexity of cross-disciplinary subject progress and requirement for forays into biology even in an engineering-based thesis such as the present one, it has been found to be prudent to join the choir of voices (e.g. Black *et al.*, 2002; Rice *et al.*, 2010; Gerbersdorf *et al.*, 2011) that auspicate for a unified effort across different research disciplines, if significant progress is to be made in Eco-Hydraulics or biostabilization research.

References

1. **Aberle J, Nikora VI and Walters R.** (2004). Effects of bed material properties on cohesive sediment erosion. *Marine Geology* **207:** 83-93.
2. **Aberle J, Nikora VI, McLean S, Doscher C, McEwan I, Green M, Goring D, Walsh J.** (2003). A straight benthic flow through flume for in situ measurement of cohesive sediment dynamics. *J. Hydraul. Eng*. **129**: 63–66.
3. **Abramoff MD, Magelhaes PJ, Ram SJ.** (2004). Image Processing with ImageJ. *Biophotonics Int*. 11: 36-42.
4. **Adrian RJ.** (1991). Particle-Imaing Techniques for experimental fluid mechanics. *Ann. Rev. Fluid. Mech.* **23**: 261-304.
5. **Adrian RJ.** (2007). Harpin vortex organization in wall turbulence. Phys Fluids **19**: 041601.
6. **Aggarwal S, Hozalski RM.** 2010. Determination of biofilm mechanical properties from tensile tests performed using a micro-cantilever method. *Biofouling* **26**: 479-486.
7. **Aggarwal S, Poppele EH, Hozalski RM.** 2010. Development and testing of a novel microcantiliver technique for measuring the cohesive strength of intact biofilm. *Biotech and Bioeng* **105**:924-934.
8. **Ahimou F, Denis FA, Touhami A, Dufrene, YF.** 2002. Probing microbial cell surface charges by atomic force microscopy. *Langmuir* **18**:9937-9941.
9. **Ahimou F, Semmens MJ, Novak PJ, Haugstad G.** 2006. Biofilm cohesiveness using a novel atomic force microscopy methodology. *App Environ Microbiol* **73**:2897-2904.
10. **Allison DG, Sutherland IW, Neu TR.** (2003). EPS: What´s an acronym? p. 381-386. *In* McBain A, Allison D, Brading M, Rickard A, Verran J, J Walker (eds.),Biofilm communities: Order from Chaos? BioLine, Cardiff.
11. **Alpkvist E, Klapper I.** (2007). Description of Mechanical Response including detachment using a novel particle model of biofilm/flow interaction. *Wat Sci Technol* **55**:265-273.
12. **Amos CL, Brylinsky M, Sutherland TF, O'Brien D, Lee S, Cramp A.** (1998). The stability of a mud flat in the Humber estuary, south Yorkshire, UK. *J Geol Soc (London)* **139**: 25-44.
13. **Amos CL, Daborn GR, Christian HA, Atkinson A, Robertson A.** (1992). In situ erosion measurements of fine-grained sediments form the Bay of Fundy. *Mar Geol* **108**: 175-196.
14. **Amos CL, Droppo IG.** (1996). The stability of remediated lakebed sediment, Hamilton Harbour, Lake Ontario, Canada. *Geological Survey of Canada Open File Report* # 2276.
15. **Ananthanarayan R, Jayaram Paniker CK.** (1996). *Textbook of microbiology*. Sangam Bks.
16. **Anderson-Glenna MJ, Bakkestuen V and Clipson NJ W.** (2008). Spatial and temporal variability in epilithic biofilm bacterial communities along an upland river gradient. *FEMS Microbiol Eco* **64**: 407–418.
17. **Andrewartha J, Sargison J, Perkins K, Walker G and Henderson A.** (2010). The turbulence structure of flows over rough surfaces and freshwater biofilm. In *Proc.17th Congress of the Asia and Pacific Division of the International Association of Hydraulic Engineering and Research*.

18. **Andrews ED.** (1983). Entrainment of gravel from naturally sorted riverbed material. *Geological Society of America Bulletin* **94:** 1225-31.
19. **Aravas N, Laspidou CS.** (2008). On the calculation of the elastic modulus of biofilm streamer. *Biotech. Bioeng.* **101**:196-200.
20. **AzeredoJ, Oliveira R.** (2000). The role of exopolymers produced by Sphingomonas paucimobilis in biofilm formation and composition. *Biofouling* **16:** 17-26.
21. **Battin TJ and Sengschmitt D.** (1999). Linking Sediment Biofilms, Hydrodynamics, and River Bed Clogging: Evidence from a Large River. *Microbial Ecology* **37**:185–196.
22. **Battin TJ, Kaplan LA, Denis Newbold J and Hansen CME.** (2003a). Contributions of microbial biofilms to ecosystem processes in stream mesocosms. *Nature* **426**: 439-442.
23. **Battin TJ, Kaplan LA, Newbold JD, Cheng X, Hansen C.** (2003b). Effects of current velocity on the nascent architecture of stream microbial biofilms. *Appl Environ Microbiol*, **69:** 5443-5452.
24. **Battin TJ.** (2000). Hydrodynamics is a major determinant of streambed biofilm activity: from the sediment to the reach scale. *Limnol Oceanogr* **46**: 1308-1319.
25. **Best JL (1992).** On the entrainment of sediments and initiation of bed defects: insights from recent developments within turbulent boundary layer research. *Sedimentology* **39**: 797-811.
26. **Best JL.** (1993). On the interactions between turbulent flow structure, sediment transport and bedform development. In Clifford, N.J., French, J.R. and Hardisty, J. (eds). *Turbulence: perspectives on flow and sediment transport*. Chichester: Wiley, 61-92.
27. **Biggs BJF and Hickey CW.** (1994). Periphyton responses to a hydraulic gradient in a regulated river in New Zealand. *Freshwater Biology* **32**:49-59.
28. **Biggs BJF, Goring DG & Nikora VI. 1998.** Subsidy and stress responses of stream periphyton to gradients in water velocity as a function of community growth form. *J Phycol* **34**: 598–560.
29. **Black KS, Tolhurst TJ, Paterson DM and Hagerthey SE.** (2002). Working with natural cohesive sediments. *Journal of Hydraulic Engineering* **128**:1-8.
30. **Borsje BW , de Vries MB, Hulscher SJMH , de Boer GJ.** (2008). Modeling large-scale cohesive sediment transport affected by small-scale biological activity. *Estuarine, Coastal and Shelf Science* **78** 468e480
31. **Boulton AJ, Findlay S, Marmonier P, Stanley EH, Valett HM.** (1998). The functional significance of the hyporheic zone in streams and rivers. *Ann Rev Ecol Syst* **29**: 59-81.
32. **Bouwer EJ, Rijnaarts HHM, Cunningham AB, Gerlach R.** (2000). Biofilms in porous media. In: Bryers J, editor. Biofilms II: process analysisand applications. New York: Wiley-Liss, Inc. pp123-158.
33. **Brown PP and Lawler DF.** (2003). Sphere Drag and Settling Velocity Revisited. *J Environm Eng* **129**: 222-231.
34. **Buffington J.M.** (1999). The legend of A.F. Shields. *Journal of Hydraulic Engineering* **125**: 376-386.
35. **Buffington JM, Montgomery DR.** (1997). A systematic analysis of eight decades of incipient motion studies, with special reference to gravel-bedded rivers. *Water Res Research* **33**:1993-2029.

36. **Buffington JM, Montgomery DR.** (1999). Effects of sediment supply on surface textures of gravel-bed rivers. *Water Resources Research* **35**: 3523–3530.
37. **Butler JB, Lane SN, Chandler JH.** (1998). Assessment of DEM quality characterising surface roughness using close range digital photogrammetry, *Photogrammetric Record*, **19**:271-291.
38. **Callow ME.** (1993). A review of fouling in freshwaters. *Biofoul* **7**: 313-326.
39. **Carling PA.** (1990). Particle over-passing on depth limited gravel bars. *Sedimentology* **37:** 345-355.
40. **Carson MA, Griffiths GA**. (1987). Bedload transport in gravel channels. *Journal of Hydrology* (New Zealand) **26**: 1-151.
41. **Casey HJ.** (1935). Uber Geschiebebewegung. *Mitteilungen der Preussischen Versuchsanstalt fu¨r Wasserbau und Schiffbau*, Heft 19, Berlin (in German).
42. **Chanson H.** (1999). *The hydraulics of open channel flow. An introduction*. London: Arnold, 495 pp.
43. **Characklis WG, Wilderer PA.** (1989). Structure and function of biofilms. Dahlem Workshop Reports. London.
44. **Cheng N-S, Chiew Y-M.** (1998). Pickup probability for sediment entrainment. *J. Hydraul. Eng.*, **124**: 232-235.
45. **Chepil W.S.** (1959). Equilibrium of soil grains at the threshold of movement by wind. *Soil. Sci. Soc. Am. Proc.,* **23**:422-428.
46. **Chepil WS.** (1958). The use of evenly spaced hemispheres to evaluate aerodynamic forces on soil surfaces. *Eos Trans A GU* **39**: 397-404.
47. **Cooper JR, Tait SJ.** (2008). Water worked gravel beds in laboratory flumes- a natural analogue?. Earth Surface Processes and Landforms. 34: 384-397.
48. **Costerton JW, Cheng KJ, Geesey GG, Ladd TI, Nickel JC, Dasgupta M, Marrie TJ.** (1987). Bacterial biofilm in nature and disease. *Ann. Rev. Microbiol*. **41**: 435-464.
49. **Costerton JW, Greesey GG, Cheng KJ.** (1978). How bacteria stick. *Sci Am* **238:** 85-95.
50. **Costerton JW, Irwin RT, Cheng KJ.** (1981). The bacterial glycocalyx in nature and disease. *Annu Rev microbial* **35**: 299-324.
51. **Cox JS, Scott Smith D, Warren LA & Ferris FG.** (1999). Characterizing heterogeneous bacterial surface functional groups using discrete affinity spectra for proton binding. *Environ Sci Technol* **33**: 4514–4521.
52. **Dade WB, Davis JD, Nichols PD, Nowell ARM, Thistle D, Trexler MB, White DC** (1990). Effects of bacterial exopolymer adhesion on the entrainment of sand. *Geomicrob J,* **8**: 1-16.
53. **Dade WB, Self RL, Pellerin NB, Moffet A, Jumars PA, Nowell ARM.** (1996). The effects of bacteria on the flowbehaviour of clay-seawater suspensions. *J. Sediment res.* **66:** 39-42.
54. **Daniels L, Hanson RS, Phillips J**. (2007). Total Carbohydrates by Phenol Reaction, p. 468. In: Reddy, C.A., Beveridge, T.J., Breznak, J.A., Marzluf, G.A., Schmidt, T.M., and L.R. Snyder (ed.), *Methods for General and Molecular Microbiology*, 3rd ed., Section III: Chemical Analysis ASM Press, Washington, DC
55. **Dantec Dynamics** (2010). 2D PIV Reference Manual.
56. **Day TJ.** (1980). A study of initial motion characteristics of particles in graded bed material. *Geological Survey of Canada, Current Research, Part A, Paper* **80**: 281-6.

57. **de Beer D, O'Flaharty V, Thaveesri J, Lens P, Verstraete W.(**1996). Distribution of extracellular polysaccharides and flotation of anaerobic sludge. *Appl Microbiol Biotechnol* **46**:197-201.
58. **de Brouwer JFC, Bjelic S, De Deckere EMGT, Stal LJ**. (2000). Interplay between biology and sedimentology in a mudflat (Biezelingse Ham, Westerschelde, The Netherlands*). Cont Shelf Res* **20**:1159–1176.
59. **de Deckere EMGT, Tolhurst TJ, De Brouwer JFC** (2001) Destabilisation of cohesive intertidal sediments by infauna. *Est, Coast and Shelf Sci* **56**:665–669.
60. **Dorigo U, Lefranc M, Leboulanger C, Montuelle B, Humbert J-F.** (2009). Spatial heterogeneity of periphytic microbial communities in a small pesticide-polluted river. *FEMS Microb Ecol* **67**:491–501. doi: 10.1111/j.1574-6941.2008.00642.x
61. **Droppo IG, Lau YL, Mitchell C.** (2001). The effect of depositional history on contaminated bed sediment stability**.** *Sci Tot Env,* **266:** 7-13.
62. **Droppo IG, Liss SN, Williams D, Nelson T, Jaskot C, Trapp B.** (2009). Dyanamic Existence of Waterborne Pathogens within River Sediment Compartments. Implications for Water Quality Regulatory Affairs. *Environ Sci Technol* **43**: 1737-1743.
63. **Egiazaroff V.** (1965). Calculation of nonuniform sediment concentrations. *J Hydraul Div Am Soc Civ Eng* **91**: 225-247.
64. **Einstein HA.** (1942). Formulas for the transportation of bed load. *Trans Amer Soc Civ Eng* **107**: 561-597.
65. **Fernández-Luqueño F, Valenzuela-Encinas C, Marsch R, Martínez-Suárez C, Vázquez-Núñez E and Dendooven L.** (2011). Microbial communities to mitigate contamination of PAHs in soil—possibilities and challenges: a review. *Environ Sci Pollut Res* **18**:12–30.
66. **Findlay S. 1995.** Importance of surface-subsurface exchange in stream ecosystems: the hyporheic zone. *Limnol Oceanogr* **40**: 159-164.
67. **Finnigan J.** (2000). Turbulence in plant canopies. *Annual Review of fluid Mechanics* **32:**519-571.
68. **Ford *A*, Roberts A.** (1998). *Color Space Conversions*, Technical report, August 11.
69. **Francus P.** (1998). An image-analysis to measure grain-size variation in thin sections of soft clastic sediments. *Sed Geol* **121**: 289-298.
70. **Fripp JB, Diplas P.** (1993). Surface sampling in gravel streams. *J Hydr Engrg* **119**: 473-490.
71. **Garcia MH.** (2000). Discussion of "The legend of A.F. Shields". *Journal of Hydraulic Engineering* **126**: 718-720
72. **Garcia-Aragon J, Droppo IG, Krishnappan BG, Trapp B, Jaskot C. 2011.** Erosion Characteristics and floc strength of Athabasca River cohesive sediments: towards managing sediment-related issues. *J Soils and Sed*
73. **Garcia-Pichel F, Wojciechowski MF.** (2009). The Evolution of a Capacity to Build Supra-Cellular Ropes Enabled Filamentous Cyanobacteria to Colonize Highly Erodible Substratums. *PLoS ONE* **4**(11): e7801.
74. **Gerbersdorf SU, Bittner R, Lubarsky H, Manz W, Paterson DM**. (2009a). Microbial assemblages as ecosystem engineers of sediment stability. *J of Soils and Sed* **9**: 640–652.
75. **Gerbersdorf SU, Hollert H, Brinkmann M, Wieprecht S, Schuttrumpf H, Manz W.** (2011). Anthropogenic pollutants affect ecosystem services of freshwater sediments: the need for a „triad plus x" approach. *J Soils Sediments* 2011.

76. **Gerbersdorf SU, Jancke T, Westrich B, Paterson DM.** (2008). Microbial stabilization of riverine sediments by extracellular polymeric substances. *Geobiol* **6**:57–69.
77. **Gerbersdorf SU, Jancke T, Westrich B.** (2005). Physico-chemical and biological sediment properties determining erosion resistance of contaminated riverine sediments—temporal and vertical pattern at the Lauffen reservoir/River Neckar, Germany. *Limnol* **35**:132–144.
78. **Gerbersdorf SU, Westrich B, Paterson DM.** (2009b). Microbial Extracellular Polymeric Substances (EPS) in FreshWater Sediments. *J of Soils and Sed* **9**:640:652.
79. **Ghosh U, Gillette JS, Luthy RG, Zare RN. 2000.** Microscale location, characterization, and association of polycyclic aromatic hydrocarbons on harbour sediment particles. *Env Sci Tech* **34:** 1729-1736.
80. **Gil JA, Túa L, Rueda AC,Rodríguez M, Prats D.** (2010). Influence of temperature variations on the cake resistance and EPS of MBR mixed liquor fractions. *Desalin and Wat Treat,* doi: 10.5004/dwt.2010.1225.
81. **Gilbert GK.** (1914). The transportation of debris by running water. *Profl. Paper* **86**, U.S. Geological Survey, Washington, D.C.
82. **Godillot R., Caussade B, Ameziane T, Capblancq J.** (2001). Interplay between turbulence and periphyton in rough open-channel flow. *J of Hydr Res* **39**: 227-239.
83. **Graba M, Moulin FY, Boulêtreau S, Garabétian F, Kettab A, Eiff O, Sánchez-Pérez JM, Sauvage S.** (2010). Effect of near-bed turbulence on chronic detachment of epilithic biofilm: Experimental and modeling approaches, *Water Resour Res* **46**: W11531.
84. **Grabowski RC, Droppo IG, Wharton G.** (2011). Erodibility of cohesive sediments: the importance of sediment properties. *Earth-Sci Rev* **105**: 101-120.
85. **Graf WH.** (1984). Hydraulics of sediment transport. Water Resources Publications, Littleton.
86. **Graham DJ, Rice SP, Reid I.** (2005). A transferable method for the automated grain sizing of river gravels. *Water Resour Res* **41**: W07020, doi:10.1029/2004WR003868.
87. **Grant J, Bathmann' UV, Mills EL**. (1986). The Interaction between Benthic Diatom Films and Sediment Transport. *Est Coast and Shelf Sci* **23:** 225-23.
88. **Grant J, Gust G.** (1987). Prediction of coastal sediment stability from photopigment content of mats of purple sulphur bacteria. *Nature* **330**: 244-246.
89. **Grass AJ. (1971).** Structural features of turbulent flow over smooth and rough boundaries. *Journal of Fluid Mechanics* **50**: 233-255.
90. **Grass AJ.** (1970). Initial instability of fine bed sand. *Journal of Hydraulic division, ASCE,* **HY3**: 619-632.

91. **Haag I, Westrich B.** (2002). Processes governing river water quality identified by principal component analysis. *Hydrol Process* **16:** 3113–3130.
92. **Hall SJ.** (1994). Physical disturbance and marine benthic communities: life in unconsolidate sediments. *Oceanography and Marine Biology Annual Review,* **32**:179-239.
93. **Halow JS.** (1973). Incipient rolling, sliding and suspension of particles in horizontal and inclined turbulent flow. *Chem Eng Sci* **28**: 1-12.
94. **Hardy RJ, Best L, Lane SN, Carbonneau PE**. (2009). Coherent flow structures in a depth-limited flow over a gravel surface: the role of near-

bed turbulence and influence of Reynolds number. *J Geophys Res* **114**:F01003.
95. **Harkes G, Feijen J, Dankert J.** (1991). Adhesion of Escherichia coli on to a series of poly(methacrylates) differing in charge and hydrophobicity. *Biomaterials* **12**: 853–860.
96. **Haynes H, Pender G.** (2007). Stress history effects on graded bed stability. *Journal of Hydraulic Engineering* **33**: 343-349.
97. **HIMOM.** (2005). Hierarchical Monitoring Methods. European Commission Fifth Framework Programme. Contract: EVK3-CT-2001-00052. Brokman Consult, Geesthacht.
98. **Hjulström F.** (1935). Studies of the morphological activity of rivers as illustrated by the river Fyris. *Bulletin of the Geological institute*, University of Uppsala **25:** 221-256.
99. **Hupp CR, Osterkamp WR, Howard AD.** (1995). Biogeomorphology-Terrestrial and Freshwater Systems. Elseiver, Amsterdam, The Netherlands. 347 pp.
100. **Huxley TH.** (1868). Letter to Ernst Haeckel, 6th October 1868.
101. ife Sciences Research Report 46. John Wiley and Sons, Chichester.
102. **Jenkinson I, Biddanda B, Turley CM, Abreu PC, Riebesell U and Metacek VS.** (1991). Rheological properties of marine organic aggregates: Importance for vertical flux, turbulence and microzones. *Oceanolog. Acta*, **11**:101-106.
103. **Jucker BA, Harms H, Zehnder AJB.** (1996). Adhesion of the positively charged bacterium Stenotrophonmonas (Xanthomonas) maltophilia 70401 to glass and Teflon. *J Bacteriol* **178**:5472–5479.
104. **Klapper I, Rupp CJ, Cargo R, Purvedorj B, Stoodley P**. (2002). Viscoelastic fluid description of bacterial biofilm material properties. *Biotechnol. Bioeng.*, **80**: 289-296.
105. **Komar PD.** (1987). Selective grain entrainment by a current from a bed of mixed sizes: a reanalysis. *Journal of Sedimentary Petrology* **57**: 203-11.
106. **Komar PD.** (1996). Entrainment of sediments from deposits of mixed grain sizes and densities. *In* Advances in fluvial dynamics and stratigraphy. (Ed) P.A. Craling and M.R. Dawson.
107. **Körstgens V, Flemming HC, Wingender J, Borchard W.** (2001). Uniaxial compression measurement device for investigation of the mechanical stability of biofilms. *J Microbiol Methods* **46**: 9-16.
108. **Kouwen N, Unny TE.** (1973). Flexible roughness in open channels. *J. of the Hydr. Div ASCE* **99**:713-728.
109. **Kramer H.** (1932). *Modellgeschiebe und schleppkraft*, Doktor-Ingenieurs dissertation, Technischen Hochschule, Dresden, Germany (in German).
110. **Kramer H.** (1935). Sand mixtures and sand movement in fluvial models. *Trans.*, ASCE, **100**: 798–838.
111. **Krumbein WC.** (1934). Size frequency distributions of sediments. *J. Sedim. Petrol*. **4**: 65-76.
112. **Labiod C, Godillot R, Caussade B.** (2007). The relationship between stream periyphyton dynamics and near-bed turbulence in rough open-channel flow. *Ecological Modelling* 209: 78-96.
113. **Larson F, Lubarsky H, Gerbersdorf SU, Paterson DM.** (2009). Surface adhesion measurements in aquatic biofilms using magnetic particle induction: MagPI. *Limnol Oceanogr: Methods* **7**: 490-496.

114. **Laspidou CS and Aravas N.** (2006). Variation in mechanical properties of a porous multi-phase biofilm under compression due to void closure. *Water Science and Technology*, **55**:447–453.
115. **Lawless M, Robert A.** (2001). Scale of boundary resistance in coarse-grained channels. *Geomorphology* **39**: 221-38.
116. **Lawrence JR, Korber DR, Hoyle BD, Costerton JW and Caldwell DE.** (1991). Optical sectioning of microbial biofilms. *J. Bact.*, **173:** 6558-6566.
117. **Le Hir P, Monbet Y, Orvain F.** (2007). Sediment erodibility in sediment transport modeling: can we account for biota effects? *Cont. Shelf Res.* **27**:1116-1142.
118. **Lelieveld SD, Pilditch CA and Green MO.** (2003). Varition in sediment stability and relation to indicators of microbial abundance in the Okura Estuary, New Zealand. *Est. Coast & Shelf Sci* **57**: 123-136.
119. **Li H, Wang Y, Shi LQ, Mi J, Song D, Pan XJ.** (2012). Distribution and Fractions of Phosphorus and Nitrogen in Surface Sediments from Dianchi Lake, China. *Intern J of Env Res* **6**: 195-208.
120. **Li Z, Komar PD.** (1986). Laboratory measurements of pivoting angles for applications to selective entrainment of gravel in a current. *Sedimentology* **33**: 413--425.
121. **Lick W, Jin L, Gailani, J.** (2004). Initiation of Movement of Quartz Particles. *J Hyd Eng* **130:** 755-761.
122. **Lick W.** (1982). The transport of contaminants in the great lakes. *Ann. Rev. Earth Planet. Sci.* **10:** 327-353.
123. **Ling CH.** (1995). Criteria for incipient motion of spherical sediment particles. *J Hydraul Eng* **121**:472–478.
124. **Little BJ, Wagner PA, Lewandowski Z**. (1996). *Spatial relationships between bacteria and mineral surfaces*. In: Banfield JF, Nealson KH, editors. Geomicrobiology: Interactions between Microbes and Minerals. Washington, DC: Mineralogical Society of America. p 123–159.
125. **Lock MA, Wallace RR, Costerton JW, Ventullo RM, Charlton SE**. (1984). River epilithon (biofilm): toward a structural functional model. *Oikos*, **42:** 10-22.
126. **Lock MA.** (1993). Attached microbial communities in rivers. *In (ed.)* T. E. Ford, Aquatic Microbiology, Blackwell scientific publications, Boston, pp. 518.
127. **Lu LJ, Smith CR.** (1991). Use of flow visualization data to examine spatial-temporar velocity and burst-type characteristics in a turbulent boundary layer. *Journal of fluid mechanics* **232**: 303-340.
128. **Luoma SN, Rainbow PS.** (2008). Metal Contamination in Aquatic Environments: Science and Lateral Management. Cambridge University Press, Cambridge. 573pp.
129. **Maa JPY, Kwon JI, Hwang KN, Ha HK.** (2007). Critical bed shear stress for cohesive sediment deposition under steady flows. *Journal of Hydraulic Engineering* **134**, 1767–1771.
130. **Maa JP-Y, Sanfort LP, Halka JP.** (1998). Sediment resuspension characteristics in Baltimore Harbor, Maryland. *Mar Geol* **146**: 137-145.
131. **Macklin MG, HudsonEdwards KA, Dawson EJ**. (1997). The significance of pollution from historic metal mining in the Pennine orefields on river sediment contaminant fluxes to the North Sea. *Science of the Total Environment* **194:** 391-396.

132. **Madsen KN, Nilsson P, Sundback K.** (1993). The influence of benthic microalgae on the stability of subtidal sediment. *J of Exp Mar Bio and Eco* **170:** 159-176.
133. **Mantz PA.** (1977). Incipient transport of fine grains are flakes by fluids—Extended Shields diagram. *J. Hydr. Div., ASCE* **103**: 601–615.
134. **Manzenrieder H**. (1983). Die biologische Verfestigung von Wattflächen aus der Sicht des Ingenieurs. *Miteilungen Leichtweiss-Instituts Wasserbau, T.U. Braunschweig* **79**:135-193.
135. **Marshall KC.** (1984). Microbial adhesion and aggregation. Dahalem Workshop Berlin. Life Sciences Research report 31. Springer Verlag, Berlin.
136. **McCabe SK, Cyr H. 2006.** Environmental variability influences the structure of benthic algal communities in an oligotrophic lake. *Oikos* **115**: 197–206.
137. **McCave IN.** (1976). *The benthic boundary layer.*Plenum, New York.
138. **Middleton G, Southard JB.** (1984). *Mechanics of sediment movement*. SEPM. Short course number 3.
139. **Miller MC, McCave IN and Komar PD.** (1977). Threshold of sediment motion under unidirectional currents. *Sedimentology* **24**: 507–526.
140. **Möhle RB, Langemann T, Haesner M, Augustin W, Scholl S, Neu T R, Hempel DC and Horn H.** (2006). Structure and shear strength of microbial biofilms as determined with confocal laser scanning microscopy and fluid dynamic gauging using a novel rotating disc biofilm reactor. *Biotech and Bioeng* **98**:747–755.
141. **Monin AS, Yaglom A M.** (1971). Statistical fluid mechanics: mechanics of turbulence. MIT Press, Cambridge, Mass., English ed. updated, augmented and rev edition.
142. **Morton LHG, Greenway DLA, Gaylarde CC, Surman SB.** (1998). Consideration of some implications of the resistance of biofilms to biocides. *Int. Biodeterio. Biodegrad* **41**: 247-259.
143. **Moulin FY *et al*.** (2008). Experimental study of the interaction between a turbulent flow and a river biofilm growing on macrorugosities, in *Advanceds in Hydro-Science and Engineering* , vol 8, edited by SSY Wang , pp 1887-1896, Int Assoc Hyrdo-Environ Eng Res, Nagoya, Japan.
144. **Neill CR, Yalin MS.** (1969). Quantitative definition of beginning of bed movement. *Proc Am Soc Civ Eng* **95**: 585-587.
145. **Neu TR.** (1994). Biofilm and microbial mats, *in* Krumbein, W.E., Paterson, D.M. and Stal, L., eds., Biostabilization of sediments: Oldenburg, Germany, Bibliotheks und Informations system der Universitat Oldenburg, pp. 9-16.
146. **Neuman AC, Gebelein CD, Scoffin GP.** (1970). The composition, structure, and erodibility of subtidal mats, Abaco, Bahamas. *J. Sed. Petrol*. **40:** 274-296.
147. **Nicklin J, Graeme-Cook K, Paget T, Killington R.** (1999). Instant Notes in Microbiology. *Bios. Scientific Ltd.*, Oxfrod, UK., pp. 76-80.
148. **Nikora VI, Goring D and Biggs B.** (1997). On stream periphyton-turbulence interactions. *New Zealand Journal of Marine and Freshwater Research* **31**:435-448.
149. **Nikora VI, Goring D, McEwan I, Griffiths G.** (2001). Spatially averaged open-channel flow over rough bed. *J Hydraulic Eng* **127**: 123–133.

150. **Nikora VI, Goring DG, Biggs BJF.** (1998). A simple model of stream *periphyton*-flow interactions. *Oikos* **81**: 607-611.
151. **Nikora VI, Goring DG, Biggs BJF.** (2002). Some observations of the effects of micro-organisms growing on the bed of an open channel on the turbulence properties. *J. of Fluid Mech*. **450**: 317-341.
152. **Nikora VI, Larned S, Nikora N, Debnath K, Cooper G, Reid M.** (2008). Hydraulic Resistance due to Aquatic Vegetation in Small Streams: Field Study. *J Hydr Eng* **134**: 1326-1332.
153. **Nikora VI.** (2010). Hydrodynamics of aquatic ecosystems: an interface between ecology, biomechanics and environmental fluid mechanics. *River Res. and Appl*. **26**: 367-384.
154. **Niño Y, Garcia MH.** (1996). Experiments on the particle-turbulence interactions in the near-wall region of an open channel flow: implications for sediment transport. *J. Fluid Mech.* **326**: 285-319.
155. **Noffke N, Gerdes G, Klenke T, Krumbein WE.** (2001). Microbially induced sedimentary structures – A new category within the classification of primary sedimentary structures. *Journal of Sedimentary Research* **71**: 649-656.
156. **Ockelford A, Haynes H.** (2011). The impact of stress history on bed structure. Submitted to *Earth Surfaces Processes and Landforms*.
157. **Ohashi A, Harada H.** (1994). Adhesion strength of biofilm developed in an attached –growth reactor. *Water Sci Technol* **29**: 201-211.
158. **Ohashi A, Harada H.** (1996). A novel method for evaluation of biofilm adhesion strength by applying tensile force and shear force. *Water. Sci. Technol.*, **34:** 201-211.
159. **Ohashi A, Koyama T, Syutsubo K, Harada H.** (1999). A novel method for evaluation of biofilm tensile strength resisting erosion. *Water Sci Technol* **39:** 261-268.
160. **Owens PN.** (2007). Introduction. Background and Summary of this Issue on Sediment Linkages. *J Soils Sediments* **7**: 273–276
161. **Paintal AS.** (1971). A stochastic model for bed load transport. Journal *of Hydraulic Research* **9**: 527–553.
162. **Paphitis D, Collins MB.** (2005). Sand grain threshold, in relation to bed stress history: an experimental study. *Sedimentology* **52**: 827 838.
163. **Parker G, Klingeman PC, McLean DG.** (1982). Bedload and size distribution in paved gravel-bed stream. *Journal of the Hydraulic Division of the American Society of Civil Engineers.* **108**: 544-571.
164. **Parker G, Klingeman PC.** (1982). On why gravel bed streams are paved. *Water Res Res* **18**:1409-23.
165. **Parker WR.** (1997). On the characterization of cohesive sediment for transport modelling. In *Cohesive sediments* (eds) Burt, N., Parker, R. and Watts, J., pp. 458.
166. **Partheniades E.** (1962) *A study of erosion and deposition of cohesive soils in salt water*. Ph.D. Thesis. University of California, Berkeley, 182pp.
167. **Paterson DM, Daborn GR**. (1991). Sediment stabilization by biological action: significance for coastal engineering. In *Developments in coastal engineering*. Peregrine, D.H. and Loveless, J.H. (eds). University of Bristol press, pp.111-119.
168. **Paterson DM.** (1989). Short-term changes in the erodibility of intertidal cohesive sediments related to the migratory behavior of epiphelic diatoms. *Limno. Oceanogr* **34**:223-234.

169. **Paterson DM.** (1994). Microbiological mediation of sediment structure and behaviour, in Stal LJ and Caumette P, eds., Microbial Mats: Berlin, Springer-Verlag, p. 97–109.
170. **Paterson DM.** (1997). Biological mediation of sediment erodibility: ecology and physical dynamics. In *Cohesive sediments*, 458. Burt, N., R. Parker, and J. Watts.
171. **Paul D, Pandey G, Pandey J, Jain RK.** (2005). Accessing microbial diversity for bioremediation and environmental restoration. *Trends Biotechnol* **23**:135–142.
172. **Phoenix VR, Holmes WM**. (2008). Magnetic resonance imaging of structure, diffusivity, and copper immobilization in a phototrophic biofilm. *Appl Environ Microbiol* **74**:4934–4943.
173. **Poppele EH, Hozalski RM.** (2003). Micro-cantilever method for measuring the tensile strength of biofilms and microbial flocs. *J Microbiol Methods* **55:** 607-615.
174. **Powers MC**. (1953). A new roundness scale for sedimentary particles. *J Seditiement Petrol* **23:** 117-119.
175. **Prandtl L.** (1925).Uber die ausgebildete Turbulenz Z. *Angew. Math. Mech.* **5**:136.
176. **Raffel M, Willert CE, Kompenhans J.** (2007) *Particle-Image Velocimetry: A Practical Guide* Springer-Verlag, Berlin.
177. **Ramanan B, Holmes WM, Sloan WT, Phoenix1 VR.** (2010). Application of Paramagnetically Tagged Molecules for Magnetic Resonance Imaging of Biofilm Mass Transport Processes. Appl Environm Mirobiol 76: 4027-4036.
178. **Rathbun RE, Guy HP.** (1967). Measurement of hydraulic and sediment transport variables in a small recirculating flume. *Wat Resour Res* **3**: 107-122.
179. **Reynolds O.** (1985). On the dynamical theory of incompressible fluids and the determination of the criterion. *Phil Trans Roy Soc London A* **186:** 123-164**.**
180. **Rice S, Church M**. (1996). „Sampling surficial fluvial gravels: The precision of size distribution percentile estimates. *J Sed Res* **66**: 654–665.
181. **Rice SP, Lancaster J and Kemp P.** (2010a). Experimentation at the interface of fluvial geomorphology, stream ecology and hydraulic engineering and the development of an effective, interdisciplinary river science. *Earth Surface Processes and Landforms* **35:**64-76.
182. **Rice SP, Little S, Wood PJ, Moir HJ and Vericat D.** (2010b). The relative contributions of ecology and hydraulics to ecohydraulics. *River Research and Applications* **26**: 363-366.
183. **Richards KS.** (1982). *Rivers. Form and Process in alluvial channels*. London: Methuen, 358 pp.
184. **Righetti M, Lucarelli C.** (2007). May the shields theory be extended to cohesive and adhesive benthic sediments? *J. Geophys. Res.* **112**: C05039.
185. **Righetti M, Lucarelli C.** (2010). Resuspension phenomena of benthic sediments: The role of cohesion and biological adhesion. *River Res. and Applic*. **26**: 404-413.
186. **Ripkka R, Deruelles J,. Waterbury JB, Herdman M, Stanier RY.** (1979). Genetic assignments, strain histories, and properties of pure cultures of cyanobacteria. *J Gen Microbiol* **111**:1–61.
187. **Rittenhouse G**. (1943). Transportation and Deposition of Heavy Minerals. *Geol. Soc. Am. Bull.*, **54:** 1725-1780.

188. **Robert A.** (1997). Characteristics of velocity profiles along riffle-pool sequences and estimates of bed shear stresses. *Geomorp* ***19***: 89–98.
189. **Robert A.** (2003). *River processes. An introduction to Fluvial Dynamics*. London: Arnold, 214 pp.
190. **Salant NL.** (2011). "Sticky business": the influence of streambed periphyton on particle deposition and infiltration. *Geomorphology* **126**: 350-363.
191. **Sanford LP, Maa JP-Y.** (2001). A unified erosion formulation for fine sediments. *Marine Geol* **179**: 9-23.
192. **Schultz MP, Swain GW.** (1999). The Effect of Biofilms on Turbulent Boundary Layers. *ASME J. Fluids Engineering*, **121**: 44-51.
193. **Scoffin TP.** (1970). The trapping and binding of subtidal carbonate sediment by marine vegetation in Bimini Lagoon, Bahamas. *J. Sed. Petrol.*, **40**:249-273.
194. **Shaoo PK, Soltani S, Wong AKC**. (1988). A survey of thresholding techniques. *Comp Vis, Graph and Image Proc* **41**: 233-260.
195. **Shields A.** (1936). Application of Similarity Principles and Turbulence Research to Bed- load Movement. In: Mitteilungen der preussischen Nersuchsanstalt fur Wassed Brau end Schiffbuar. Report 167, California Institute of Technology, Pasedena, California.
196. **Shvidchenko AB, Pender G, Hoey TB.** (2001). Critical shear stress for incipient motion of sand/gravel streambeds. *Proceedings of the Institute of Civil Engineering; Waters and Maritime Engineering* **142**; 217-226.
197. **Sigee, D.** (2005). *Freshwater microbiology*. Wiley, West Sussex
198. **Smith GA, Nickels JS, Kerger BD, Davis JD, Collins SP, Wilson JT, McNabb JF, White DC.** (1986). Quantitative characterization of microbial biomass and community structure in subsurface material: a prockaryotic consortium responsive to organic contamination. *Can. J. Microbiol*. **32:** 104-111.
199. **Smith JD, McLean SR.** (1977). Spatially averaged flow over a wavy surface. J. *of Geoph. Res.* **82**: 1735-46.
200. **Soulsby RL, Whitehouse RJSW.** (1997). *Threshold of sediment motion in coastal environments*. In: Proceedings of the Pacific coasts and ports, Christchurch, University of Canterbury, New Zealand, 7–11 September 1997, pp 149–154
201. **South Yakima Conservation District.** (2008). Dissolved Oxygen and pH in the Lower Yakima River. South Yakima Conservation District at (509) 837-7911.
202. **Sparks TH, Collinson N, Crick H, Croxton P, Edwards M, Huber K, Jenkins D, Johns D, Last F, Maberly S, Marquiss M, Pickup J, Roy D, Sims D, Shaw D, Turner A, Watson A, Woiwod I, Woodbridge K.** (2006). Natural Heritage Trends of Scotland: phenological indicators of climate change. Scottish Natural Heritage Commissioned Report No. 167 (ROAME No. F01NB01).
203. **Spears BM, Saunders JE, Davidson I, Paterson DM.** (2008). Microalgal sediment biostabilisation along a salinity gradient in the Eden Estuary, Scotland: unravelling a paradox. *Mar & Freshwat Res* **59**: 313-321.
204. **Stal LJ.** (2003). Microphytobenthos, their extracellular polymeric substances, and the morphogenesis of intertidal sediments. *Geomicrobiol Journ* **20:** 463-478.

205. **Standford JA, Ward JV.** (1988). The hyporheic habitat of river ecosystems. *Letters to Nature* **335**: 64-66.
206. **Stoodley P, Cargo R, Rupp CJ, Wilson S, Klapper I**. (2002). Biofilm mechanics and shear induced deformation and detachment. *J Ind Microbiol Biotechnol* **29**:361 – 368.
207. **Stoodley P, Lewandowski Z, Boyle JD, Lappin-Scott HM.** (1999). Structural deformation of bacterial biofilms caused by short-term fluctuations in fluid shear: an in situ investigation of biofilm rhehology. *Biotech and Bioeng* **65:**83-91.
208. **Stoodley P., Wilson S., Hall-Stoodley L., Boyle J.D., Lappin-Scott H.M., Costerton J.W.** (2001). Growth and detachment of cell clusters from mature mixed species biofilms. *Applied Environmental Microbiology*, **67**:5608 – 5613.
209. **Taylor BD, and Vanoni VA.** (1972). Temperature effects in flat-bed flows. *J Hydr Div* ASCE **98**: 1427–1445.
210. **Teng F, Guan YT, Zhu WP**. (2008). Effect of biofilm on cast iron pipe corrosion in drinking water distribution system: Corrosion scales characterization and microbial community structure investigation. *Corr. Sci.* **50**:2816–2823.
211. **Ternat F, Boyer P, Anselmet F, and Amielh M.** (2008). Erosion threshold of saturated natural cohesive sediments: modeling and experiments. *Waer Reour. Res.***44:** W11434
212. **Tolhurst TJ, Black KS, Paterson DM.** (2009). Muddy sediment erosion: insight from field studies. *J Hydr Eng Forum*:73-86.
213. **Tolhurst TJ, Black KS, Shayler SA, Mather S, Black I, Baker K, Paterson DM.** (1999). Measuring the in situ erosion shear stress of intertidal sediments with the Cohesive Strength Meter (CSM). *Est Coast Shelf Sci* **49**:281-294.
214. **Tolhurst TJ, Consalvey M and Paterson DM.** (2008). Changes in cohesive sediment properties associated with the growth of a diatom biofilm. *Hydrobiology* **596**: 225-239.
215. **Tolhurst TJ, Gust G, and Paterson DM.** (2001). The influence of an extacellular polymeric substance (EPS) on cohesive sediment stability. *Proc. Of INTERCOH 2000,* 409-425.
216. **Tolhurst TJ, Reithmüller R, Paterson DM.** (2000). *In situ* versus laboratory analysis of sediment stability from intertidal mudflats. *Continental Shelf Research* **20**: 1317-1334.
217. **USWES.** (1935). Study of riverbed material and their use with special reference to the Lower Mississippi River. Paper 17, U.S. Waterways Experiment Station, Vicksburg, Miss.
218. **Van Hullebusch ED, Zandvoort M H, Lens PNL.** (2003). Metal immobilisation by biofilms: Mechanisms and analytical tools. *Re/Views in Environ. Sci. Bio/Technol*. **2**: 9–33.
219. **Vardy S, Saunders JE, Tolhurst TJ, Davies PA, Paterson DM**. (2007). Calibration of the high-pressure cohesive strength meter (CSM). *Cont Shelf Res* **27**:1190-1199.
220. **Vignaga E, Haynes H, Sloan WT.** (2011). Quantifying The Tensile Strength of Microbial Mats Grown Over Non Cohesive Sediments. *Biotechnology and Bioengineering*. doi: 10.1002/bit.24401.
221. **von Karman** (1930). *Mechanische Ahnlichkeit and Turbulenz Nachr. Ges.Wiss. Go¨ettingen*, Math.-Phys. Kl. 68.

222. **Walker TR, Grant J.** (2009). Quantifying erosion rates and stability of bottom sediments at mussel aquaculture sites in Prince Edward Island, Canada. *J of Mar Sys* **75**:46-55.
223. **Wallbridge G, Voulgaris BN, Tomlinson B, Collins MB.** (1999). Initial motion and pivoting characteristics of sand particles in uniform and heterogeneous beds: experiments and modelling. *Sedimentology* **46**: 17–32.
224. **Wathen SJ, Ferguson RI, Hoey TB, Werritty A.** (1995). Unequal mobility of gravel and sand in weakly bimodal river sediments. *Water Resources Research* **31**: 2087-2096.
225. **Wentworth CK.** (1922). A scale of grade and class terms for clastic sediments. *J. Geol.* **30**: 377-392.
226. **Wheaton JM, Gibbins C, Wainwright J, Larsen L, McElroy B.** (2011). Preface: Multiscale Feedbacks in Ecogeomorphology. *Geomorphology* **126:** *265–268.*
227. **White CT.** (1940). The equilibrium of grains on the bed of an alluvial Channel, *Proceedings of the Royal Society of London, Series A,* 174:332-338.
228. **Wiberg PL, Smith JD.** (1987). Calculation of the Critical Shear Stress for Motion of Uniform and Heterogeneous Sediments. *Water R Res* **8:**1471-14
229. **Wilcock PR, Barta AF, Shea CC, Kondolf GM, Matthews GV, Pitlick J.** (1996). Observations of flow and sediment entrainment on a large gravel-bed river. *Water Resources Research* **32**: 2897–2909.
230. **Wilcock PR, Kenworthy ST.** (2002). A two-fraction model for the transport of sand/gravel mixtures. *Wat Res Res* **38**: 1194, doi:10.1029/2001WR000684.
231. **Wilcock PR.** (1988). Methods for estimating the critical shear stress of individual fractions in mixed-size sediment. *Water Resources Research* **24**: 1127-1135.
232. **Wilcock PR.** (1993). Critical shear stress of natural sediments. *Journal of Hydraulic Engineering* **119**: 491-505.
233. **Wilcock PR.** (1996). Estimating local bed shear stress from velocity observations. *Water Resources Research* **32**: 3361-3366.
234. **Williams DD.** (1984). The hyporheic zone as a habitat for aquatic insects and associated arthropods. In Resh V.H. and Rosenberg D.M. (eds) *The ecology of aquatic insects*. Praeger, New York.
235. **Williams JJ.** (1996). Turbulent flow in rivers. *In* Advances in Fluvial Dynamics and sratigraphy, (ed.) P.A. Carling and M.R. Dawson.
236. **Wilson CAME, Stoesser T, Bates PD, Batemann Pinzen A.** (2003). Open Channel Flow through Different Forms of Submerged Flexible Vegetation. *J Hydr Eng* **129**: 847-853.
237. **Wu F.-C. and Chou Y.-J.** (2003). Rolling and lifting probabilities for sediment entrainment. Journal of Hydraulic Engineering, 129, pp. 110-119.
238. **Yalin MS, Karahan E.** (1979). Inception of sediment transport. *Journal of the Hydraulics Division, American Society of Civil Engineers* **105**: 1433-43.
239. **Yalin MS.** (1972). *Mechanics of sediment transport,* Oxford, Pergamon: pp. 290.
240. **Yallop ML, Dewinder B, Paterson DM, et al.** (1994).Comparative structure, primary production and biogenic stabilization of cohesive and

non-cohesive marine sediments inhabited by microphytobenthos. *Est Coas and Shelf Sci,* **39:** 565-582.

241. **Yang CT.** (1973). Incipient motion and sediment transport. *J of Hydr Div ASCE* **99**: 1679-1704.

242. **Yang CT.** (2003). Sediment Transport: Theory and Practice, Krieger Publishing Company, Malabar, FL.

243. **Yeung AKC, Pelton R.** (1996). Micromechanics: a new approach to studying the strength and breakup of flocs. *J Colloid Interface Sci* **184**:579-585.

244. **Young RN, Southard JB.** (1978). Erosion of fine-grained marine sediments: sea-floor and laboratory experiments. *Geol Soc Am Bull* **89**: 663-672.

245. **Zahid WM, Ganczarczyk JJ**. (1990). Suspended solids in biological filter effluents. *Water Res* **24**: 215–220.

Appendices

Appendix 3.A: Experimental program

Exp N.	Material	Biotic/ Abiotic	Growth T (weeks)	Scale (mm)	Light at growth (µmol m^{-2} s^{-1})	Light cycle (h)	% τ_b at growth relative to τ_c	Testing Flow steps	Large Scale images analyzed	Small Scale Videos analyzed (min)	PIV
1	SGS	Abiotic		200*200*20				9		18	No
2	SGS	Biotic	1	200*200*20	~120	24	35-50%	9	10	18	No
3	SGS	Biotic	2	200*200*20	~120	24	35-50%	9	10	18	No
4	SGS	Biotic	3	200*200*20	~120	24	35-50%	9	10	18	No
5	SGS	Biotic	4	200*200*20	~120	24	35-50%	9	10	18	No
6	SGS	Biotic	5	200*200*20	~120	24	35-50%	9	10	18	No
7	SGS	Biotic	6	200*200*20	~120	24	35-50%	9	10	18	No
8	SGS	Biotic	7	200*200*20	~120	24	35-50%	9	10	18	No
9	SGS	Biotic	8	200*200*20	~120	24	35-50%	9	10	18	No
10	SGS	Biotic	9	200*200*20	~120	24	35-50%	9	10	18	No
11	SGS	Biotic	10	200*200*20	~120	24	35-50%	9	10	18	No
12	Sand	Abiotic		200*200*20				11		22	No
13	Sand	Biotic	1	200*200*20	~120	12	35-50%	11	22	22	No
14	Sand	Biotic	2	200*200*20	~120	12	35-50%	11	22	22	No
15	Sand	Biotic	3	200*200*20	~120	12	35-50%	11	22	22	No
16	Sand	Biotic	4	200*200*20	~120	12	35-50%	11	22	22	No
17	Sand	Biotic	5	200*200*20	~120	12	35-50%	11	22	22	No
18	LGS	Abiotic		200*200*20				11		22	No
19	LGS	Biotic	1	200*200*20	~120	12	25-30%	11	22	22	No
20	LGS	Biotic	2	200*200*20	~120	12	25-30%	11	22	22	No
21	LGS	Biotic	3	200*200*20	~120	12	25-30%	11	22	22	No
22	LGS	biotic	4	200*200*20	~120	12	25-30%	11	22	22	No
23	LGS	biotic	5	200*200*20	~120	12	25-30%	11	22	22	No

24	Gravel	abiotic		200*200*20				15		30	No
25	Gravel	biotic	1	200*200*20	~120	12	25-30%	15	35	30	No
26	Gravel	biotic	2	200*200*20	~120	12	25-30%	15	35	30	No
27	Gravel	biotic	3	200*200*20	~120	12	25-30%	15	35	30	No
28	Gravel	biotic	4	200*200*20	~120	12	25-30%	15	35	30	No
29	Gravel	biotic	5	200*200*20	~120	12	25-30%	15	35	30	No
30	**SGS**	**abiotic**		**1000*300*20**				**6**		**12**	**yes**
31	**SGS**	**biotic**	**1**	**1000*300*20**	**~26**	**12**	35-50%	**6**	**13**	**12**	**yes**
32	**SGS**	**biotic**	**2**	**1000*300*20**	**~26**	**12**	35-50%	**6**	**13**	**12**	**yes**
33	**SGS**	**biotic**	**3**	**1000*300*20**	**~26**	**12**	35-50%	**6**	**13**	**12**	**yes**
34	**SGS**	**biotic**	**4**	**1000*300*20**	**~26**	**12**	35-50%	**6**	**13**	**12**	**yes**
35	**Sand**	**abiotic**		**1000*300*20**				**6**		**12**	**yes**
36	**Sand**	**biotic**	**1**	**1000*300*20**	**~26**	**12**	35-50%	**6**	**13**	**12**	**yes**
37	**Sand**	**biotic**	**2**	**1000*300*20**	**~26**	**12**	35-50%	**6**	**13**	**12**	**yes**
38	**Sand**	**biotic**	**3**	**1000*300*20**	**~26**	**12**	35-50%	**6**	**13**	**12**	**yes**
39	**Sand**	**biotic**	**4**	**1000*300*20**	**~26**	**12**	35-50%	**6**	**13**	**12**	**yes**
40	**LGS**	**abiotic**		**1000*300*20**				**6**		**12**	**yes**
41	**LGS**	**biotic**	**1**	**1000*300*20**	**~26**	**12**	35-50%	**6**	**13**	**12**	**yes**
42	**LGS**	**biotic**	**2**	**1000*300*20**	**~26**	**12**	35-50%	**6**	**13**	**12**	**yes**
43	**LGS**	**biotic**	**3**	**1000*300*20**	**~26**	**12**	35-50%	**6**	**13**	**12**	**yes**
44	**LGS**	**biotic**	**4**	**1000*300*20**	**~26**	**12**	35-50%	**6**	**13**	**12**	**yes**
45	**Gravel**	**abiotic**		**1000*300*20**				**6**		**12**	**yes**
46	**Gravel**	**biotic**	**1**	**1000*300*20**	**~26**	**12**	35-50%	**6**	**13**	**12**	**yes**
47	**Gravel**	**biotic**	**2**	**1000*300*20**	**~26**	**12**	35-50%	**6**	**13**	**12**	**yes**
48	**Gravel**	**biotic**	**3**	**1000*300*20**	**~26**	**12**	35-50%	**6**	**13**	**12**	**yes**
49	**Gravel**	**biotic**	**4**	**1000*300*20**	**~26**	**12**	35-50%	**6**	**13**	**12**	**yes**

Appendix 3.B: Full strength BG-11 (with NaNO3) nutrient medium

The nutrient medium used at the full strength BG-11 (with NaNO3) according to Ripkka *et al*. (1979) is presented below:

- 1 ml/l of: Ag, $NaCO_3$, citric acid, $MgSO_4*7H_2O$, $CaCl_2*2H_2O$, EDTA, K_2HPO_4, fettic ammonium citrate;
- 5 ml/l of: $NaNO_3$.

Appendix 4.A: Flow steps and hydraulic characteristics

Appendix 4.A shows the different flow steps used for the testing of SGS, sand, LGS and gravel. Whilst SGS and sand have different flow steps because the bed was resettled after SGS experimental testing as concluded, for LGS and gravel the same bed was used; also in this case though new quasi-uniform flow steps higher in magnitude than for sand sediments had to be generated due to the larger size of the gravel sediments.

- **SGS experiments.**

Flow (l/s)	H (mm)	R_h (m)	Bed slope	WL slope	Energy Slope	Froude	U (m/s)	DS u^* (cm/s)	Einstain (1942) u^*(cm/s)	MPM u^*(cm/s)	MPM τ_b (Pa)
0.52	16.9	0.015	0.0054	0.0046	0.0046	0.24	0.10	2.84	2.76	2.63	0.69
0.94	22.0	0.019	0.0058	0.0045	0.0046	0.37	0.17	3.31	3.14	2.95	0.87
1.31	25.2	0.022	0.0056	0.0044	0.0045	0.34	0.17	3.44	3.31	3.10	0.96
1.63	27.1	0.023	0.0057	0.0043	0.0045	0.36	0.19	3.58	3.40	3.17	1.00
1.95	30.1	0.025	0.0054	0.0041	0.0043	0.40	0.22	3.64	3.50	3.25	1.05
2.27	32.2	0.027	0.0053	0.0041	0.0043	0.40	0.23	3.71	3.62	3.34	1.11
2.44	33.6	0.028	0.0053	0.004	0.0042	0.40	0.23	3.78	3.65	3.37	1.13
3.40	39.6	0.031	0.0051	0.0038	0.004	0.44	0.28	3.96	3.86	3.53	1.22
4.52	46.5	0.036	0.0052	0.0038	0.0041	0.48	0.32	4.25	4.19	3.78	1.24

Table 4A. 1 Flow parameters for SGS: H is the flow depth (mm); R_h is the hydraulic radius (m), WL is the water level, DS is the depth-slope shear velocity obtained from the depth slope equation, Einstein (1942) is the shear velocity obtained for side wall correction and MPM is the Meyer-Peter and Müller shear velocity.

- **Sand experiments.**

Flow (l/s)	H (mm)	R_h (m)	Bed slope	WL slope	Energy slope	Froude	U (m/s)	MPM u^* (cm/s)	MPM τ_b (Pa)
1.31	25.2	0.022	0.0061	0.0043	0.0045	0.35	0.17	3.09	0.96
1.70	25.3	0.022	0.0055	0.0045	0.0047	0.45	0.22	3.16	1.00
1.98	27.4	0.023	0.0055	0.0043	0.0046	0.47	0.24	3.22	1.03
2.26	29.8	0.025	0.0054	0.0043	0.0045	0.47	0.25	3.33	1.10
2.47	31.8	0.026	0.0056	0.0042	0.0045	0.46	0.26	3.40	1.15
2.94	34.1	0.028	0.0055	0.0042	0.0045	0.50	0.29	3.51	1.23
3.41	37.0	0.030	0.0060	0.0041	0.0046	0.51	0.31	3.66	1.33
4.06	42.5	0.033	0.0052	0.0040	0.0043	0.49	0.32	3.73	1.37
5.06	48.0	0.036	0.0052	0.0041	0.0044	0.51	0.35	3.96	1.60
6.00	51.9	0.039	0.0061	0.0041	0.0047	0.54	0.38	4.21	1.79
7.00	55.4	0.040	0.0054	0.0041	0.0045	0.57	0.42	4.24	1.96

Table 4A. 2 Flow parameters for Sand: H is the flow depth (mm); R_h is the hydraulic radius (m), WL is the water level, and MPM is the Meyer-Peter and Müller shear velocity. During the sand experiments different flow steps were employed compared to SGS ones: this was due to the fact that the flume was emptied once between the 2 experiments and hence the uniform flow calibration had to be re run; moreover higher flow steps were applied for sand to investigate further the biostabilization potential.

- **LGS and gravel experiments.**

Flow (l/s)	H (mm)	R_h (m)	Bed slope	WL Slope	Energy Slope	Froude	U (m/s)	MPM u^* (cm/s)	MPM τb (Pa)
1.31	25.2	0.022	0.0061	0.0043	0.0045	0.35	0.17	3.09	0.95
1.70	25.3	0.022	0.0055	0.0045	0.0047	0.45	0.22	3.16	1.00
1.98	27.4	0.023	0.0055	0.0043	0.0046	0.47	0.24	3.22	1.03
2.26	29.8	0.025	0.0054	0.0043	0.0045	0.47	0.25	3.33	1.11
2.47	31.8	0.026	0.0056	0.0042	0.0045	0.46	0.26	3.40	1.16
2.94	34.1	0.028	0.0055	0.0042	0.0045	0.50	0.29	3.51	1.23
3.41	37.0	0.030	0.006	0.0041	0.0046	0.51	0.31	3.66	1.34
4.06	42.5	0.033	0.0052	0.0040	0.0043	0.49	0.32	3.73	1.39
4.50	43.3	0.034	0.0046	0.0045	0.0045	0.53	0.35	3.86	1.49
5.06	48.0	0.036	0.0052	0.0041	0.0044	0.51	0.35	3.96	1.56
5.50	48.8	0.037	0.0044	0.0047	0.0046	0.54	0.38	4.08	1.66
6.00	51.9	0.039	0.0061	0.0047	0.0047	0.54	0.38	4.21	1.77
6.50	54.1	0.040	0.0045	0.0046	0.0046	0.55	0.40	4.22	1.78
7.00	55.4	0.040	0.0054	0.0041	0.0045	0.57	0.42	4.24	1.79
7.50	58.7	0.042	0.0040	0.0048	0.0045	0.56	0.43	4.34	1.88
8.00	60.6	0.043	0.0047	0.0046	0.0046	0.57	0.44	4.43	1.96
8.50	64.1	0.045	0.0049	0.0047	0.0048	0.56	0.44	4.58	2.09
9.00	66.7	0.046	0.0051	0.0047	0.0048	0.56	0.45	4.67	2.18
10.00	69.1	0.047	0.0047	0.0049	0.0048	0.59	0.48	4.73	2.24

Table 4A. 3 Flow parameters for LGS and gravel: H is the flow depth (mm); R_h is the hydraulic radius (m), WL is the water level, and MPM is the Meyer-Peter and Müller shear velocity.

Appendix 5.A: Biofilm coverage LS: Beginning vs End of flow step

Appendix 5.A shows the hydraulic parameters obtaining setting up UF conditions for the testing of box1.

Flow (l/s)	H (mm)	R_h (m)	Bed Slope	WL slope	Froude	U (m/s)	τ_b DS (R_h) (Pa)	τ_b Einst. 1942 (Pa)	τ_b DS (H) (Pa)
1.6	18.0	0.016	0.0048	0.0050	0.71	0.30	0.78	0.84	0.88
2.6	24.8	0.021	0.0054	0.0055	0.71	0.35	1.04	1.14	1.22
3.6	29.0	0.024	0.0055	0.0053	0.78	0.41	1.19	1.31	1.42
5	36.8	0.030	0.0047	0.0050	0.75	0.45	1.45	1.64	1.80
7	44.2	0.034	0.0047	0.0053	0.80	0.53	1.67	1.91	2.16
9	52.5	0.039	0.0046	0.0052	0.80	0.57	1.90	2.23	2.57
11	59.3	0.043	0.0050	0.0055	0.81	0.62	2.08	2.48	2.90

Table 5A. 1. Flow parameters for the erosion testing of box1: H is the flow depth (mm); R_h is the hydraulic radius (m), WL is the water level, DS is the depth-slope τ_b shear stress obtained from the depth slope equation respectively using H or R_h; Einstein (1942) is the shear velocity obtained for side wall correction, which would be used as the reference value in the experiments.

Appendix 5.B: EPS -Carbohydrate quantification with phenol assay

Modified after **Daniels, L., Hanson, R.S, and J. Phillips**. 2007. Total Carbohydrates by Phenol Reaction, p. 468. In: Reddy, C.A., Beveridge, T.J., Breznak, J.A., Marzluf, G.A., Schmidt, T.M., and L.R. Snyder (ed.), *Methods for General and Molecular Microbiology*, 3rd ed., Section III: Chemical Analysis ASM Press, Washington, DC

Sample Preparation

Supernatants

1. 200mg of biofilm plus sediment sample into a 15ml tube;
2. Add 1.5ml dH_2O water;
3. Rotate for 1.5h;

4. Place the test tube in an ice bath and sonicate with 20 % of the amplitude for 180 seconds;

5. Centrifuge (at 10,000 rpm) for 10 minutes;

6. Remove the supernatant to a fresh tube (2ml).

Preparation of Standards

Prepare Glucose standards in distilled water in the concentrations of 5; 10; 25; 50; 75; and 100µg/ml.

Photometric Assay

1. Pipet 500µl of each standard, blank and sample or sample dilution into a glass 15ml tube;

2. Under the fume hood add 500µl of the Phenol solution (5% v/v) and 2.5ml of concentrated sulphuric acid.

3. Mix thoroughly.

4. Incubate at 95°C for 1h.

5. Pipet 300µl into separate wells of a microplate.

6. Measure the absorbance at 488nm using the microplate reader.

Materials and Dispensable

Water, distilled; Phenol Solution, 5% (v/v) in distilled water; Sulphuric Acid, >95%; D (+) – Glucose (Monohydrate); Phenol cryst., extra pure; 15ml tubes.

Standards EPS Curve

Below the calibration curve for the glucose standards, prepared in distilled water in the concentrations of 5; 10; 25; 50; 75; and 100µg/ml.

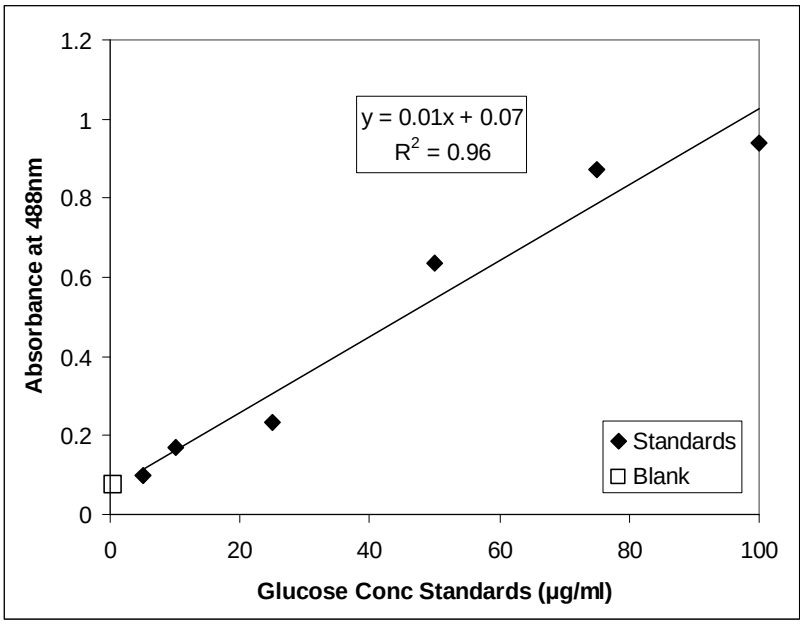

Figure 5.B: Calibration curve of the Standards glucose concentration of 5; 10; 25; 50; 75; and 100µg/ml.

Appendix 5.C: Biofilm coverage LS: beginning vs end of flow step

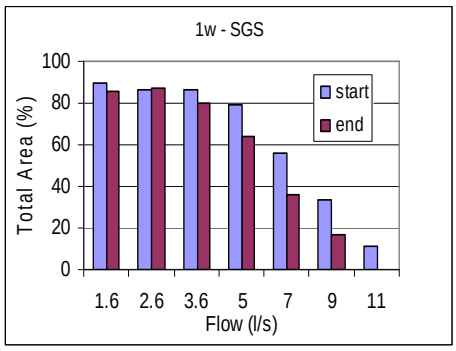

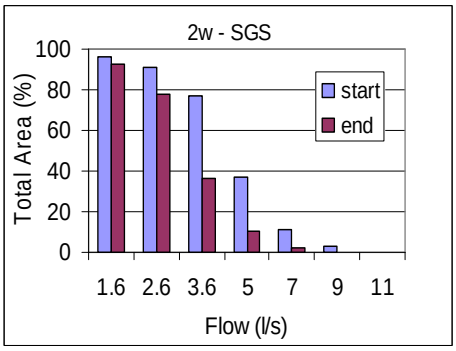

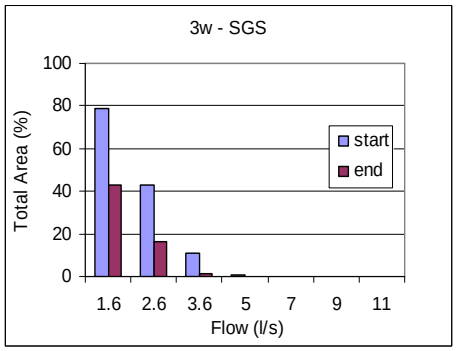

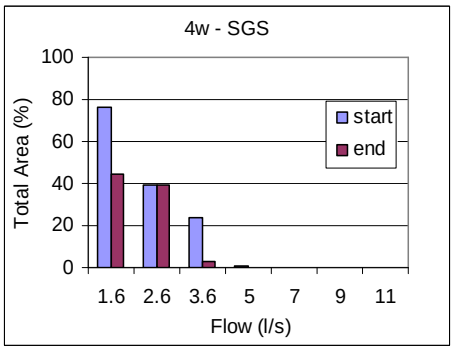

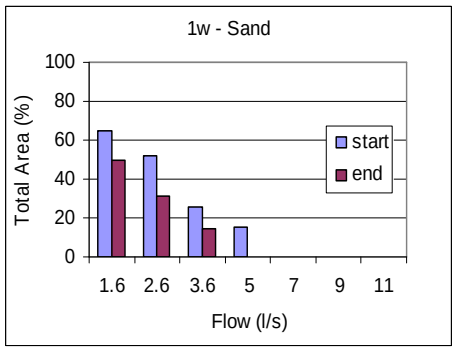

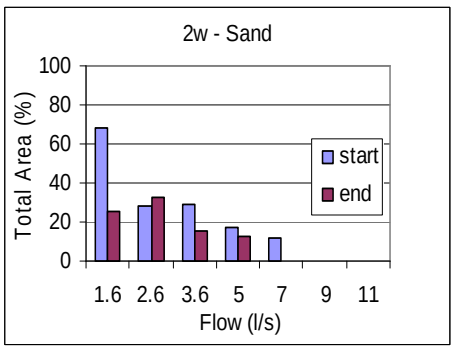

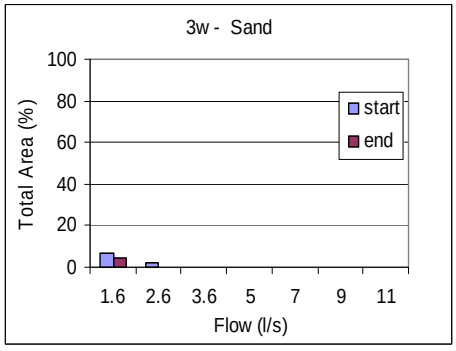

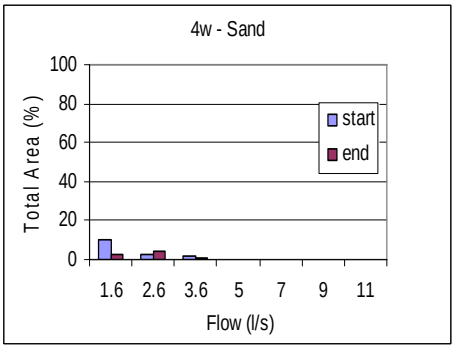

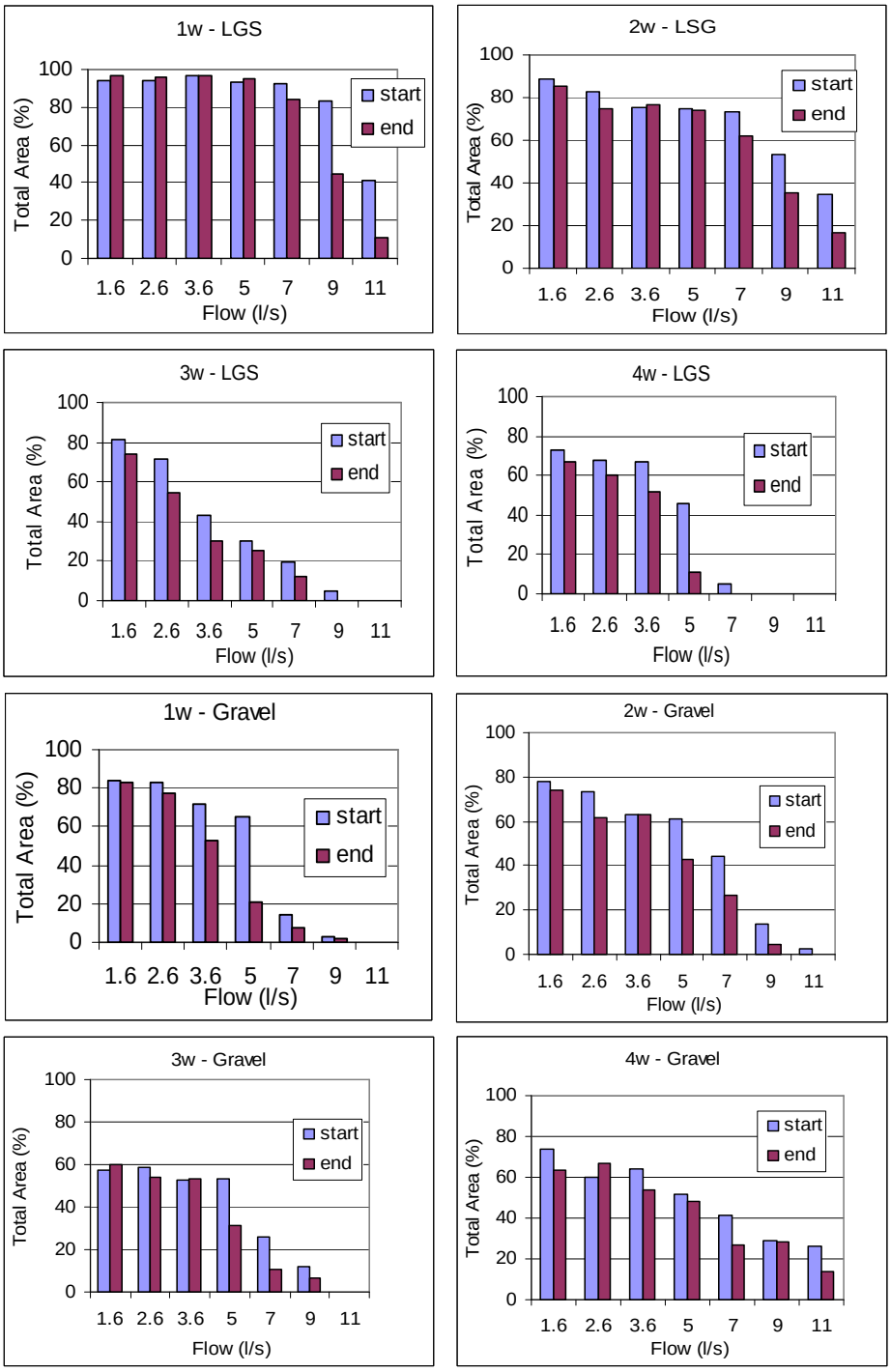

Figure 5.C 1. Biofilm coverage at the LS (% of the total, equal to 500mm by 280mm) for the four materials (SGS, Sand, LGS and Gravel) at the beginning and at the end of every flow step. Spheres are subjected to an error of up to 9% and natural sediment to an error up to 5% (a reasoning for this can be find in Chapter 4, Section 4.3.3).

Appendix 5.E: Average PIV double averaged statistics comparison

Time and Space averaged flow statistics for SGS.

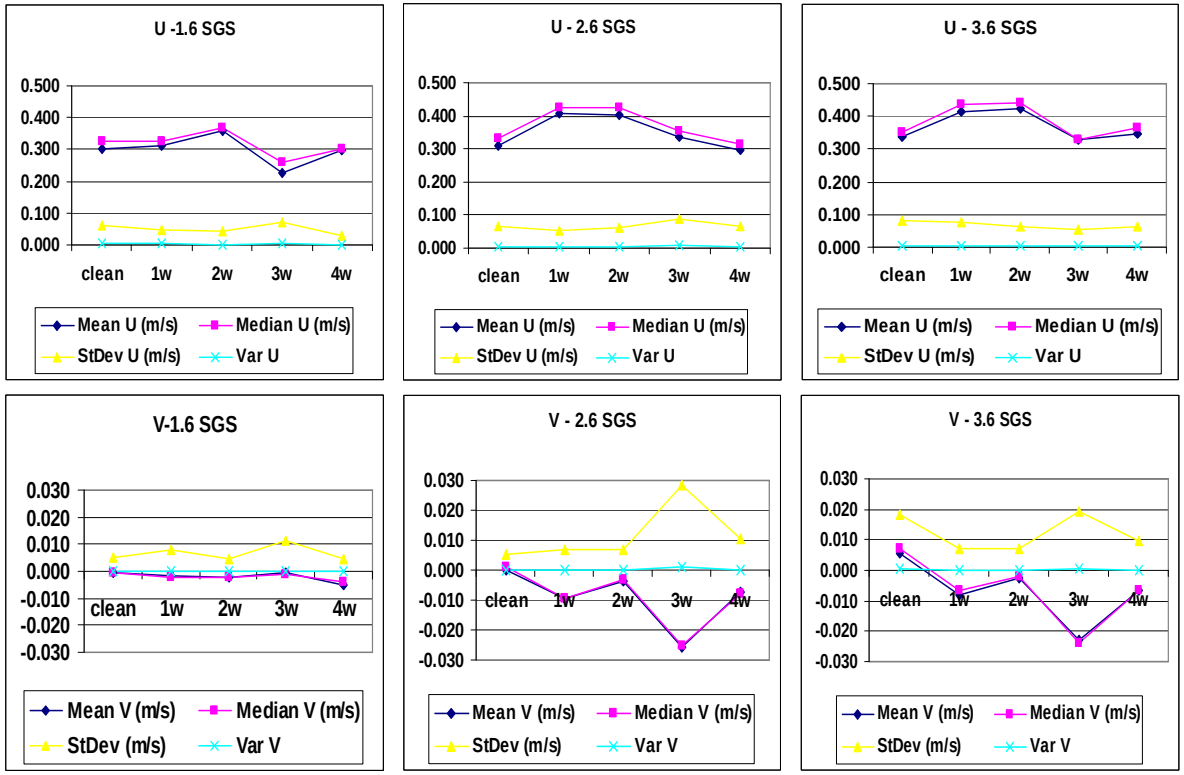

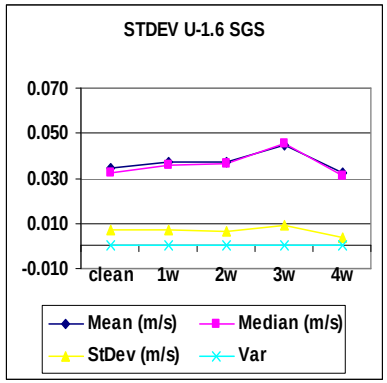
STDEV U-1.6 SGS
0.070
0.050
0.030
0.010
-0.010
clean
1w
2w
3w
4w
Mean (m/s)
Median (m/s)
StDev (m/s)
Var

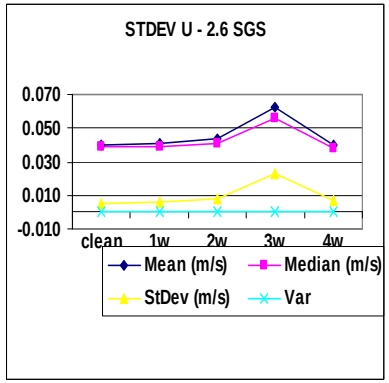
STDEV U - 2.6 SGS
0.070
0.050
0.030
0.010
-0.010
clean
1w
2w
3w
4w
Mean (m/s)
Median (m/s)
StDev (m/s)
Var

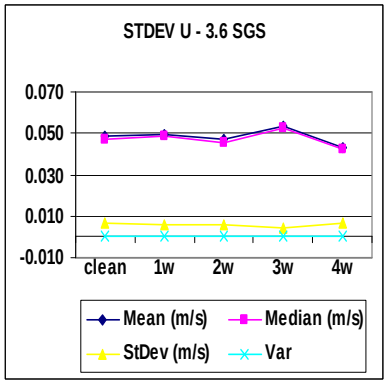
STDEV U - 3.6 SGS
0.070
0.050
0.030
0.010
-0.010
clean
1w
2w
3w
4w
Mean (m/s)
Median (m/s)
StDev (m/s)
Var

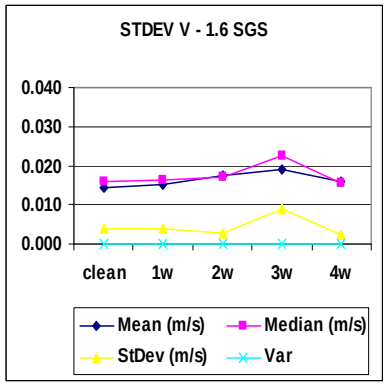
STDEV V - 1.6 SGS
0.040
0.030
0.020
0.010
0.000
clean
1w
2w
3w
4w
Mean (m/s)
Median (m/s)
StDev (m/s)
Var

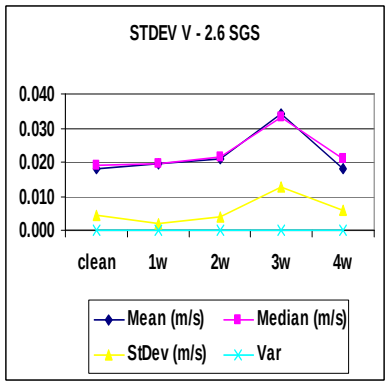
STDEV V - 2.6 SGS
0.040
0.030
0.020
0.010
0.000
clean
1w
2w
3w
4w
Mean (m/s)
Median (m/s)
StDev (m/s)
Var

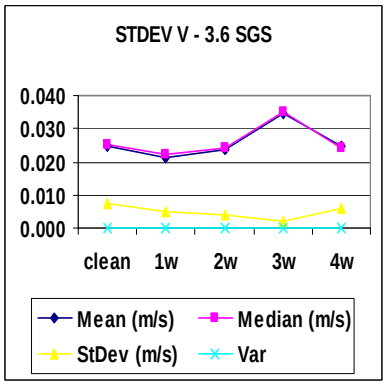
STDEV V - 3.6 SGS
0.040
0.030
0.020
0.010
0.000
clean
1w
2w
3w
4w
Mean (m/s)
Median (m/s)
StDev (m/s)
Var

Time and Space averaged flow statistics for Sand.

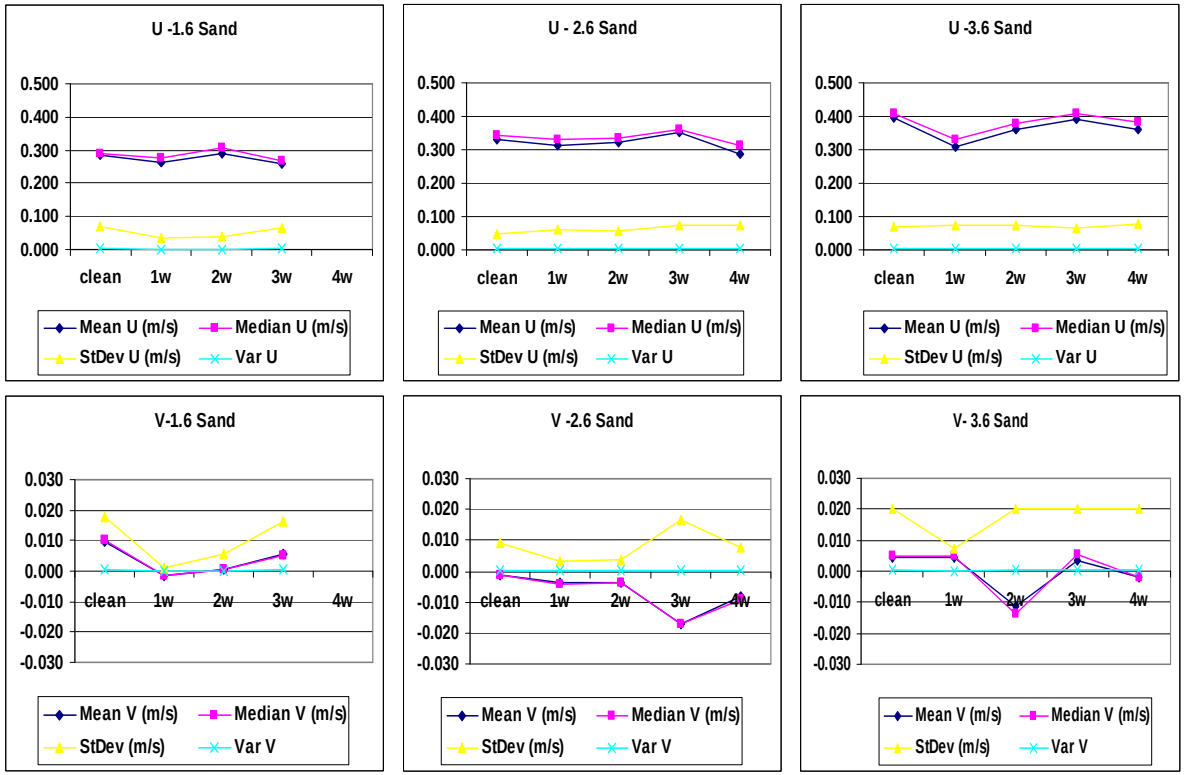

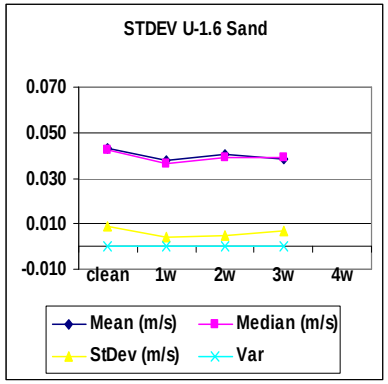
STDEV U-1.6 Sand
0.070
0.050
0.030
0.010
-0.010
clean
1w
2w
3w
4w
Mean (m/s)
Median (m/s)
StDev (m/s)
Var

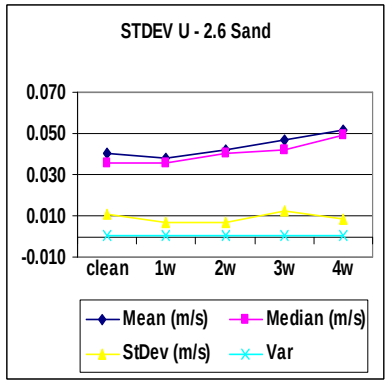
STDEV U - 2.6 Sand
0.070
0.050
0.030
0.010
-0.010
clean
1w
2w
3w
4w
Mean (m/s)
Median (m/s)
StDev (m/s)
Var

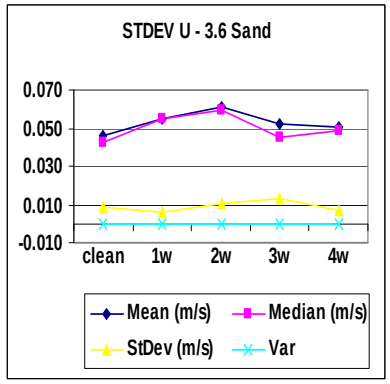
STDEV U - 3.6 Sand
0.070
0.050
0.030
0.010
-0.010
clean
1w
2w
3w
4w
Mean (m/s)
Median (m/s)
StDev (m/s)
Var

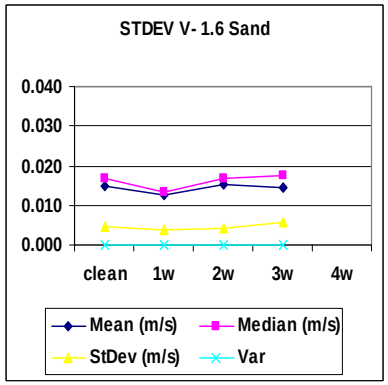
STDEV V- 1.6 Sand
0.040
0.030
0.020
0.010
0.000
clean
1w
2w
3w
4w
Mean (m/s)
Median (m/s)
StDev (m/s)
Var

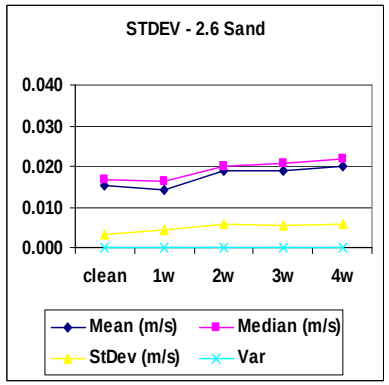
STDEV - 2.6 Sand
0.040
0.030
0.020
0.010
0.000
clean
1w
2w
3w
4w
Mean (m/s)
Median (m/s)
StDev (m/s)
Var

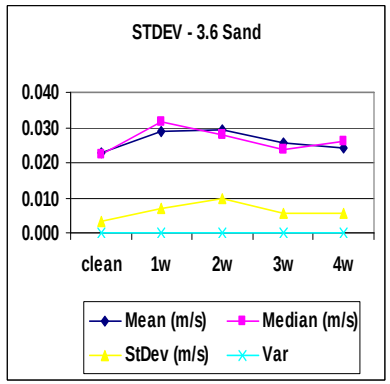
STDEV - 3.6 Sand
0.040
0.030
0.020
0.010
0.000
clean
1w
2w
3w
4w
Mean (m/s)
Median (m/s)
StDev (m/s)
Var

Time and Space averaged flow statistics for LGS.

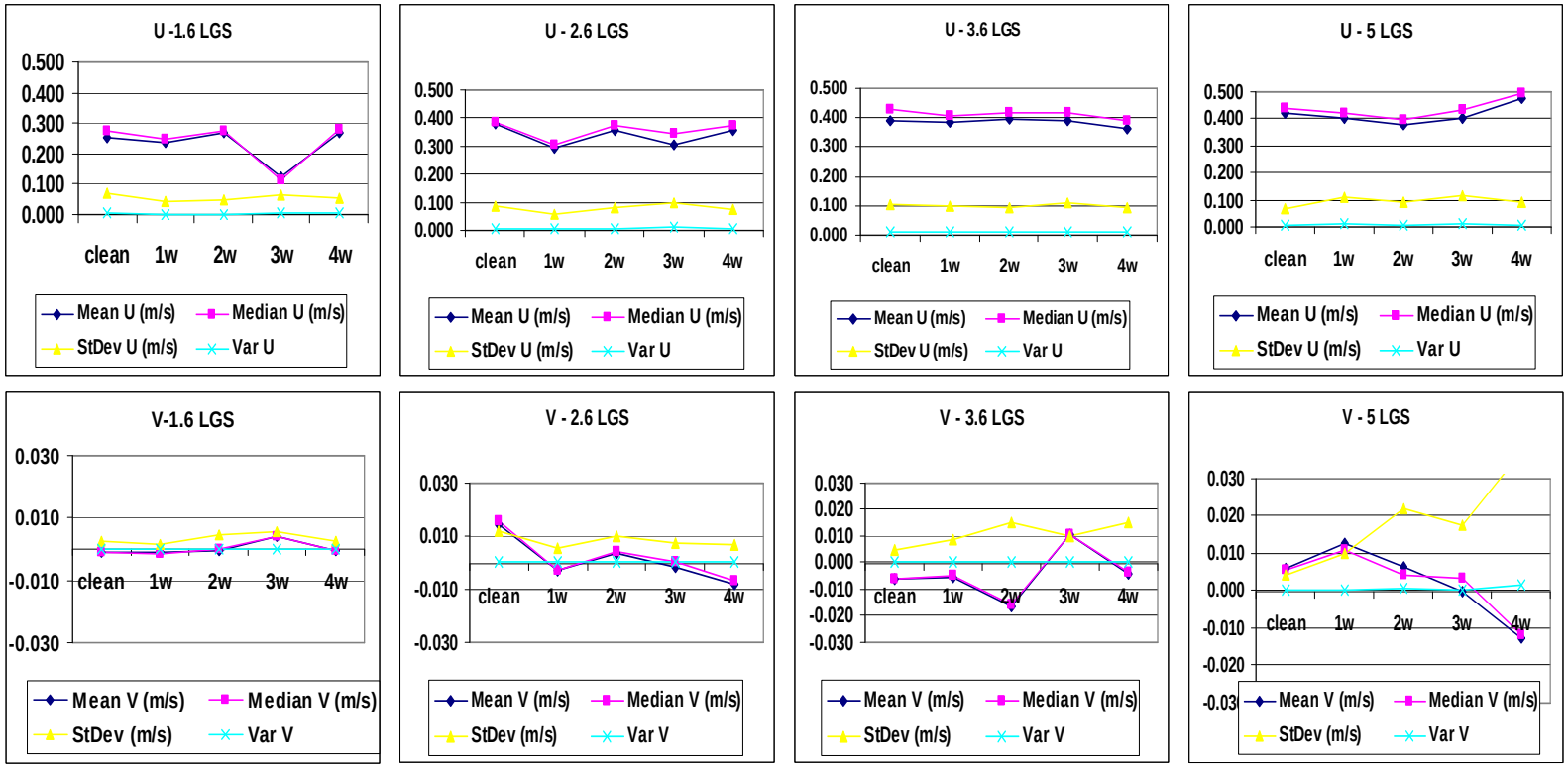

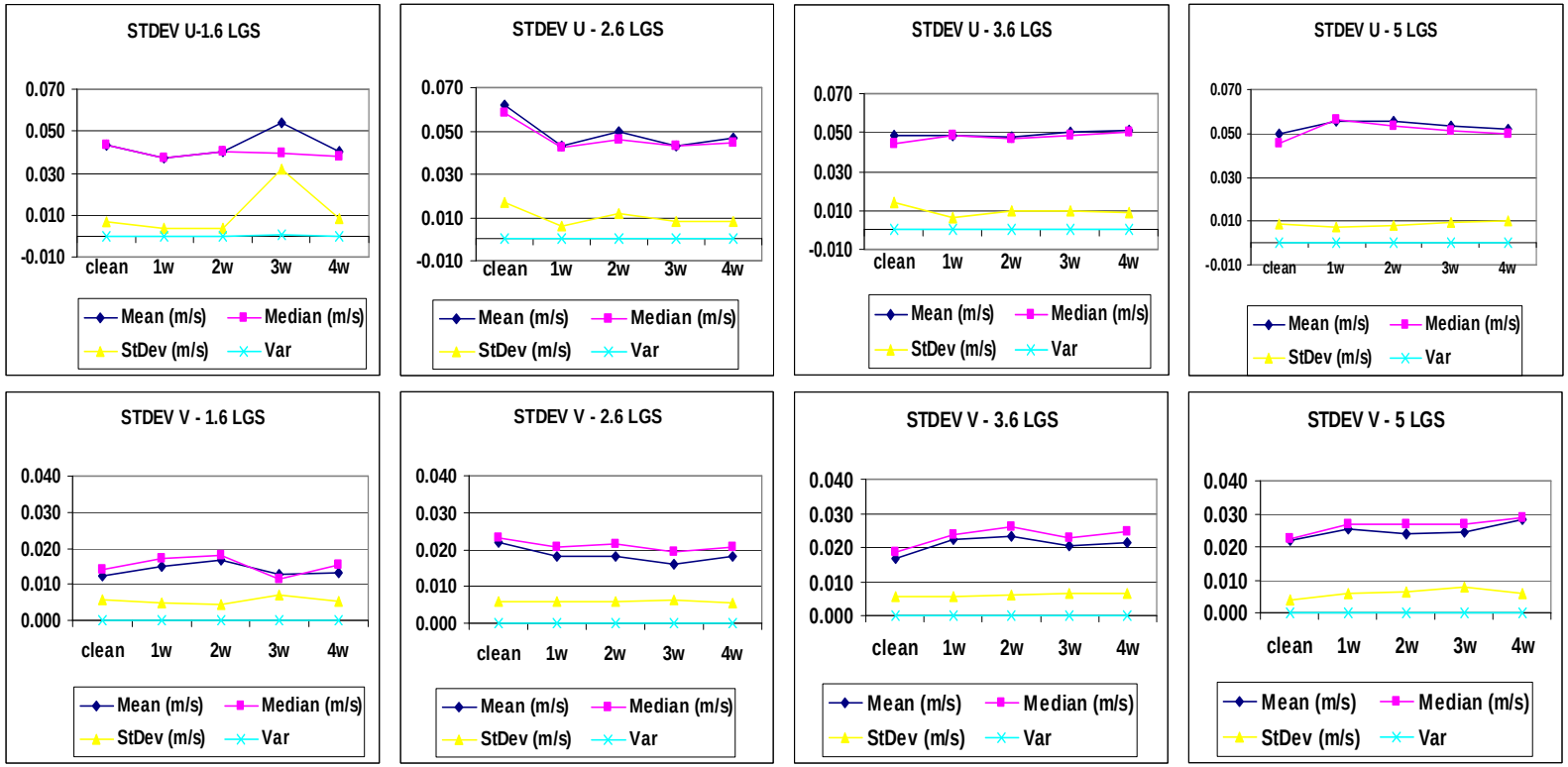
STDEV U-1.6 LGS
0.070
0.050
0.030
0.010
-0.010
clean 1w 2w 3w 4w
Mean (m/s) Median (m/s)
StDev (m/s) Var
STDEV U - 2.6 LGS
0.070
0.050
0.030
0.010
-0.010
clean 1w 2w 3w 4w
Mean (m/s) Median (m/s)
StDev (m/s) Var
STDEV U - 3.6 LGS
0.070
0.050
0.030
0.010
-0.010
clean 1w 2w 3w 4w
Mean (m/s) Median (m/s)
StDev (m/s) Var
STDEV U - 5 LGS
0.070
0.050
0.030
0.010
-0.010
clean 1w 2w 3w 4w
Mean (m/s) Median (m/s)
StDev (m/s) Var
STDEV V - 1.6 LGS
0.040
0.030
0.020
0.010
0.000
clean 1w 2w 3w 4w
Mean (m/s) Median (m/s)
StDev (m/s) Var
STDEV V - 2.6 LGS
0.040
0.030
0.020
0.010
0.000
clean 1w 2w 3w 4w
Mean (m/s) Median (m/s)
StDev (m/s) Var
STDEV V - 3.6 LGS
0.040
0.030
0.020
0.010
0.000
clean 1w 2w 3w 4w
Mean (m/s) Median (m/s)
StDev (m/s) Var
STDEV V - 5 LGS
0.040
0.030
0.020
0.010
0.000
clean 1w 2w 3w 4w
Mean (m/s) Median (m/s)
StDev (m/s) Var

Time averaged flow statistics for Gravel.

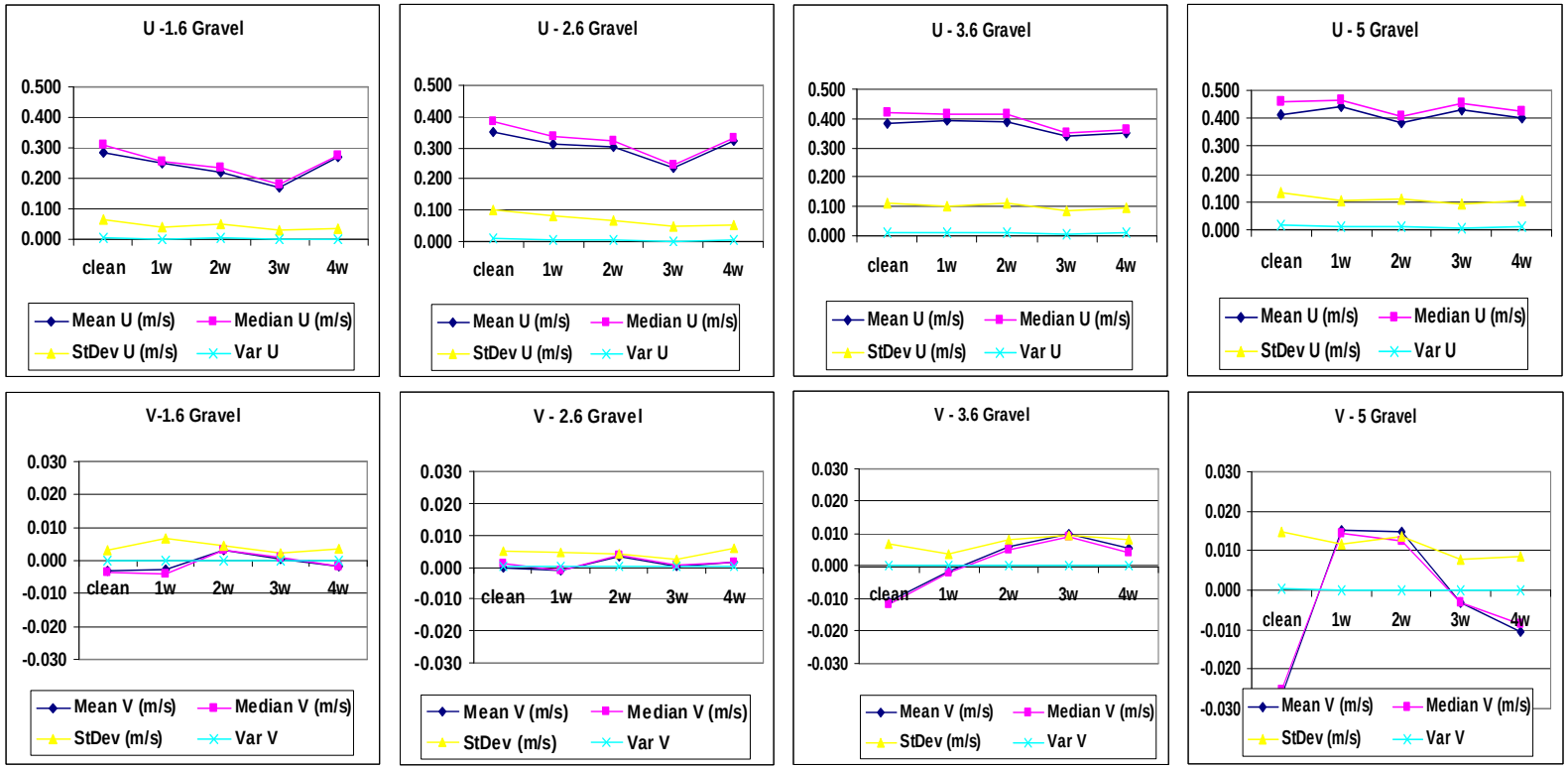

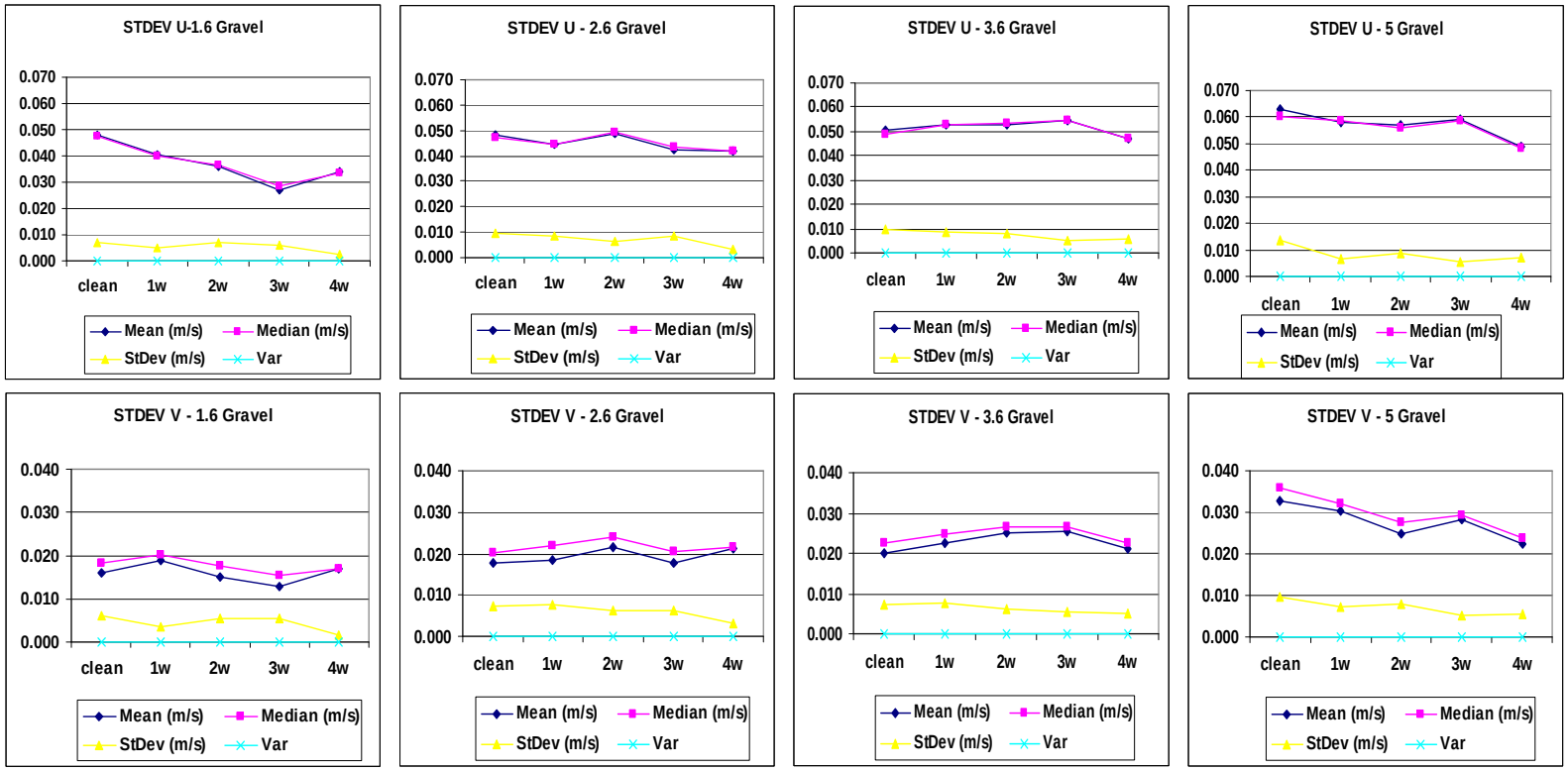
STDEV U-1.6 Gravel
STDEV U - 2.6 Gravel
STDEV U - 3.6 Gravel
STDEV U - 5 Gravel
STDEV V - 1.6 Gravel
STDEV V - 2.6 Gravel
STDEV V - 3.6 Gravel
STDEV V - 5 Gravel
clean
1w
2w
3w
4w
Mean (m/s)
Median (m/s)
StDev (m/s)
Var

Appendix 8.A: Real river biofilm: site selection

This Appendix relates to Section 8.2.1.1 of this thesis. It outlines the field site locations, characteristics and sampling that underpins choice of Camps Water as the real river sample location; these data are provided in Table 8.A1 and figure 8.A4. All sedimentological information from the field sites is also provided in Table 8.A2 and in figures 8.A1-A3.

Table 8A. 1. Catchment, hydraulic, sediment and ecological descriptors of three field sites; R. Eden, R. Devon and Camps Water. Qx values for the hydraulic data are gauged discharge values which are exceeded x% of the time, thus, a Q95 is a low flow and Q10 is a high flow. Catchment descriptor information is sourced from Centre for Ecology and Hydrology (CEH: http://www.ceh.ac.uk/).

Catchment	General river description	Sample Location (O.S. grid ref.)	Biofilm observations	Hydraulic gauge data	Catchment descriptor	Sediment analysis
Eden	Located in Fife (nr. St. Andrew's). Catchment area = 307.4 km^2. Generally single thread meandering. Two tributaries: Motray Water (rural) and Ceres Burn (rural)	NO415158	Brown bio-mat; mature and spongy character. Cover relatively homogeneous. (figure 8A.4). Presumed diatom dominant.	Kemback Gauge. Average daily flow: Q=3.97m^3/s Q10=8.14m^3/s Q95 = 0.97m^3/s.	Gently-sloping, low-altitude catchment. Land-use is arable, pasture and woodland.	Bimodal coarse sand and fine gravel (Table 8A.2, figure 8A.1).
Devon	The Devon River is a left tributary of the river Forth in Clackmannanshire. Catchment area = 181 km^2. After descending from the Blairdenon Hill in the Ochils, it flows east and southeast through Glendevon, turning southwest at Crook of Devon and then continuing westwards. It then reaches the River Forth at the small village of Cambus. It is a meandering river and it is prone to floodings.	NS858960	Evidence of different photosynthetic biofilms: a green one (possibly a filamentous cyanobacteria) and a brown one (presumably diatoms). Cover patchy, mature biofilm (figure 8A.4).	Glenochil Gauge. Average daily flow: Q=4.64m^3/s Q10=9.63m^3/s Q95=1.03m^3/s.	The headwaters are steep whereas the lower valley is broad and very flat. The land use is arable in the valley, grassland in headwaters and some forest.	Unimodal very fine/fine gravels (Table 8A.2, figure 8A.2).

Camps	It rises, in several head-streams, on heights contiguous to the boundary with Peeblesshire, and runs about 6 miles west-south-westward, through a moorish, mountainous tract, to the river Clyde opposite Crawford village.	NT 003 225	Brown biofilm, spongy character and filaments. Cover patchy. (figure 8A.4). Presumed diatom dominant.	No info	It source is the Camps reservoir, which is a dammed artificial reservoir. Rural.	Bimodal distribution of coarse sand and fine gravels (Table 8A.2, figure 8A.3).

Table 8A. 2. Sediment characteristics over 400 grains for the three field sites. Standard statistics are provided in terms of the mean, median (D_{50}), mode, geometric standard deviation and range. Full grain size distributions can be found in figure from 8A.1 - 8A.3.

	Eden	Devon	Camps Water
Mean (mm)	1.91	2.05	1.79
Median (mm)	1.13	1.82	1.27
Mode (mm)	0.48	2.02	1.41
Standard Deviation	2.04	1.22	1.54
Range (mm)	14.00	16.93	13.41
Wentworth class	Coarse sand	Fine gravel	Coarse sand
Grade	Bimodal	Unimodal	Weakly bimodal

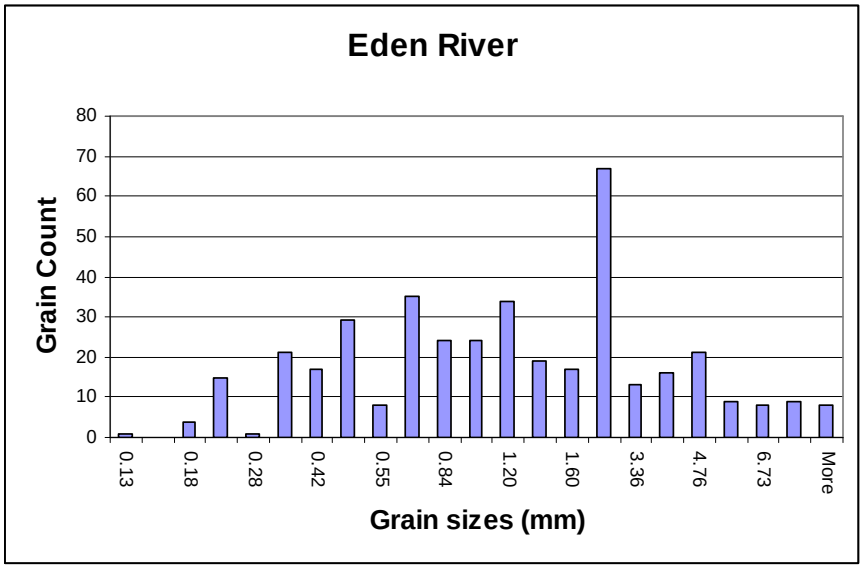

Figure 8A. 1. Grain size distribution for the Eden River (out of 400 grains). The graph shows a clear bimodal bed.

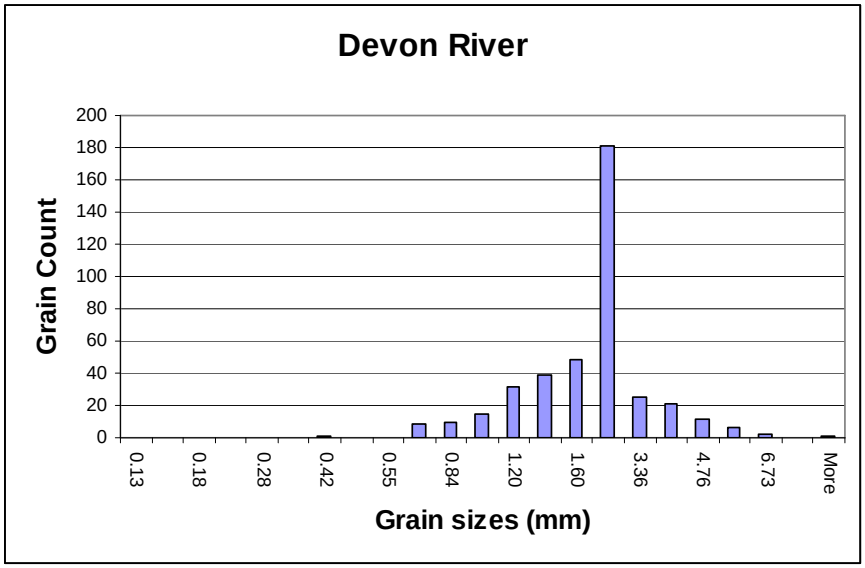

Figure 8A. 2. Grain size distribution for the Devon River (out of 400 grains). A clear unimodal distribution is visible with a peak in the fine gravel range.

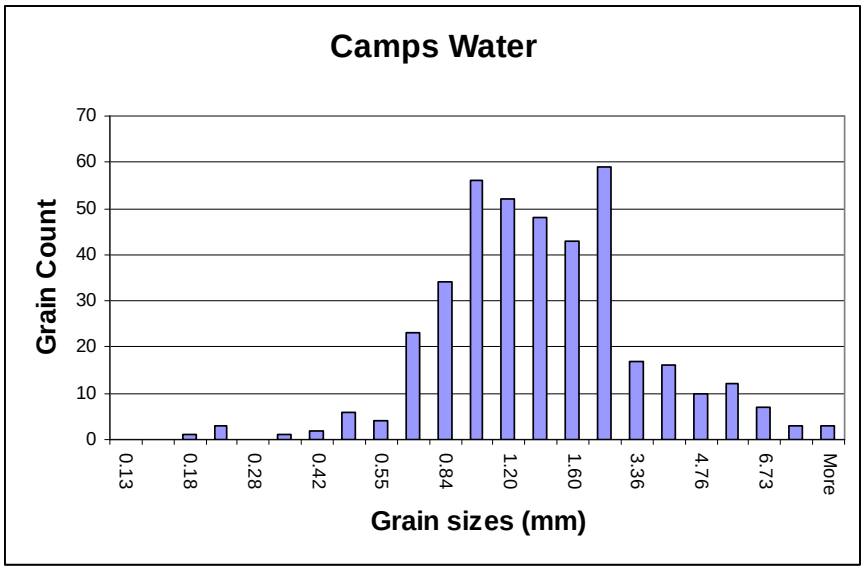

Figure 8A. 3. Camps Water sediment sizes distribution (out of 400 grains). The distribution is bimodal with a mean peak in the range of coarse sand and a second peak in the range of coarse gravel.

(i) River Eden: 1) view of the vegetated river bed, River Eden; 2) view of the vegetated river bed; 3) Light microscope of the biofilm collected (scale 3.53mm*2.65mm).

(ii) River Devon: 1-2) more gravely than the Eden river; 3) Biofilm from the Devon river: prevalence of filamentous cyanobacteria; 4) brown biofilm, possibly diatoms (scale 2.34mm*1.75mm)

(iii) Camps Water: 1) generally a gravely bed; 2) finer material at the bends; 3) Photosynthetic brown biofilm (scale 3.53mm*2.65mm).

Figure 8A. 4: Field sample locations at the reach (10's m) and patch scale (m) and light microscope images of biofilm samples at approximately 3.5 x 2.5mm scale: (i) River Eden - brown spongy biofilm tending towards a homogeneous coating but not a well developed mat, possible diatom dominant biofilm; (ii) River Devon – brown/green spongy biofilm well established in patches, possible cyanobacteria (green) and diatom (brown) present; (iii) Camps Water – brown spongy and filamentous biofilm, patchy; possibly (diatoms).

Appendix 8.B: Real river biofilm: flume, growth and light set up

The selected flume (figure 8B.1) for the pilot experiment presented in section 8.2.1 was ideal for the experiment where real river water was used to culture a sediment substratum because equipped with a small tank that could be filled up with 150l of water. It was a 5m long flume (3m working section), 0.081m wide and fitted with a 4l/s pump. The bed was set to be 50mm deep and mainly comprised by gravel with diameter (*D*) in the range of 5.6mm-8mm. The testing section was located 3.8m downstream the inlet and far enough to not be disturbed by the outlet. The length of the test area was approximately 240mm; here glass beads with D_{50}=0.85mm were placed and screeded at the level of the adjacent bed. The fitted pump was not controlled by a power inverter, so picks of flow (roughly 20-30% more water depth, lasting for only a short amount of time) have been experienced during growth.

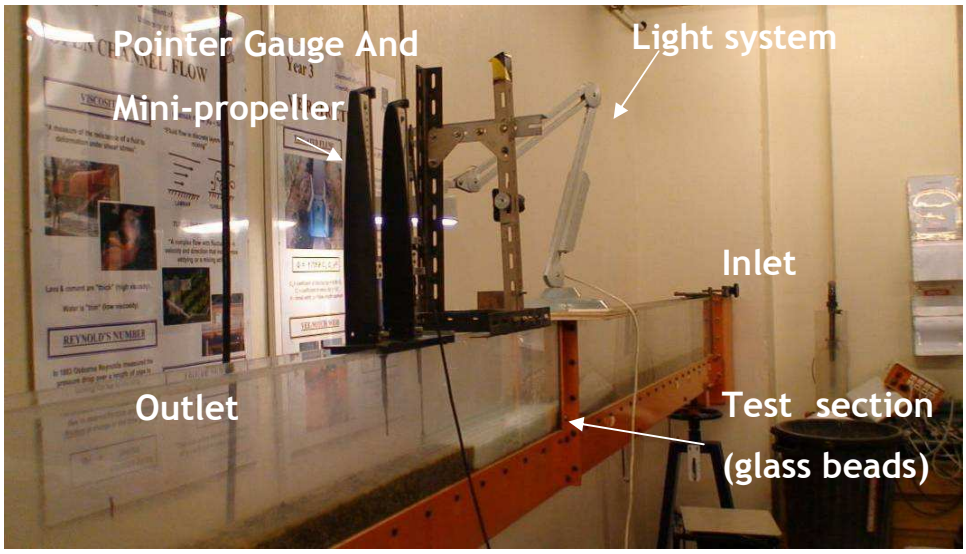

Figure 8B. 1. Narrow flume used for real river biofilm colonisation and testing. Full working length of 5m, test width of 81mm. Facility is equipped with 12:12h lighting cycles. The pointer gauge for depth readings and mini-propeller for are crude methods for calculating discharge through the flow section (max. 4l/s). The test section of glass beads is 240mm in length, located 3.8mm downstream of the inlet in the region of best uniform flow; 5.6-8mm gravel surrounds this section.

Uniform flow conditions for growth (lower than the critical threshold conditions for the glass beads) and at threshold were established: the maximum error on the slope experienced was up to 15% due to the absence of an adjustment of the

tail gate on the flume. The bed shear stress (τ_b) was derived from the depth-the Einstein (1942) equation for side wall correction with ρ, the density of the water, set at 21ºC (equal to 997.9kg/m^3) (see chapter 4, equation 4.2) To use this equation it was required to obtain the flow depths at each step and flow velocity using a mini-propeller (*Nixon 403*), which had a calibration chart (HZ values were related to flow velocity). The propeller was placed at 40% of the flow depth (from the bed), location that is considered in engineering practice to be where the average velocity takes place in a turbulent velocity profile. Knowing the cross-sectional area (b, width of the channel, was equal to 0.081m) and the average velocity for that position, flow could be estimated (See table 6.4 below).

Flow	Depth *H* (mm)	*U* (m/s)	DS $\tau_{b\,(Pa)}$	Einstein (1942) τ_b (Pa)
1st (at growth)	20	0.27	0.66	0.60
2nd	33	0.37	0.89	0.77
3rd	40	0.39	0.99	0.84
4th	47	0.44	1.06	0.88
5th	55	0.52	1.14	0.89

Table 8B. 1. Hydraulic variable for the 5 flows used in the experiments. DS τ_b is the shear stress obtained for the depth slope equation; Einstein τ_b and u^*_c are values corrected for the walls effect (Einstein, 1942).

Critical threshold of the abiotic beads was calculated using the Yalin Criterion (1972) (See chapter 4). The selected area A was equal to 35mm by 20mm, which meant having in the field of view approximately 1234 particles. For a period of time equal to 60s, the number of particle required to move in the field of view were 8 to define such a flow at threshold. To maximize the precision we analyzed 3 minutes: the 1st, the 5th and the 9th minute. The calculations showed that 8 particles were at threshold in each of the minutes analyzed for an average velocity *U* equal to 0.30m/s and a corrected shear stress τ_c equal to 0.70Pa (u^*_c equal to 2.65cm/s).

Once the uniform flow set up was established, the real river water was added to the tank (first 150l and then the tank was topped up to compensate for evaporation) and the experiment started, letting the bacteria in the water colonize the sediment in the tested area. This was obtained by having a lamp constantly illuminating the test section (15.6 µmol m^{-2} s^{-1}) and positioned 400mm away from the bed. Of interest is that the first flow, which was the flow at

growth, was approximately 86% of the critical entrainment threshold, hence quite a strong flow that should have created a strong biofilm.

A high speed camera (*Sony HDR-SR5E*) was placed on top of the testing area and it allowed to get full view pictures of the entire testing area (240mm in length) and high resolution video of a smaller area in the centre line of the flume (35mm in length) for the duration of each flow step (10 minutes). The growth achieved after 10 weeks can be seen below (figure 5B.2). A brown biofilm, similar to the one seen in the Camps Water was seen colonizing the artificial sediments.

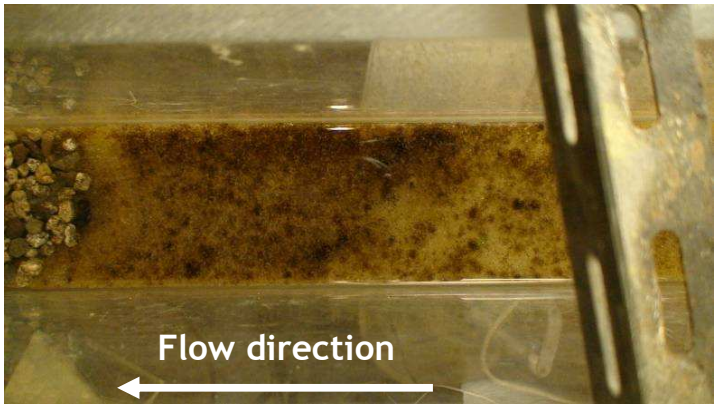

Figure 8B. 2. Laboratory biofilm over substratum area 240mm*81mm following 10 weeks of growth. Laboratory sample is clearly appropriate in terms of colour and coverage, compared to that of the field Biofilm coverage after 10 weeks of growth (length scale 240mm)

Before starting the test, a sample was collected at the downstream end of the test section. This was done in order to calculate the biomass (Himom, 2005) and the EPS (Daniels *et al.*, 2007) produced at this stage of growth.

Appendix 8.C: Real River: Results

- **Biomass**

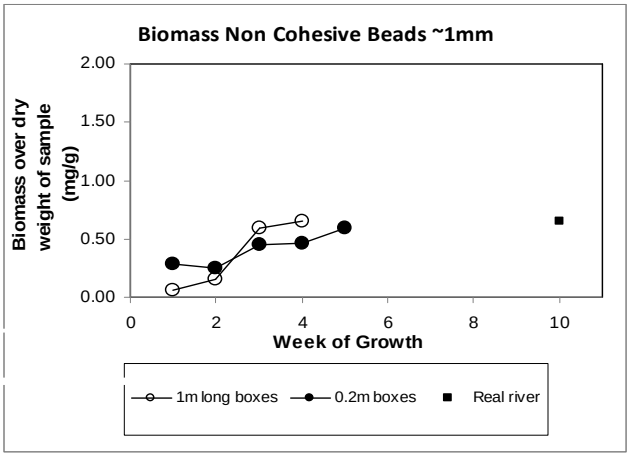

Figure 8C. 1. Biomass over weight of the sample (g) for non cohesive spherical glass beads for 200mm, and 1m boxes (SGS) compared to the real river experiment (D_{50}=0.85). The value of biomass obtained showed that 10 weeks of colonization allowed 17.70mg of biomass to be generated using the same methodology as in chapter 4 and chapter 5 (see chapter 3). The biomass value for this experiment sits in the middle of the largest biomass experienced in previous chapters for SGS.

- **EPS**

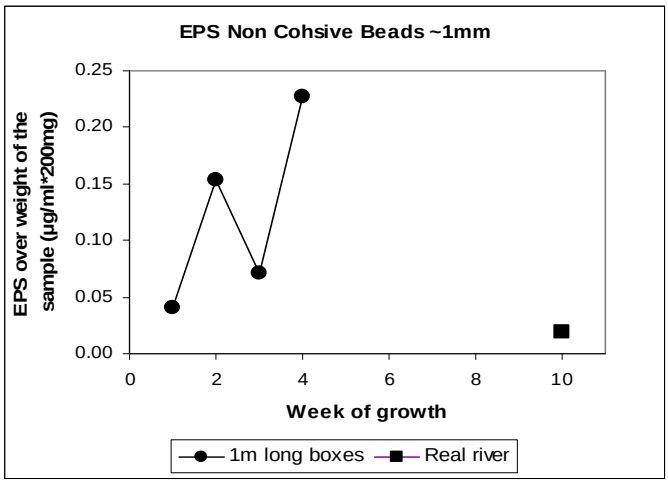

Figure 8C. 2. EPS over weight of the sample (200mg) for non cohesive spherical glass beads ~1mm for 1m boxes compared to the real river experiment. When comparing the results for the real river experiments with previously collected data (only for 1m long boxes) for SGS, it is evident that the value of EPS in this experiment was the lowest. This might have consequences in the stability of the substratum: in chapter 5 low EPS content was associated to high stabilization potential (week 1 of growth).

- **Percentage erosion at the Large Scale:**

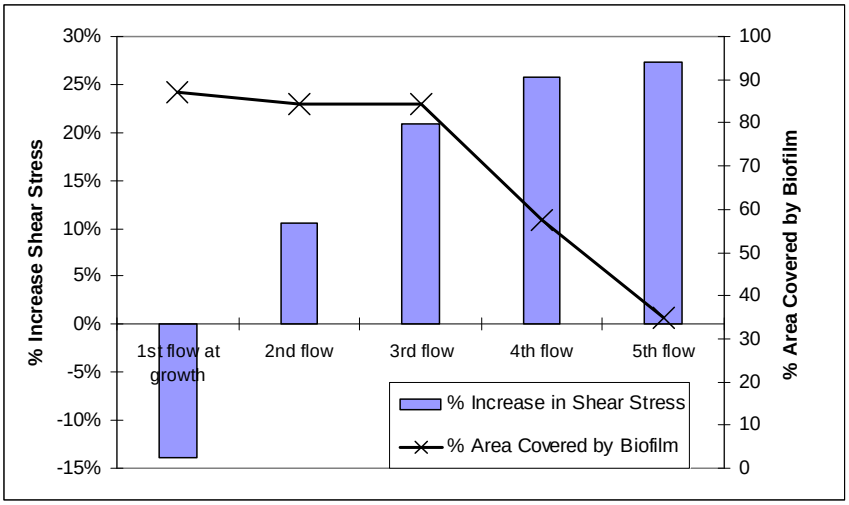

Figure 8C. 3. Area erosion at the end of every flow step (10min) for the 5 different flows. The bars relate to the % increase in shear stress compared to the critical, whereas the line is the % coverage of the biofilm at the full view (~24.00 in length).

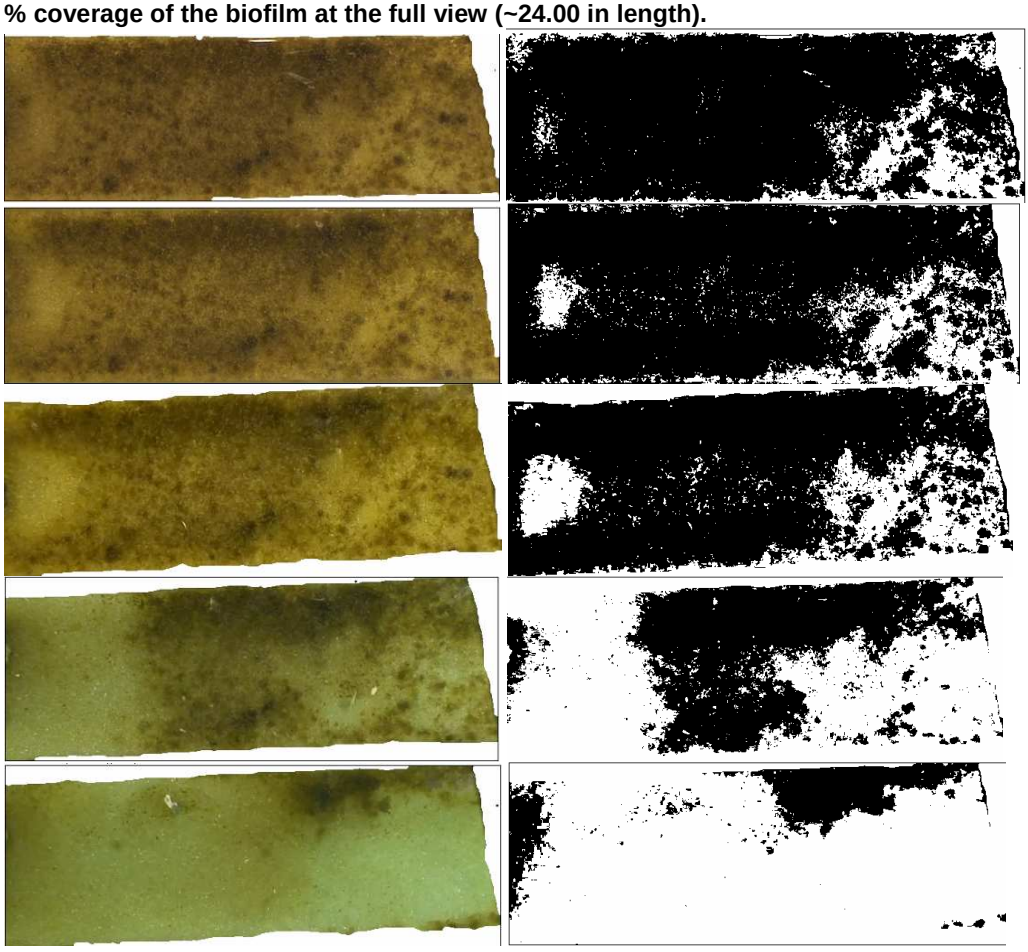

Figure 8A. 5. Area eroded (%) for original and thresholded image using Iso Data technique through *ImageJ* for the five flow steps used in the testing of the real river experiments (see Appendix 5B; Length 240mm).

Appendix 8.D: Wiberg and Smith (1987) modification including the force induced by biofilms

Derivation of the modified Wiberg and Smith model, after adding the elastic force due to the biofilm F_e=*KdL*, where k is the constant of elasticity and dl is the elongation of the biofilm before breaking. The other forces acting on the sediment particle are as seen in figure 8.2 are: Gravity (F_G), Buoyancy (F_B), Lift and Drag over the particle (F_L *and* F_D), Resisting force (F_R). $F_{G'}$ is defined as the difference between the gravity and the buoyancy force (see Wiberg and Smith, 1987).

$$(F_D + F_G \sin\beta)\cos\Phi = (F_G \cos\beta - F_L)\sin\Phi + KdL;$$

$$F_D + F_G \sin\beta = (F_G \cos\beta - F_L)tg\Phi + \frac{KdL}{\cos\Phi};$$

$$\left(\frac{F_D}{F_L}\right)\left[(F_G \cos\beta - F_L)tg\Phi + \frac{KdL}{\cos\Phi}\right] = \left(\frac{F_D}{F_L}\right)\left[F_D + F_G \sin\beta\right];$$

$$F_G(\cos\beta tg\Phi - \sin\beta) + \frac{KdL}{\cos\Phi} = F_D + F_L tg\Phi;$$

$$\frac{F_G}{F_D} = \frac{1 + \frac{F_L}{F_D}tg\Phi - \frac{KdL}{F_D\cos\Phi}}{\cos\beta tg\Phi - \sin\beta};$$

Using the Law of the Wall and knowing that α=A_xD/V, where A_x is the cross sectional area of a grain, and V is the volume of the grain, the equation above can be re written as:

$$\frac{\frac{1}{2}\tau_c C_D f^2\left(\frac{z}{z_0}\right) A_x D}{(\rho_s - \rho)Ug} = \frac{\cos\beta tg\Phi - \sin\beta}{1 + \frac{F_L}{F_D}tg\Phi - \frac{KdL}{F_D\cos\Phi}};$$

Hence:

$$\tau_c = \frac{2}{\alpha}\frac{1}{C_D f^2\left(\frac{z}{z_0}\right)}\frac{(\cos\beta tg\Phi - \sin\beta)D}{1 + \frac{F_L}{F_D}tg\Phi - \frac{KdL}{F_D\cos\Phi}}$$

Where C_D is the drag coefficient, *U* is the temporal mean velocity at height *z*, z_0 the zero velocity level of the logarithmic profile.

Interesting to notice is that *KdL* and $F_D cos\Phi$ are applied to the same plane and in opposite direction.